JAIST Repository
https://dspace.jaist.ac.jp/

Title	ケイホウ酸ガラス型有機・無機ハイブリッドの設計とその二次電池デバイスへの電気化学的応用
Author(s)	Kumar Sai Smaran
Citation	
Issue Date	2015-03
Type	Thesis or Dissertation
Text version	ETD
URL	http://hdl.handle.net/10119/12768
Rights	
Description	Supervisor:松見　紀佳，マテリアルサイエンス研究科，博士

JAIST
JAPAN
ADVANCED INSTITUTE OF
SCIENCE AND TECHNOLOGY

Japan Advanced Institute of Science and Technology

Doctoral Dissertation

Borosilicate Type Organic-inorganic Hybrid Ion-gels and Their Electrochemical Applications in Secondary Batteries

KUMAR SAI SMARAN

Supervisor: Professor Noriyoshi Matsumi

School of Materials Science

Japan Advanced Institute of Science and Technology

March 2015

Borosilicate Type Organic-inorganic Hybrid Ion-gels and their Electrochemical Applications in Secondary Battery Devices

Kumar Sai Smaran, s1240004

ABSTRACT

Nowadays, lithium ion batteries are widely employed as energy storage media in numerous electrical appliances. Although these batteries have higher energy density, flammability of electrolyte and lower transference number endanger their reliability for persistent usage in daily life. With the Boeing Dreamliner mishap due to faulty lithium-ion batteries, a deliberate and conscientious effort towards improvement safety parameters of the batteries apart from production efficiency in terms of cost, conductivity and other mechanical and thermal factors.

The present doctoral work mainly concerns with the design of novel ionic liquid based lithium ion conducting electrolytes for LiBs aiming at the improvement of the abovementioned issues, divided n the chapters 2,3 and 4 in the doctoral thesis. Hybrid ion-gel electrolytes via borosilicate glass formation is one of approach for such novel electrolytes. In-situ sol-gel condensation reactions of alkoxysilane/alkoxyborane in ionic liquid media resulted in the formation of organic-inorganic hybrids, which constitutes the principle subject of Chapter-2. Such, organic-inorganic hybrids have the dual advantages of high ionic conductivity due to the organic component and high thermal stability due to the inorganic component. Incorporation of boron improves ionic conductance by facilitated salt dissociation. Enhanced salt dissociation may be due to the possible interactions between the empty p-orbital of boron atom and the anion moiety. The main aspects of this chapter are highlighted in Fig. 1.

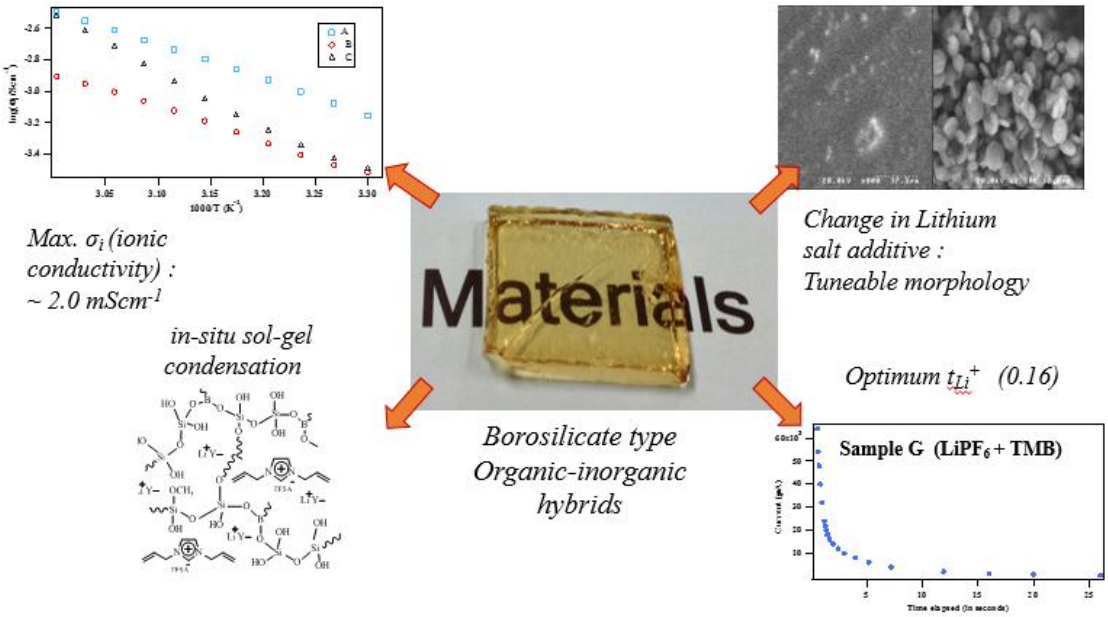

Figure 1. Highlights of Chapter 2

In the subsequent chapter, i.e. Chapter-3, the viability of the organic-inorganic hybrids as electrolytes for lithium batteries was studied by the fabrication of anodic half-cells, and their subsequent cycling at various charging current rates. The conventional protocol was employed for charge-discharge studies. Having obtained results not in terms with the typical patterns of batteries, a variant of the

Electrochemical Impedance spectroscopic technique was further employed to determine the causes of such anomalous behaviour. Given the novelty of the material, to get a clear view of the internal kinetics of cells, the impedance profiles of the anodic half-cells were studied over a range of potential utilising Dynamic Electrochemical Impedance Spectroscopy. It was observed that high capacitive tail-ends were observed at higher potentials in these anodic-half cells, with anomalous charge-discharge profiles at such potentials. Hence, utilising such non-destructive DEIS technique, and interpreting the results in terms effect of potential on the passivation of the electrolyte, the voltage cut-offs were revised. The revised protocol, which comprised of DEIS experiments followed by charge-discharge studies, provided notable results. The gist of this chapter is shown in Figure 2. The $LiPF_6$ based hybrids with various alkoxyboranes were considered for the studies in this chapter on account of their high ionic conductivities.

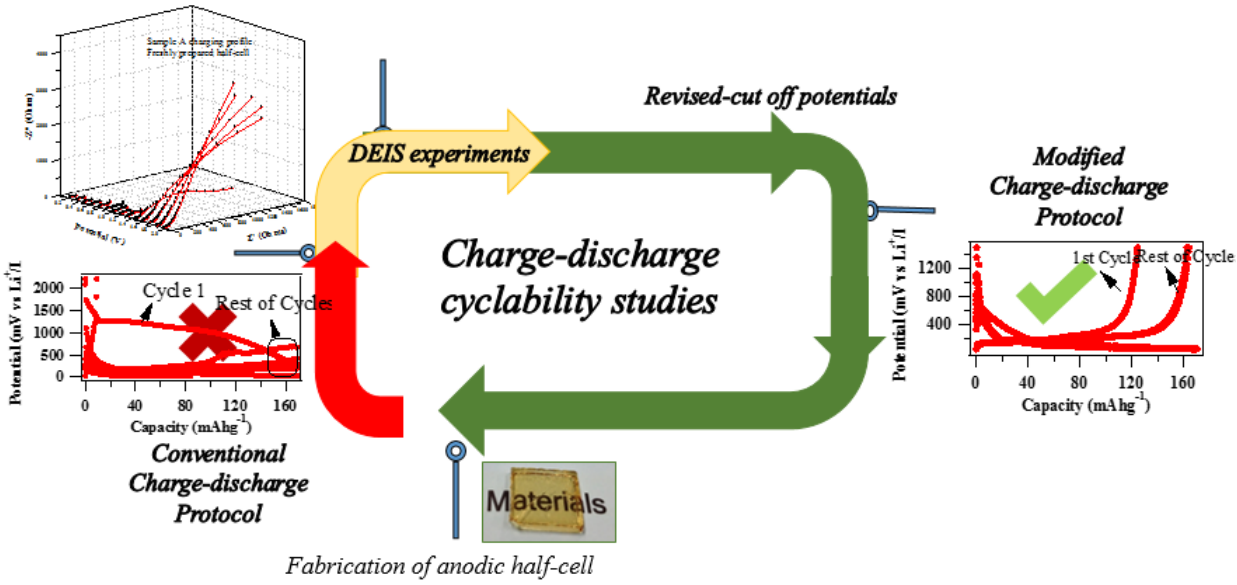

Figure 2. Highlights of Chapter 3

The major focus of the final chapter (Chapter-4) was on the flammability studies and thermogravimetric studies of the organic-inorganic hybrids to evaluate their thermal stability in a comparative manner with that of the commercially available electrolytes for lithium-ion batteries. Thermogravimetric analysis (TGA) showed morphologically uniform hybrids were stable up to 350°C. The highly homogenous hybrids with LiTFSA salt additive showed greater thermal stability in naked flame studies as well. While $LiPF_6$ based hybrids which characteristically showed heterogeneous behaviour showed higher susceptibility to flame tests, and showed lower range of thermal stability in thermogravimetric experiments. However, the hybrid electrolytes showed self-extinguishing features, which is absent in case of commercially used electrolytes in lithium ion batteries.

Thus, the doctoral work encompasses an overall study comprising of three steps. The first step being the design and synthesis of novel borosilicate type organic-inorganic hybrids along with the study of its conductivity and lithium-ion diffusivity aspects. The second phase includes the study of fabricated anodic half-cells using organic-inorganic hybrids for a practical demonstration of these hybrids in lithium batteries. In addition, Dynamic electrochemical impedance spectroscopy was used as a diagnostic tool to evaluate an optimum working rage for these cells. In the third and final step, the thermal stability of these hybrids was verified through thermogravimetric and naked flame studies.

Keywords: Organic-inorganic hybrids, ion-gels, in-situ sol-gel condensation, lithium-ion borosilicate, charge-discharge

Preface

The present dissertation is the consolidation of results of the works on the topic "Borosilicate type Organic-inorganic hybrids and their electrochemical applications in secondary batteries" under the direction of *Prof. Noriyoshi Matsumi* at the School of Materials Sciences, Japan Advanced Institute of Science and Technology during 2012-2015.

With the constant depletion of conventional energy resources and increasing needs for energy by the society has led to the scarcity of energy sources which has become evident in recent times. Lithium-ion batteries is one of the trendsetter among the existing energy technologies, widely popular, commercialised due to its various attractive features. However, as a means of improvement of its electrolyte system, to deem it safe from flame hazards, various kinds of research works are being undertaken. The author's main focus is to address the above mentioned drawbacks by the synthesis of mechanically robust, yet highly conductive borosilicate type organic-inorganic hybrid ion-gels for use as electrolytes in Lithium-ion batteries.

The work presented in this thesis covers the synthesis and characterisation of novel borosilicate organic-inorganic hybrids along with their performance parameters as observed in lithium-ion batteries by employment of novel experimental protocol as devised by dynamic electrochemical impedance spectroscopy. Also the sturdiness against flame unlike other conventional electrolytes has also been showcased. Finally, the conclusions of the studies are summarised in the final chapter.

Kumar Sai Smaran

School of Materials Science

Japan Advanced Institute of Science and Technology

March 2015

Acknowledgement

The studies presented in this thesis have been carried out under the direction of *Prof. Noriyoshi Matsumi* at the School of Materials Sciences, Japan Advanced Institute of Science and Technology during 2012-2015. The studies are concerned with the design and synthesis of novel borosilicate Organic-inorganic Hybrids along with their electrochemical applications in Lithium-ion batteries.

The author expresses his deep gratitude to my supervisor *Prof. Noriyoshi Matsumi* for his kind guidance, valuable suggestions and heartfelt encouragements throughout this work.

I would also like to thank the members of my Review committee *Prof. Masayuki Yamaguchi*, *Prof. Kensuke Naka*, *Assoc. Prof. Yuki Nagao* and *Assoc. Prof. Kazuaki Matsumura*, who have spent their valuable time to read my manuscript and gave valuable comments and remarks to enhance the quality of my thesis.

The author is thankful to *Prof. Vito Di Noto*, for giving him an opportunity to carry out experiments at his laboratory at Department of Chemical Sciences, University of Padua, Padua, Italy. Furthermore, the author wishes to express his special thanks to *Prof. Vito Di Noto* and members at his laboratory for their active collaboration, warm support and valuable suggestions during the author's stay in Italy.

The author also takes an opportunity to thank *Assistant Prof. Raman Vedarajan* for his guidance and encouragement at a professional and personal level. I am also grateful to other laboratory members, for the valuable inputs, cooperation and active discussions throughout my time at JAIST.

The author would also like to thank *Dr. Kitano Takahiro* san, General Manager, TEC ONE Co. Ltd., who graciously helped at the time of need.

The author expresses his heartfelt gratitude to his parents and dear ones, for their relentless encouragement at difficult times. Finally, the author expresses his humble gratitude to the Almighty for all the good things.

Kumar Sai Smaran

School of Materials Science

Japan Advanced Institute of Science and Technology

March 2015

List of Figures

Figure 1.1 *Maximum volumetric energy density and maximum gravimetric energy density profiles for various batteries* 6

Figure 1.2 *Graphic timeline of the evolutionary trend in batteries, with futuristic insights* 8

Figure 1.3 *Estimated output of various emergent technologies alongside present technologies* 9

Figure 1.4 *Lithium-ion transport mechanism in a polymer electrolyte formed by a complex between lithium salt and a coordinating poly (ethyleneoxide) PEO chain* 10

Figure 1.5 *Chemical reactions taking at individual electrodes in a lithium-ion battery* 11

Figure 1.6 *Typical set-up of a lithium-ion battery, with the constituent graphite anode, lithium cobalt oxide cathode separated by a separator and electrolyte* 12

Figure 1.7 *Broad classification of anode materials used in lithium-ion batteries* 13

Figure 1.8 *Lithium intercalation into Graphite* 13

Figure 1.9 *Anomalous expansion of silicon anode in 110 plane in lithium-ion cells* 14

Figure 1.10 *Formation of crystalline phases upon electrochemical lithium insertion and de-insertion from a Sn anode* 15

Figure 1.11 *Hysteresis profiles of various Cobalt based materials* 16

Figure 1.12 *TEM images of pulverization of Aluminium anode in lithium-ion cells at different magnifications* 16

Figure 1.13 *Broad classification of cathode materials used in lithium-ion batteries* 18

Figure 1.14 *Crystal structure of* $LiCoO_2$ 18

Figure 1.15 *a) Crystal structure of* $LiFePO_4$ *b) TEM images of* $LiFePO_4$ *cathode coated MWCNT* 20

Figure 1.16 *Structure of* Li_2MnSiO_4 21

Figure 1.17 *Classification of electrolytes of Lithium-ion batteries* 22

Figure 1.18 *Comparative chart of various lithium salts over a wide category of parameters* 24

Figure 1.19 *Some other lithium salts which have been considered in the lithium-ion battery research* 25

Figure 1.20 *Visuals of pure Ionic liquids* 26
Figure 1.21 *Advantages of Ionic liquids along with few common examples of ionic liquids* 26
Figure 1.22 *Classification of Polymer electrolytes* 27
Figure 1.23 *Structural formula poly(methoxyethoxyethoxyphosphazene), MEEP* 29
Figure 1.24 *Few other polymer structures which are used in lithium ion-batteries* 30
Figure 1.25 *Elaboration on the classification of Hybrid electrolytes* 30
Figure 1.26 *Aliphatic ionic liquids employed for studies in LiBs* 37
Figure 1.27 *Some of the popular anions and newly designed anions studied employed in LiBs* 38
Figure 1.28 *Few of the constituents of ionic liquids employed by Passerini et al as electrolytes in LiBs* 39
Figure 1.29 *Few of the constituents of ionic liquids employed by Zaghib et al as electrolytes in LiBs* 39
Figure 1.30 *The possible ways of polymerisation of ionic liquids* 40
Figure 1.31 *Structure of poly(N-vinyl-3-methylimidazolium TFSA), first polymerised ionic liquid* 40
Figure 1.32 *Polycation type ionic liquid based polymers* 41
Figure 1.33 *Block copolymer comprising of styryl and functionalised styryl units with ionic liquid pendant groups* 42
Figure 1.34 *Illustration depicting the anion-trapping mechanism corresponding salt dissociation in the presence of boron compounds* 42
Figure 1.35 *Boroxine ring type anion receptors* 43
Figure 1.36 *Boronate type anion receptors* 43
Figure 1.37 *Boric ester type anion receptors* 44
Figure 1.38 *Organoboron compounds derived from reaction between borane compounds and ionic liquids* 44
Figure 1.39 *Ionic liquid based organoboron polymer* 45
Figure 1.40 *Reaction scheme for synthesis of organoboron ion-gels by condensation of cellulose with boric acids in ionic liquids* 45
Figure 1.41 *Reaction scheme of the synthesised inorganic-organic hybrids showing the incorporation of boron via borosilicate network* 46
Figure 1.42 *Computer enhanced image of the Mayan fresco* 47
Figure 1.43 *Commonly observed interactions highlighted as observed in hybrid materials* 48

Figure 1.44 *General strategies towards the synthesis of organic-inorganic hybrids* 50
Figure 1.45 *Representation of the hydrolysis and condensation reactions of a silicate alkoxide* 53
Figure 1.46 *Reaction mechanisms of aqueous hydrolysis of alkoxysilane precursors* 54
Figure 1.47 *Highlights of in-situ sol-gel condensation of organic-inorganic hybrids* 57
Figure 2.1 *Characteristics of Electrochemical Impedance Spectroscopic (EIS) technique* 71
Figure 2.2 *Flowchart depicting the experimental for Electrochemical impedance spectroscopic (EIS) Experiments* 72
Figure 2.3 *a) A typical Nyquist or Cole-Cole plot b) Commonly used Randle's circuit for electrochemical circuit fitting analysis* 72
Figure 2.4 *LiTFSA based organic-inorganic hybrids with differing concentrations of alkoxyborane (MDMB) precursor* 74
Figure 2.5 *Comparative chart of various lithium salts over a wide category of parameters* 76
Figure 2.6-a *FT-IR spectra of LiTFSA based hybrids A-C* 77
Figure 2.6-b *FT-IR spectra of $LiPF_6$ based hybrids G-I* 78
Figure 2.7 *SEM micrographs of LiTFSA based hybrids* 78
Figure 2.8 *SEM micrographs of $LiPF_6$ based hybrids* 79
Figure 2.9 *Flowchart showing the classification of all the synthesised organic-inorganic hybrids* 79
Figure 2.10 *Temperature dependence of ionic conductivity of LiTFSA hybrids A-C* 80
Figure 2.11 *Temperature dependence of ionic conductivity of LiTFSA hybrids D-F* 81
Figure 2.12 *Temperature dependence of ionic conductivity of $LiPF_6$ hybrids G-I* 82
Figure 2.13 *Temperature dependence of ionic conductivity of $LiPF_6$ hybrids J-L* 82
Figure 2.14 *VFT plots of LiTFSA based hybrids A-C* 83
Figure 2.15 *VFT plots of LiTFSA based hybrids D-F* 84
Figure2.16 *VFT plots of $LiPF_6$ based hybrids G-I* 85
Figure2.17 *VFT plots of $LiPF_6$ based hybrids J-L* 86
Figure 2.18 *Polarisation curve of the organic-inorganic hybrid in Li/electrolyte/Li sandwich cell* 87

Figure 3.1 *Charge-discharge as indicated by the intercalation of lithium in the graphite anode* *91*
Figure 3.2 *Correlation between Nyquist plot and transport of lithium ions in a battery* *93*
Figure 3.3 *Designation of electrochemical circuit model for transport of lithium ions in batteries* *94*
Figure 3.4 *Set-up of the assembled anodic-half cells* *97*
Figure 3.5 *The DEIS experimental protocol highlighting the stages of experimental data extraction* *98*
Figure 3.6 *Comparative plot depicting the ionic conductivity profiles of various organic-inorganic hybrids as a function of alkoxyborane concentration and lithium salt additive* *99*
Figure 3.7 *Flowchart depicting the conventional protocol employed for charge-discharge studies* *100*
Figure 3.8 *Charge- discharge profile of anodic half-cell fabricated with Sample A at 0.5C charging rate (voltage cut-off 0.03 V-2.1 V)* *101*
Figure 3.9 *Modified protocol employed including DEIS for charge-discharge studies of organic-inorganic hybrids* *102*
Figure 3.10 *Physical circuit used for electrochemical fitting of DEIS data* *101*
Figure 3.11 *DEIS charging profile of a freshly prepared anodic-half cell fabricated using Sample A (voltage cut off range 0.03 V-2.2 V) alongside the derived R_{ct} values* *103*
Figure 3.12 *DEIS discharging profile of a freshly prepared anodic-half cell fabricated using Sample A (voltage cut off range 0.03 V-2.2 V) alongside the derived R_{ct} values* *103*
Figure 3.13 *Charge-discharge profile of assembled anodic-half cell fabricated using Sample A(voltage cut-off 0.03 V-1.5 V)* *103*
Figure 3.14 *Charge-discharge profile of assembled anodic-half cell fabricated using Sample A(voltage cut off range 0.03 V-1.5 V, at 0.5C, 1C and 1.5C charging rates)* *105*
Figure 3.15 *Couolumbic efficiency chart for Sample A run over 70 cycles at different charging rates* *105*
Figure 3.16 *DEIS charging profile of an already pre-cycledanodic-half cell fabricated using Sample A (voltage cut off range 0.03 V-0.9 V)* *106*
Figure 3.17 *R_{ct} parameters as obtained from the DEIS charging profile of an already pre-cycled anodic-half cell fabricated using Sample A* *107*
Figure 3.18 *DEIS discharging profile of an already pre-cycled anodic-half cell fabricated using Sample A (voltage cut off range 0.03 V-0.9 V)* *107*
Figure 3.19 *R_{ct} parameters as obtained from the DEIS discharging profile of an already pre-cycled anodic-half cell fabricated using Sample A* *108*
Figure 3.20 *Charge discharge profile of anodic half-cell fabricated with Sample B*

at 0.5C charging rate voltage cut-off 0.03 V-2.1 V 109
Figure 3.21 *DEIS charging profile of an already pre-cycled anodic-half cell fabricated using Sample B (voltage cut off range 0.03 V-2.2 V) alongside the derived R_{ct} values* 109
Figure 3.22 *DEIS discharging profile of an already pre-cycled anodic-half cell fabricated using Sample B (voltage cut off range 0.03 V-2.2 V) alongside the derived R_{ct} values* 110
Figure 3.23 *Charge-discharge profiles anodic half-cell fabricated with Sample B at 0.5C charging rate (voltage cut-off 0.03V-1.5V)* 110
Figure 3.24 *Couolumbic efficiency chart for Sample B run for 50 cycles at 1C charging rate* 111
Figure 3.25 *DEIS charging profile of an already pre-cycled anodic-half cell fabricated using Sample B (voltage cut off range 0.03 V-1.6 V)* 112
Figure 3.26 *R_{ct} parameters as obtained from the DEIS charging profile of anodic-half cell fabricated using Sample B* 112
Figure 3.27 *DEIS discharging profile of an already pre-cycled anodic-half cell fabricated using Sample B (voltage cut off range 0.03 V-1.6 V)* 113
Figure 3.28 *R_{ct} parameters as obtained from the DEIS discharging profile of anodic-half cell fabricated using Sample B* 113
Figure 4.1 *Broad classification of major flame-retardant electrolyte alternatives* 119
Figure 4.2 *Flowchart showing the classification of all the synthesised organic-inorganic hybrids* 121
Figure 4.3 *Representative TGA plots of LiTFSA based organic-inorganic hybrids A-C* 122
Figure 4.4 *Representative TGA plots of $LiPF_6$ based organic-inorganic hybrids (J-L)* 123
Figure 4.5 *DSC plots of LiTFSA based organic-inorganic hybrids A-F* 124
Figure 4.6 *DSC plots of $LiPF_6$ based organic-inorganic hybrids J-L* 125
Figure 4.7 *Flammability studies of Hybrid A* 126
Figure 4.8 *Flammability studies of Hybrid B* 126
Figure 4.9 *Flammability studies of Hybrid C* 127
Figure 4.10 *Flammability studies of Hybrid D* 127
Figure 4.11 *Flammability studies of Hybrid E* 128
Figure 4.12 *Flammability studies of Hybrid F* 129
Figure 4.13 *Flammability studies of Hybrid G* 130
Figure 4.14 *Flammability studies of Hybrid H* 130
Figure 4.15 *Flammability studies of Hybrid I* 131
Figure 4.16 *Flammability studies of Hybrid J* 131
Figure 4.17 *Flammability studies of Hybrid K* 132

Figure 4.18 *Flammability studies of Hybrid L* *132*
Figure 4.19 *Flammability studies of 1M $LiPF_6$ (1:1 EC-DEC) solution* *134*

List of Tables

Table 1.1 *Time line of evolutionary trend major breakthroughs in batteries* *3*

Table 1.2 *Multilayer system composed of four layers and five phases* *5*

Table 1.3 *Comparison of the performance characteristics of secondary batteries* *6*

Table 1.4 *Promising futuristic technologies* *9*

Table 1.5 *Chart of commonly used solvents in lithium ion batteries* *24*

Table 1.6 *Some of the soft anions with a delocalised structure* *29*

Table 2.1 *Stoichiometric quantities of the initial reaction mixture* *75*

Table 2.2 *VFT parameters of LiTFSA based hybrids A-C* *84*

Table 2.3 *VFT parameters of LiTFSA based hybrids D-F* *85*

Table 2.4 *VFT parameters of* $LiPF_6$ *based hybrids G-I* *86*

Table 2.5 *VFT parameters of* $LiPF_6$ *based hybrids J-L* *86*

Table 3.1*. Compositional matrix employed for the synthesis of organic-inorganic hybrids* *97*

Table 3.2 *Overview of obtained results from charge-discharge and DEIS results* *115*

Table 4.1 *Thermo gravimetric data of organic-inorganic hybrids* *123*

Table 4.2 *Table showing the observed weight loss associated during flame tests* *133*

Chapter 1

Introduction

Abstract

This chapter deals with an evolutionary account of batteries with a detailed and comprehensive account of lithium ion batteries. An exhaustive review about the various types of materials employed in the cathode, anode and electrolyte sections are discussed. Further, the advantages of ionic liquids as electrolytes in lithium ion batteries and a brief account of boron compounds as successful anion trapping agents is presented. Further, an overview about the utility of organic-inorganic hybrids both in terms of synthesis and design by virtue of precursor materials is introduced. In a nutshell, the foundation for the research methodology implemented in the doctoral work is laid down in this chapter.

1.1 Introduction to batteries

1.1.1 General background

The technical evolution has been hugely dependent on the productivity of fossil fuels. With limited supply and uneven distribution of these non-renewable resources, humans are at the verge of depleting these sources of energy. Besides, the side-effects like pollution looming large, overt demands in terms of consumption to production ratio, in addition with the ever increasing carbon foot prints, have led to an increased and concerted efforts by the world community towards improvised energy sources. In order to maintain a harmony between the natural capability and artificial needs, and further a sustainable future, a need to reform the present energy practices is desirable. The present day concerns have led to utilization of various renewable resources including solar, geothermal, wind etc. On a parallel methodology, material innovations and improvisations are further being carried out as well, in order to strike a balance between the present technologies with the upcoming futuristic trends. Indeed, these technological drives have led to the development of present hybrid and electric vehicles. In this respect, batteries of different genres and types have been constantly pursued for improving the evolving lifestyle of humans. Batteries have been designed to suffice the interest of the consumers, based on various factors, starting from efficiency, production feasibility, safety, and more recently environment-friendliness. Undoubtedly, our daily lives are filled up with variety of energy sources ranging from lead-acid or Ni-metal batteries in automobiles, lithium-ion batteries in variety of electronic gadgets etc. With environmental awareness taking a great role in decisive actions in the improvement of new technologies, constant scrutiny of the present or emergent technologies is inevitable. Lithium-ion batteries are the most popular and well-established category of energy resources in the present days. Applications of lithium ion batteries has been phenomenal ranging from cell phones and laptops, to even hybrid vehicles. But, a constant redesign of individual components of the battery is ongoing suiting the energy and environmental needs. Lithium-ion batteries or the emerging technologies like lithium-metal batteries or other metal batteries are not spared in this respect. The need for better and efficient constituents has

paved the way for many researches around. With the hybrid vehicles researches picking up pace, not only lithium ion batteries, but battery market as a whole is still expected to make a stride ahead.[1]

A battery consists of electrochemical cells, acting as a transducer for electrochemical to chemical conversion and also the reverse. The cells are either connected in series or in parallel depending on the output voltage requirements. Individually, a cell comprises of a cathode or positive electrode, an anode or negative electrode along with ion-conducting electrolyte. The electrolyte performs the dual role:

- Acting as a separator between the electrodes
- Ion-conducting media between the electrodes

Further, an external connection between the electrodes provides the pathway for the electron movement, thereby resulting in the completion of the electrochemical circuit. Conceptually, the batteries are relatively simple, as mentioned; unfortunately, the evolution of battery sector has not been so superfluous unlike other areas in electronics. Given, the variables required to be addressed in this sector, the R&D of the batteries, an ideal battery is indeed a Herculean task.

1.1.2 Historical perspective

A chronological sequence of the development of the battery technology can be tabulated in the following manner in Table 1.1:

Table 1.1 Time line of evolutionary trend major breakthroughs in batteries[2–4]

Year	*Contributing scientist*	*Details of the battery*
1799	Alessandro Volta	Voltaic cell-Alternate piles of (Silver or Brass or Copper) and (Zinc or Tin discs) separated by a cloth saturated with brine.
1836	John Daniell	Daniell Cell
1859	Gaston Plante	First secondary cell- Lead-acid battery. Voltage output: 2 V.
1866	John Leclanche	Leclanche cell-Zinc (negative electrode), Carbon rod (positive electrode) in Ammonium chloride. Voltage output:1.5 V.

1899	Waldemar Jungner	Ni-Cd battery ($Ni(OH)_2$– positive electrode; mixture of Cadmium and Iron powders– negative electrode) in KOH Voltage output: 1.2V. [commercialised]
1905	Thomas Edison	Similar to Ni-Cd battery except for all-iron negative electrode Voltage output: 1.2 V. [commercialised]
1932	Shlecht and Ackerman	Porous nickel electrodes- improved battery performances
1945	Samuel Ruben	Zn-HgO battery Zinc amalgam as negative electrode, HgO-carbon mixture as positive electrode in conc. KOH solution.
1970s	Researchers at Oxford University	Discovery of lithium intercalation in crystal lattice of Cobalt or Nickel oxides to give $LiCoO_2$ and LiNiO.
Late 1970s	Exxon	First production of Lithium metal based batteries with TiS_2 along with lithium metal.
1990s	Sony corporation	Commercialisation of Lithium-ion batteries.

Undoubtedly, battery technology has grown leaps and bounds over its historical precursors. With the considerable advancement in technology, the last century marked the consistent use of MnO_2 based primary batteries along with secondary batteries based on Lead/acid or Nickel or Zinc systems. With the Nickel or Zinc-metal batteries and Lead/acid batteries reaching a saturation threshold in terms of efficiency and output, parallel emerging technologies like lithium-ion batteries have caved in their foundations. Due to evolving needs, with the concept of “survival of the fittest” even applicable to industrial chemistry, lithium-ion batteries have emerged out as a popular choice in recent times. Aiming towards a highly technology-driven future, without bluntly compromising on earth’s resources is the motivation behind the current energy research scenario. Although, renewable energy sources have been aptly utilised, the need for portable energy sources for domestic needs necessitates the re-development of many of the present technologies. From 1990 onwards, lithium-ion batteries, have undergone tremendous developments notably with respect to power and safety, besides giving rise to allied technologies, which are essentially offshoots of the present extensive researches.

1.1.3 Battery

A battery, in its simplest qualification, essentially carries out two basic functions:

- Energy output over a time period,
- Energy storage.

A primary battery manages to serve energy output, while a secondary battery, does an additional job of energy storage after a process of charging. These processes are governed by the charge-discharge processes related with the internal components of the batteries. As shown in the Table 1.2, the energy conversion is a multistep and multiphase process, involving the electron /ion transfer over the electrode and electrolyte systems.

Table 1.2 Multilayer system composed of four layers and five phases

Phase (I)		*Phase (II)*		*Phase (III)*		*Phase (IV)*		*Phase (V)*
e^-	$\rightleftharpoons$	e^- ion	$\rightleftharpoons$	ion	$\rightleftharpoons$	e^- ion	$\rightleftharpoons$	$\mathbf{e^-}$
Electronic conductor		Metal electrode		Ionic conductor		Solid matrix		**Electronic conductor**
Negative terminal		Anode		Electrolyte		Cathode		**Positive terminal**

The interphase is determined by the concerned phase. Moreover, the time-dependence of these interfacial regions yet plays another significant role in dictating the shelf-life of the battery. The cell voltage is reflected by the electric double layer existent over these interfacial regions, between the electrode and electrolytic regions.[5] To surmise, the secondary battery technology is essentially the interplay of factors between the materials consisting of the electrodes and electrolytes. Hence, a great emphasis is laid on understanding the nature of chemistry played by the individual components which finally determines the performance of a battery.

Lithium-ion batteries are quite popular energy sources in recent times due to their various advantages over other conventional secondary energy sources. Way back in 2001, Tarascon and Armand, documented in *Nature* about the historical cum developmental perspective of lithium-ion

batteries followed by an in-depth analysis of the various contributions concerning the three major constituents in a battery viz., the anode, cathode and electrolytes. A comprehensive outlook was

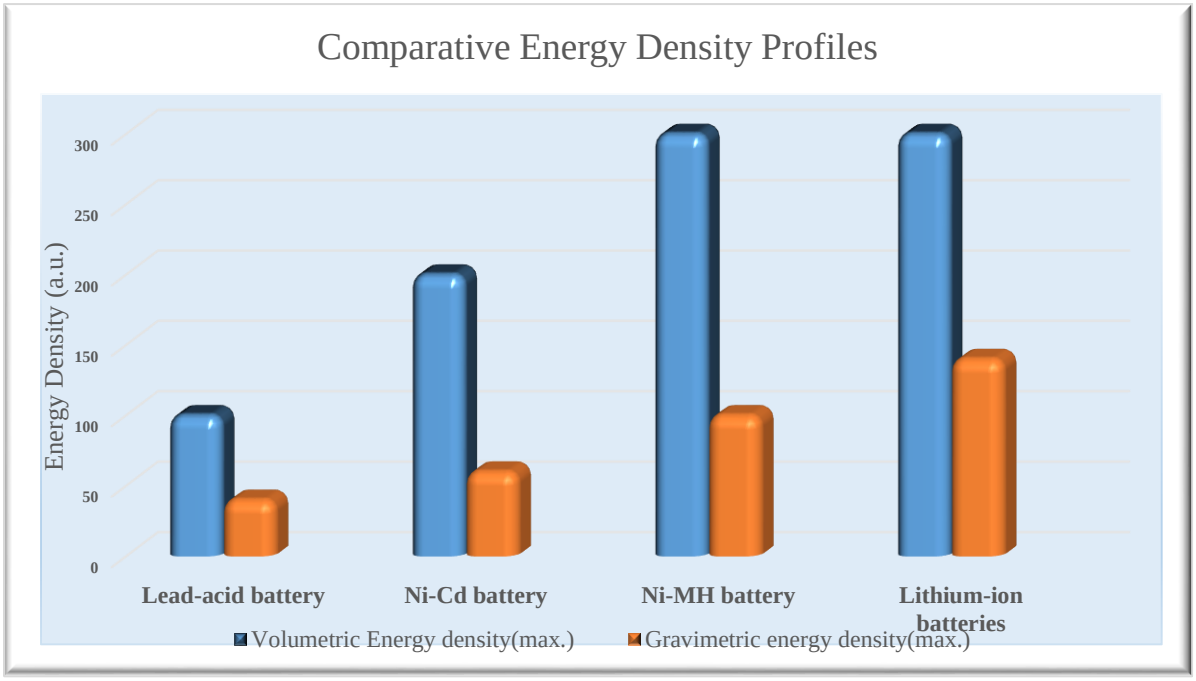

Figure 1.1 Maximum volumetric energy density and maximum gravimetric energy density profiles for various batteries (adapted from 6a)

provided by the authors about the notable developments with due acknowledgements to the grey areas. Figure 1.1, adapted from the concerned article, highlights the status quo of battery technology during that time frame.[6a]

The above figure reportedly rates lithium ion battery as the front runner in terms of energy density among other conventional energy sources. The following table (Table 1.3) also details a comparative account of the technical aspects of lithium ion batteries over other batteries.

Table 1.3 Comparison of the performance characteristics of secondary batteries (adapted from 6b)

Battery type	*Nominal voltage (V)*	*Specific energy ((Theoretical) ($Whkg^{-1}$)*	*Specific energy (Practical) ($Whkg^{-1}$)*	*Energy density (Practical) (WhL^{-1})*
Pb-acid	2.0	120	35	70
Ni-Cd	1.2	181	35	100

Ni-MH	1.2	178	75	240
Ag-Zn	1.5	283	105	180
Li-ion	4.1	100	150	400

In a recent article, in *Nature*[7], the same authors, presented another perspective about the growth of lithium ion batteries citing at length about the progressive evolutions with respect to the overhaul of architecture and design of lithium-ion batteries alongside highlighting other futuristic insights. Figure 1.2 represents a brief timeline about the battery technologies as of now and further scope beyond. The inevitable situations of ever increasing energy demands coupled with depleting fossil resources and environmental concerns, essentially necessitate the need for a constant search of technological breakthroughs. Thus, need of the hour is the motivation to the scientific community towards discovery of new technologies as energy sources.

The popularity of Lithium-ion batteries over other sources was primarily due to its superior energy density additionally being environment friendly over its conventional counterparts, like lead-acid or Ni-Cd batteries.[3] There are numerous advantages linked to this technology, which can be enumerated in the following manner[3]**:**

- High energy density (gravimetric and volumetric);
- High average operating voltage (4.1 V);
- Low self-discharge profiles;
- Stable operational window;
- Rapid recharging ability.

Although, lithium-ion battery technology has been proven to be an established arena in terms of portability, efficiency and adaptability, its glory has been marred due to factors such as reliability, longevity, safety (especially thermal safety) and also cost concerns. An intensive quest is being pursued

by the scientific community towards an improvised, re-designed architecture of the key elements of the lithium ion batteries.

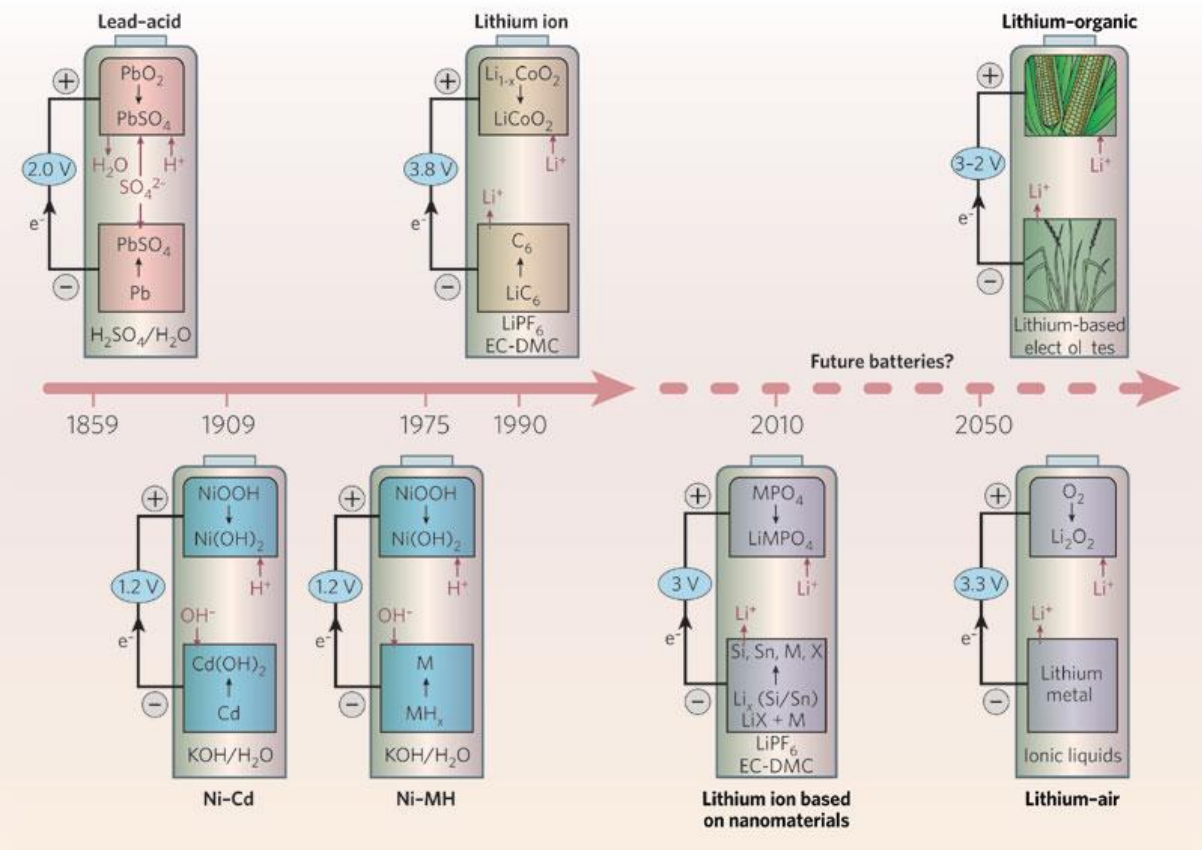

Figure 1.2 Graphic timeline of the evolutionary trend in batteries, with futuristic insights (adapted from 7)

Incessant energy demands have further resulted in the mushrooming of various divergent yet complementary technologies in addition to the lithium ion batteries. In recent years, concerted research works have led to the output of various emergent technologies with an aim towards supplementing the existing technologies. Lithium-metal batteries[8–10], Aluminium batteries[3], Magnesium batteries[11], Sodium batteries[12] etc., are a few examples in this category. With impressive energy density profiles, these smart juvenile alternatives are giving stiff competition to the already established lithium-ion batteries. Considering the early phase of such technologies, it will take a while before these technologies have a solid footprint in terms in viability, capacity, durability, safety and commercial reproducibility. In contrast, it's easier in terms of improvising or enhancing the already established technology of lithium-ion batteries. In fact, lithium-ion batteries are presently the most adapted form of portable

energy source with developmental evolution still taking place. The following Figure 1.3 showcases some of the most promising successors to the lithium-ion legacy. Magnesium systems is a step ahead of Li-ion technology, while Li-metal technology though boasting of next generation profiles are in early stages of development. In other words, theoretically, magnesium batteries, and Li-metal batteries have extremely high potential; practically it has not been successfully tapped so far.

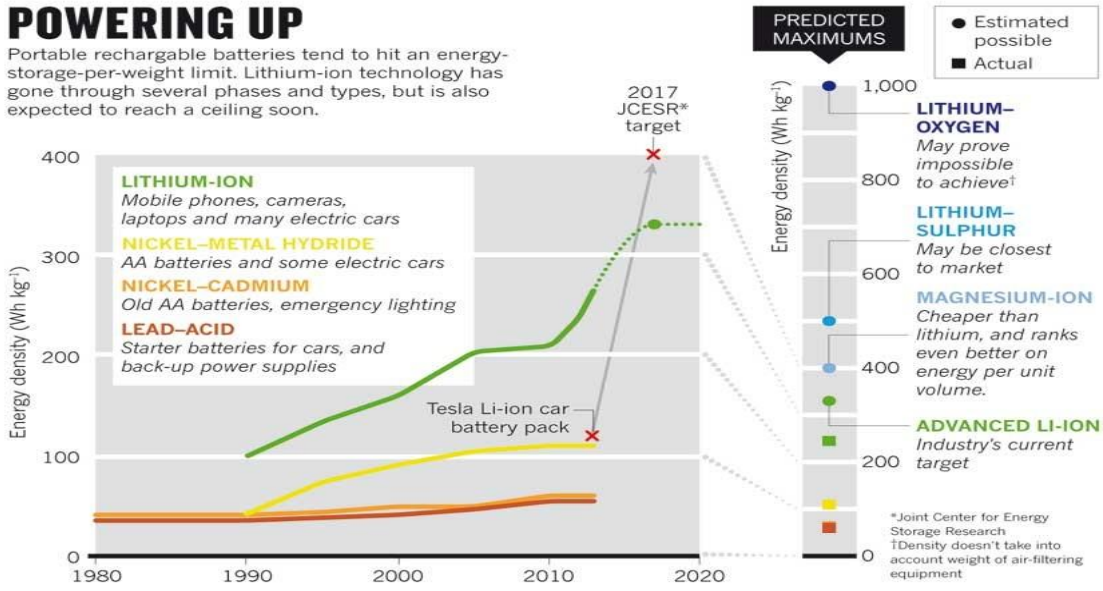

Figure 1.3 Estimated output of various emergent technologies alongside present technologies (adapted from 13a,b)

To sum-up, a few promising futuristic technologies which might probably solve the ongoing energy crisis are enlisted in Table 1.4:

Table 1.4 Promising futuristic technologies (adapted from 7)

Emergent battery technology	*Technical expertise known so far*	*Advantages or noteworthy aspects*
Magnesium-sulphur	Predicted: high energy density, unknown power density and unknown cycle life	Green, recyclable, smaller carbon footprint
Lithium-organic	High capacity, energy density limited power rate, low-cost technology	Rechargeable, excellent carbon footprint renewable electrodes easy recycling
Lithium-air	High energy density, low efficiency and rate capability	Recharge ability-issues excellent carbon footprint renewable electrodes easy recycling
Aluminium-CF	Predicted, moderate energy density, unknown power density	Green components non-recyclable

Proton battery	Predicted, all organic, low voltage, moderate energy density, unknown power density	Green components, biodegradable

1.2 Lithium-ion batteries

The concept of commercialization of lithium ion batteries was deemed feasible after the discovery of intercalation materials, which were hailed as the prospective electrode materials. Exxon employed lithium metal anodes, however, it proved dangerous due to its aggressive reaction with the electrolyte moisture. Armand *et al*., in the late 70s, discovered a solid-state polymer electrolyte formed by an aggregation between a coordinating polymer and a lithium salt. This technical breakthrough was hugely beneficial to the energy research scenario then. The coordination of lithium ions through columbic attraction with the negatively charged oxygen atoms on the PEO chains led to their facile dissociation of lithium salts and further dissolution in the PEO matrix. With the flexibility of the PEO chains, it was possible for the lithium ions to move in the electrolyte matrix in a coordinated manner.[15] The schematic representation of the mechanism of such systems can be shown in Figure 1.4 as follows: The development of gel polymer electrolytes was further strengthened while working on the issues of

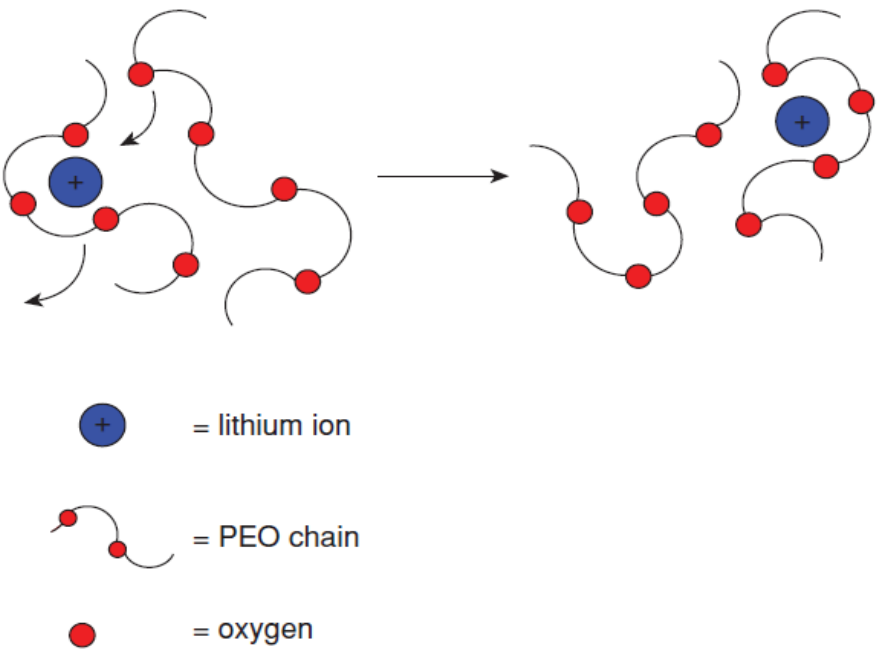

Figure 1.4 Lithium-ion transport mechanism in a polymer electrolyte formed by a complex between lithium salt and a coordinating poly (ethyleneoxide) PEO chain (adapted from 15b)

low ionic conductivity of PEO-based electrolytes. In these electrolytes, a liquid electrolyte was used to

plasticize the polymer, resulting in a highly conductive solid polymer electrolyte with conductivity at par with that of liquid electrolyte. Variants of these gel polymer electrolytes are currently used in many of the present-day electronic devices. Hence, within the limited frame of available resources, it led to an understanding that a successful lithium battery can be manufactured, if the lithium metal anode was replaced with a reliable anode. With the discovery of insertion electrodes, it was thus a winning match for the manufacturers, to realise the two combinations of electrodes:

a. An electrode capable of accepting lithium ions, i.e. an anode,
b. An electrode capable of releasing lithium ions, i.e. a cathode.

In a detailed way as dealt in Figure 1.5, the lithium-ion batteries could be charged by an application of electric potential, which forces the movement of the lithium ions from the cathode and electrolyte layer to the anode. Thereafter, the lithium ions are intercalated into the anodic material. The discharge or de-intercalation of the lithium ions from anodic matrix is reflected by the increase in the output voltage monitored by an external circuit. The resultant flow due to *x* equivalents of lithium ion migration is the reason for such voltage increment. These systems, in other words, concentration cells, in which lithium ions rock between alternate electrodes, gave birth to a new system, known as the *lithium rocking chair battery*. Thus, it can be tapped for various useful purposes as per need. The typical charge discharge setup in a lithium ion battery can be visualised in the following manner:

CATHODE	$LiMO_2$	$\underset{\text{discharging}}{\overset{\text{charging}}{\rightleftharpoons}}$	$Li_{1-x}MO_2 + xLi^+ + xe^-$
ANODE	$C + xLi^+ + xe^-$	$\underset{\text{discharging}}{\overset{\text{charging}}{\rightleftharpoons}}$	Li_xC
OVERALL	$LiMO_2 + C$	$\underset{\text{discharging}}{\overset{\text{charging}}{\rightleftharpoons}}$	$Li_{1-x}MO_2 + Li_xC$

where M = Co, Ni, Mn etc.

Figure 1.5 Chemical reactions taking at individual electrodes in a lithium-ion battery

Although, the conceptualization of rocking chair batteries was established by 80s, it was only due to pioneering efforts of Japanese manufacturer Sony Corporation which popularized the system.

The company recognised graphite as the lithium sink anode while the lithium source cathode was lithium cobalt oxide. This was a win-win combination which was hugely successful in the commercial market. Use of graphite as anode material held its roots in the defining work by Peled[16] about the ensuing passivating layer i.e., Solid Electrolyte Interphase (SEI) layer between the electrode and

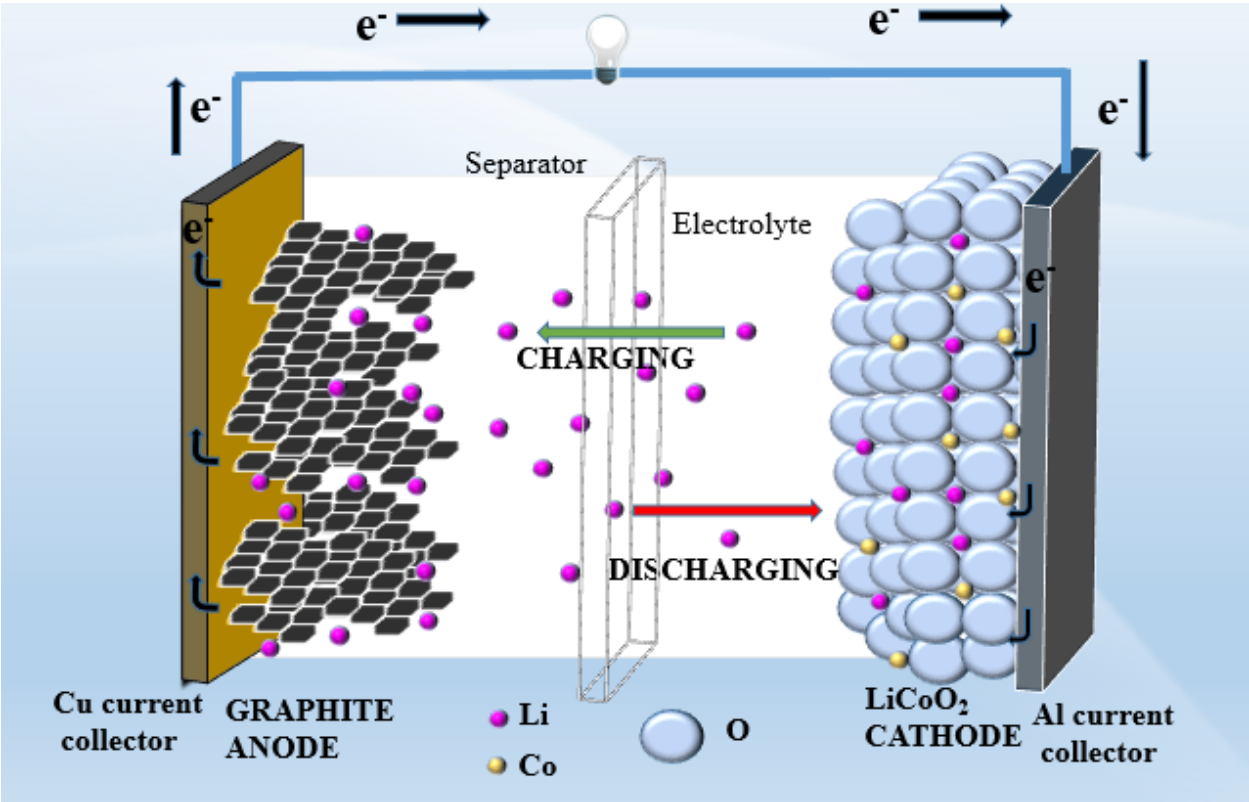

Figure 1.6 Typical set-up of a lithium-ion battery, with the constituent graphite anode, lithium cobalt oxide cathode separated by a separator and electrolyte

electrolyte. Figure 1.6 shows the conventional set-up in a lithium battery or colloquially, the lithium rocking chair battery.

The ongoing portions of this chapter will further discuss about lithium ion batteries, their component materials before talking at length about the electrolytic materials used so far in lithium ion batteries. Although, this literature review is focussed on over-all aspects of lithium-ion batteries, the focus is mainly on the electrolyte materials and motivation behind such design of novel electrolyte materials.

1.2.1 Anode or Negative electrode

An electrode with very low potential vs. Li/Li^+ and high degree of efficiency with regard to lithiation delithiation is highly desirable. Technically, lithium is the perfect match for this combination. However, learning from the drawbacks encountered in the first lithium based batteries produced by Exxon, which had resulted in accidents due to short circuits caused by lithium dendrites, it was thought upon to have materials with intercalation lattices, considering safety issues. Of the various materials used so far, carbonaceous materials have been very popular after the commercial success of Sony Corporation which used carbonaceous material in its batteries as anode. Although, the problem linked with dendritic growth was addressed by this material, the compromise on capacity could not be avoided. Reportedly, carbonaceous materials show only a tenth of the theoretical capacity by lithium anode. The anodic materials used so far in the development of lithium-ion batteries can be enlisted in a broad classification in Figure 1.7:

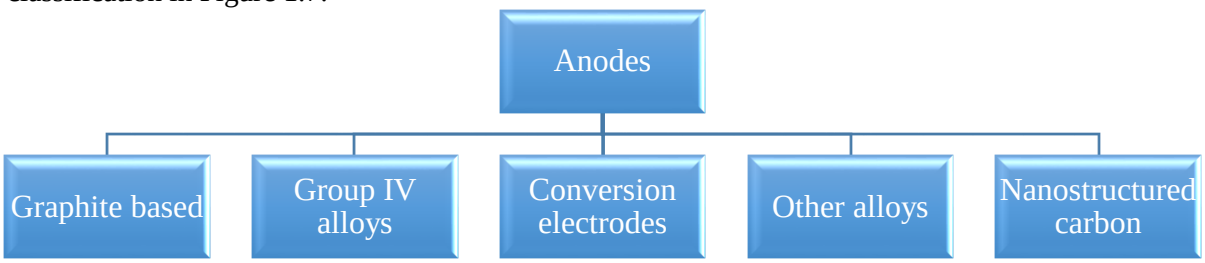

Figure 1.7 Broad classification of anode materials used in lithium-ion batteries (adapted from 17)

1.2.1.1 *Graphite based materials*:

The application oriented use of graphite as an anode material was first reported by Armand and Touzain.[18] Thereafter, numerous researchers have carried out exhaustive studies in understanding the

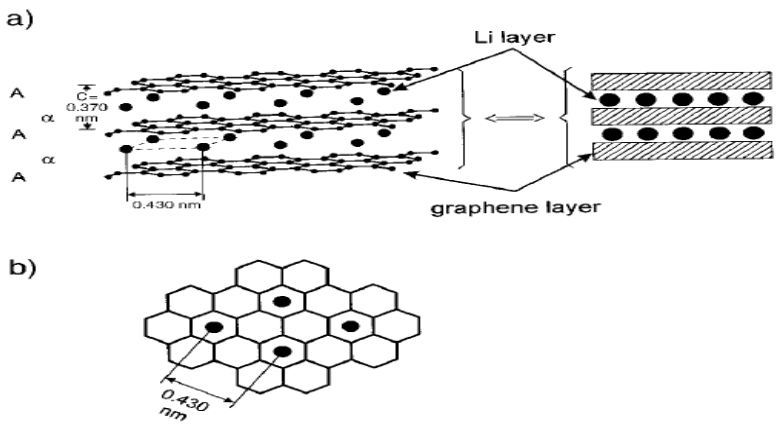

Figure 1.8 Lithium intercalation into Graphite (adapted from 20)

mechanism of lithiation and de-lithiation in the graphitic matrices. Intercalation of lithium ions as guest species in the host matrix of graphite is largely reversible and topotactic.[19] The process proceeds in a sequential manner with lithium intercalation leading to the nominal composition Li_xC_6 where $0<x<1$. At the highest intercalation point, the designation becomes LiC_6 (represented in Figure 1.8).[20] Extensive studies have been carried out by Peled[16] and Aurbach[21] concerning the SEI layer formation which is in fact a passivating film, which protects the anode simultaneously acting as a channel for lithium ions.

1.2.1.2 *Group-IV alloys based anodes*:

A variety of lithium-metal alloys are employed as anode materials in lithium-ion batteries (Si, Ge, Sn)[22] Si: In case of Si alloys, the practical limit is as high as 3579 $mAhg^{-1}$ in pure form, during a fully lithiated state of $Li_{15}Si_4$.[23,24] However, its performance is mainly marred due to large volume

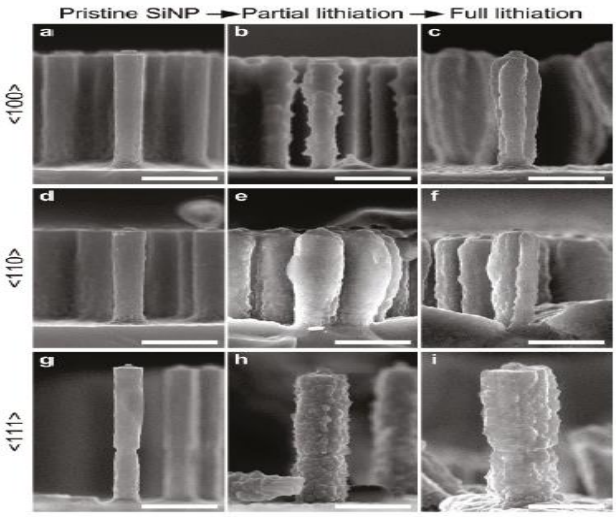

Figure 1.9 Anomalous expansion of silicon anode in 110 plane in lithium-ion cells (adapted from 28)

expansion-contraction process, during charge-discharge especially at higher charging rates as shown in Figure 1.9. This often leads to mechanical disintegration and subsequently electrode failure.[17,23,25–29] The remedy has been discovered by changing to nanostructure instead of bulk material consideration. The use of nanostructure relieves the stress at the surfaces and provides necessary void space for expansion.[30]

Ge: Although Ge is super expensive compared with Si, it is still considered due to superior conductivity and diffusivity of lithium ions. Intercalation of lithium leads to an intermediate crystalline

state finally forming a $Li_{15}Ge_4$ state. However, upon delithiation, an amorphous, porous phase is observed.[31,32] Although, the optimization of thickness of Ge sheets have not been achieved, it is evident from the studies so far, it has excellent capacity retention profiles whilst withstanding high currents without any cracking on its surface. Recent reports by Haro *et al.*, suggest that germanium coating on Si nanotubes enhances the rate capabilities, evaluated by electrochemical impedance studies.[33]

Sn: Theoretical limit of Sn based anodes is restricted to 990 $mAhg^{-1}$. However, its volumetric capacity is comparable with that of Si. In fully lithiated state, it reaches Li_2Sn_5 state as shown in Figure 1.10, possibly brittleness of this state doesn't permit to reach the theoretical capacity. Sn nanoparticles,[34] Sn-O_2 composites and even Sn-Co-C alloys based anodes[35,36] are other popular forms of Sn alloys used commercially.

Pb: Toxicity of lead compounds have limited their utilities in research. High volumetric capacity and abundance are factors, which give a scope of research of these compounds. However, so far the theoretical capacity of Pb based anodes have not been achieved.[16]

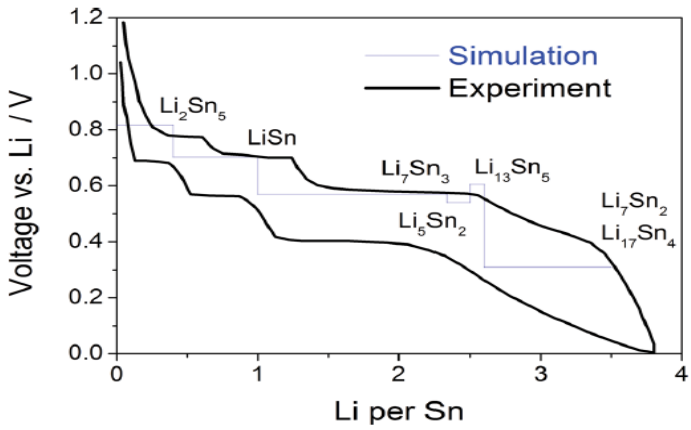

Figure 1.10 Formation of crystalline phases upon electrochemical lithium insertion and de-insertion from a Sn anode (adapted from 17)

1.2.1.3 *Conversion electrodes*:

Conversion electrodes, often synthesised by simple conversion reactions as shown below, might possibly show higher specific capacities over graphitic carbon, given by the equation:

$$Li + M_nX_b \leftrightarrow aM + bLi_nX$$

where M= transition metal, X = O in case of anodes. However, great difficulty is observed in terms of encountered large over potential (0.1-1 V) to proceed the reaction. To overcome this issue, large voltage

ranges vs. Li is employed while using conversion electrodes. The trend of over potentials in case of cobalt metal is as follows: fluoride > oxide > sulphide > nitride > phosphide > hydride. Due to these high over potentials (Figure 1.11), there is an evident irreversible capacity loss observed in these systems. Although, numerous attempts have been made to solve this issue, they pose serious concerns compromising safety and durability of these cells. They also face issues due to high surface area and thus, unstable SEI layer.

Alloying elements: Various other metal alloys have been studied as alloying elements for the

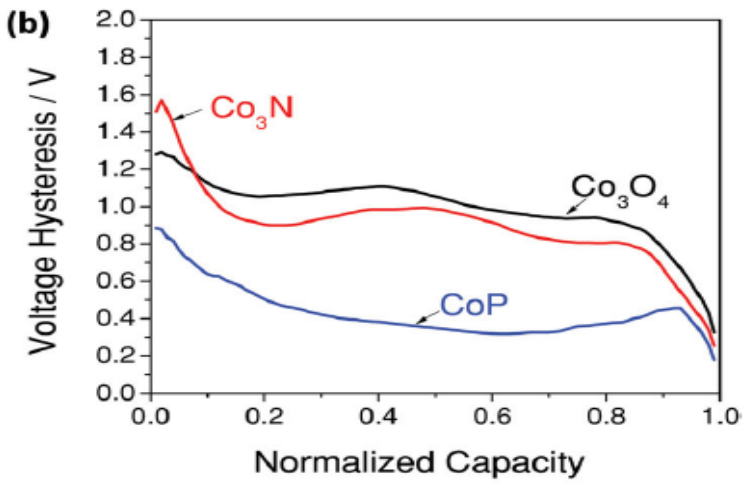

Figure 1.11 Hysteresis profiles of various cobalt based materials (adapted from 17)

employment as anodes in lithium-ion batteries.

Mg: Very few reports exist, on the use of Mg as anodic materials. Due to issues such as dissolution of Li in Mg, sluggish kinetics parameters, and a certainly resistive SEI, this type of anode material has seldom practical implications.

Al: Although factors such as abundance, economical, and high capacity and low potential vs. Li, diffusion coefficient of Al is higher than Li are the attractive attributes of Aluminium based materials.

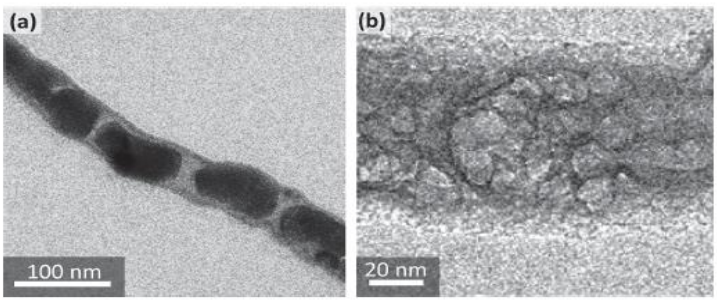

Figure 1.12 TEM images of pulverization of aluminium anode in lithium-ion cells at different magnifications (adapted from 17)

However, pulverization of Al (even in nanostructure) is a serious concern of Al based anodes (Figure 1.12). Hence, reversible cyclability of Al based anodes have not been reported so far.

Ga: Although, expensive like Ge, it is being hailed as a promising anode material due to its low range mp at ~30 ^{o}C. It exhibits electrochemically tunable self-healing properties. Although, reports on reversible lithiation/delithiation have been reported, high capacity stable cyclability has not been reported so far.[16]

Zn: The intercalation/de-intercalation of lithium ions does lead to a LiZn crystalline phase. However, issues such as low rate capability and stable cyclability are yet to be addressed.[16]

1.2.1.4 *Nanostructured carbon*

Although nanostructured carbon materials as anodes reportedly show high capacity, they are also afflicted by high irreversible capacity, possibly due to high surface area, nanopore accumulation and functional groups on the surface. Limited volumetric capacities are observed in these materials. It's observed that reversible delithiation capacity of pure nanostructure materials does not exceed that of graphite. While differently coated nanostructured materials, show notable capacities.

1.2.2 Cathodes

A few characteristic features required in good cathode materials are as follows:

- Should possess a low lithium chemical potential against an anode which should have high lithium chemical potential. This in turn affects the cell voltage capacity.
- Maximum and easily accessible sites for insertion or extraction of lithium ions in the electrode matrix.
- Should allow reversible lithiation and delithiation processes with or without minimal change in its crystal structure, thereby increasing the longevity.
- Should strike a right balance between electronic and lithium ion conductivity, in order to reduce the polarization losses during cycling. This is directly dependent on the crystal geometry, energy density profiles and sites of intercalation.

- Redox energy of the cathode should be well within a range of the electrolyte, which in turn should be in close range with that of anode.
- Economical, thermal and chemical stability and most importantly, environment friendliness are other concerns of a good cathode.

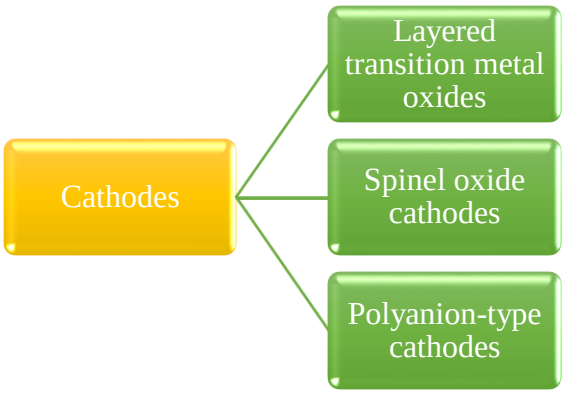

Figure 1.13 Broad classification of cathode materials used in lithium-ion batteries (adapted from 17)

1.2.2.1 *Layered metal oxides*

Oxides with the general formula $LiMO_2$ (M = V, Cr, Co, and Ni) crystallize in a layered structure in which the Li^+ and M^{3+} ions occupy interstitial sites in an octahedral fashion, facilitating easy movement of the lithium ions in and out of the matrix.[38]

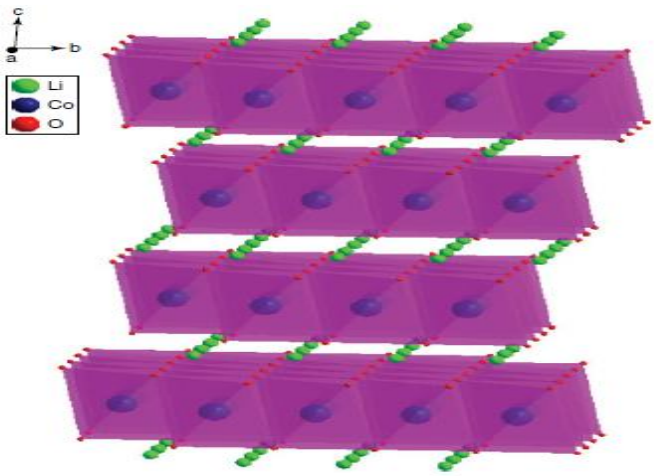

Figure 1.14 Crystal structure of $LiCoO_2$ (adapted from 38)

$LiCoO_2$, first reported by Goodenough and co-workers in 1979[37], is one of the most popular cathode material offering a high theoretical capacity (274 $mAhg^{-1}$ assuming complete Li extraction) and an intercalating and deintercalating voltage around 3.9 V. Although, it's practical capacity has been

restricted to half its theoretical capacity due to structural degradation when in contact with organic solvents, it's still the best commercial combination so far along with graphite material.[38] Various improvements such as metal oxide coatings on cathode have been extensively studied[39–44], still toxicity and cost issues have propelled further research for newer materials.

$LiNiO_2$ shares an iso-structural attribute with that of $LiCoO_2$. It almost resembles in properties such as intercalation process voltage close to 3.8 V. However, due to similar radii of lithium and nickel cations, its synthesis is cumbersome and intercalation behaviours are often found to be unsuccessful in long periods of cycling.[45]

$LiMnO_2$ shares a similar theoretical capacity profile with $LiCoO_2$, it has concerns for long term stability runs due to conversion into spinel structure during successive cycling.[46]

Further evolutionary offshoots of these layered transition metal oxides using a combination of transition metals are proposed, which provide milder thermal stability at charged state, lower cost and less toxicity than $LiCoO_2$. Some of the examples in this category include: $LiNi_{1/3}Co_{1/3}Mn_{1/3}O_2$ (NCM)[47,48], $LiNi_{0.8}Co_{0.2}O_2$[49], and $LiNi_{0.5}Mn_{0.5}O_2$.[50–52]

Another variant of these mixed transition metal oxides include the over lithiated transition metal oxides which have higher lithium in their matrices useful for efficiency of the batteries.

1.2.2.2 *Spinel oxide cathodes*

Spinel materials have a 3D framework based on λ-MnO_2. The 3D geometry provides a convenient platform for lithium ion diffusion. $LiMn_2O_4$ gained commercial interest due to its cost-effectiveness, durability and robustness. This material offers favourable safety and intrinsic rate capability, which arise from the chemically stable Mn^{3+}/Mn^{4+} couple apart from being a safe media for lithium ion diffusion.[19] These materials also face similar issues like the layered metal oxides concerning the structural changes over cycling. Remedial procedures have been quite similar to their counterparts. Although, the nanostructural approach of cathode won't completely overcome the structural change issue, it certainly does ease the stress related problems. Doping with other metals as well improves the cyclability; Kumagai *et al.*, demonstrated the easy substitution of Mn with Ni to form $LiNi_{0.5}Mn_{1.5}O_4$ through an emulsion drying method.[53]

1.2.2.3 *Polyanion based materials*

Tetrahedral polyanion structure units $(XO_4)^{n-}$ along with MO_x (M denotes transition metal) polyhedral constitute polyanion based materials.[54] The most common examples in this category are phospho-olivines and lithium metal orthosilicates. These materials have higher thermal stability than conventional layered transition metal oxides. Hence, these materials are now regarded as the most promising cathode candidates for use in next-generation Li-ion batteries. Their desirable traits include enhanced stability, safety and natural abundance. The most commonly studied materials in this category include lithium iron phosphate ($LiFePO_4$) and lithium iron/manganese silicate (Li_2MSiO_4 (M = Fe, Mn or combinations).

$LiFePO_4$

Following the reports of Goodenough *et al.*, in late 90s, $LiFePO_4$ has emerged as the most promising cathode material for lithium ion batteries. As shown in Figure 1.14a, olivine $LiFePO_4$ has a slightly distorted hexagonal closed-packed geometry (*hcp*). The phosphorus atoms occupy tetrahedral sites; iron and lithium atoms occupy octahedral 4*a* and 4*c* sites respectively. The representative Figure 1.15a shows the structure.[54–59] The TEM images of $LiFePO_4$ cathode coated Multi Walled Carbon Nano Tubes (MWCNT) is shown in the adjoining Figure 1.15b.

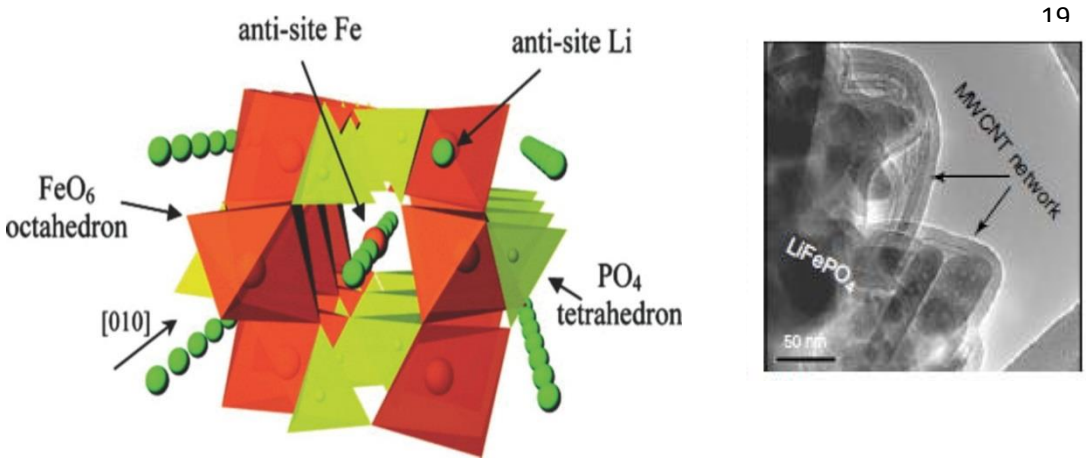

Figure 1.15 a) Crystal structure of $LiFePO_4$ b) TEM images of $LiFePO_4$ cathode coated MWCNT (adapted from 17)

$LiMSiO_2$

These are a new class of materials i.e. Li_2MSiO_4 where M =Fe, Mn or Co which boasts of handling two lithium ions per unit of material (Figure 1.16). The structure can be shown as such:

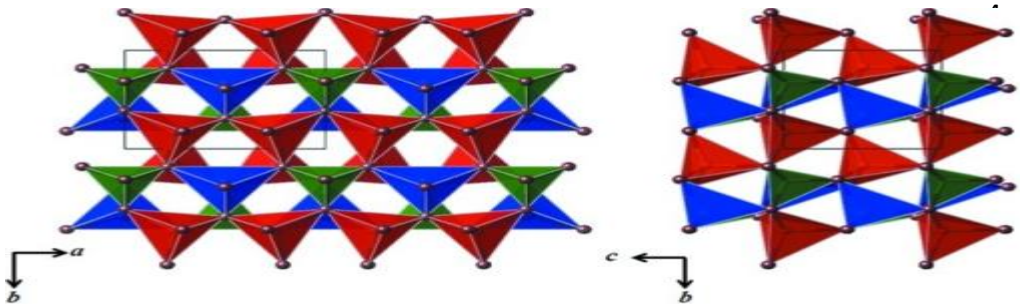

Figure 1.16 Structure of Li_2MnSiO_4 (adapted from 60)

Although, the theoretical capacity is around 333 $mAhg^{-1}$, practical capacity has not been found exceeding 160$mAhg^{-1}$. Li_2MSiO_4 crystallizes in an orthorhombic β-Li_3PO_4 structure, with all the cations occupying tetrahedral sites. The de-lithiation of lithium ions from Li_2FeSiO_4, can be expressed as

$$Li_2FeSiO_4 \leftrightarrow LiFeSiO_4 + Li^+ + e^-$$

Early research evaluated the possibility of the application of Li_2FeSiO_4 in Li-ion batteries. Nyten *et al*., first reported the application of Li_2FeSiO_4 as a new cathode material for Li-ion batteries, which can deliver a reversible capacity of 130 mAh g^{-1} at 60 °C at 0.062*C*.

However, Li_2MnSiO_4 suffers from poor cycle life, which is most likely caused by Jahn–Teller distortion and loss of crystallinity during cycling. In addition, these materials also suffer from poor electronic conductivity and consequent slow reaction kinetics. Recently, Gaberscek group demonstrated the possibility of a reversible exchange of more than one Li per unit by using the Mn/Fe solid solution with a general formula $Li_2Mn_xFe_{1-x}SiO_4$. The $Li_2Mn_{0.5}Fe_{0.5}SiO_4$ sample achieved a capacity of 214 $mAhg^{-1}$ and energy density of 593 $Whkg^{-1}$. Other dopants, such as Ni and V, could also improve the performance of Li_2FeSiO_4. For example, Ni-doped Li_2FeSiO_4 has been reported by Li to have an initial discharge capacity of 160 mAh g^{-1} at 0.062C, which was a much higher capacity than the bared one and almost close to the theoretical capacity.

1.2.3 Electrolytes

Electrolytes play a decisive role in the performance of the batteries, the simple reason being their location between the anode and cathode as the medium for lithium conduction pathway. Moreover, considering the viability of the cell over a period of time, this component is ideally sought to be unchanging over cycling whilst providing means for lithium ion conduction. From 70s onwards, after the discovery of PEO based electrolytes, there have been continuous strides of development of novel electrolyte systems, catering to the evolving needs. With a never-ending evolutionary trend of electrolytes, it's a Herculean task to provide a substantial classification for these electrolytes. Although, there's no formal way of classification of the electrolyte as a whole, a simple classification as dealt with in the Figure 1.17 [38]:

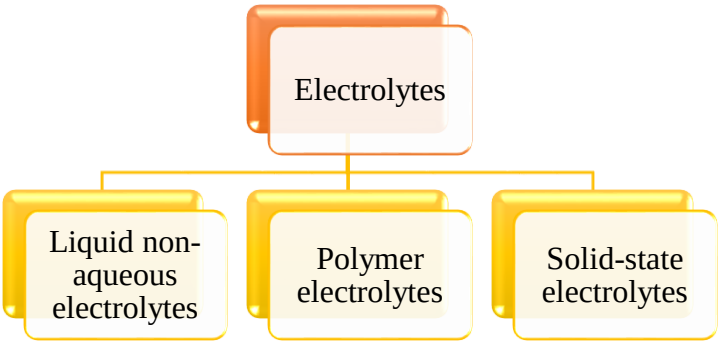

Figure 1.17 Classification of electrolytes of Lithium-ion batteries (adapted from 38)

1.2.3.1 *Liquid non aqueous electrolytes*

Typically these electrolyte solutions, contain a solvent and salt, typically a lithium salt. The solvent considerations are made based on various structural factors such as polarizability along with several thermodynamic or kinetic factors such as Donor number or Taft's parameters etc. Careful evaluation of the material parameters, have resulted in the list of some commonly used solvents which can be considered for use in lithium ion batteries are as mentioned in Table 1.5 .

Coming to the salts which constitute the other half in the liquid electrolyte systems, some of the basic features are enlisted here:

Table 1.5 List of commonly used solvents in Lithium ion batteries (adapted from 5)

Solvent	*Acronym*	*DN*	*Et(30)*	*An*	*α*	*β*	*π*
Acetonitrile	AN	14.1	46.0	18.9	0.19	0.31	0.75
Γ-butyrolactone	GBL	-	-	18.6	0.00	0.49	0.87
Dimethoxy ethane	DME	-	38.2	10.2	0.00	0.41	0.53
Dimethyl carbonate	DMC	15.1[a]	-	-	-	0.00	0.38
Dimethyl sulfoxide	DMSO	29.8	45.0	19.3	0.00	0.76	1.00
Ethylene carbonate	EC	16.4	-	-	-	-	-
Methyl acetate	MA	16.5	40.0	-	0.00	0.42	0.60
Methyl formate	MF	-	-	-	0.00	0.37	0.62
2-methyltetrahydrofuran	MTHF, 2-Me-THF	-	36.5	-	-	-	-
Propylene carbonate	PC	15.1	46.6	18.3	0.00	0.40	(0.83)
Sulfolane	SL	14.8	44.0	19.2	0.00	-	0.98
Tetrahydrofuran	THF	20.0	37.4	8.0	0.00	0.55	0.58

- High ionic conductivity in the electrolyte solutions
- Optimum solubility in various solvents of choice
- Electrochemical stability
- Thermal stability
- Stability factor in the presence of anode and cathode
- Economic considerations
- Low toxicity.

A variety of lithium salts are used for instance $LiPF_6$, $LiBF_4$, $LiN(CF_3SO_2)_3$, $LiClO_4$, $LiAsF_6$, $LiCF_3SO_3$, etc. However, $LiPF_6$ seems to be the most commonly used salt mainly due to following attributes:

- High conductivity on dissolution in alkyl carbonates, as high as 10 $mScm^{-1}$ at RT.
- High oxidative stability close to 5 V, ease in terms of formation of passivation layer. Besides, it's soluble in most of the commonly employed solvent systems.

However, the grey areas are the thermal instability and hygroscopic nature. Even in the presence of trace amounts of moisture, the salt decomposes to give LiF and PF_5 which further undergoes hydrolysis resulting in corrosive gases.

The following figure gives information about various lithium salts and their features.

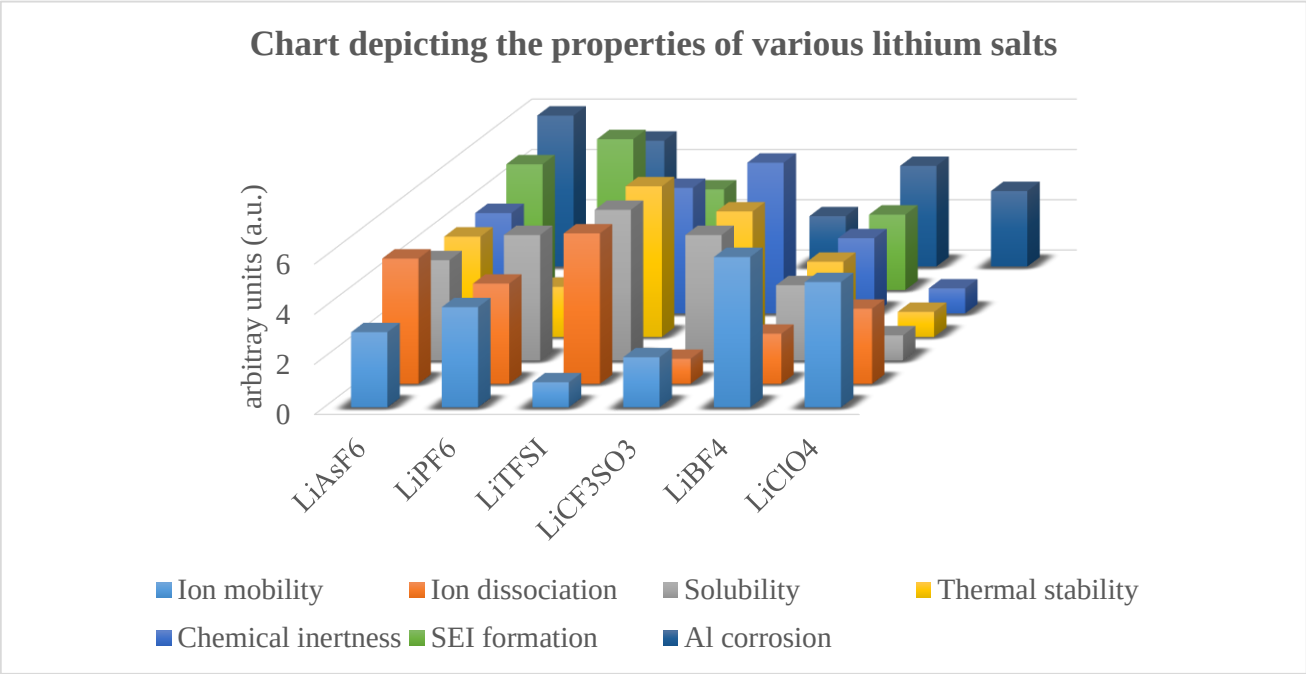

Figure 1.18 Comparative chart of various lithium salts over a wide category of parameters (adapted from 15)

As indicated by the Figure 1.18, LiTFSI features good ratings in average, however it is extremely expensive. So $LiPF_6$ is widely used in the commercial market as a decent compromise amongst all the factors. There exist various other salts in this category which have been explored so far in the research field. Lithium bis(oxalato)borate (LiBOB) type salt and its derivatives are also well researched in recent times due to their advantageous SEI features. Some of the popular derivatives in this category are shown in Figure 1.19

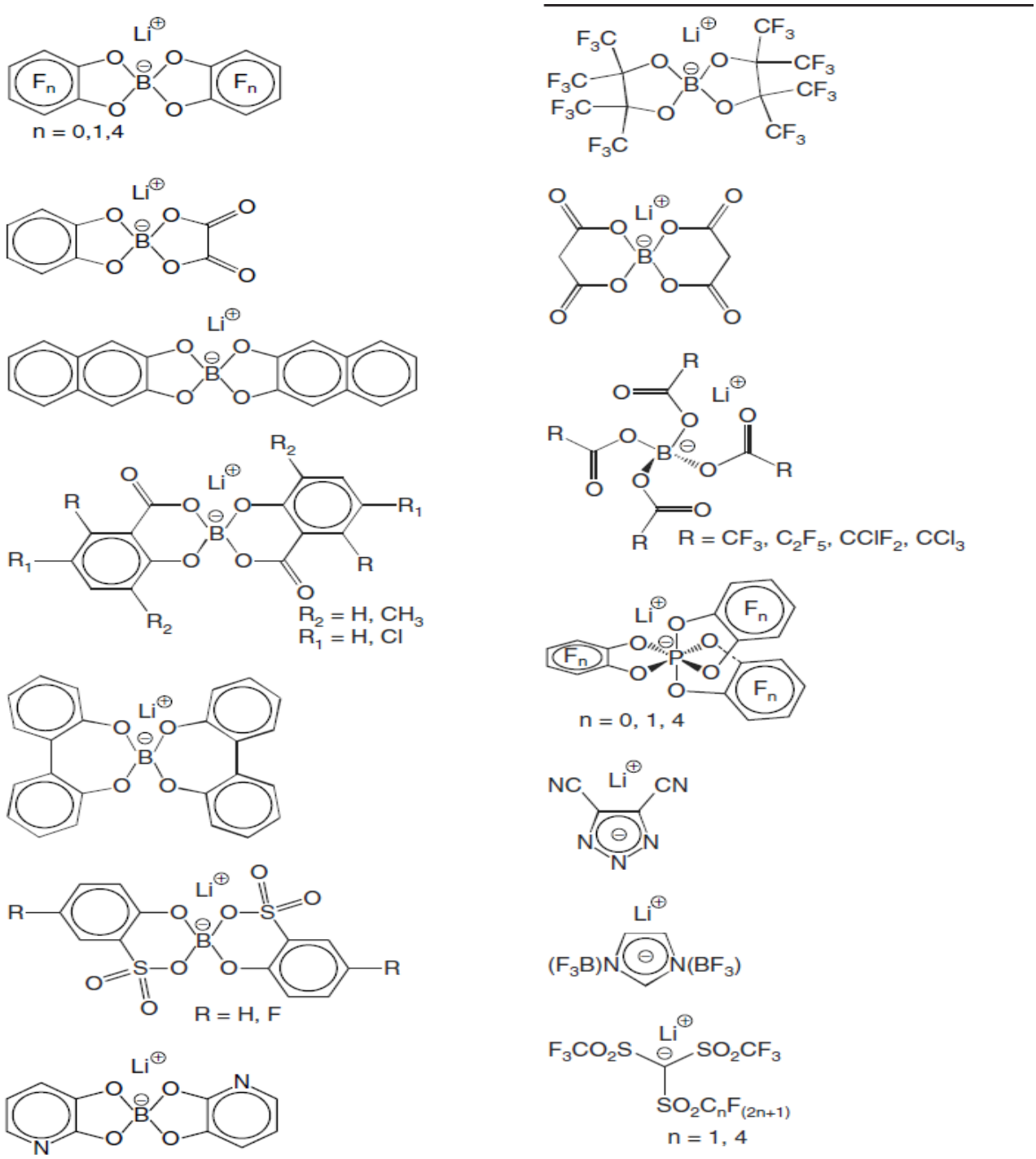

Figure 1.19 Some other lithium salts which have been considered in the lithium ion battery research (adapted from 5)

Ionic liquids as electrolytes

Ionic liquids, also known as molten salts, are liquids (Figure 1.20) composed of ions discretely. Due to the presence of a large cation and a charge-delocalized anion, resultant weak interactions characterize these ionic liquids. Flexibility of the anion and dissymmetry of the cation often leads to a lower tendency towards crystallization. The various possible combinations of ionic liquids include, among others, imidazolium, pyrrolidinium and quaternary ammonium salts as cations and bis(trifluoromethanesulphonyl)imide, bis(fluorosulphonyl)imide and tetrafluoroborate as anions. This fluid combination often registers high ionic conductivity in the order of $mScm^{-1}$ and thermal stability over 300–400 °C. Ionic liquids have various advantages shown in Figure 1.21. An elaborate discussion is dealt in the later part of this chapter.

Figure 1.20 Visuals of pure Ionic liquids

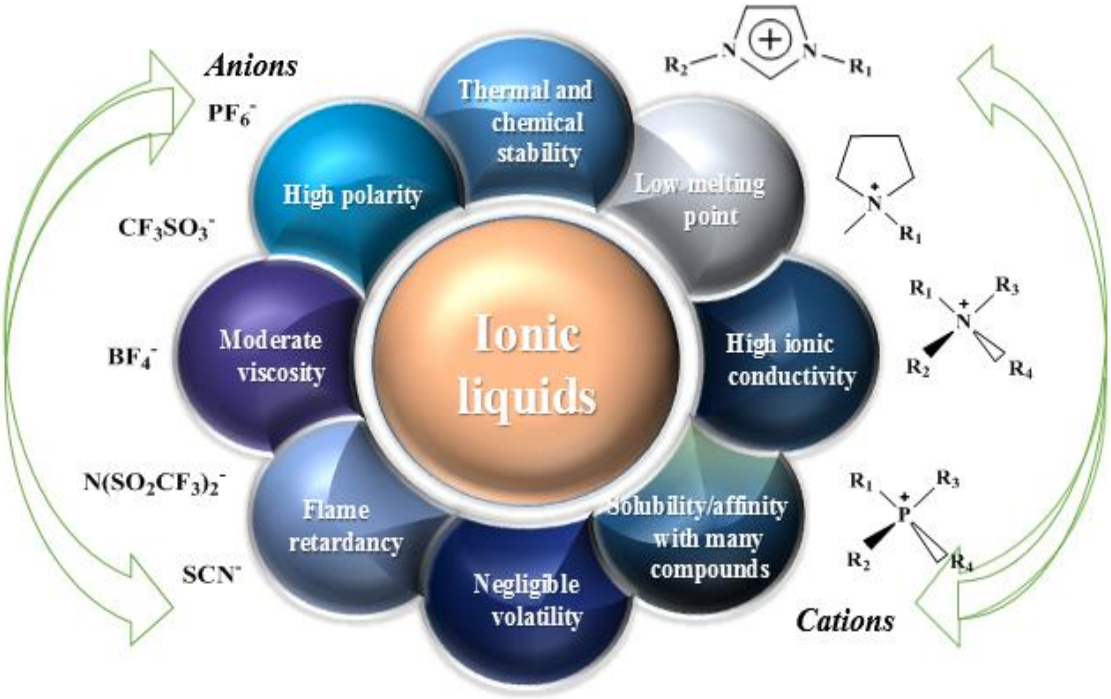

Figure 1.21 Advantages of Ionic liquids along with few common examples of ionic liquids

1.2.3.2 *Polymer electrolytes*

The term '*polymer electrolyte*' encompasses an extensively broad family of various ion-conductive materials. The typical classification in this category can be outlined (restricted to lithium ion batteries) as shown in Figure 1.22:

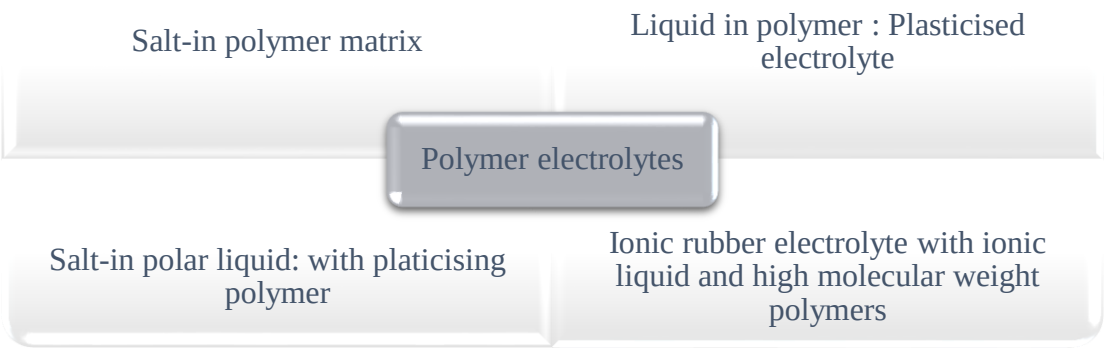

Figure 1.22 Classification of polymer electrolytes

On a structural level, these electrolytes have some features in common with gel electrolytes. They were first reported in the literature in 1993 and are still in the early stages of development. A thorough discussion about the classification abovementioned is beyond the scope of this thesis work. However, considering the interest, the authors will focus mainly on the polymer based solvent-free systems generally used for lithium ion secondary batteries. The review of literature suggests that polymer electrolytes are often used in conjunction with ceramic electrolytes under solid-state electrolytes. However, for the ease of classification, the author has chosen to classify polymer electrolytes separately from that of ceramic electrolytes. Ease of preparation, unique physico-electrochemical properties makes these materials a preferred choice in a wide range of studies.

Solvent-free polymer electrolytes

Polymer electrolytes include many compounds such as polyethers, polyimines, polyesters and even polythioethers. The solvation enthalpy of a metal salt-in polymer matrix is governed by several factors:

- Interactive parameters between the cation and the coordinating atoms in the polymer,
- Lattice energy parameters of the concerned salt,
- Interactions, predominantly electrostatic in the matrix of the dissolved ions.

The solvation sphere around the cation plays a major role in these systems. This in principle is determined by the Hard Soft Acid Base (HSAB) concept as proposed by Pearson, where a hard acid-hard base react well on the basis of mainly ionic interactions, while soft acid-soft base bank on covalent interactions. For instance, in case of low-molecular weight solvents, the number of surrounding molecules around the cation affect its dissociation from the ion-pair. However, the characteristics of a repeating unit in a higher polymeric systems have a significant role. Polyethylene oxide type high molecular weight chains (PEO) or Polypropylene oxide (PPO) chains are often considered choices as polymer matrices. For instance, in case of polyethers, the order of interactive parameters with the cations are observed in the following manner:

$$-(CH_2O)^{n-} << -(CH_2CH_2O)^{n-} >> -(CH_2CH_2CH_2O)^{n-}$$

in the presence of hard cations such as Li^+, Na^+, Mg^{2+}, Ca^{2+}. Similarly, O is often the best candidate over other Lewis bases in the Periodic table.

The ion association and dissociation constants of a salt in a polymeric matrix plays a major role, since ion-association is often an undesirable trait. Ion-pair formation or aggregation in higher concentrations of salt or even steric factors of the polymeric structure often plays a negative role towards ionic conductivity. Anion stability also has a significant contribution in conductivity. For example, large anions with the negative charge delocalized is often a good choice for the polymeric systems, mainly due to their lower solvation energy requirements over the conventional halides.

Some typical example in this category include: ClO_4^-, $CF_3SO_3^-$, $(CF_3SO_2)_2N^-$, BF_4^-, BPh_4^-, AsF_6^-, SCN^- etc.

Table 1.6 Some of the soft anions with a delocalised structure

Name	*Abbreviation*	*Structure*
Bis(trifluoromethanesulfonyl)imido	TFSI	$[(CF_3SO_2)_2N]^-$
(Methoxypropyltrifluoromethanesulfonyl)amino	MPSA	$[(CF_3SO_2)N(CH_2)_3OCH_3]^-$
Bis(trifluoromethanesulfonyl)-methyl	TFSM	$[(CF_3SO_2)_2CH]^-$

So, in conclusion, a polymeric matrix with low crystallinity and with a constituent anion with a negative charge delocalized is an ideal matrix in this category (Other examples are shown in Table 1.6).

Second generation polymer electrolytes

Considering the inherent drawback of high crystallinity of PEO based polymers, new class of polymer electrolytes were devised in the past, basically random copolymers resembling PEO with amorphous geometry. One of the earliest known examples in this category was oxyethylene-oxymethylene repeating unit with high molecular weights. Structurally,

$$-[-(OCH_2CH_2)_mOCH_2-]_{n-m} \; (\textit{ where } n = 5-10)$$

A similar example in this category is dimethylsiloxane based amorphous polymer with low T_g values and tunable ionic conductivity attributes. Block copolymers of various architectures with mechanical stability are also registered are in this category. A notable example in this category includes, poly(methoxyethoxyethoxyphosphazene), also known as *MEEP* (Figure 1.23). Appropriate cross-linking or inclusion of side chains, is helpful in enhancing the dimensional stability of the material.

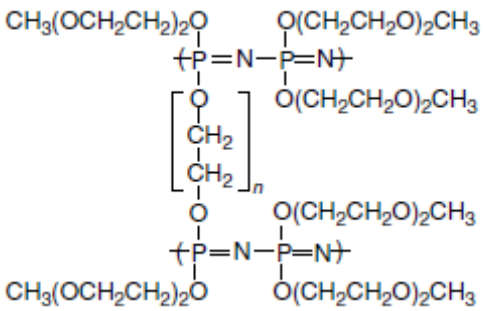

Figure 1.23 Structural formula poly(methoxyethoxyethoxyphosphazene), MEEP

However, electrochemical stability is one of the most important worrying factors in these polymers. Presence of carbonyl or siloxane function, alcohol or urethane functionalities adversely affect its stability in lithium batteries.

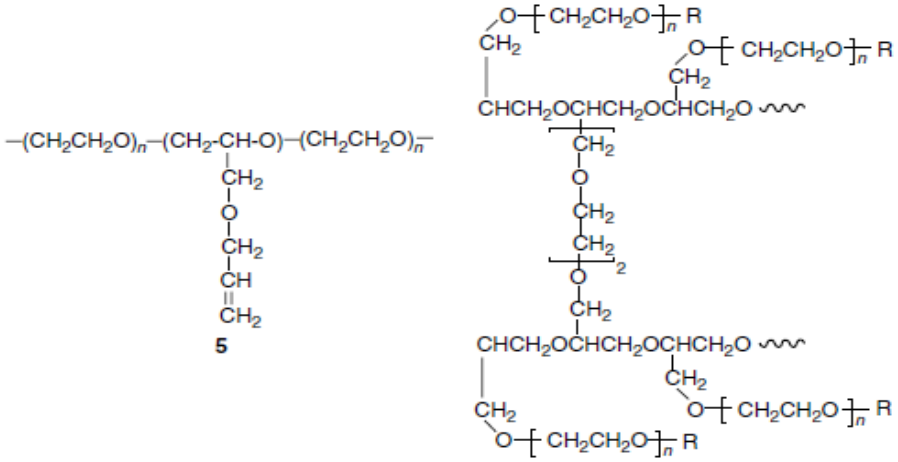

Figure 1.24 A few other polymer structures which are used in lithium ion batteries

To sum it up, all polymer electrolytes (Figure 1.24) share a resemblance in structural aspects. Inter chain as well as intra chain dynamics affect the ion coordination and movement. The mechanics of ion-conduction is usually defined by two models:

1. Arrhenius model: Classical model concerning ion motion in solid electrolytes.
2. VFT model (Vogel Fulcher Tammann model): This model takes ideal T_g value into consideration, and provides more clearer understanding about the activation energy parameters.

Hybrid electrolytes

Considering the diversity of hybrid polymer electrolytes, Di Noto *et al.*, have proposed another classification (Figure 1.25) where, they reconsider this class as Hybrid Inorganic-Organic Polymer Electrolytes and further divide it in the following manner:

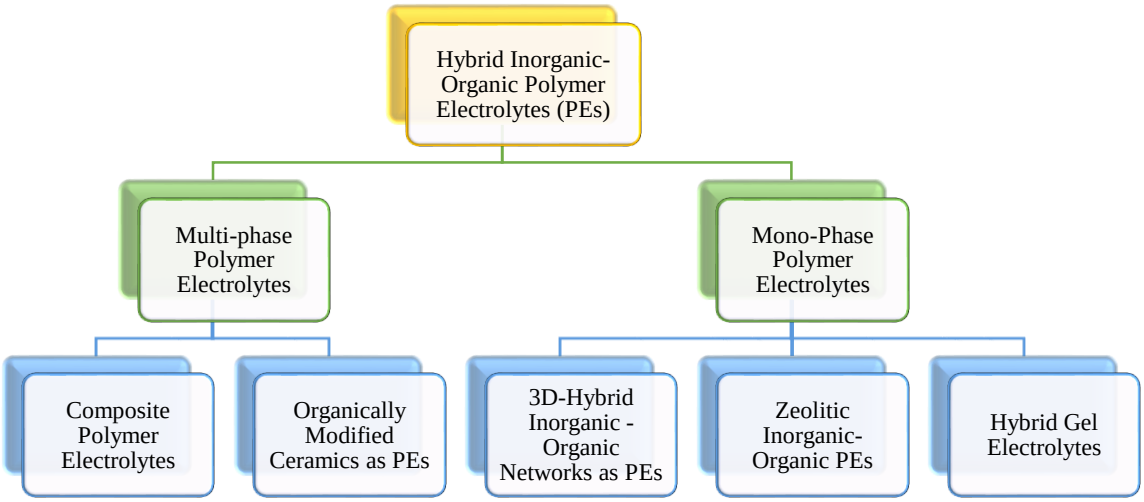

Figure 1.25 Elaboration on the classification of hybrid electrolytes (adapted from 212)

Multiphase Polymer Electrolytes

a. The first subclass in this category includes (nano) Composite Polymer Electrolytes wherein nano sized materials of various oxides are introduced into conventional polymer electrolytes with an aim of improving conductivity, chemical, mechanical and electrochemical properties.

b. The second subclass is referred to as Organically Modified Ceramics as Polymer Electrolytes (ORMOCERS-APE). This class includes sol-gel derived matrices containing synergistic organic and inorganic domains, like silicon and conventional PE blocks as starting materials.

Mono-phase Polymer Electrolytes

a. 3D-Hybrid Inorganic-Organic Networks as PE: This predominantly includes materials with 3D ion-conducting materials, with metal or non-metal atoms bridging between macromolecular chains. This class is further divided into two subclasses, differing mainly on the role of the Lewis acid in the structural framework.

The first sub class in this category includes "-ate" structures, precisely Lewis acidic moieties with single mobile cations in the matrix. The bridging Lewis acidic moieties are often affixed in the polymer structure, resulting in single ion conductors.

The second sub-class in this category are resultant of incorporation of weak Lewis acidic moieties into the polymeric matrix.

b. Zeolitic Organic-organic Polymer Electrolytes: (Z-IOPES) are formed by agglomeration of inorganic coordination complexes comprising of Sn, Pd, Fe or Co which are bridged by organic macromolecular moieties such as PEO or smaller moieties such as glycerol. Example in this category include: $[Fe_xPd_y(CN)_z]Cl_y(CH_{2n}H_{4n+2}O_{n+1}Li_1)$.

c. Hybrid Gel electrolytes: This class includes electrolyte matrices involving sol-gel processes, starting from inorganic (Si) or organometallic precursors with constituent ion-conducting cation and low molecular or macromolecular liquids.

Gel electrolytes

Boasting of notably higher ionic conductivities over their dry counterparts, gel electrolytes are another variant of electrolytes in the reckoning. Two of the common approaches as followed in practice in this category include:

- Addition of a soluble polymer towards immobilization of liquid solvent (PEO, PMMA, PAN, PVdF etc.);
- Loading of liquid electrolyte into microporous matrix. eg. porous polyethylene

Considering the entanglements in the matrix which result in the solidification of the matrix, the electrolytes show a liquid type behaviour at higher temperatures, while they show a rubber kind of behaviour at low temperatures. Accordingly, the VFT dependence of the electrolytes is markedly different at different temperatures.

PVdF based Gel polymer electrolytes: Poly(vinylidene fluoride) PVdF and its copolymer with hexaflouropropylene (PVdF-HFP) suffice all the requisites of a polymer matrix as gel electrolyte.[60,61,62] Electrochemical stability and incombustibility features are high among these polymers due to the strong electron-withdrawing substituents in the polymer chain. The polymer is often known to react with lithium anode forming LiF, thereby restricting their use in lithium batteries with graphite anode alone. Porosity of the polymeric membranes is another significant pre-requisite.[63] Often these membranes are prepared by phase inversion or electrospinning[64] methods. Microporous polymer electrolytes also have been reported with improved conductivity and porosity profiles.[65] Ceramic porous additives such as $BaTiO_3$ and TiO_2 also result in improvement of ionic conductivity.[66,67] In such microporous electrolytes, the liquid electrolyte which occupies the micro pores, thus, plays a decisive role in the ionic conductivity. Similarly, the amorphous parts which are plasticized by the liquid electrolyte provide the channels for the movement of lithium cations. Thus, porosity and increase in amorphous parts improve the conductivity profiles. Also, mixing of similar polymer structures like PEO or PMMA etc., improves the mechanical stability.

PMMA based electrolytes: PMMA based PE are often related with homogenous matrices prepared commonly by solution-casting procedures in the presence of a wide variety of initiators. The

main drawback of this polymer is low conductivity[68] even in the presence of other polymers like poly (vinyl acetate)[69] or even ionic liquids.[70] However, there are reports on improved ionic conductivity in the presence of PEG based copolymer[71] and PMMA or poly(vinylacetate) PVC based polymers.[72–74]

PAN based electrolytes: PAN based electrolytes, including lithium salts and various plasticizers, show electrochemical stability as high as 4.5V (vs Li/Li^+) and high transference numbers. Besides, its thermal resistant property is an inherent additional merit.[75] However, PAN based PEs individually or in the presence of other polymers or lithium salts do not provide high ionic conductive profiles.[75,76] Isolated reports of improve ionic conductivity in the presence of $LiClO_4$ and succinonitrile SN (an organic plastic) are known. [77,78]

Poly(vinylchloride) PEs: Poly(vinylchloride) have several advantages like commercial availability, low ignition susceptibility besides its chemical stability. Facile salt dissociation and further solvation is facilitated by the lone pair present in the chlorine atom.[68] However, similar to the PAN based systems, these systems also register low ionic conductivity values except in the case of PEMA based system. Often batteries using this electrolyte show lowering in capacity due to an anodic passivating layer of LiCl.[79]

1.2.3.3 *Solid State Electrolytes*

Solid state electrolytes are beneficial due to the ease of fabrication unlike voluminous liquid electrolytes, safe and durable over other electrolytes. The two major classes in this category are:

- Inorganic ceramics
- Organic polymers

The major factor behind this classification includes the mechanical property. On one hand, ceramics boast of merits such as high elastic moduli and adjustability at higher temperatures or aggressive environments. While, organic polymers are known to be processable and flexible *per se* making their fabrication properties easier and economically viable over ceramics.

1.2.3.3.1 Ceramic electrolytes

Defect points such as vacancies and interstitial ions in the ceramic electrolytes are the driving force for cation movement, which in fact, is an energy consuming process. As a result, often it is observed that ionic conductivity in such electrolytes increases with increase in temperature, making it suitable for high temperature applications. However, some of these electrolytes also register exceptional conductivity at room temperature(RT), finding applications in lithium ion batteries.[80–84]

Sulfides

The typical example in this category includes a Li_2S-P_2S_5 glass or glass-ceramic. The phase composition of the electrolyte determines the composition.[85] Tatsumisago *et al.*, have carried out extensive research in this area and reported the conductivity trend dependent on the crystalline or amorphous nature of the sample. It is often observed that samples with crystalline phases produce better ionic conductive profiles over corresponding glasses.[83,86–92] However, anomalies do exist. For example, in case of Li_2S-$P_2S_5Li_4SiO_4$ crystallization adversely affects ionic conductivity. Various transition metal sulfides like nickel, copper and copper-molybdenum sulfides are employed as cathode materials for sulfide electrolytes against various cathodes including the most common $LiCoO_2$ and $Li_4Ti_5O_{12}$.

Thio-LISICONs are another variant of sulfide electrolytes given by the general formula $Li_2SGeS_2P_2S_5$.[93–95] These electrolytes reportedly show an increase in ionic conductivity in an oxygen atmosphere up to an optimum concentration, on account of increased coordination sphere of lithium.

Oxides

Perovskites, of the general formula $(LaLi)TiO_3$ (LLTO), is one of the popular oxide solid state electrolyte.[96–100] The ratio of La/Li determines the ionic conductivity in the composition $Li_{3y}La_{2/3-y}TiO_3$. Reports so far indicate that the high ratio of La/Li typically >>1, results in notable ionic conductivity. However, various structural features such as grain size variations and grain boundaries also play an active role in ionic conductivity. Incorporation of other elements have mixed response in these electrolytes. While Titanium when replaced by Aluminium in small amounts improves ionic

conductivity, sodium seldom does have the same effect, while, silica fillers improve conductivity profiles.

Garnet type oxides reported so far show ionic conductivity in the order of $mScm^{-1}$. [101–104] Strontium or barium doped garnet oxides show improved conductivity profiles over niobium or antimony based oxides.[105,106]

Phosphates

Phosphates based solid state electrolytes resemble closely with sodium (Na) Super Ionic CONductor (NASICON) type of electrolytes. The general formula of these type of compounds is $LiAlM(PO_4)_3$. It has been differently doped with either tantalum or silicate simultaneously or Cr or Ge or Zr as the metal atom with applications in both lithium ion and lithium-air batteries.[107–113] Although, Fe metal centred compounds have also been reported, they are preferred as cathode materials over electrolytes.[114] Organic polymers have already been dealt in the category of polymer electrolytes.

1.3 Ionic liquids as electrolytes in Lithium ion batteries

Ionic liquids, on the strength of their diverse advantages are being extensively studied as electrolytes in various forms of battery technology. Lithium-ion technology has also witnessed the frequent experimentation of ionic liquids over the course of last 20 years. Performance of ionic liquids as electrolytes involves a critical combination of various factors such as ionic conductivity, viscosity, electrochemical stability, stability towards electrodes etc. There exists no clear demarcation regarding the classification of such electrolytes, however, a simple yet comprehensive categorisation can be brought in the following way, on the basis of various available literature:

1. Monomeric form of Ionic liquids: In this category, only monomers or mixture of monomers with various additives are considered. This includes

   a) Pure ionic liquids or Mixtures of ionic liquids

   b) Ionic liquids with organic electrolyte additives

   c) Ionic liquids with polymer electrolytes or gels

2. Polymeric ionic liquids

1.3.1 Monomers of ionic liquids

Some excellent and elaborate reviews on use of ionic liquids as electrolytes in batteries have been reported by Lewandowski *et al.* [193,213] These comprehensive reviews provide an overview of ionic liquids as electrolytes in lithium battery technology. The most common prototype of ionic liquids viz., the bifunctional imidazolium ionic liquids have been vastly researched upon as an electrolyte. However, the free proton on the unsubstituted C-2 position makes it vulnerable at higher voltages. Despite, the myriads of benefits against conventional electrolytes, this particular factor is an area of concern due to it's vulnerability at higher potentials. Although a gradual shift towards C-2 substituted imidazolium ionic liquids or aliphatic ionic liquids (pyridinium, pyrrolidinium, phosphonium or quarternary

ammonium type of ionic liquids etc.) is gradually taking place, the archetypal ionic liquids still are being considered in the research works linked to batteries.

Tatsumi *et al.*, have reported in depth about the viability of ionic liquids as electrolytes exploring various cations and counter ions along with organic electrolyte additives such as ethylene carbonate(EC), Diethyl carbonate(DEC) etc., in the electrolyte segment. The group maintains that ratio of ionic liquid: organic additives principally affects the flammability of the electrolytes, with advantages of being flame-retardant electrolyte even in the presence of organic additives.[214] Some of the ionic liquids studied by the group are shown in the following Figure 1.26.

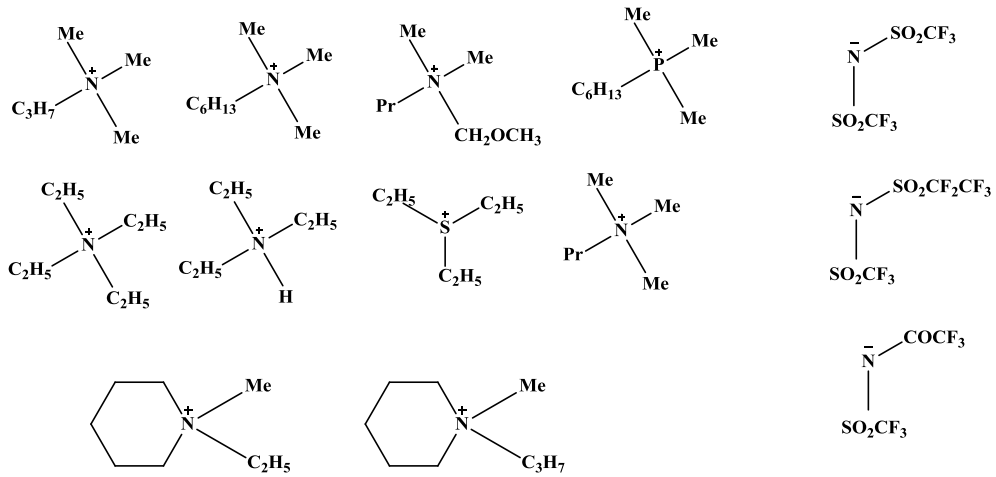

Figure 1.26 Aliphatic ionic liquids employed for studies in LiBs (adapted from 216)

The group further affirms the utilisation of ionic liquids quaternary cations, in the presence of lithium salts as front runners in the electrolyte section for lithium batteries. Incorporation of bis(trifluoromethylsulfonyl)imide anion often results in enhancing the fluidity of the system, resulting in lower viscosities, a desirable attribute for battery applications. Phosphonium ionic liquids containing a methoxy group, triethyl(methoxymethyl)phosphonium bis(trifluoromethylsulfonyl)imide and triethyl(2-methoxyethyl)phosphonium bis(trifluoromethylsulfonyl)imide, were found to very extremely low viscous even at RT, with excellent thermal stability upto 400 ^{o}C. [215] However, reports about cointercalation of TFSI along with cations during the cycling of batteries, often mars the useful attributes of ionic liquids as electrolytes, especially in graphite based cells. [216] Hence, there seems to be a search for a highly efficient counter ion suitable for battery applications. Some of the recent amide and borate types of anions employed in LiBs are shown in Figure 1.27.

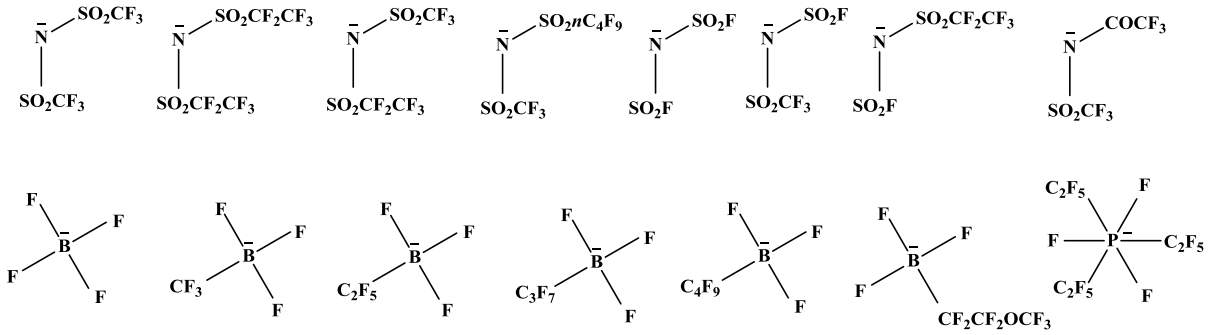

Figure 1.27 Some of the popular anions and newly designed anions studied employed in LiBs (adapted from 15)

Ishikawa *et al.*, have reported largely about the use of various FSI based ionic liquids, in the presence of lithium salts as electrolytes for lithium batteries, with their focus on the enhanced cyclability by virtue of FSI anion in the electrolyte. The group claims that presence of FSI anion leaves out the need for any solvents or additives.[217] Similar compositions were explored as electrolytes for Electric Double Layer capacitors as well. [218] Further, the group also reports the usefulness of FSI counter ion as a competitive facilitator for enhanced lithium ion mobility towards the electrodes. [219] The group also investigated the practicality of FSI based ionic liquids at various temperature ranges. The study suggests the use of LiBOB to be instrumental in stabilisation of SEI layer especially in low temperature studies. Further claims about the superiority of FSI anion as the only perflouroanion suitable for use in battery applications are also reported. [220]

Similarly, Matsumoto *et al.*, have reported extensively about the use of ionic liquids as electrolytes for lithium-ion batteries. The group has extensively surveyed on the functionality of ammonium and phosphonium type ionic liquids with reports suggestive about the higher compatibility of aliphatic counter cations over aromatic imidazolium systems.[221] A similar view about the versatility of the FSI anion along with the previously reported superiority of aliphatic ionic liquids was also reported. *N*-methyl-*N*-propylpyrrolidinium (Py_{13}^{+}) and *N*-methyl-*N*-propylpiperidinium (PP_{13}^{+}) salts of [FSI] showed better results compared with the imidazolium counterpart with the same FSI anion. [222] Similarly, Mcfarlane *et al*., profess that aliphatic ionic liquids (phosphonium type of ionic liquids) are better capacity retention responses over imidazolium systems.[223]

Passerini *et al.*, have extensively studied pyrrolidinium type of ionic liquids in lithium batteries.[224] Some of the ionic liquids employed by the group are illustrated in Figure 1.28.

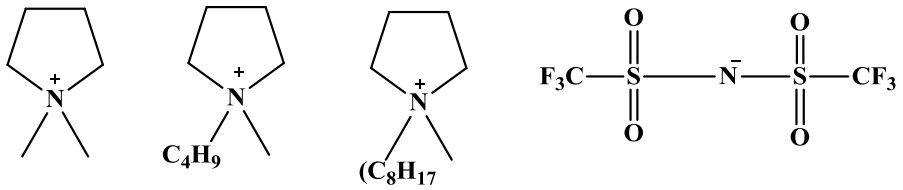

Figure 1.28 Few of the constituents of ionic liquids employed by Passerini et al., as electrolytes in LiBs (Ref. 224)

Similarly, Zaghib *et al.*, strongly profess the use of aliphatic ionic liquids predominantly piperidinium type of ionic liquids in several of their recent works. Recently, the group reported about a comparative account of the aromatic and aliphatic in terms of charge-discharge profiles in LiBs. (Figure 1.29) [225]

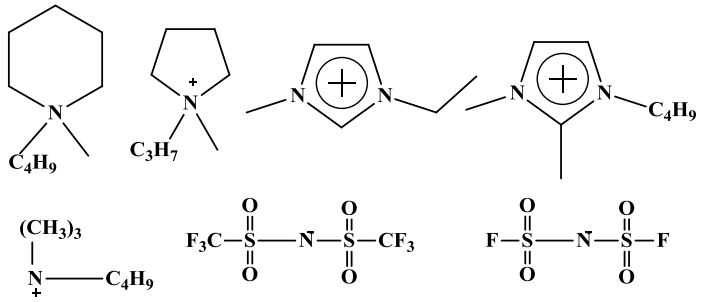

Figure 1.29 Few of the constituents of ionic liquids employed by Zaghib et al., as electrolytes in LiBs (Ref. 225)

1.3.2 Polymeric ionic liquids

Polymerised ionic liquids were reported for the first time by Ohno et al in 1998.[226] From there on, many types of polymerised ionic liquids have been synthesised utilising various strategies for

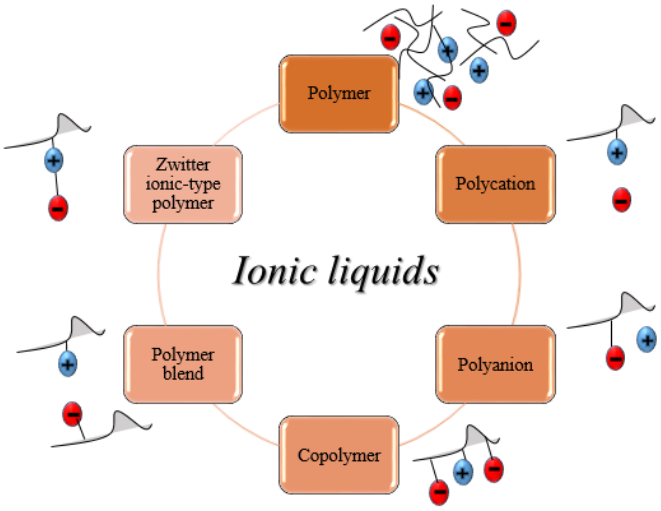

Figure 1.30 The possible ways of polymerisation of ionic liquids (Ref. 227)

applications in different research fields.[227] Some of the common types of polymeric forms of ionic liquids are enlisted in the following Figure 1.30

1.3.2.1 Polymer

The first report of a polymeric ionic liquid was the radical initiated polymer of *N*-vinyl-3-ethylimidazolium TFSA, shown in Figure 1.31. The polymeric form almost decreased to half the ionic conductivity of its monomer precursor, which was partially compensated by external addition of lithium salt. This strategic approach of external addition of salt is often employed in the polymerised ionic

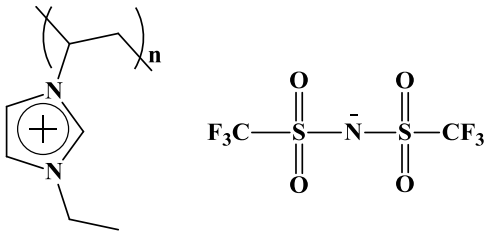

Figure 1.31 Structure of poly(N-vinyl-3-methylimidazolium TFSA) , first polymerised ionic liquid (Ref. 226)

liquids. Since polymers lose the mobile cations into the polymer matrix leading to an appreciable dip, external addition of salt is often beneficial.[226]

1.3.2.2 Polycation type polymers

In an effort to overcome the dip in ionic conductivity issues, and to avoid the structural inefficiency of being only an anion-conducting polymer, introduction of external salt was deemed necessary. Further, to enhance the structural relaxations of the polymer chains, spacers were introduced as well viz., oligoether or oligoethylene spacers, resulting in enhanced conductivity compared with polymers sans spacers. The structures of the polymers are illustrated in Figure 1.32. The choice of such spacers played a crucial role in determining the order of ionic conductivity. For instance,

Oligoethylene >> oligoether (in terms of enhancement of ionic conductivity)

The functionality on the imidazolium moiety also played as a manipulator towards ion conductive behaviour.

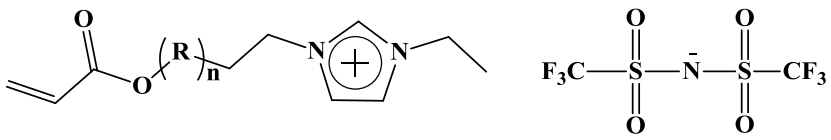

where R = -(C_2H_4)- or -(CH_2OCH_2)-

Figure 1.32 Polycation type ionic liquid based polymers (adapted from 228)

1.3.2.3 Copolymer

Various ionic liquid based copolymers have been extensively studied. Block copolymers by themselves present an attractive domain of designable ordered macromolecules. Many of the self-assemblies are principally on four main factors being the Flory-Huggins interactions parameter, number of repeating units, volume fraction of individual constituent units, and the structural arrangement of the units. Further, the constituted self-assemblies are either cubic or close-packed spheres or hexagonally packed or gyroid or lamellar morphologies which play a significant role in the ion-conductive behaviour.[229] Moving on to ionic liquid based block copolymers which encompass superior features compared with PEO based block copolymers in conductivity, lithium transference and also in film formation properties and tunable morphological attributes. Glass transition temperature dictates the ion-conductive behaviour since the polymer segmental motion is dependent on the T_g values. Several

reserachers led by Ohno , Colby and Elabd reported either direct or indirect use of ionic liquid towards the synthesis of block copolymers.[230] Elabd et al in a recent article reported the synthesis of a series of block polymers between a styryl unit and another styryl unit bearing an ionic liquid pendant (Structure is shown in Figure 1.33). The functionality on the ionic liquid was modified with the polymerisation carried out by nitroxide mediated polymerisation pathway. The study highlighted the role of morphology playing an instrumental role in the ion-conductive behaviour of the block polymer.

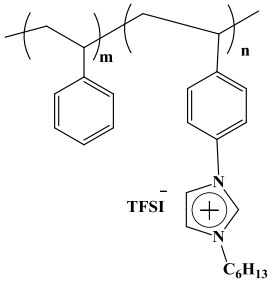

Figure 1.33 Block copolymer comprising of styryl and functionalised styryl units with ionic liquid pendant (adapted from 230)

1.4 Boron as anion receptors in electrolytes

Anion receptors in electrolyte matrices are often meritorious due to the potential advantage of increasing the localised lithium ion concentration in the electrolyte by binding with the counter anion. The anion of the lithium salt binds with the Lewis acidic moiety thereby helping in a facile lithium salt dissociation. Further, the free lithium ions in the matrix leads to improved lithium-ion transference number whilst enhancing the ionic conductivity simultaneously. Among various anion receptors, boron based anion receptors have been well studied in the recent past, due to their excellent Lewis acidic nature along with the electrochemical stability. The empty *p*-orbital in the boron atom presents with electron-accepting attributes. The graphical representation of the working mechanism of boron type anion receptors is shown:

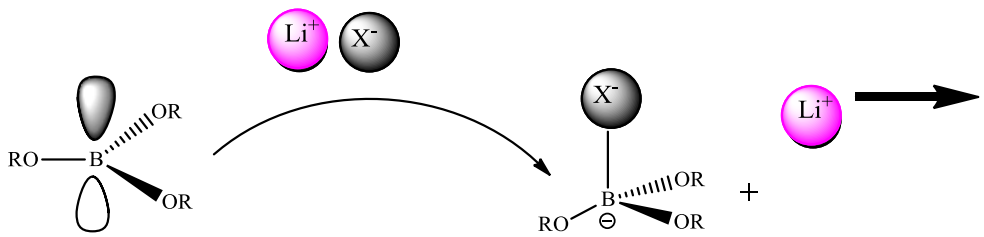

Figure 1.34 Illustraton depicting the anion-trapping mechanism and corresponding salt dissociation in the presence of boron compounds

The abovementioned illustration in Figure 1.34 shows the complexation of the anion (of the lithium salt), with that of the boron moiety, also known as "anion-trapping effect" which helps in the dissociation of the lithium salt in the electrolytic matrix.

The earliest reports about use of boron as anion receptors was reported in 1997 by Fujinami *et al.*, who reported boroxine ring receptors (Figure 1.35) as effective agents towards enhanced ionic conductivity and high lithium transference numbers by virtue of its Lewis acidic properties. A family

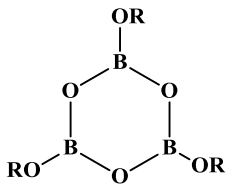

Figure 1.35 Boroxine ring type anion receptors (adapted from 199)
where R = methyl, ethyl,isopropyl or butyl groups

of boroxine type anion receptors were explored by this group, by modification of the structural fabric by various functionalities.[199-201]

Subsequent research works about boron based anion receptors were reported by McBreen *et al.*, who synthesised a number of trialkyl/triaryl borates. The anion receptors in the aprotic electrolyte media including LiF in dimethoxymethane, showed improved ionic conductivity. Further, reports about improved cyclability of such electrolytic mixtures in batteries were reported as well.[231] The family of boron compounds synthesised by the group are highlighted in the following Figure 1.36 :

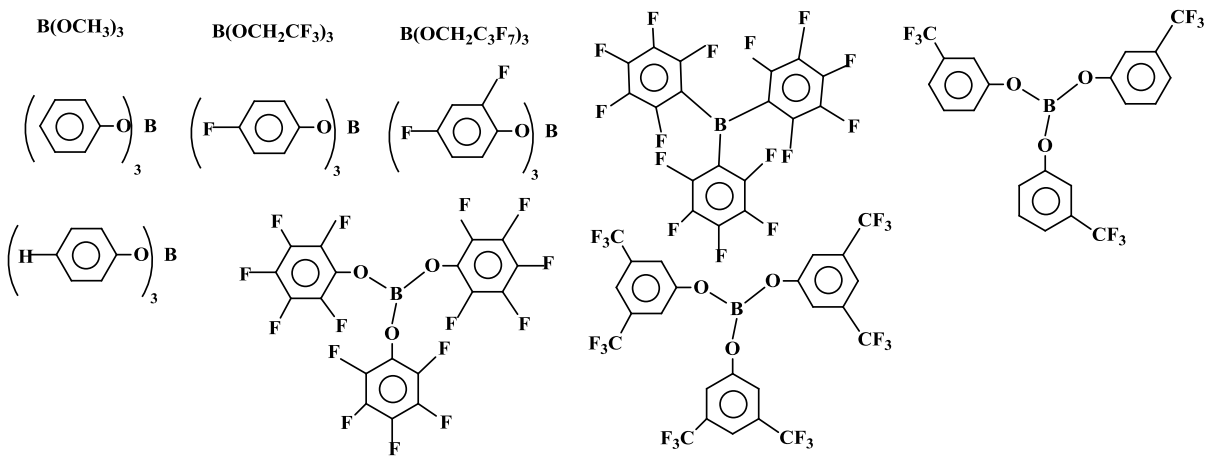

Figure 1.36 Boronate type of anion-receptors devised by McBreen et al., (adapted from 231)

Aihara *et al*., [232]Watanabe *et al*., [233] reported about different types of polymerizable novel boric esters exploiting the principles of Lewis acidic nature of Boron. (Figure 1.37) The incorporation of boron moiety in the electrolyte matrices showed improvement in ionic conductivity and transference numbers when compared with the pristine polymers without boron incorporation.

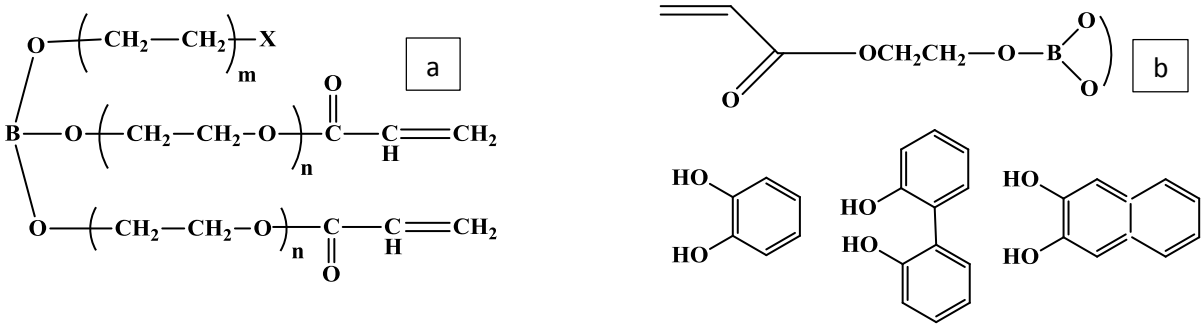

Figure 1.37 Boric ester type anion receptors, a) Aihara et al., b) Watanabe et al., (adapted from 232, 233)

The first ever report on incorporation of boron into ionic liquids was reported by Matsumi *et al*.,[234] A series of organoboron based imidazolium type ionic liquids with various borane compounds. (borane, mesityldimethoxyborane and 9-BBN 9-boracyclononane). The synthesised compounds showed improved ionic conductivity and higher transference numbers. (Figure 1.38)

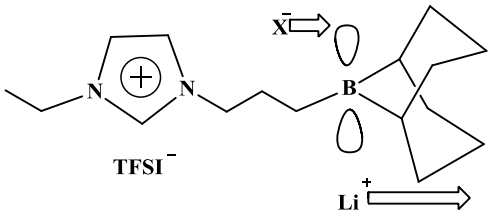

Figure 1.38 Organoboron compound derived from reaction between borane compounds with ionic liquids (adapted from 234)

Similarly, further reports about polymerised ionic liquids with organoboron compounds successfully demonstrated the capability of anion-trapping. Again the group focussed on the incorporation of various boron moieties such as borane, mesitylborane and 9-BBN as potentially advantageous anion-trapping agents (Figure 1.39). [209]

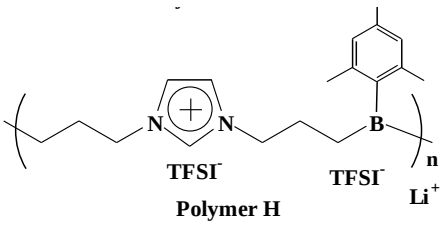

Figure 1.39 Ionic liquid based organoboron polymer as synthesised by Matsumi et al. (Ref. 209)

Another significant improvisation by taking an environmentally benign material towards utilisation in batteries was cellulization of ionic liquid based organoboron compounds (Figure 1.40). This work was once again reported by Matsumi *et al*., which include a reaction between cellulose with boric acid and pentafluorophenylbenzoic acid,[236] in the presence of ionic liquid and external lithium salt

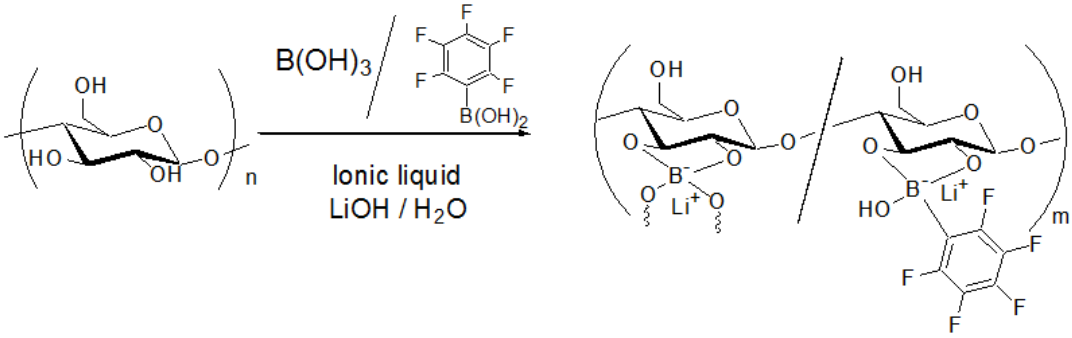

Figure 1.40 Synthetic scheme for synthesis of organoboron ion-gels by condensation of cellulose with boric acids in ionic liquids (adapted from 236)

additive. This study on the cellulose based macromolecular network also reported an increase in ionic conductivity values due to the pronounced anon trapping effect due to the presence of boron moiety.

Organic-inorganic hybrids are yet another type of functional materials, with several desirable and tunable precursorial attributes. Matsumi *et al*., reported boron incorporation in such hybrid materials by synthesising an interpenetrating network of an ionic liquid network and a boro-silicate/silicate network, formed by in-situ sol-gel condensation polymerisation reaction. A radical (AIBN) initiated reaction of 1-ethyl-3-vinyl imidazolium TFSI in the presence of alkoxysilane and various alkoxyborane precursors via acidic hydrolysis resulted in such inorganic-organic hybrids.[235] The reaction scheme illustrating the synthesis of such hybrids is referred in Figure 1.41. Borosilicate type hybrids with incorporated ionic liquids are formed from *in-situ* condensation methods provide dual benefits such as the inorganic moiety provides mechanical and thermal stability while the organic

moiety aids in ionic conductivity. These benefits are further supported by ease of synthesis, simple film-fabrication, riddance of organic solvents etc.

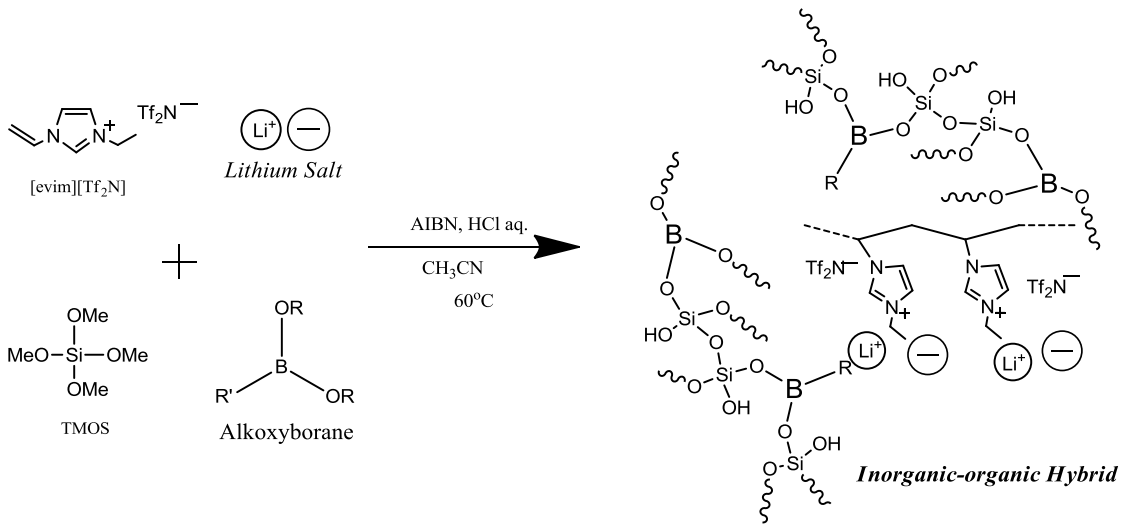

Figure 1.41 Reaction scheme of the synthesised inorganic-organic hybrid showing the incorporation of boron via borosilicate network (adapted from 235)

1.5 Organic-inorganic Hybrid Materials

Nature has been instrumental in production of materials unmatched in terms of beauty, aesthetics and even durability (shells of marine organisms like crustaceans). The perfection in terms of integration of multiple components at a nano level resulting in functionally smart materials is simply awesome. For instance, bones are perfect examples of such interactive matrices between organic and inorganic building blocks, where the inorganic part contributes mechanical strength while the organic part acts as the linking moiety. Even history of various civilizations is replete with examples where humans have used hybrid materials as inks, paints which have withstood the impact of time.[115] For instance, in Figure 1.42, a computer enhanced image of Maya blue fresco has been shown. These frescoes, characterised by bright blue colours, are hardly discoloured although subjected to hostile environments over centuries. This pigment is composed of a blue indigo natural dye within mineral encapsulation.[116]

Figure 1.42 Computer enhanced image of the Mayan fresco (adapted from 116)

The concept of "hybrids" arose yet again, in the early industrial era, although it was not defined in a wholesome manner. However, the historic links of hybrid materials, certainly interested many of the chemists. With the popularity of "chemie douce" or soft inorganic chemistry, the concept of "hybrids" was re-discovered. A hybrid material can be defined in the simplest terms as two moieties blended at a molecular level. They can be defined as nanocomposites at the molecular level, having at least one component (either organic or biological) with a characteristic length scale of nanometer size. Over the period of technological advancement, it was understood that interfacial interaction between the constituents in such hybrid materials determines their properties. Attempts towards hybridisation of the components aim at two aspects: Firstly, bridging the gap between individual capacities simultaneously,

secondly, resulting in an additive synergistic or limiting reinforced aspect of the hybridised material. It would be naïve to mention hybrid materials, as just a simple physical mixture of individual components. To reiterate, hybrid materials are resultant materials due to nanolevel interactions between inorganic and organic moieties. Such an interplay between organic and inorganic components provides a synergistic and productive effect in terms of mechanical strength and durability. Compatibility of organic-inorganic components might result in homogenous or heterogeneous materials. Thus, hybrid materials present an interfacial connection of varying degrees highlighting either precursor level or even superior level features with advantages and limitations.[117–119] The unparalleled benefits of a sol-gel process in terms of cost, efficiency, labileness and efficiency paved path to myriads of arenas opening up to embrace the usefulness of such functional hybrids. Tuning of the interfacial aspects between the two phases, presents a great variety of materials. Based on the interactive parameters (Figure 1.43), a broad yet distinct classification divides these materials into two classes:

Class I: Weak interactions: Hydrogen bonds, Ionic, coordinate bond, van der Waals interactions,

Class II: Strong interactions: Chemical covalent bonds.

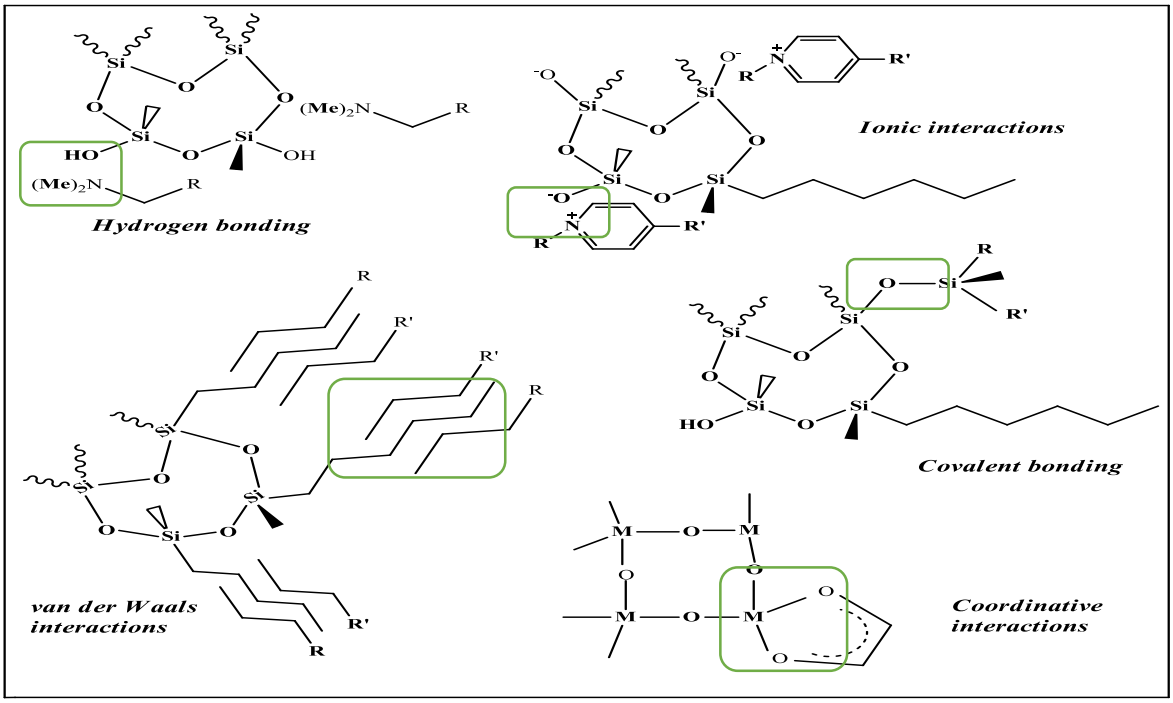

Figure 1.43 Commonly observed interactions highlighted as observed in hybrid materials (adapted from 117)

In class I, organic-inorganic hybrids are linked together by the presence of weak interactions such as hydrogen, coordinative, van der Waals or ionic bonds. The most preferred classification in this regard, corresponds in this manner:

1. Organic dyes embedded (enclosed) in sol-gel matrices,
2. Organic monomers embedded (enclosed) in sol-gel matrices,
3. Inorganic polymers embedded (enclosed) in sol-gel matrices.

Organic dyes embedded (enclosed) in sol-gel matrices

Maya blue is the perfect example for the first class of hybrids, where an organic dye is encompassed within a sol-gel matrix. As already mentioned, this dye has been able to resist centuries of climatic and bio-degradation. This dye consists of natural indigo dye encapsulated within a mineral clay viz., palygokorskite. The resultant material, possesses the colour properties of the organic component and the abrasion resistance of the inorganic component, which is simply not possible in terms of physical mixing of different components.

Organic monomers embedded (enclosed) in sol-gel matrices

In this class, the two counterparts are linked by strong chemical bonds. Orbital overlap which occurs due to bonding is the cause of increased interactions between various moieties. The choice of various functionalities of metal alkoxide in addition to the metal itself presents a wide spectra of possibilities in terms of variability. For instance, chloro- or alkoxy- precursors of precursor reagents, undergo aqueous or non-aqueous hydrolysis to result a metal oxo polymer network (M-OR bonds, where M= metal). Post condensation, the silicon based materials are resistant to hydrolysis, while other M-C bonds (when, M =Ti, Zr) hydrolyse in the presence of water.

There exist certain notable advantages of class II over class I as follows:

- Capacity of synthesis of radically new materials from unpresumed precursors,
- Tuning of degree of phase-separation,
- Control of interfacial aspects.

Most of the hybrid materials, can roughly be accommodated into one of the classes of abovementioned classification.

Novel materials with high degree of mechanical durability and superior range of flexibility in various categories is the need of the hour, due to a fast-paced technological evolution aimed at maintaining a harmonious balance in the environmental elements. Many of the conventionally used materials (metals, ceramics and plastics) are giving way to new materials owing to the inherent drawbacks of disposability. Research on hybrid materials have gained prominence off late due to the aforementioned reasons. Scientists are on a constant learning curve about understanding the interaction parameters of such hybrid materials of natural origin in order to produce materials which mimic the nature. Novel materials with multiple attributes such as environmental compatibility, desirable architecture at nano-level, yet feasible in terms of production costs are on the hunt. Hybrid materials which can be tailor-made as per requirement are a promising and attractive prospect to be ventured upon.

1.5.1 General strategies for the design of hybrid materials

Given the significance of interfacial aspects towards the synthesis of hybrid materials, the choice of the synthetic pathway plays a major role. The main chemical routes employed for typical synthesis are as summarized in Figure 1.44 as follows:

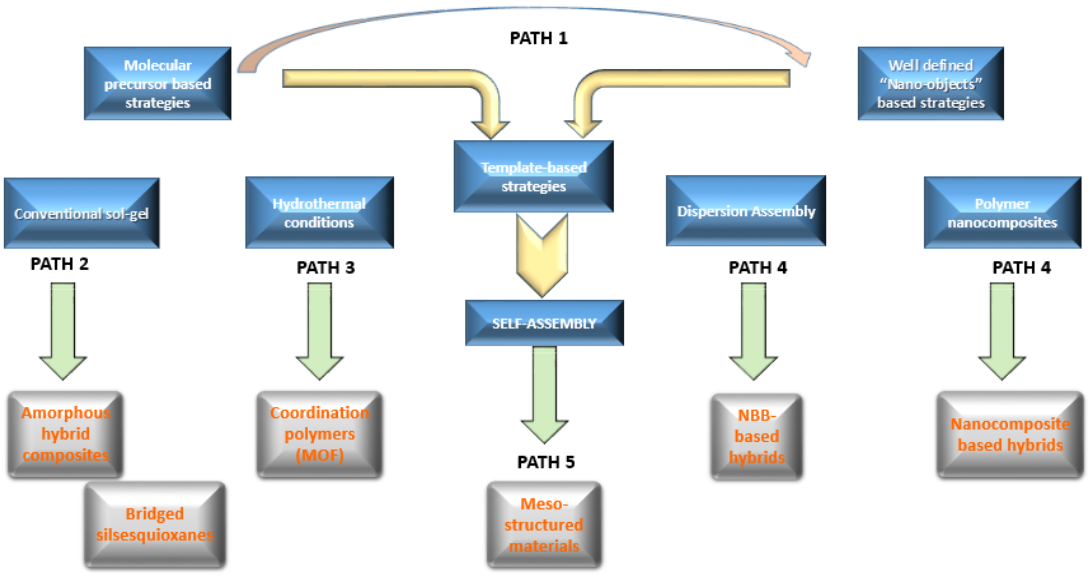

Figure 1.44 General strategies towards the synthesis of organic-inorganic hybrids (*NBB= Nano building blocks, *MOF=Metal-organic frameworks)(Ref. 119b)

Path 1: Path 1 conforms to the synthesis of well-defined non aggregated single Nano Building Block (NBB). Precursors can be aptly chosen from nano particles or nano lamellae based compounds or even macromolecular clusters.[120–137] The flexibility of composition can also be tuned in these hybrids. The control of reaction parameters such as nucleation process, growth and aggregation processes specifically define the nanoparticle specifications.[138–177] The choice of reaction media can be either organic solvents, water, inorganic molten salts, ionic liquids or even ionic liquid based gels (aerogels or xerogels) with the reaction triggering chosen as per the solvent media. The range of thermal agitation is further chosen as per the choice of the precursors.[178–184] On the basis of the abovementioned methods and strategies, a wide class of hybrid materials are synthesised.

Path 2: It refers to the conventional sol-gel pathways including both hydrolytic and non-hydrolytic routes. The precursor's choice ranges from simple metal alkoxides or halides (Zr, Ti, Al, Sn, Si alkoxides) to specific bridged or polyfunctional precursors (bridged or functionalized polysilsesquioxanes). Typically, hybrids conforming to homogeneity at nano levels are produced, with tailor-made degree of control in terms of micro or semi-micro level of control. The bridged or polyfunctional precursors, further offer greater degree of control, with the flexibility of a specific organic moiety of choice as a linker, offering improved supramolecular materials with higher precision in terms of degree of organization.[13,185–189a]

Path 3: In this path, all the hydrothermal or solvothermal based processes are included, which are often performed in polar solvents, resulting in crystalline materials. Templated organic zeolites known for their micro porous attributes are a specific class of hybrids produced in this category. Syntheses of metal organic frameworks (MOFs), which are basically coordination polymers made out of telechelic and polyfunctional spacers coordinating with various metal atoms or even link with in-situ generated metal atoms containing oligomers also pertains to this category.

Path 4: It is more or less an extension to Path 1 in various measures. It aims at the synthesis of various NBBs employing step-wise synthetic pathways, to provide comprehensively designed and structured hybrid materials with precision at the nanolevel. Such nanomaterials can be used for capping with polymerizable ligands or with organic spacers. Considering the wide range of available NBBs in

terms of material, structural and designable functionalities, it results in multitudes of architectural hybrid materials with great flexibilities in tunability.

Path 5: This path allows the templated growth or organization of inorganic or hybrid materials. The typically considered templates include micelles, lyotropic liquid crystals, silica beads etc.

1.5.1.1 Sol-gel method

The sol-gel pathway is low-temperature chemical synthesis for glass-like materials and ceramics. A *sol* can be referred to as a dispersion of colloidal particles viz., the reaction constituents or precursors in a liquid; while the *gel* is the rigid interconnected network of reactive precursors, post-condensation. It consists of polymeric chains and porous attributes of different degrees. Typically, the precursors are mixed with water or other solvents along with co-solvents (usually methanol or ethanol); subjected to either aqueous or non-aqueous hydrolysis. Further, condensation reactions and progressive densification of the compositional matrix results in the formation of gel. [189b]

Typical precursors employed in the sol-gel process include either alkanols ($M(OH)_n$) or metal alkoxides ($M(OR)_n$) or even both. The most commonly utilised elements are Si, Ti, Sn, Zr, Al, B while R refers to an alkyl group of different lengths, while n is the multiplicity of such substituents. Often, hydrolysis and condensation reactions can be accelerated by catalytic and thermal means. Catalysts are commonly employed for silicate alkoxides, while other metal alkoxides do not require any catalysts for hydrolytic initiations.

The sequence of reactivity order often observed follows this order: [189c]

$$Zr(OR)_4,\ Al(OR)_4 > Ti(OR)_4 > Sn(OR)_4 >> Si(OR)_4$$

The general scheme of hydrolysis and further condensation can be schematically represented in the following manner:

Hydrolysis

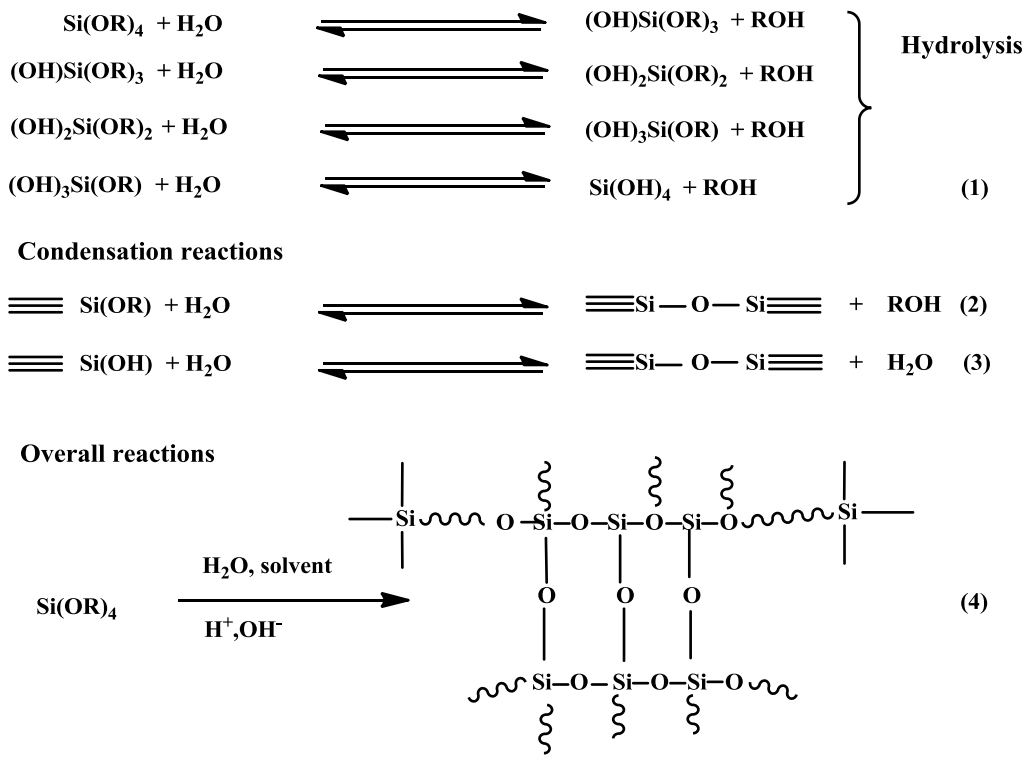

Figure 1.45 Representation of the hydrolysis and condensation reactions of a silicon alkoxide.

The abovementioned scheme, in Figure 1.45, represents the whole sequence in a silicate alkoxide based sol-gel condensation reaction. In step 1, hydrolysis of the alkoxides takes place in solutions containing an acid or base catalyst, resulting in the $\equiv Si(OH)$ formation of silanol groups, further, condensation reactions proceed, involving these silanol groups resulting in the formation of siloxane networks. The progressive densification occurs as a function of the siloxane network formation.

Several factors influence the sol-gel process, for instance, catalyst employed, H_2O/Si ratio, type of solvent, pH, catalyst employed, temperature and additives.

Catalyst: Choice of catalyst also plays a major role in the hydrolysis and condensation reactions. Acids, and bases are commonly employed as catalysts. Acids are known to increase the straight chain polymers while bases are known to increase the ramification. The mechanisms of each, the acidic and basic hydrolytic processes, depicted in Figure 1.46 are employed as follows:

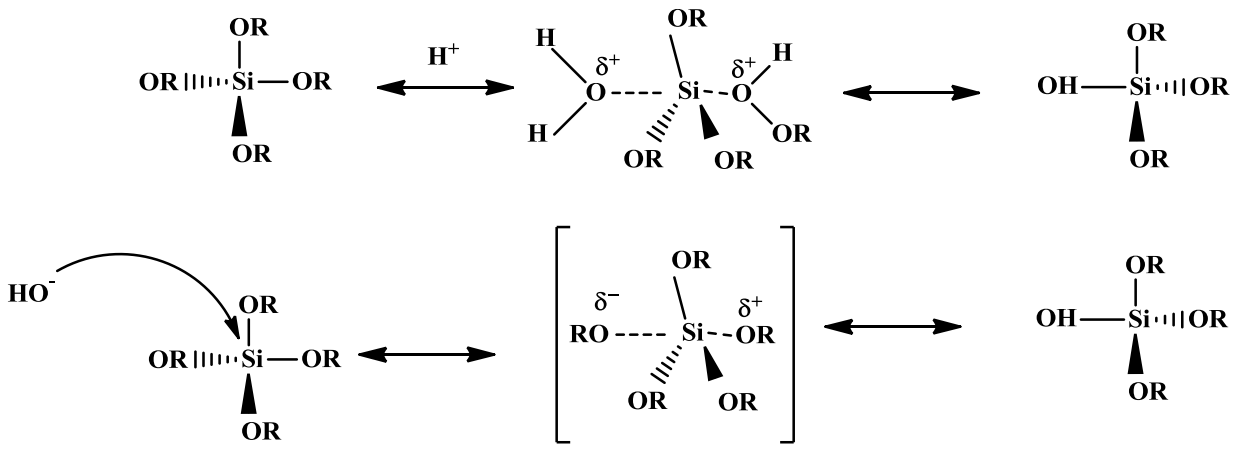

Figure 1.46 Reaction mechanisms of aqueous hydrolysis of alkoxysilane precursor

Molar ratio H_2O/Si (R): This ratio plays a major role in the hydrolysis reactions. The initiation of hydrolysis is favoured when the ratio is R>>2. While, the silanol formation through various intermediate stages is favoured when R<<2.

pH: pH is effective in the overall mechanism of the gelation and is instrumental in the microstructure formulation in the materials. Often, at the isoelectric point of silica, the reaction time is minimal. However, variations in pH lead to change in the reaction time. A classification devised by Iller,[189d] divides the polymerization process into three distinct pH regions: pH<2, 2<pH>7, pH>7.

Temperature: Temperature often plays an accelerating role in gelation. Often, sol-gel processes at room temperature takes a long time. However, increasing the temperature, decreases the reaction time, due to quicker removal of solvents, co-solvents and water.

1.6 Statement of Problem

In recent times, a great deal of research has been carried out in the development of electrolytes which have multiple attributes such as enhanced ionic conductivity, alongside properties such as mechanical durability, thermal stability and longer shelf life. This isn't restricted to lithium ion technology alone, it further covers areas such as magnesium systems and even lithium metal systems.

1.6.1 Electrolyte systems in lithium-ion batteries

Electrolytes are the third most significant parameter towards its functioning apart from anode and cathode. Although, role of electrolyte is considered trivial, it is deemed crucial with respect to the choice of electrode materials. Highly oxidizing cathode material would demand a higher electrolyte possessing greater electrochemical window. In a similar manner, polymer electrolytes are often preferred due to their highly favourable range of electrochemical stability. Such properties have resulted in popularisation of PEO based electrolytes along with alkyl carbonate based additives. In case of the additives, the whole class of electrolytes used so far can be divide into three classes such as: esters, ethers and alkyl carbonates based salts. Alkyl carbonate based solvents are often devised as popular electrolyte materials in lithium-ion batteries. The key features which define an ideal electrolyte would be as follows:

- Cation transport properties and ionic conductivity: Great deal of understanding about the parameters governing ionic conductivity and Li ion transference number is quintessential,
- Wide electrochemical window: With recent development in various high voltage cathode materials, it is very significant to have materials with optimum electrochemical windows,
- Operational temperature range: With diverse applications of lithium ion batteries, it is indeed necessary to find electrolytes with wider temperature viability,
- Safety aspects: With recent news of thermal runway accidents due to its hermetic packages, it's a grey area which needs to be addressed.

An arsenal of electrolyte options are currently used including polymer PEO based electrolytes, glassy ceramic electrolytes or even ionic liquid based electrolytes. Due to numerous variables requiring

attention, it's practically impossible to discover an *ad hoc* solution to the electrolyte concerns in the lithium ion systems. However, a modular approach towards decimating the known lacunae in this field would ultimately lead to a hierarchical evolution of electrolytes.

1.7 Importance of Study

Guided by the need of the hour, all the existent alongside emerging technologies are subjected to intense scrutiny towards a superior all-round performance in their respective areas of applications. With numerous variable parameters seeking attention in every technology, it's a matter of time how we excel in these technologies without compromising quality or safety in anyways.

The present area of interest lies in the *design and development of novel electrolytes for the lithium ion batteries*. There is an urgent need to develop novel electrolytic materials with improved thermal retardancy properties without compromising on conductivity issues and mechanical stability. The strategic and modular approach in this study comprises of "Utilisation of Ionic liquids and Boron Chemistry" in a complementary manner to address the issues of electrolytes in lithium-ion batteries.

The synthesis of novel borosilicate banks on several foundations of principles of solid-state materials. The ionic liquid enhances ion-conductive parameters, encompassed in an inorganic network composed of borosilicate network aided by the alkoxysilane and alkoxyborane precursors. Furthermore, the presence of boron moiety is useful in anion-trapping thereby facilitating facile salt dissociation of the lithium salt additive present in the matrix. An in situ sol-gel synthesis is a rather facile mode of synthesis, avoiding high-temperature and bulk solvent requirements.

The resultant hybrid which is mechanically stable owing to its borosilicate network, acquires flame retardancy properties due to its ionic liquid content, besides the inorganic fabric. The thermal

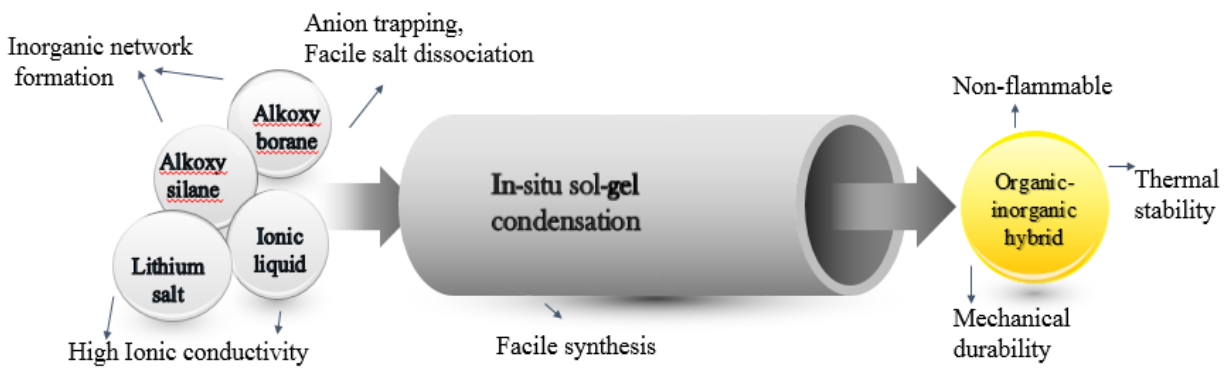

Figure 1.47 Highlights of in-situ sol-gel condensation of organic-inorganic hybrids

stability is indeed aided by the ionic liquid components besides the structural borosilicate linkages. The graphic illustration in Figure 1.47 talks about the mentioned advantages.

The whole work can be categorically classified into these three sections:

a) Design and synthesis of novel hybrid electrolyte material for Lithium-ion battery,

b) Evaluation of the efficiency of hybrid electrolyte in Lithium-ion batteries,

c) Evaluation of the thermal and flammability properties of the synthesised electrolytes.

1.8 Objectives and Scope of Research

To address a few of the major concerns in the electrolyte section of Lithium-ion batteries, a multidimensional approach was employed in the present work.

Ionic liquids generally show unique characteristics such as non-volatility, non-flammability and high ionic conductivity, and preparation of ionic liquids based electrolyte material is also a promising approach and is presently trending well. After ionic liquids emerged as a novel class of electrolytes[190], polymer and monomer homologues of ionic liquids have also been vigorously studied as solid polymer electrolytes, microwave absorption materials and so forth.[191] Particularly, in the field of ionics and energy devices such as lithium ion secondary batteries and other allied emergent fields , there has been growing interest towards ionic liquids.[192–198]

Fujinami *et al.*, reported way back in late 90s about the anion trapping ability of boron compounds in electrolyte matrices.[199–201] From thereon, multitudes of studies have been conducted to ascertain the concept highlighted. Guided by the needs for superior electrolyte systems with enhanced ionic conductivity and lithium transference numbers, it was deemed necessary to explore the worthiness of boron moiety in the electrolyte matrices along with the highly promising ionic liquid as the cofactor. Boron compounds are known to be as ideal Lewis acids, due to their empty *p*-orbitals, which have pronounced anion trapping effect, often leading to facile salt dissociation.[202–211]

The scope of this research is to design and synthesize novel organic-inorganic hybrid electrolytes showing both good thermal stability and ionic conductivity at the same time so that efficient charge-discharge is attained with greater safety. Electrochemical characterizations for an in-depth understanding of the changes occurring in the electrolyte matrices is also under the purview of this research.

The first chapter includes a literature review spanning the areas of lithium ion batteries with an insight into the electrolyte components used so far, use of ionic liquids as electrolytes, significance of organic-inorganic hybrids and blends as electrolytes.

The second chapter deals with the design of novel borosilicate type organic-inorganic hybrid ion-gel electrolytes synthesized utilising low-viscous type allylimidazolium type ionic liquid. It covers the sol-gel mediated synthetic procedure, subsequent characterisations, ionic conductivity studies and morphological studies.

The third chapter deals with the implementation of such hybrid electrolyte as an electrolyte for lithium ion batteries. This covers the fabrication of cells, their electrochemical characterizations using electrochemical impedance spectroscopy besides charge-discharge studies at various charging rates as a means to evaluate them as an electrolyte for LiBs.

The fourth chapter deals with the thermo gravimetric studies and the differential scanning calorimetric studies of the hybrid electrolytes apart from the flammability studies. This study shows the advantages of the synthesised electrolytes over other electrolytes in terms of susceptibility to flammability.

Finally, the main results and achievements of this doctoral research work are summarized and concluded in the fifth chapter.

References

(1) Goodenough, J. B.; Park, K.-S. *J. Am. Chem. Soc.*, **2013**, *135*, 1167–1176.
(2) Zhou G.; Li F.; Cheng H-M. *Energy & Environ. Sci.*, **2014**, *7*, 1307-1338.
(3) Kurzweil, P. *J. Power Sources*, **2010**, *195*, 4424–4434.
(4) Cheng, F.; Liang, J.; Tao, Z.; Chen, J. *Adv. Mater.*, **2011**, *23*, 1695–1715.
(5) Ozawa K.; Eds, in *Lithium Ion Rechargeable Batteries*; **2009**, Wiley.
(6) a) Tarascon, J.-M.; Armand, M. *Nature*, **2001**, *414*, 359–367.
b) Linden, D.; Reddy, T.B.; Eds, in *Handbook of Batteries*, **1995**, McGraw Hill.
(7) Armand, M.; Tarascon, J.-M. *Nature*, **2008**, *451*, 652–657.
(8) Song, M.-K.; Zhang, Y.; Cairns, E. J. *Nano Lett.*, **2013**, *13*, 5891–5899.
(9) Wang, K.; Jiang, K.; Chung, B.; Ouchi, T.; Burke, P. J.; Boysen, D. A.; Bradwell, D. J.; Kim, H.; Muecke, U.; Sadoway, D. R. *Nature*, **2014**, *514*, 348–350.
(10) Jung, H.-G.; Hassoun, J.; Park, J.-B.; Sun, Y.-K.; Scrosati, B. *Nat Chem*, **2012**, *4*, 579–585.
(11) Doe, R. E.; Han, R.; Hwang, J.; Gmitter, A. J.; Shterenberg, I.; Yoo, H. D.; Pour, N.; Aurbach, D. *Chem. Commun.*, **2014**, *50*, 243–245.
(12) Hartmann, P.; Bender, C. L.; Vračar, M.; Dürr, A. K.; Garsuch, A.; Janek, J.; Adelhelm, P. *Nat. Mater.*, **2013**, *12*, 228–232.
(13) a) Van Noorden, R. *Nature*, **2014**, *507*, 26-28.
b) Zu, C.-X.; Li, H. *Energy & Environ. Sci.*, **2011**, *4*, 2614–2624.
(14) Muldoon, J.; Bucur, C. B.; Oliver, A. G.; Sugimoto, T.; Matsui, M.; Kim, H. S.; Allred, G. D.; Zajicek, J.; Kotani, Y. *Energy & Environ. Sci.*, **2012**, *5*, 5941–5950.
(15) a) Scrosati, B., Abraham, K.M., van Schalkwik W.; Hassoun, J.; Eds., in *Lithium Batteries-Advanced Technologies and Applications*, **2013**, Wiley.
b) Daniel, C.; Besenhard, J.O.; Eds in *Handbook of Battery Materials*, **2011**, Wiley.
(16) Peled, E. *J. Electrochem. Soc.*, **1979**, *126*, 2047-2051.
(17) Nitta, N.; Yushin, G. *Part. & Part. Syst. Charact.*, **2014**, *31*, 317–336.
(18) Aurbach, D. *et al*., *J. Power Sources*, **2007**, *165*, 491-499.
(19) Kaskhedikar, N. A.; Maier, J. *Adv. Mater.*, **2009**, *21*, 2664–2680.
(20) Winter, M.; Besenhard J.O.; Spahr, M.E.; Novak, P. *Adv. Mater.*, **1998**, *10*, 725-763.
(21) Aurbach, D.; Markovsky, B.; Weissman, I., Levi, E.; Ein-Eli, Y. *Electrochim. Acta*, **1999**, 45, 67-86.
(22) Cho, J. *J. Mater. Chem.*, **2010**, *20*, 4009-4014.
(23) Obrovac, M. N.; Krause, L. J. *J. Electrochem. Soc.*, **2007**, *154*, A103–A108.
(24) Obrovac, M. N.; Christensen, L. *Electrochem. Solid-State Lett.*, **2004**, *7*, A93–A96.
(25) Liu, X. H.; Liu, Y.; Kushima, A.; Zhang, S.; Zhu, T.; Li, J.; Huang, J. Y. *Adv. Energy Mater.*, **2012**, *2*, 722–741.
(26) Liu, X. H.; Fan, F.; Yang, H.; Zhang, S.; Huang, J. Y.; Zhu, T. *ACS Nano*, **2012**, *7*, 1495–1503.
(27) Hatchard, T. D.; Dahn, J. R. *J. Electrochem. Soc.*, **2004**, *151*, A838–A842.
(28) Lee, S. W.; McDowell, M. T.; Choi, J. W.; Cui, Y. *Nano Lett.*, **2011**, *11*, 3034–3039.
(29) Zhao, K.; Pharr, M.; Cai, S.; Vlassak, J. J.; Suo, Z. *J. Am. Ceram. Soc.*, **2011**, *94*, s226–s235.
(30) Goldman, J. L.; Long, B. R.; Gewirth, A. A.; Nuzzo, R. G. *Adv. Funct. Mater.*, **2011**, *21*, 2412–2422.
(31) Liu, X. H.; Huang, S.; Picraux, S. T.; Li, J.; Zhu, T.; Huang, J. Y. *Nano Lett.*, **2011**, *11*, 3991–3997.
(32) Park, M.-H.; Cho, Y.; Kim, K.; Kim, J.; Liu, M.; Cho, J. *Angew. Chem. Int. Ed.*, **2011**, *123*, 9821–9824.
(33) Haro, M.; Song, T.; Guerrero, A.; Bertoluzzi, L.; Bisquert, J.; Paik, U.; Garcia-Belmonte, G. *Phys. Chem. Chem. Phys.* **2014**, *16*, 17930–17935.
(34) Ren, W.; Kong, D.; Cheng, C. *ChemElectroChem*, **2014**, *in press*.
(35) Liu, C.; Huang, H.; Cao, G.; Xue, F.; Paredes Camacho, R. A.; Dong, X. *Electrochim. Acta*, **2014**, *144*, 376–382.
(36) Menkin, S.; Barkay, Z.; Golodnitsky, D.; Peled, E. *J. Power Sources*, **2014**, *245*, 345–351.
(37) Mizushima, K.; Jones, P. C.; Wiseman, P. J.; Goodenough, J. B. *Mater. Res. Bull.*, **1980**, *15*,

783–789.
(38) Alcántara, R.; Lavela, P.; Tirado, J. L.; Zhecheva, E.; Stoyanova, R. *J. Electroanal. Chem.*, **1998**, *454*, 173–181.
(39) Pu, X.; Yu, C. *Nanoscale*, **2012**, *4*, 6743–6747.
(40) Hao, Q.; Xu, C.; Jia, S.; Zhao, X. *Electrochim. Acta*, **2013**, *113*, 439–445.
(41) Li, X.; Liu, J.; Meng, X.; Tang, Y.; Banis, M. N.; Yang, J.; Hu, Y.; Li, R.; Cai, M.; Sun, X. *J. Power Sources*, **2014**, *247*, 57–69.
(42) Miyashiro, H.; Yamanaka, A.; Tabuchi, M.; Seki, S.; Nakayama, M.; Ohno, Y.; Kobayashi, Y.; Mita, Y.; Usami, A.; Wakihara, M. *J. Electrochem. Soc.*, **2006**, *153*, A348–A353.
(43) Dai, X.; Wang, L.; Xu, J.; Wang, Y.; Zhou, A.; Li, J. *ACS Appl. Mater. & Interfaces*, **2014**, *6*, 15853–15859.
(44) Cho, J.; Lee, J.-G.; Kim, B.; Park, B. *Chem. Mater.*, **2003**, *15*, 3190–3193.
(45) Dahn, J. R.; von Sacken, U.; Michal, C. A. *Solid State Ionics*, **1990**, *44*, 87–97.
(46) Capitaine, F.; Gravereau, P.; Delmas, C. *Solid State Ionics*, **1996**, *89*, 197–202.
(47) He, P.; Wang, H.; Qi, L.; Osaka, T. *J. Power Sources*, **2006**, *160*, 627–632.
(48) Wang, Z.; Sun, Y.; Chen, L.; Huang, X. *J. Electrochem. Soc.*, **2004**, *151*, A914–A921.
(49) Idemoto, Y.; Takanashi, Y.; Kitamura, N. *J. Power Sources*, **2009**, *189*, 269–278.
(50) Ohzuku, T.; Makimura, Y. *Chem. Lett.*, **2001**, *30*, 744–745.
(51) Zhang, B.; Chen, G.; Xu, P.; Lv, Z. *Solid State Ionics*, **2007**, *178*, 1230–1234.
(52) Lee, K.-S.; Myung, S.-T.; Moon, J.-S.; Sun, Y.-K. *Electrochim. Acta*, **2008**, *53*, 6033–6037.
(53) Myung, S.-T.; Komaba, S.; Kumagai, N.; Yashiro, H.; Chung, H.-T.; Cho, T.-H. *Electrochim. Acta*, **2002**, *47*, 2543–2549.
(54) Padhi, A. K.; Nanjundaswamy, K. S.; Goodenough, J. B. *J. Electrochem. Soc.*, **1997**, *144*, 1188–1194.
(55) Meethong, N.; Huang, H.-Y. S.; Speakman, S. A.; Carter, W. C.; Chiang, Y.-M. *Adv. Funct. Mater.*, **2007**, *17*, 1115–1123.
(56) Morgan, D.; Van der Ven, A.; Ceder, G. *Electrochem. Solid-State Lett.*, **2004**, *7*, A30–A32.
(57) Molenda, J.; Ojczyk, W.; Marzec, J. *J. Power Sources*, **2007**, *174*, 689–694.
(58) Fergus, J. W. *J. Power Sources*, **2010**, *195*, 939–954.
(59) Okada, S.; Sawa, S.; Egashira, M.; Yamaki, J.; Tabuchi, M.; Kageyama, H.; Konishi, T.; Yoshino, A. *J. Power Sources*, **2001**, *97–98*, 430–432.
(60) Choe, H. S.; Giaccai, J.; Alamgir, M.; Abraham, K. M. *Electrochim. Acta*, **1995**, *40*, 2289–2293.
(61) Ameduri, B. *Chem. Rev.*, **2009**, *109*, 6632–6686.
(62) Du Pasquier, A.; Warren, P. C.; Culver, D.; Gozdz, A. S.; Amatucci, G. G.; Tarascon, J.-M. *Solid State Ionics*, **2000**, *135*, 249–257.
(63) Shi, Q.; Yu, M.; Zhou, X.; Yan, Y.; Wan, C. *J. Power Sources*, **2002**, *103*, 286–292.
(64) Kim, J. R.; Choi, S. W.; Jo, S. M.; Lee, W. S.; Kim, B. C. *Electrochim. Acta*, **2004**, *50*, 69–75.
(65) Huang, H.; Wunder, S. L. *J. Power Sources*, **2001**, *97–98*, 649–653.
(66) Raghavan, P.; Zhao, X.; Kim, J.-K.; Manuel, J.; Chauhan, G. S.; Ahn, J.-H.; Nah, C. *Electrochim. Acta*, **2008**, *54*, 228–234.
(67) Li, Z. H.; Zhang, H. P.; Zhang, P.; Wu, Y. P.; Zhou, X. D. *J. Power Sources*, **2008**, *184*, 562–565.
(68) Ramesh, S.; Wong, K. C. *Ionics*, **2009**, *15*, 249-254.
(69) Rajendran, S.; Bama, V. S.; Prabhu, M. R. *Ionics*, **2010**, *16*, 27-32.
(70) Egashira, M.; Todo, H.; Yoshimoto, N.; Morita, M. *J. Power Sources*, **2008**, *178*, 729–735.
(71) Liang, Y.-H.; Wang, C.-C.; Chen, C.-Y. *J. Power Sources*, **2008**, *176*, 340–346.
(72) Zhou, D. Y.; Wang, G. Z.; Li, W. S.; Li, G. L.; Tan, C. L.; Rao, M. M.; Liao, Y. H. *J. Power Sources*, **2008**, *184*, 477–480.
(73) Rao, M. M.; Liu, J. S.; Li, W. S.; Liang, Y.; Liao, Y. H.; Zhao, L. Z. *J. Power Sources*, **2009**, *189*, 711–715.
(74) Liao, Y. H.; Zhou, D. Y.; Rao, M. M.; Li, W. S.; Cai, Z. P.; Liang, Y.; Tan, C. L. *J. Power Sources*, **2009**, *189*, 139–144.
(75) Perera, K. S.; Dissanayake, M. A. K. L.; Skaarup, S.; West, K. *J. Solid State Electr.*, **2008**, *12*, 873-877.

(76) Pu, W.; He, X.; Wang, L.; Tian, Z.; Jiang, C.; Wan, C. *Ionics*, **2008**, *14*, 27-31.
(77) Patel, M.; Chandrappa, K. G.; Bhattacharyya, A. J. *Electrochim. Acta*, **2008**, *54*, 209–215.
(78) Bhattacharyya, A.; Patel, M.; Das, S. *Monatsh Chem.*, **2009**, *140*, 1001-1010.
(79) Baskakova, Y. V.; Efimov, O. N. *Russ. Chem. Rev.*, **2012**, *81*, 367-380.
(80) Thangadurai, V.; Weppner, W. *Ionics*, **2006**, *12*, 81-92.
(81) Thangadurai, V.; Weppner, W. *J. Solid State Chem.*, **2006**, *179*, 974–984.
(82) Liu, Z.; Huang, F.; Yang, J.; Wang, B.; Sun, J. *Solid State Ionics*, **2008**, *179*, 1714–1716.
(83) Minami, K.; Hayashi, A.; Tatsumisago, M. *Solid State Ionics*, **2008**, *179*, 1282–1285.
(84) Money, B. K.; Hariharan, K. *Solid State Ionics*, **2008**, *179*, 1273–1277.
(85) Muñoz, F.; Montagne, L.; Pascual, L, Durán, A. *J. Non-Cryst. Solids*, **2009**, *355*, 52-54.
(86) Teragawa, S.; Aso, K.; Tadanaga, K.; Hayashi, A.; Tatsumisago, M. *J. Power Sources*, **2014**, *248*, 939–942.
(87) Noi, K.; Hayashi, A.; Tatsumisago, M. *J. Power Sources*, **2014**, *269*, 260–265.
(88) Nagao, M.; Kitaura, H.; Hayashi, A.; Tatsumisago, M. *J. Power Sources*, **2009**, *189*, 672–675.
(89) Minami, K.; Hayashi, A.; Ujiie, S.; Tatsumisago, M. *J. Power Sources*, **2009**, *189*, 651–654.
(90) Ohtomo, T.; Hayashi, A.; Tatsumisago, M.; Tsuchida, Y.; Hama, S.; Kawamoto, K. *J. Power Sources*, **2013**, *233*, 231–235.
(91) Ohtomo, T.; Mizuno, F.; Hayashi, A.; Tadanaga, K.; Tatsumisago, M. *J. Power Sources*, **2005**, *146*, 715–718.
(92) Hayashi, A.; Konishi, T.; Tadanaga, K.; Minami, T.; Tatsumisago, M. *J. Power Sources*, **2005**, *146*, 496–500.
(93) Murayama, M.; Kanno, R.; Irie, M.; Ito, S.; Hata, T.; Sonoyama, N.; Kawamoto, Y. *J. Solid State Chem.*, **2002**, *168*, 140–148.
(94) Kanno, R.; Hata, T.; Kawamoto, Y.; Irie, M. *Solid State Ionics*, **2000**, *130*, 97–104.
(95) Kanno, R.; Murayama, M. *J. Electrochem. Soc.*, **2001**, *148*, A742–A746.
(96) Jimenez, R.; Rivera, A.; Varez, A.; Sanz, J. *Solid State Ionics*, **2009**, *180*, 1362–1371.
(97) Mei, A.; Wang, X.-L.; Feng, Y.-C.; Zhao, S.-J.; Li, G.-J.; Geng, H.-X.; Lin, Y.-H.; Nan, C.-W. *Solid State Ionics*, **2008**, *179*, 2255–2259.
(98) Mei, A.; Jiang, Q.-H.; Lin, Y.-H.; Nan, C.-W. *J. Alloy. Compd.*, **2009**, *486*, 871–875.
(99) Stramare, S.; Thangadurai, V.; Weppner, W. *Chem. Mater.*, **2003**, *15*, 3974–3990.
(100) Thangadurai, V.; Kaack, H.; Weppner, W. J. F. *J. Am. Ceram. Soc.*, **2003**, *86*, 437–440.
(101) Murugan, R.; Thangadurai, V.; Weppner, W. *J. Electrochem. Soc.*, **2008**, *155*, A90-A101.
(102) Murugan, R.; Thangadurai, V.; Weppner, W. *Appl. Phys. A-Mater.*, **2008**, *91*, 615-620.
(103) Zeier, W. G. *Dalton Trans.*, **2014**, *43*, 16133–16138.
(104) Awaka, J.; Kijima, N.; Takahashi, Y.; Hayakawa, H.; Akimoto, J. *Solid State Ionics*, **2009**, *180*, 602–606.
(105) Percival, J.; Kendrick, E.; Slater, P. R. *Solid State Ionics*, **2008**, *179*, 1666–1669.
(106) Narayanan, S.; Thangadurai, V. *J. Power Sources*, **2011**, *196*, 8085–8090.
(107) Shimonishi, Y.; Zhang, T.; Imanishi, N.; Im, D.; Lee, D. J.; Hirano, A.; Takeda, Y.; Yamamoto, O.; Sammes, N. *J. Power Sources*, **2011**, *196*, 5128–5132.
(108) Hasegawa, S.; Imanishi, N.; Zhang, T.; Xie, J.; Hirano, A.; Takeda, Y.; Yamamoto, O. *J. Power Sources*, **2009**, *189*, 371–377.
(109) Shimonishi, Y.; Zhang, T.; Johnson, P.; Imanishi, N.; Hirano, A.; Takeda, Y.; Yamamoto, O.; Sammes, N. *J. Power Sources*, **2010**, *195*, 6187–6191.
(110) Kosova, N. V.; Devyatkina, E. T.; Stepanov, A. P.; Buzlukov, A. L. *Ionics*, **2008**, *14*.
(111) Adachi, G.; Imanaka, N.; Aono, H. *Adv. Mater.*, **1996**, *8*, 127–135.
(112) Pérez-Estébanez, M.; Isasi-Marín, J.; Díaz-Guerra, C.; Rivera-Calzada, A.; León, C.; Santamaría, J. *Solid State Ionics*, **2013**, *241*, 36–45.
(113) Trevey, J. E.; Gilsdorf, J. R.; Miller, S. W.; Lee, S.-H. *Solid State Ionics*, **2012**, *214*, 25–30.
(114) Nagamine, K.; Hirose, K.; Honma, T.; Komatsu, T. *Solid State Ionics*, **2008**, *179*, 508–515.
(115) Sanchez, C.; Arribart, H.; Giraud Guille, M. M. *Nat Mater*, **2005**, *4*, 277–288.
(116) Gomez-Romero, P.; Sanchez, C. *New J. Chem.*, **2005**, *29*, 57–58.
(117) Kickelbick, G; Eds, in *Introduction to Hybrid Materials*, **2006**, Wiley.
(118) Gomez-Romero, P. *Adv. Mater.*, **2001**, *13*, 163–174.
(119) a) Sanchez, C.; Julian, B.; Belleville, P.; Popall, M. *J. Mater. Chem.*, **2005**, *15*, 3559–3592.

b) Sanchez, C.; Boissiere, C.; Cassaignon, S.; Chaneac, C.; Durupthy, O.; Faustini, M.; Grosso, D.; Laberty-Robert, C.; Nicole, L.; Portehault, D.; Ribot, F.; Rozes, L.; Sassoye, C. Chem. Mater., **2014**, *26*, 221-238.
(120) Antonietti, M.; Berton, B.; Goltner, C.; Hemtze, H-P *Adv. Mater*. **1998**, *10*, 154-159.
(121) Yang, P. *Science*, **1998**, *282*, 2244–2246.
(122) Moller, K.; Bein, T. *Chem. Mater.*, **1998**, *10*, 2950–2963.
(123) Kresge, C. T.; Leonowicz, M. E.; Roth, W. J.; Vartuli, J. C.; Beck, J.S. *Nature*, **1992**, *359*, 710-712.
(124) Levy, D. *Chem. Mater*. **1997**, *9*, 2666-2670.
(125) Mann, S.; Burkett, S. L.; Davis, S. A.; Fowler, C. E.; Mendelson, N. H.; Sims, S. D.; Walsh, D.; Whilton, N. T. *Chem. Mater.*, **1997**, *9*, 2300-2310.
(126) Sanchez, C.; Ribot, F.;Libeau, B. *J. Mater. Chem*., **1999**, *9*, 35-44.
(127) Yaghi, O. M.; Li, H.; Davis, C.; Richardson, D.; Groy, T. L. *Acc. Chem. Res.*, **1998,** 31, 474-484.
(128) Yanagisawa, T.; Shimizu, T.; Kuroda, K.; Kato, C. *Bull. Chem. Soc. Jpn.*, **1990**, *63*, 988-992.
(129) Andrianainarivelo, M.; Corriu, R.; Leclercq, D.; Mutin, P.H.; Vioux, A. *J. Mater. Chem.*, **1996**, *6*, 1665-1671.
(130) Corma, A. *Chem. Rev.*, **1997**, *97*, 2373- 2419.
(131) Schubert, U.; Husing, N.; *Chem. Mater.*, **1995**, *7*, 2010-2027.
(132) Schmidt, W. R.; Interrante, L. V.; Doremus, R. H.; Trout, T. K.; Marchetti, P.S.;Maciel, G.E. *Chem. Mater*. **1991**, *3*, 257-267.
(133) Goltner, C. G.; Antonietti, M. *Adv. Mater*. **1997**, *9*, 431–436.
(134) Zhao, D. *Science*, **1998**, *279*, 548–552.
(135) Loy, D. A.; Shea, K. J. *Chem. Rev*., **1995**, *95*, 1431-1442.
(136) Forster, S.; Antonietti, M. *Adv. Mater*., **1998**, *10*, 195-217.
(137) Livage, J.; Henry, M.; Sanchez, C. *Prog. Solid State Chem*., **1988**, *18*, 259-341.
(138) Nassif, N.; Liavge, J. *Chem. Soc. Rev*., **2011**, *40*, 849-859.
(139) Carbone, L.; Cozzoli, P. D. *Nano Today*, **2010**, *5*, 449–493.
(140) Skrabalak, S. E.; Chen, J.; Sun, Y.; Lu, X.; Au, L.; Cobley, C. M.; Xia, Y. *Acc. Chem. Res.*, **2008**, *41*, 1587–1595.
(141) Grzelczak, M.; Vermant, J.; Furst, E. M.; Liz-Marza´n, L. M. *ACS Nano*, **2010**, *4*, 3591–3605.
(142) Gonzalez, E.; Arbiol, J.; Puntes, V. F. *Science*, **2011**, *334*, 1377–1380.
(143) Cölfen, H.; Antonietti, M. *Angew. Chem. Int. Ed.*, **2005**, *44*, 5576–5591.
(144) Hoffmann, F.; Cornelius, M.; Morell, J.; Fröba, M. *Angew. Chem. Int. Ed.*, **2006**, *45*, 3216–3251.
(145) Mutin, P. H.; Vioux, A. *Chem. Mater.*, **2009**, *21*, 582–596.
(146) Niederberger, M.; Garnweitner, G. *Chemistry - Eur. J.*, **2006**, *12*, 7282–7302.
(147) Avnir, D.; Coradin, T.; Lev, O.; Livage, J. *J. Mater. Chem.*, **2006**, *16*, 1013-1030.
(148) Park, J.; Joo, J.; Kwon, S. G.; Jang, Y.; Hyeon, T. *Angew. Chem. Int. Ed.*, **2007**, *46*, 4630–4660.
(149) Cölfen, H.; Mann, S. *Angew. Chem. Int. Ed.*, **2003**, *42*, 2350–2365.
(150) Vallet-Regí, M.; Balas, F.; Arcos, D. *Angew. Chem. Int. Ed.*, **2007**, *46*, 7548–7558.
(151) Soler-Illia, G. J. de A. A.; Sanchez, C.; Lebeau, B.; Patarin, J. *Chem. Rev*,. **2002**, *102*, 4093–4138.
(152) Stein, A. *Micropo Mesopor Mater*., **2001**, *44*, 227-239.
(153) Niederberger, M. *Acc. Chem. Res.*, **2007**, *40*, 793–800.
(154) Ruiz-Hitzky, E.; Darder, M.; Aranda, P.; Ariga, K. *Adv. Mater.*, **2010**, *22*, 323–336.
(155) Ryoo, R.; Joo, S. H.; Kruk, M.; Jaroniec, M. *Adv. Mater*., **2001**, *13*, 677-681.
(156) Cotí, K. K.; Belowich, M. E.; Liong, M.; Ambrogio, M. W.; Lau, Y. A.; Khatib, H. A.; Zink, J. I.; Khashab, N. M.; Stoddart, J. F. *Nanoscale*, **2009**, *1*, 16-39.
(157) Jun, Y.; Choi, J.; Cheon, J. *Angew. Chem. Int. Ed.*, **2006**, *45*, 3414–3439.
(158) Wang, X.; Maeda, K.; Thomas, A.; Takanabe, K.; Xin, G.; Carlsson, J. M.; Domen, K.; Antonietti, M. *Nat. Mater.*, **2009**, *8*, 76–80.
(159) Ozin, G. A. *Chem. Commun.*, **2000**, 419–432.
(160) Wan, Y.; Shi, Y.; Zhao, D. *Chem. Mater.*, **2008**, *20*, 932–945.

(161) Robinson, R. D.; Sadtler, B.; Demchenko, D. O.; Erdonmez, C. K.; Wang, L.-W.; Alivisatos, A. P. *Science*, **2007**, *317*, 355–358.
(162) Corma, A.; García, H. *Chem. Rev.*, **2003**, *103*, 4307–4366.
(163) Miszta, K.; Graaf, J. de; Bertoni, G.; Dorfs, D.; Brescia, R.; Marras, S.; Ceseracciu, L.; Cingolani, R.; Roij, R. van; Dijkstra, M.; Manna, L. *Nat Mater*, **2011**, *10*, 872–876.
(164) Férey, G. *Chem. Mater.*, **2001**, *13*, 3084–3098.
(165) Ye, X.; Collins, J. E.; Kang, Y.; Chen, J.; Chen, D. T. N.; Yodh, A. G.; Murray, C. B. *Proc. Natl. Acad. Sci.*, **2010**, *107*, 22430–22435.
(166) Meldrum, F. C.; Cölfen, H. *Chem. Rev.*, **2008**, *108*, 4332–4432.
(167) Antonietti, M.; Ozin, G. A. *Chemistry - Eur. J.*, **2004**, *10*, 28–41.
(168) Yin, Y.; Alivisatos, A. P. *Nature*, **2005**, *437*, 664–670.
(169) Sanchez, C.; Soler-Illia, G. J. de A. A.; Ribot, F.; Lalot, T.; Mayer, C. R.; Cabuil, V. *Chem. Mater.*, **2001**, *13*, 3061–3083.
(170) Shi, Y.; Wan, Y.; Zhao, D. *Chem. Soc. Rev.*, **2011**, *40*, 1107-1150.
(171) Kalsin, A. M. *Science*, **2006**, *312*, 420–424.
(172) Sanchez, C. *et al.*, *Chem. Mater.*, **2014**, 26, 221-238.
(173) Schüth, F. *Chem. Mater.*, **2001**, *13*, 3184–3195.
(174) Parak, J.W. *et al.*, *Nanotechnology*, **2003**, *14*, R15-R27.
(175) Kanamori, K.; Nakanishi, K. *Chem. Soc. Rev.*, **2011**, *40*, 754-770.
(176) Deka, S.; Miszta, K.; Dorfs, D.; Genovese, A.; Bertoni, G.; Manna, L. *Nano Lett.*, **2010**, *10*, 3770–3776.
(177) Kitagawa, S.; Kitaura, R.; Noro, S. *Angew. Chem. Int. Ed.*, **2004**, *43*, 2334–2375.
(178) Chung, I.; Kanatzidis, M. G. *Chem. Mater.*, **2014**, *26*, 849–869.
(179) Duguet, E.; Desert, A.,Perro, A., Ravaine, S. *Chem. Soc. Rev.*, **2011**, *40*, 941-960.
(180) Aifantis, K.E.; Hackney, S.A.; Kumar, R.V.; Eds, in *High Energy Density Lithium Batteries*: *Materials, Engineering, Applications*, **2010**, Wiley.
(181) Kim, J. Y.; Voznyy, O.; Zhitomirsky, D.; Sargent, E. H. *Adv. Mater.*, **2013**, *25*, 4986–5010.
(182) Mizoshita, N.; Tani, T.; Inagaki, S. *Chem. Soc. Rev.*, **2011**, *40*, 789-800.
(183) Baghbanzadeh, M.; Carbone, L.; Cozzoli, P. D.; Kappe, C. O. *Angew. Chem. Int. Ed.*, **2011**, *50*, 11312–11359.
(184) Grosso, D.; Ribot, F.;Biossiere, C.; Sanchez, C. *Chem. Soc. Rev.*, **2011**, *40*, 829-848.
(185) Corriu, R.; Leclercq, D.; *Angew. Chem. Int. Ed.*, **1996**, *35*, 1420–1436.
(186) Loy, D. A.; Shea, K. J. *Chem. Rev.*, **1995**, 95, 1431-1442.
(187) Ruiz-Hitzky, E.; Aranda, P.; Darder, M.; Ogawa, M. *Chem. Soc. Rev.*, **2011**, *40*, 801-828.
(188) Muramatsu, H.; Corriu, R.; Boury, B. *J. Am. Chem. Soc.*, **2003**, *125*, 854–855.
(189) a) Boury, B.; Corriu, R. *Chem. Rec.*, **2003**, *3*, 120–132.
b) Brinker, C. J.; Scherer, G.W.; Eds, in *Sol-gel Science: The Physics and Chemistry of Sol-Gel Processing*, **1990**, Academic Press.
c) Ribot, F.; Toledano, P.; Sanchez, C. Chem. Mater., **1991**, *3*, 759-764.
d) Iler, R.K., in *The Chemistry of Silica*, **1979**, Wiley.
(190) Welton, T. *Chem. Rev.*, **1999**, *99*, 2071–2084.
(191) Armand, M.; Endres, F.; MacFarlane, D. R.; Ohno, H.; Scrosati, B. *Nat. Mater.*, **2009**, *8*, 621–629.
(192) Garcia, B.; Lavallée, S.; Perron, G.; Michot, C.; Armand, M. *Electrochim. Acta*, **2004**, *49*, 4583–4588.
(193) Lewandowski, A.; Świderska-Mocek, A. *J. Power Sources*, **2009**, *194*, 601–609.
(194) Fernicola, A.; Croce, F.; Scrosati, B.; Watanabe, T.; Ohno, H. *J. Power Sources*, **2007**, *174*, 342–348.
(195) Sato, T.; Maruo, T.; Marukane, S.; Takagi, K. *J. Power Sources*, **2004**, *138*, 253–261.
(196) Guerfi, A.; Dontigny, M.; Charest, P.; Petitclerc, M.; Lagacé, M.; Vijh, A.; Zaghib, K. *J. Power Sources*, **2010**, *195*, 845–852.
(197) Sugimoto, T.; Atsumi, Y.; Kikuta, M.; Ishiko, E.; Kono, M.; Ishikawa, M. *J. Power Sources*, **2009**, *189*, 802–805.
(198) Galiński, M.; Lewandowski, A.; Stępniak, I. *Electrochim. Acta*, **2006**, *51*, 5567–5580.
(199) Fujinami, T.; Mehta, M. A.; Sugie, K.; Mori, K. *Electrochim. Acta*, **2000**, *45*, 1181–1186.

(200) Mehta, M. A.; Fujinami, T.; Inoue, T. *J. Power Sources*, **1999**, *81–82*, 724–728.
(201) Mehta, M. A.; Fujinami, T. *Solid State Ionics*, **1998**, *113–115*, 187–192.
(202) Shankar, S.; Matsumi, N. *Polym. Bull.*, **2012**, *68*, 721-727.
(203) Miyata, M.; Matsumi, N.; Chujo, Y. *Polym. Bull.*, **1999**, *42*, 505-510.
(204) Matsumi, N.; Mizumo, T.; Ohno, H. *Polym. Bull.*, **2004**, *51*, *389-394*.
(205) Matsumi, N.; Nakashiba, M.; Ohno, H. *Polym. Bull.*, **2003**, *50*, 259-264.
(206) Matsumi, N.; Sugai, K.; Ohno, H. *Macromolecules*, **2003**, *36*, 2321–2326.
(207) Matsumi, N.; Kotera, K.; Chujo, Y. *Macromolecules*, **2000**, *33*, 2801–2806.
(208) Matsumi, N.; Sugai, K.; Ohno, H. *Macromolecules*, **2002**, *35*, 5731–5733.
(209) Matsumi, N.; Sugai, K.; Miyake, M.; Ohno, H. *Macromolecules*, **2006**, *39*, 6924–6927.
(210) Matsumi, N.; Sugai, K.; Sakamoto, K.; Mizumo, T.; Ohno, H. *Macromolecules*, **2005**, *38*, 4951–4954.
(211) Smaran, K. S.; Vedarajan, R.; Matsumi, N. *Int. J. Hydrog. Energy*, **2014**, *39*, 2936–2942.
(212) Di Noto, V.; Lavina, S.; Giffin, G. A.; Negro, E.; Scrosati, B. *Electrochim. Acta*, **2011**, *57*, 4-13.
(213) Galiński, M.; Lewandowski, A.; Stępniak, I. *Electrochim. Acta*, **2006**, *51*, 5567-5580.
(214) Nakagawa, H.; Fujino, Y.; Kozono, S.; Katayama, Y.; Nukuda, T.; Sakaebe, H.; Matsumoto, H.; Tatsumi, K. *J. Power Sources*, **2007**, *174*, 1021-1026.
(215) Tsunashima, K.; Sugiya, M. *Electrochim. Commun.*, **2007**, *9*, 2353-2358.
(216) Matsumoto, H.; Sakaebe, H.; Tatsumi, K. *J. Power Sources*, **2005**, *146*, 45-50.
(217) Ishikawa, M.; Sugimoto, T.; Kikuta, M.; Ishiko, E.; Kono, M. *J. Power Sources*, **2006**, *162*, 658-662.
(218) Handa, N.; Sugimoto, T.; Yamagata, M.; Kikuta, M.; Kono M; Ishikawa, M. *J. Power Sources*, **2008**, *185*, 1585-1588.
(219) Sugimoto, T.; Atsumi, Y.; Kikuta, M.; Ishiko, E.; Kono, M.; Ishikawa, M. *J. Power Sources*, **2009**, *189*, 802-805.
(220) Matsui, Y.; Yamagata, M.; Murakami, S.; Saito, Y.; Higashizaki, T.; Ishiko, E.; Kono, M.; Ishikawa, M. *J. Power Sources*, **2015**, *279*, 766-773.
(221) Tsunashima, K.; Sugiya, M. *Electrochem. Commun.*, **2007**, *9*, 2353-2358.
(222) Sakaebe, H.; Matsumoto, H. *Electrochem. Commun.*, **2003**, *5*, 594-598.
(223) Macfarlane, D.R.; Pringle, J.M.; Howlett, P.C.; Forsyth, M.; *Phys Chem Chem Phys*, **2010**, *12*, 1659-1669.
(224) Moretti, A.; Jeong, S.; Giffin, G.A.; Jeremias, S.; Passerini, S. *J. Power Sources*, **2014**, *269*, 645-650.
(225) Guerfi, A.; Dontigny, M.; Charest, P.; Petitclerc, M.; Lagace, M.; Vijh, A.; Zaghib, A. *J. Power Sources*, **2010**, *195*, 845-852.
(226) Ohno, H.; Ito, K. *Chem Lett*, **1998,** *27*, 751-752.
(227) Nishimura, N.; Ohno, H. *Polymer*, **2014**, *55*, 3289-3297.
(228) Ohno, H.; Yoshizawa, M.; Ogihara, W. *Electrochim. Acta*, **2004**, *50*, 255-261.
(229) Young, W.S.; Kuan, W.F.; Epps, T.H. J. *Polym. Sci. B Polym. Phys.*, **2013**, *52*, 1-16.
(230) Elabd. Y. *et al.*, *Macromolecules*, **2011**, *44*, 5727–5735.
(231) McBreen, J.; Lee, H.S.; Yang, X.Q.; Sun, X. *J. Power Sources*, **2000**, *89*, 163-167.
(232) Aihara, Y.; Kuratomi, J.; Bando, T.; Iguchi, T.; Yoshida, H.; Ono, T.; Kuwana, K. *J. Power Sources*, **2003**, *114*, 96-104.
(233) Tabata, S.; Hirakimoto, T.; Tokuda, H.; Susan, M. A. B.; Watanabe, M. *J. Phys. Chem. B*, **2004**, *108*, 19518-19526.
(234) Matsumi, N.; Miyake, M.; Ohno, H. *Chem. Commun.*, **2004**, 2852-2853.
(235) Mizumo, T.; Watanabe, T.; Matsumi, N.; Ohno, H. *Polym. Adv. Technol.*, **2008**, *19*, 1445-1450.
(236) Matsumi, N.; Nakamura, K.; Aoi, K.; Watanabe, T.; Mizumo, T.; Ohno, H. *Polym J.*, **2009**, *41*, 437-441.

Chapter 2

Design of Organic-inorganic Hybrid Ion-gel Electrolytes Composed of Borosilicate and Allylimidazolium Type Ionic Liquids

2.1 Abstract

Research towards the design of novel electrolytes for the development of safer and efficient Li-ion batteries has gained widespread momentum in recent years. Design of novel borosilicate glass/ionic liquid hybrid type electrolyte was undertaken. Organic-inorganic hybrids have the dual advantages of high ionic conductivity due to the organic component and high thermal stability due to the inorganic component. In the present work, an *in-situ* sol-gel method using alkoxysilanes and alkoxyboranes was carried out, in the presence of low viscous ionic liquids. This resulted in the formation of highly homogenous organic-inorganic hybrids. A low viscous diallylimidazolium type ionic liquid was employed as the organic component. Arrhenius plots evinced constant temperature dependence of ionic conductivity. A maximum ionic conductivity of 2.0 $mScm^{-1}$ at 51°C, was observed among the prepared hybrids. $LiPF_6$ based hybrids showed higher ionic conductivity due to larger phase separation order of organic and inorganic components which enables better connection of ion-conductive organic components. LiTFSA based hybrids were highly homogenous while $LiPF_6$ based hybrids were heterogeneous in nature, with an external porous layer followed by a homogenous layer underneath.

2.2 Introduction

With increasing dependence on portable electronic gadgets in our daily lives, there is an increasing demand for safe and time-durable energy storage devices. Lithium ion secondary batteries (LiBs) are widely employed in various electronic appliances like laptops, mobiles and even in the automobile hybrids. LiBs have greater energy density compared with the conventional batteries such as Ni-Cd and Ni-hydrogen batteries. However, safety issue with the presently used electrolytes in the LiBs is a grey area which needs to be addressed. Ethylene carbonate and propylene carbonate are commonly used electrolytes in the LiBs, and both of them are highly flammable. Thus, extensive researches have been conducted to explore novel non-flammable electrolyte materials.[1,2]

LiBs using non-liquid electrolytes are deemed safer and reliable than the conventional liquid electrolytes. Much attention has been focussed on the use of dry solid polymer or polymer gel electrolytes or composite polymer electrolytes. On the other hand, ionic liquids (ILs) have gained considerable popularity in research field on account of their properties such as low viscosity, non-volatility, thermal stability etc.[3–6] Use of ionic liquids in the design of novel electrolytes in the lithium rechargeable batteries has been a significant area of research.[7]

Ionic liquids have been valuable component in the design of these electrolytes on account of their stability at high temperatures and considerable ionic conductivity.[3,8–15] To further improve the ion conductive characteristics of IL based electrolytes, incorporation of boron into the matrices was found to be an effective approach.[16–18] Boron atom facilitates the dissociation of the lithium salt and further traps the anion, enhancing the cationic conduction. Various types of organoboron polymers with enhanced ionic conductance profiles have been reported.[19–33] Keeping in view the enhancement of ionic conductivity or lithium ion transference number via boron incorporation, the concept of organic-inorganic composite hybrids including borosilicate glass should be an attractive approach.

Borosilicates are relatively softer material compared with silicates, and are also more stable than organoboron compounds.

Previously, borosilicate based ion-gel electrolytes prepared via *in-situ* polymerization of the ionic liquid component was reported by Ohno *et al*.[34] In those systems, significant enhancement of ionic conductivity was observed in the presence of appropriate amount of boron in borosilicate glass. However, such hybrids prepared by *in-situ* polymerization of ionic liquid monomer was mechanically too brittle to allow device fabrication. In the present work, preparation of a series of novel borosilicate based ion-gels were undertaken in the presence of low viscous allylimidazolium type ionic liquids without the polymerization of ionic liquid component. Use of low viscous allylimidazolium type ionic liquid should lead to improved ion-conductive properties of the resulting hybrids. Effect of morphological factor on ion-conductive properties of the hybrids was also studied.

2.3 Experiment

2.3.1 Materials and Instruments

The ionic liquid, 1,3-diallylimidazolium TFSA was synthesized by the reaction between 1-allylimidazole and allylchloride, followed by an ion-exchange reaction using LiTFSA (lithium bis(trifluoromethylsulfonyl)amide). Commercially available trimethoxyborane (TMB), LiTFSA and $LiPF_6$ (Wako chemicals), tetramethylorthosilicate (TMOS) (Shin-Etsu Chemical Co. Ltd.) were purchased and were used without further purification. Similarly, lithium sheets were purchased from Honjo Chemical Co. Ltd. Mesityldimethoxyborane (MDMB) was synthesized according to the literature.[20a] The IR spectra of the hybrids were measured on a JASCO FT-IR420 (JASCO). The ionic conductivity for the organic-inorganic hybrids were evaluated by complex impedance method on a Solartron 1260 impedance analyser using an AC amplitude of 100 mV and in the frequency range of1MHz-0.1Hz over a temperature range of 30-60 ^{o}C. The sample was sandwiched between two blocks of gold-plated blocking electrodes. All samples were thoroughly dried *in vacuo* at 100 ^{o}C overnight before use. The temperature dependence of ionic conductivity was studied over a range of

30-60 °C . Ionic conductivity was measured at an interval of every 3 degree starting from 30 °C extending till 60 °C. Comparison of ionic conductivity value was done at 51°C as general operational temperature of LiBs is around 50 °C. The present study is a purely empirical study which focusses the behaviour of the electrolyte over a range of temperature. When it comes to fabrication of devices using such electrolytes, it's imperative to know the behaviour of an electrolyte around this temperature range. The apparent lithium ion transference number (t_{Li}^{+}) was estimated according to the method of Evans *et al*. (Equation 1)[20b] The polarization current obtained from DC chronoamperometric data and the charge transfer resistance values between the electrolyte/lithium metal electrodes observed from the impedance spectra were substituted in the Evans-Vincent-Bruce equation, where I_o and I_s, respectively denote the initial state and steady state current. Here, R_o and R_s denote the charge transfer resistance at the initial and at steady state, respectively

$$t_{Li^+} = \frac{I_{(s)}\ [\Delta V - I_o R_o]}{I_{(o)}\ [\Delta V - I_s R_s]} \qquad [1]$$

All the measurements were carried out under an argon atmosphere. Estimation of lithium ion transference number was carried out by sandwiching the organic-inorganic hybrid between identical Li electrodes using potentiostat coupled with Frequency Response Analyser (Versastat-3; Princeton Applied Research Co. Ltd.). Scanning Electron Microscopy (SEM) analyses were carried out on a Hitachi S-4600. Before detailing the results and discussion section on the temperature dependence of ionic conductivity of the organic-inorganic hybrids, it will be imperative to bring a perspective on the underlying theory behind such experimental protocol.

2.3.2 Electrochemical Impedance Spectroscopy

Electrochemical Impedance Spectroscopy (EIS) technique is a powerful and effective technique. It is employed in the investigation of mechanisms in electrochemical reactions, in the measurement of dielectric and transport properties of materials, in the exploration of porous

electrodes, and in the analysis of passive surfaces. The following Figure 2.1, gives an idea about the various characteristic features of EIS technique:

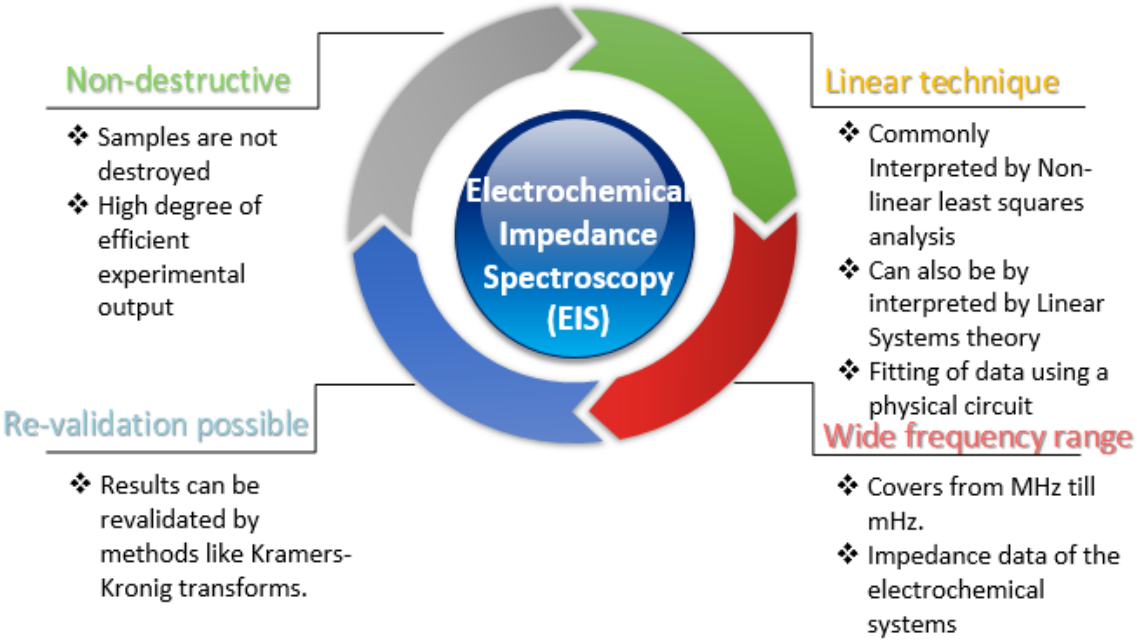

Figure 2.1 Characteristics of Electrochemical Impedance Spectroscopic (EIS) technique

Thus, impedance data has been regarded as a gateway towards understanding the internal principles of batteries. The cell impedance receives its contributions not only from the electrodes but the electrolyte as well. It's a well-known fact that SEI (Solid-Electrolyte Interphase) layer on the electrode surface plays a significant role in determining the performance, stability and durability of the batteries. Considering the complexity of the physical elements, the impedance response in a cell or battery project the following inferences:

- R_s (resistance of the bulk electrolyte)
- C_{dl} (double layer capacitance at the interfacial region)
- R_{ct} (charge-transfer resistance)
- Z_w or W (Warburg impedance)

R_s is the resistance offered to the mobile ions due to the inherent features of the electrolyte material and is often independent of potential, since, it's driven by concentration gradient. While C_{dl} is observed due to charge accumulation on the interfacial regions, R_{ct} (charge-transfer resistance)

refers to the transfer of the charge from the bulk electrolyte to electrode material, at the interfacial region. Since, it's a solid-state diffusion process, it's often a potential dependent process, which is observed as a semicircle in the Nyquist plot. Further, Warburg impedance is also observed in the Nyquist plots, which often arises due to the slow solid-state diffusion of the ions. Due to several of these factors operational in the cell, an ideal capacitor element is hardly observed. Instead a constant phase element (CPE) is observed which, more or less refers to a capacitor afflicted by non-uniform charge distribution. (These elements are depicted in Figure 2.3)

The experimental and analysis protocol of Impedance experiments can be shown in the following flowchart (Figure 2.2):

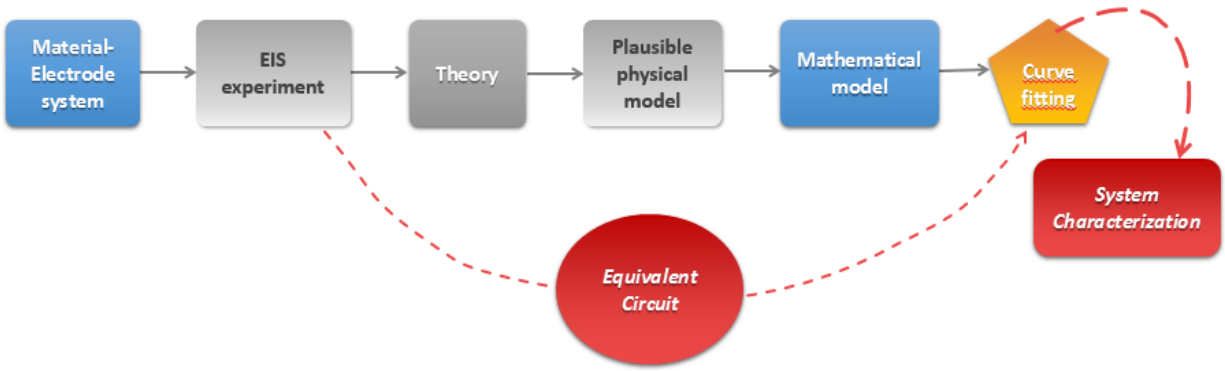

Figure 2.2 Flowchart depicting the experimental for Electrochemical Impedance Spectroscopic (EIS) Experiments

An equivalent circuit model amounting to an electrical circuit consists of various elements such as resistor (R), Capacitor (C), Constant Phase element (CPE), Warburg impedance (W), etc. A Nyquist plot along with a commonly used equivalent circuit is shown below in Figure 2.3:

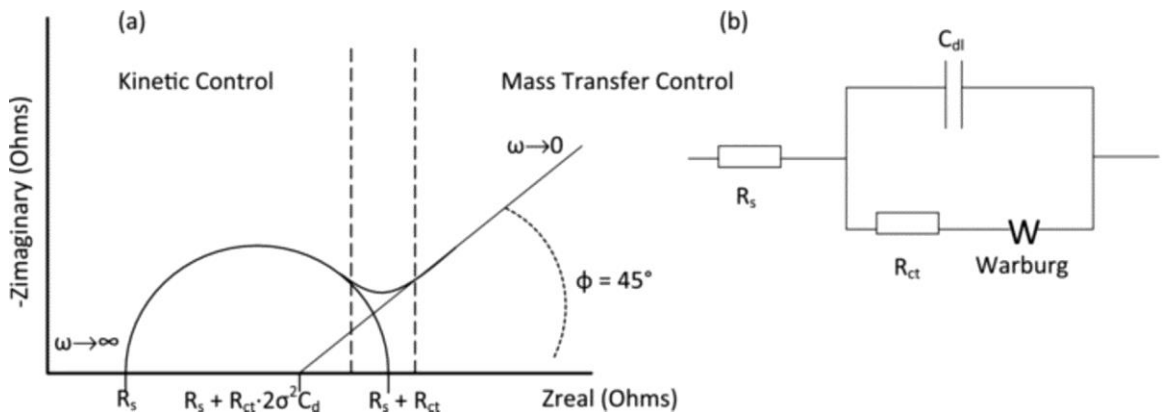

Figure 2.3 a) A typical Nyquist or Cole-Cole plot b) Commonly used Randle's circuit for electrochemical circuit fitting analysis

2.3.3 Models for Ionic conductivity

Impedance profiles are often obtained over a range of temperature, to see the behavioural pattern of the electrode and the electrolyte. The conductivity data processed from the impedance profiles is further studied with the help of several models which define the conductivity-temperature relationships in a system.

2.3.3.1 Arrhenius model

The Arrhenius equation can be represented by the equation:

$$\sigma = \sigma_o e^{\left(\frac{-E_a}{kT}\right)} \text{ Or } \sigma = Ae^{\left(\frac{-E_a}{kT}\right)}$$

where σ_o or A refers to the pre-exponential factor or the carrier ion number. E_a refers to the activation energy, κ ($1.38e^{-23}$ $m^2kgs^{-2}K^{-1}$)is the Boltzmann constant, while, T is the absolute temperature. A linear plot of ln σ vs $10^3/T$ is referred to as the typical Arrhenius behaviour. While, a non-linear plot indicates about a transition state in the material within the experimental range.

2.3.3.2 Vogel-Fulcher Tammann (VFT) model

The VFT model explains the ionic conduction by the help of free volume theory. This theory claims that, the segmental motion of polymer electrolyte systems assists the coordinated movement of the concerned mobile charge, resulting in the diffusion of the ions in the matrix, under the influence of an electric field. The VFT equation can be represented as:

$$\sigma = \frac{A}{\sqrt{T}} e\left(\frac{-B}{k(T - T_o)}\right)$$

where σ_o or A refers to the pre-exponential factor or the carrier ion number. B refers to the pseudo-activation energy, k is the Boltzmann constant, while T is the absolute temperature, while T_o is the ideal glass transition temperature, ideally in the range of 50K-70K lower than the experimental glass transition temperature.

2.3.4 Preparation of organic-inorganic hybrid ion-gels

A typical procedure for the preparation of the organic-inorganic hybrid ion-gel is as follows; to 0.43g (1.0 mmol) of 1,3-diallylimidazolium TFSA, 0.38g (2.5 mmol) of tetramethylorthosilicate (TMOS) was added. Further, requisite amount of alkoxyboranes [$B(OCH_3)_3$ or $MesB(OCH_3)_2$] was added along with unimolar quantity of lithium salt (LiTFSA or $LiPF_6$). Then, 0.16g (5.0 mmol) of methanol was added in the presence of 0.06g of 1.0 N HCl aq., as the catalyst. Finally, 2.5 ml of acetonitrile was added and the mixture was stirred at room temperature for 3 hours. The resulting mixture was further dried at 60 °C for a week. The mixture gradually converted into a film. The reaction scheme concerning the sol-gel synthesis is illustrated in Scheme 2.1.

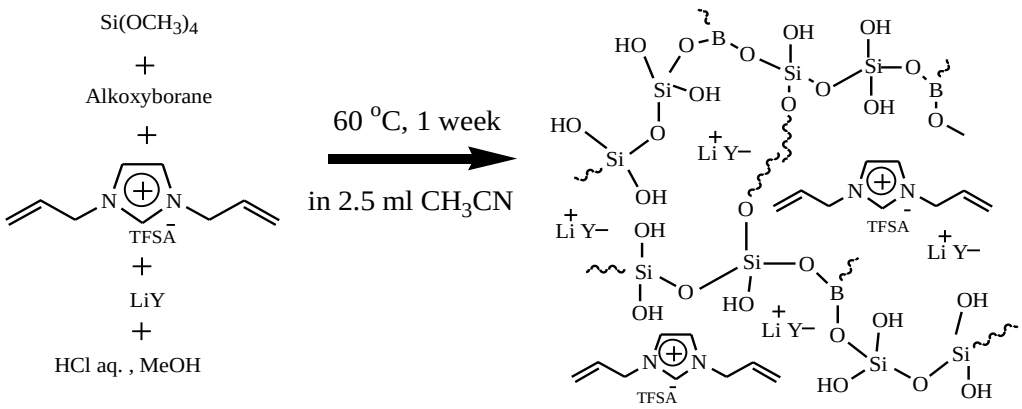

Scheme 2.1 Synthesis of Organic-inorganic hybrids

alkoxyboranes = [trimethoxyborane or mesityldimethoxyborane] LiY = [LiTFSA or $LiPF_6$]

The hybrids with different loading of alkoxyborane concentrations, as observed by the naked eyes are shown in Figure 2.4

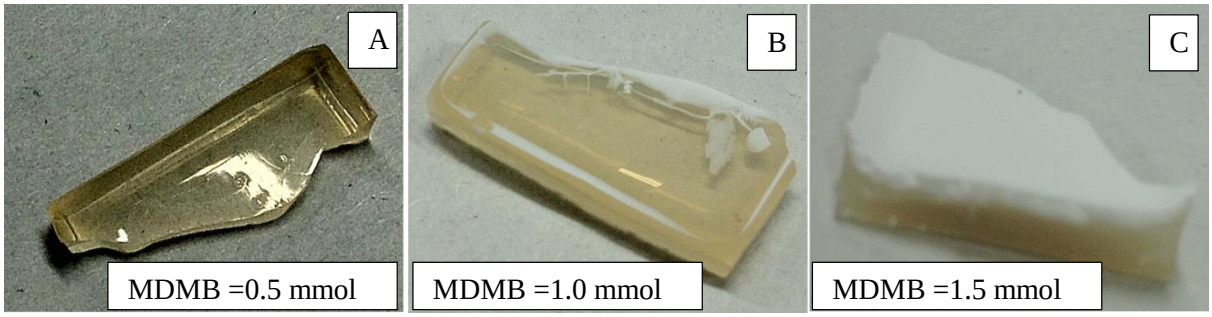

Figure 2.4 LiTFSA based organic-inorganic hybrids with different concentrations of alkoxyborane (MDMB) precursor

2.4 Results and discussion

A series of organic-inorganic hybrids were synthesized by the sol-gel condensation reaction of alkoxysilanes (TMOS=tetramethylorthosilicate) / alkoxyboranes (TMB=trimethoxyborane, MDMB=mesityldimethoxyborane) in the presence of ionic liquid and a lithium salt additive. (Scheme 2.1). The composition chart of the parent matrix of the ion-gel electrolyte matrix is shown in Table 2.1.

Table 2.1 Stoichiometric quantities of the initial reaction mixture

Sample	*IL*	*TMOS*	*TMB*	*MDMB*	*LiTFSA/ $LiPF_6$*	*σ_i at 51°C*	*Appearance*
	g (mmol)	g (mmol)	g (mmol)	g (mmol)	g (mmol)	$mScm^{-1}$	
A	0.43 (1.0)	0.38 (2.5)	-	0.09 (0.5)	0.29 (1.0)	0.20	transparent
B	0.43 (1.0)	0.38 (2.5)	-	0.19 (1.0)	0.29 (1.0)	0.08	transparent
C	0.43 (1.0)	0.38 (2.5)	-	0.28 (1.5)	0.29 (1.0)	0.14	turbid
D	0.43 (1.0)	0.38 (2.5)	0.05 (0.5)	-	0.29 (1.0)	0.30	transparent
E	0.43 (1.0)	0.38 (2.5)	0.1 (1.0)	-	0.29 (1.0)	0.20	transparent
F	0.43 (1.0)	0.38 (2.5)	0.15 (1.5)	-	0.29 (1.0)	0.34	turbid
G	0.43 (1.0)	0.38 (2.5)	-	0.09 (0.5)	0.15 (1.0)	0.10	turbid
H	0.43 (1.0)	0.38 (2.5)	-	0.19 (1.0)	0.15 (1.0)	1.50	turbid
I	0.43 (1.0)	0.38 (2.5)	-	0.28 (1.5)	0.15 (1.0)	0.60	turbid
J	0.43 (1.0)	0.38 (2.5)	0.05 (0.5)	-	0.23 (1.5)	2.00	turbid
K	0.43 (1.0)	0.38 (2.5)	0.1 (1.0)	-	0.23 (1.5)	2.00	turbid
L	0.43 (1.0)	0.38 (2.5)	0.15 (1.5)	-	0.23 (1.5)	1.50	turbid

The transparent and turbid aspects of these samples were determined based on the appearances as depicted in Figure 2.4. Either the presence of white opaque layer or the loss of transparency in a relative basis was termed as turbid. The concentration of boron source was chosen to be the variable component in the compositional matrix in every set of hybrids. Thus, the temperature dependence of ionic conductivity was analyzed for various hybrid ion-gels under different boron concentrations. A comparative account of ionic conductivity in each set of synthesized hybrids can be an effective way to narrow down the anion-trapping effect under doping carriers of hybrid type electrolytes. This approach would help us to determine the optimum concentration of alkoxyborane required for the enhancement of ionic conductivity without excessive anion-trapping

effect. LiTFSA and $LiPF_6$ were used as doping carriers in this study. The molar concentration of the lithium salt was optimized to be equimolar to that of the ionic liquid. The LiTFSA based hybrids

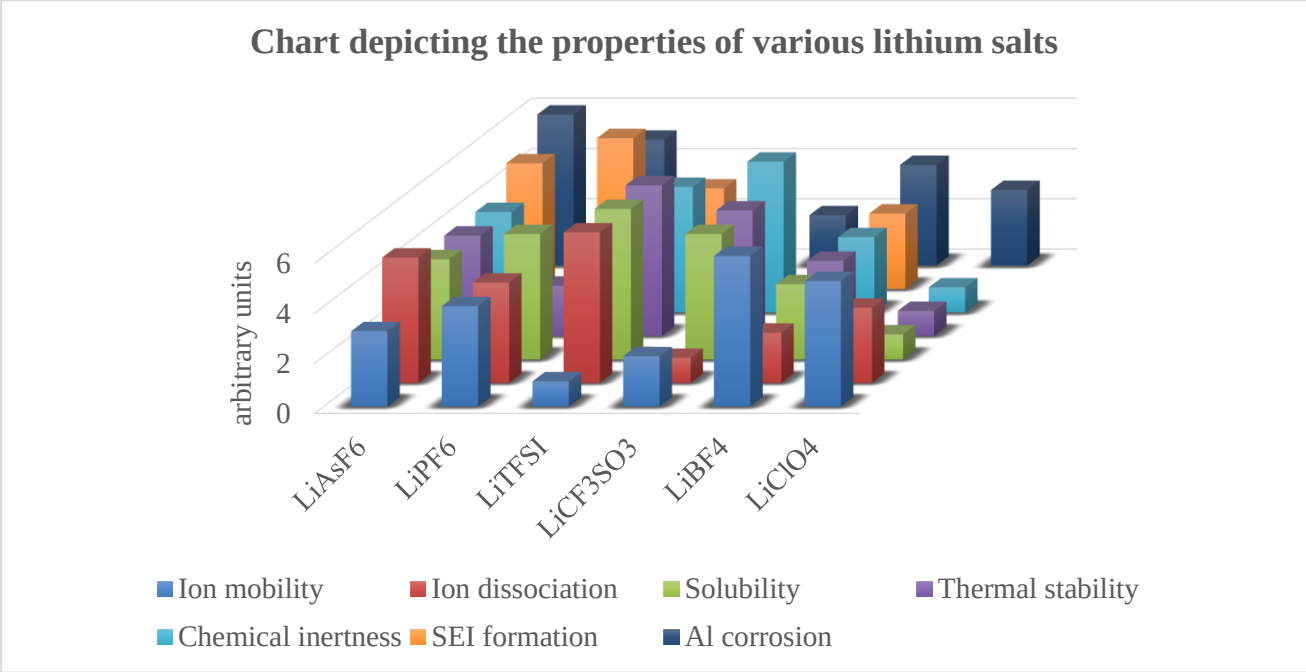

Figure 2.5 Comparative chart of various lithium salts over a wide category of parameters (adapted from 35)

consistently showed a transparent structural fabric, while the $LiPF_6$ based hybrids were almost turbid in all the cases. The choice of lithium salts was based on several factors. The following chart gives a better understanding about such parameters;

Choice of lithium salts: A comparative chart of various commercially available lithium salts such as $LiAsF_6$, $LiPF_6$, LiTFSI, $LiCF_3SO_3$, $LiBF_4$, $LiClO_4$ shows their behaviour in ion mobility, ion dissociation, solubility behaviour, thermal stability, chemical inertness, SEI formation and corrosive properties in arbitrary units. Most of the abovementioned features, play a significant role in determining the longevity and proper functioning of the cell. No particular salt is a clear frontrunner in all the categories. There exists a concerning compromise depending on the area of interest. In this regard, $LiAsF_6$, $LiPF_6$ and LiTFSA/LiTFSI provide a competitive challenge. Due to toxic concerns, $LiAsF_6$ is often not considered. Hence, we are left with two options of salt additives as LiTFSA and $LiPF_6$.

2.4.1 Characterisation of the hybrids

Formation of the borosilicate linkage in the ion-gel matrix was supported by the peaks observed in the FT-IR spectra. Weak absorption bands corresponding to B-O-Si linkage were also observed around 950 cm^{-1}. The absorption bands =C-H vibrations for allylimidazolium groups were observed at around 3100 cm^{-1}. Absence of bands around 2850 cm^{-1} indicate the complete consumption of alkoxysilane moieties in the matrix. Strong bands corresponding to the Si-O stretching were observed in the range of 1000-1100 cm^{-1}. Similarly, B-O stretching was confirmed by strong bands at 1350-1390 cm^{-1}. Representative FT-IR spectra are shown in Figure 2.6-a and Figure 2.6-b.

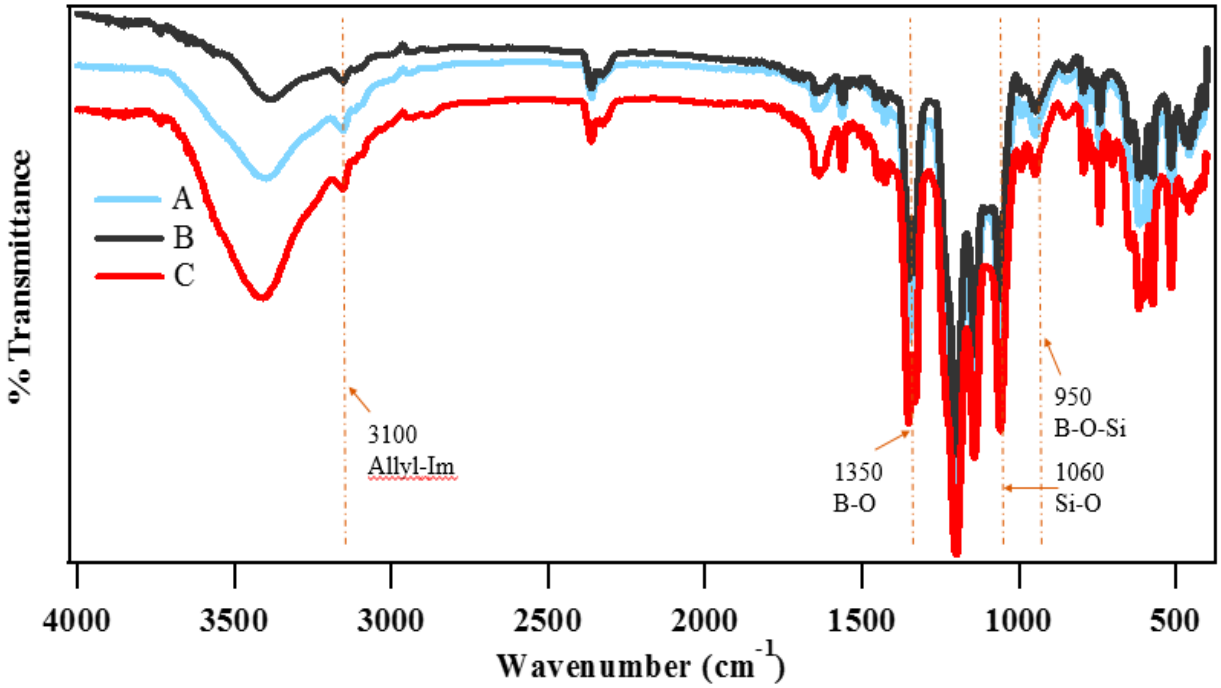

Figure 2.6-a FT-IR spectra of LiTFSA based hybrids A-C

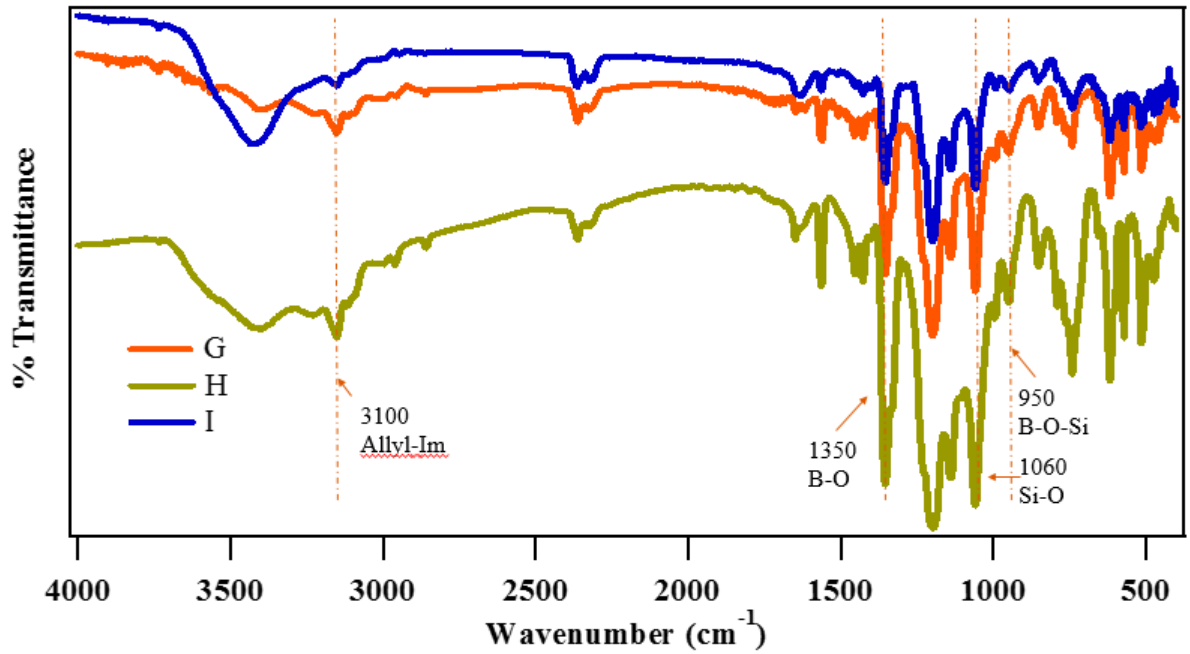

Figure 2.6-b FT-IR spectra of $LiPF_6$ based hybrids G-I

2.4.2 Morphological studies of the hybrids

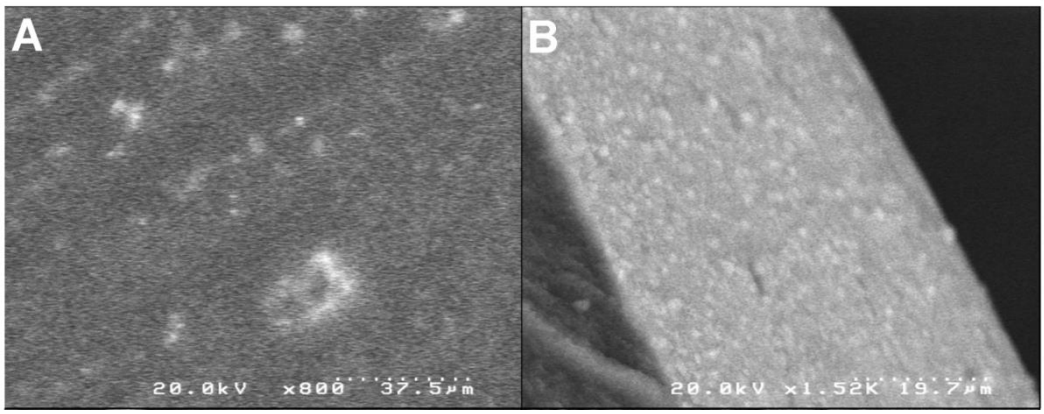

Figure 2.7 SEM micrographs of LiTFSA based hybrids

A) Surface view B) Cross-sectional view

Morphological profiles of the hybrids were determined significantly by the type of lithium salt additive. Figure 2.7, corresponds to a hybrid with LiTFSA additive. The surface view of the LiTFSA based hybrids indicated a homogenous surface which can be attributed to homogenous composition with stronger interactive features between the inorganic and organic matrices mediated by the lithium salt. The cross-section of the samples further revealed that the homogeneous profile of

the LiTFSA based hybrids through the entire thickness of the sample, which was evident from the transparency of the hybrids.

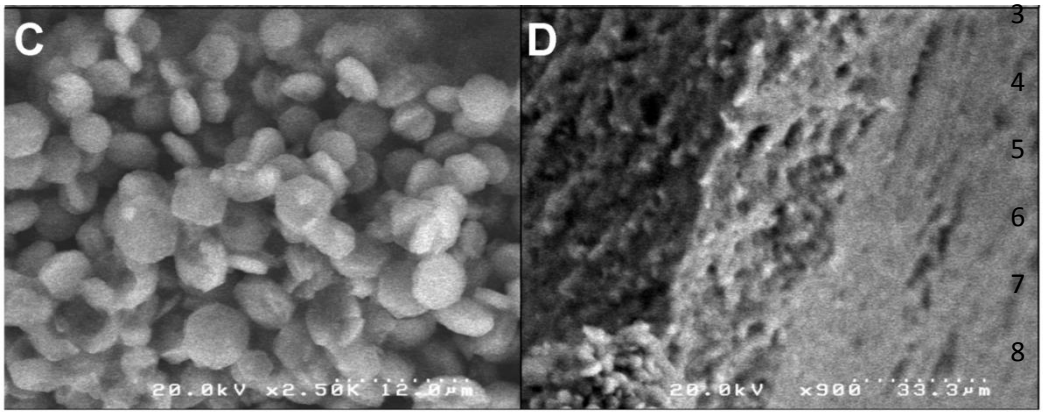

Figure 2.8 SEM micrographs of $LiPF_6$ based hybrids

A) Surface view B) Cross-sectional view

In Figure 2.8, $LiPF_6$ based hybrids showed a heterogenous profile, with discoidal structures on the surface. Further a cross-sectional analysis of the hybrids revealed two layer film, with an external porous layer and a homogenous layer in the bulk. This type of attributes were observed in $LiPF_6$ based hybrids. The morphological studies provided a good understanding about the interactive parameters operating within the sol-gel matrix. Synthesis of silica nanoparticles of similar morphology have been reported via an *in-situ* sol-gel condensation of alkoxysilane precursors in ionic liquids. This explains the discoidal particles on the external layer of the $LiPF_6$ based hybrids.[34] However, any particular mechanism has not been clearly mentioned in any literatures.

2.4.3 Temperature dependence of ionic conductivity of the hybrids

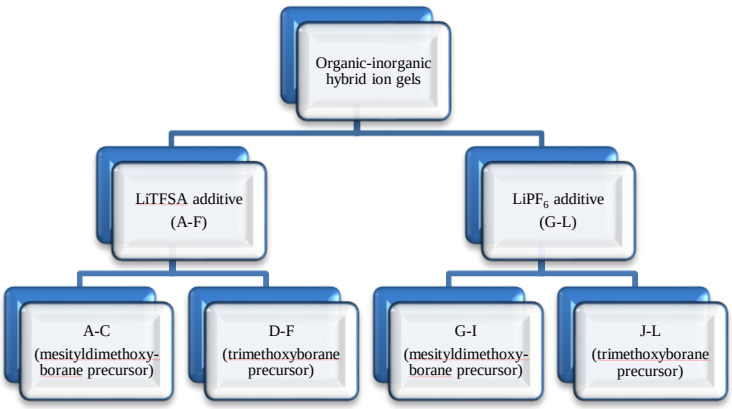

Figure 2.9 Flowchart showing the classification of all the synthesised organic-inorganic hybrids

The overall classification of hybrids, classified on the basis of the type of lithium salt additive and alkoxyborane precursor is shown in the flowchart above. (Figure 2.9)

LiTFSA was used as an additive in the first set of hybrids (A-F). The second set of hybrids (G-L) contained $LiPF_6$ as a lithium salt additive. Hybrid sets (A-C) and (G-I) contained mesityldimethoxyborane (MDMB) as the boron source while sets (D-F) and (J-L) contained trimethoxyborane (TMB). Generally, the samples with LiTFSA additive were transparent in nature at lower concentrations of boron, which can be attributed to the high plasticizing property of LiTFSA. However, transparency was lost and turbid matrices were observed at higher concentrations of boron, possibly because of different kinetics of alkoxy metal monomers.

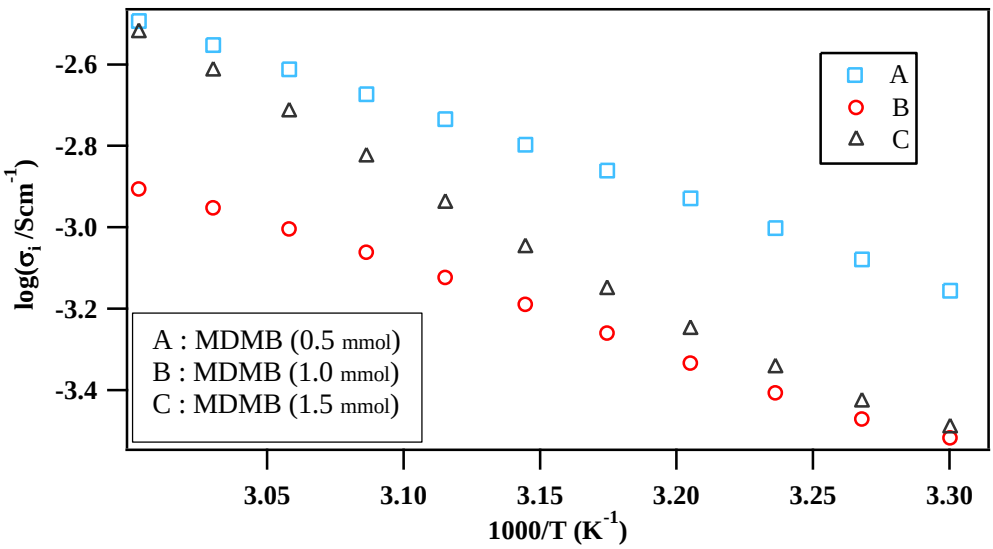

Figure 2.10 Temperature dependence of ionic conductivity of LiTFSA based hybrids A-C

Transparency (homogeneity) of the many LiTFSA based systems can be explained considering the highly plasticizing property of TFSA anion. Ionic conductivity of the obtained organic-inorganic hybrids was evaluated by ac impedance technique after thorough drying of the samples at 100 ºC *in vacuo*. The ionic conductivity observed was in the range of 0.2-2.0 $mScm^{-1}$. The hybrids (A-C) and (G-I) showed constant increase of ionic conductivity with increasing temperature. (Figure 2.10 & 2.11). With the increase of concentration in alkoxyborane above 0.1 mmol, the ionic conductivity decreased. However, there was an improvement in the ionic conductivity after further increase in alkoxyborane concentration.

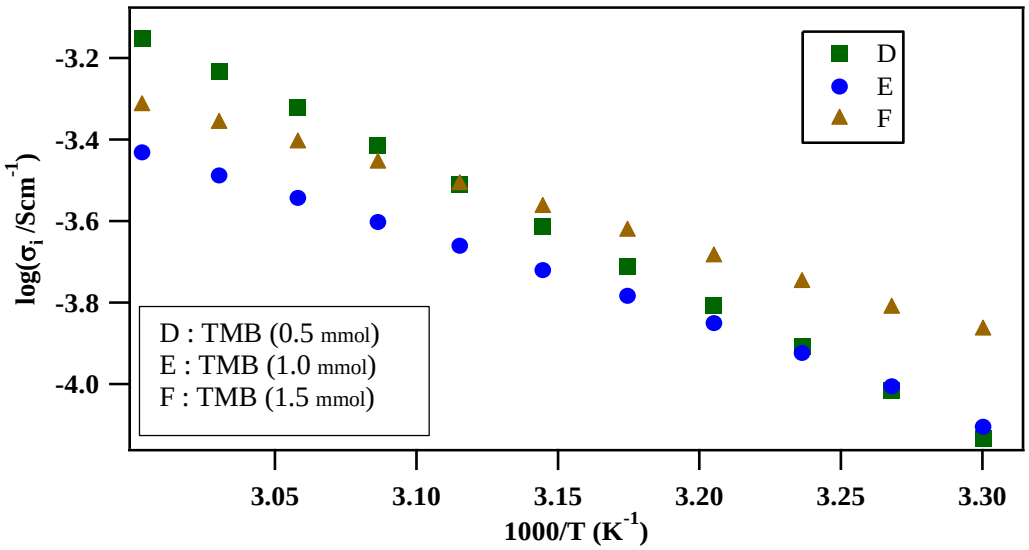

Figure 2.11 Temperature dependence of ionic conductivity of LiTFSA based hybrids D-F

This pattern of ionic conductivity was observed in LiTFSA based hybrids irrespective of the boron sources. The initial drop in ionic conductivity can be explained by considering the decreased carrier ion number under anion trapping of boron. Increase in conductivity parameters is mostly due to morphological factors, due to higher order of phase separation between the constituent phases of organic and inorganic parts, which is evident from the morphological profiles at higher alkoxyborane concentration.

Moreover, the inclusion of $LiPF_6$ additive resulted in a turbid appearance irrespective of the boron concentration. Preliminary investigations have shown that a simple binary mixture of allylimidazolium TFSA and $LiPF_6$ resulted in a heterogenous system. Similarly, a simple silicate matrix containing allylimidazolium TFSA and $LiPF_6$ resulted in a turbid matrix. Therefore in the case of $LiPF_6$ based system, incompatibility of [Allyl Im][TFSA]/ $LiPF_6$ is responsible for the turbidity of the hybrid ion-gel composed of these components. Increase of ionic conductivity under higher borane concentration might be due to the morphological factor.

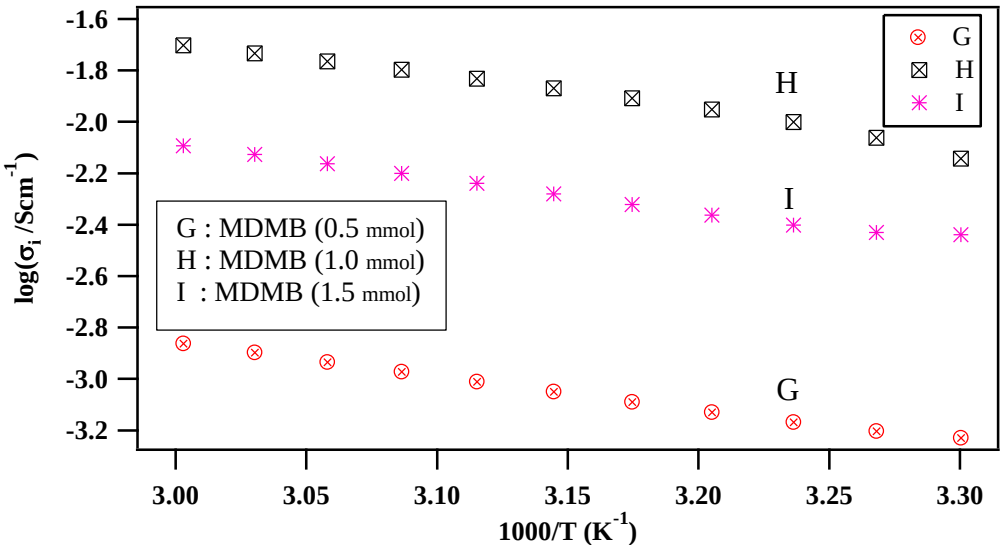

Figure 2.12 Temperature dependence of ionic conductivity of $LiPF_6$ based hybrids G-I

The ionic conductivity range for $LiPF_6$ based hybrids was significantly higher compared to the LiTFSA based hybrids. The ionic conductivity for this class of hybrids also showed monotonous increase with increasing temperature. The ionic conductivity showed a steady rise with the increase in the concentration of borane. However, after a certain concentration, ionic conductivity started to decrease. The enhanced ionic conductivity under low borane concentration should be due to the facilitated lithium salt dissociation via anion-boron interaction. However, with increase in the concentration of boron, the reduced carrier ion numbers was observed owing to the prominent anion trapping effect of the boron moiety.

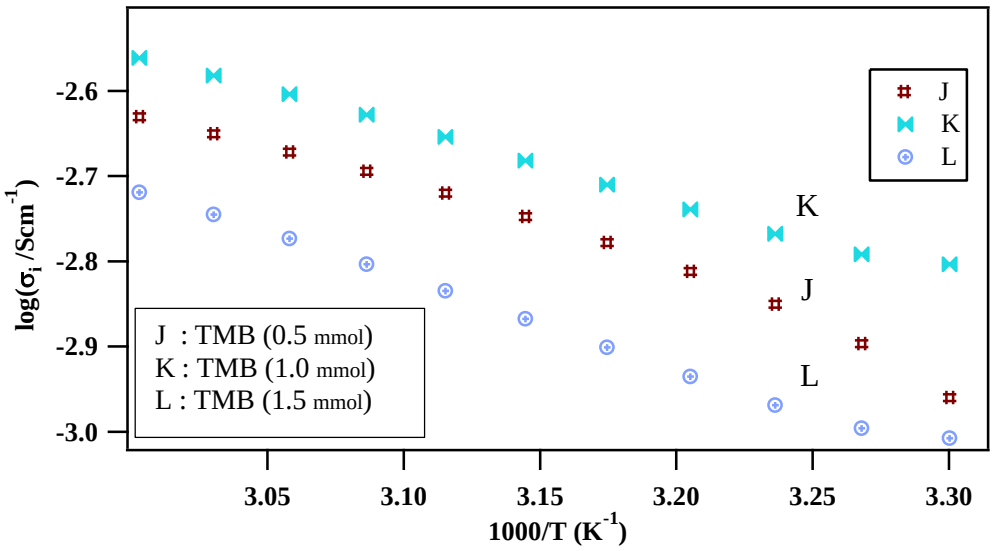

Figure 2.13 Temperature dependence of ionic conductivity of $LiPF_6$ based hybrids J-L

Hence, it hints at the fact that the optimum alkoxyborane concentration for pronounced anion trapping effect differs from trimethoxyborane and mesityldimethoxyborane. While, Set A-C and D-F showed a similar trend. Sets G-I and J-L (Figures 2.12 & 2.13) resembled each other in the conductivity profile.

2.4.4 Study of VFT parameters of the hybrids

VFT (Vogel-Fulcher-Tammann) plots were also fitted as per the linear regression equation to obtain further information on ionic conductivity and other related parameters.

$$\sigma_{i(T)} = \frac{A}{\sqrt{T}} e\left(\frac{-B}{k(T-T_o)}\right) \qquad [\,2\,]$$

In the VFT equation (Equation 2), $\sigma_{i(T)}$ is the ionic conductivity at the temperature T, T_o is ideal glass transition temperature which was optimized to give linear VFT plot. A and B correspond to carrier ion number and activation energy for ion transport, respectively. These parameters along with the respective plots are further discussed in a detailed manner set wise.

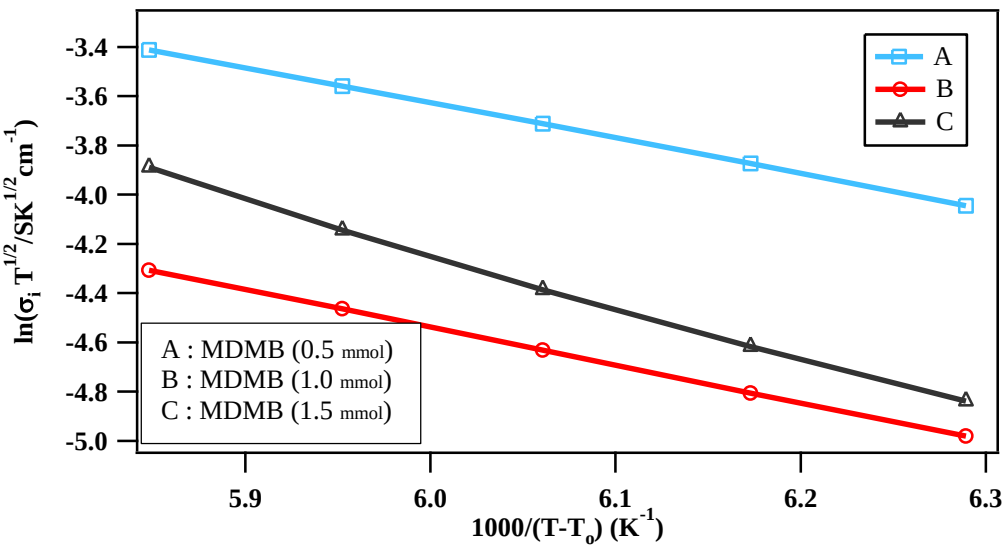

Figure 2.14 VFT plots of hybrids LiTFSA based hybrids A-C

Table 2.2 VFT parameters of LiTFSA based hybrids A-C

Sample	*T_o (K)*	*A ($Scm^{-1}K^{1/2}$)*	*B (K)*	*R^2*	*σ_i ($mScm^{-1}$) at 51°C*
A	150	170.0	1460	0.991	0.20
B	150	40.00	1140	0.994	0.08
C	150	8340	2200	0.990	0.14

The VFT plots of hybrids A-C are shown in Figure 2.14. The hybrid A shows considerably high carrier ion number (A) resulting in high ionic conductivity. While Sample B, although shows reduced activation energy (B), the conductivity is lowered due to lower A values as tabulated in Table 2.2. Further, the values register a decrease in hybrid B. The carrier ion number (A) reaches a maximum in the hybrid C, though a simultaneous increase in activation energy (B) is also observed. This factor along with the morphological factor i.e. increased turbidity helps in improved ionic conductivity although lesser than that of Sample A. Hence, in this set, the observed experimental values are in good correlation with the morphological attributes in defining the ionic conductivity parameters.

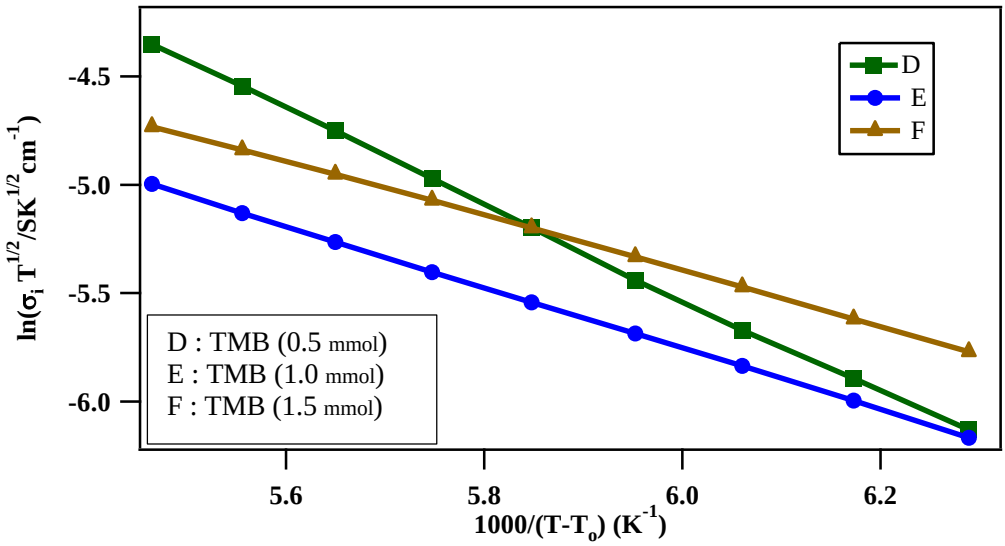

Figure 2.15 VFT plots of hybrids LiTFSA based hybrids D-F

Table 2.3 VFT parameters of LiTFSA based hybrids D-F

Sample	*T_o (K)*	*A ($Scm^{-1}K^{1/2}$)*	*B (K)*	*R^2*	*σ_i ($mScm^{-1}$) at 51°C*
D	150	1660	2160	0.999	0.30
E	150	20.00	1460	0.998	0.20
F	150	8.000	1250	0.999	0.34

The next set of hybrids D-F follows a similar pattern like that of A-C. In the VFT parameters of this set, D-F as depicted in Table 2.3, D is observed to have a balancing effect between carrier ion number (A) and Activation Energy (B), both nullifying each other and thus registering a normal conductivity profile. However, with further increase in the concentration of alkoxyborane precursor, pronounced anion trapping effect is observed due to the dip in ionic conductivity (Figure 2.15). However, further increase in the concentration of alkoxyborane leads to increase in ionic conductivity which is explained well by the morphological studies.

The set (G-I) consisting of $LiPF_6$ salt additive along with different concentrations of mesityldimethoxyborane (MDMB) presents an ionic conductivity pattern quite different from that of TFSA based hybrids. It's evident from the VFT profiles (Figure 2.16) that increase in alkoxyborane concentration increases the conductivity. However, after a threshold concentration there is a downward pattern observed. The low activation energy parameters as shown in Table 2.4 of the given set is well understood by virtue of their heterogeneous structure.

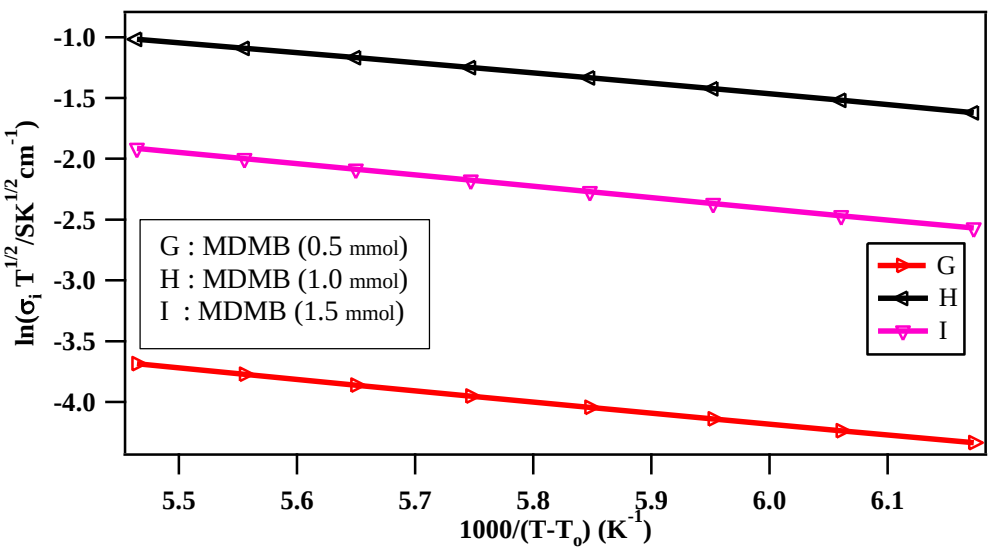

Figure 2.16 VFT plots of hybrids $LiPF_6$ based hybrids G-I

Table 2.4 VFT parameters of $LiPF_6$ based hybrids G-I

Sample	*T_o (K)*	*A ($Scm^{-1}K^{1/2}$)*	*B (K)*	*R^2*	*σ_i ($mScm^{-1}$) at 51°C*
G	150	3.0	860.0	0.995	0.10
H	150	70	950.0	0.990	1.50
I	150	15	840.0	0.987	0.60

The next set of hybrids with trimethoxyborane (TMB) based hybrids with $LiPF_6$ additive also showed a similar pattern like that of its predecessor set G-I as depicted in Figure 2.17. The VFT parameters (Table 2.5) are suggestive about low carrier ion number and low activation energy as well. However, higher order of phase separation, leading to turbidity in the matrix is imminent reason for the increase in ionic conductivity.

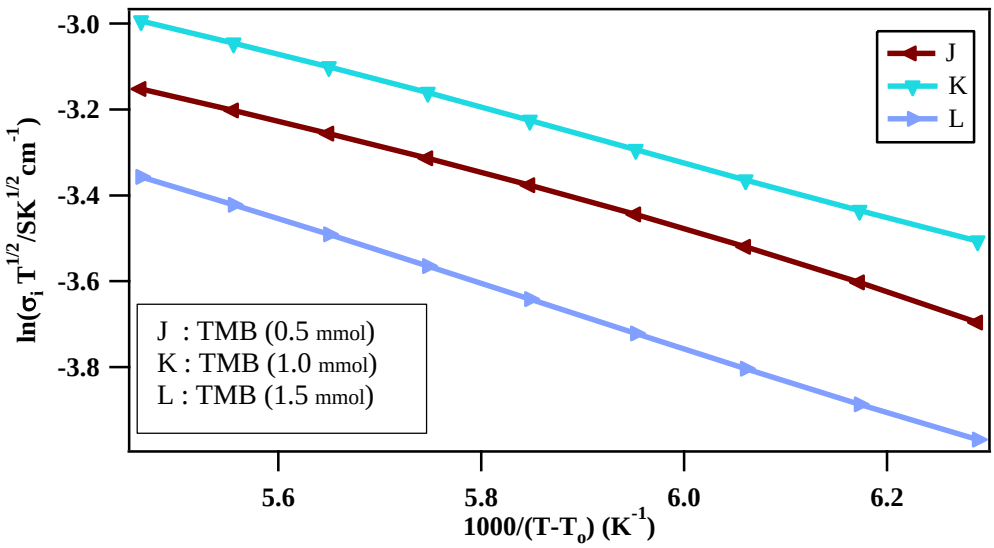

Figure2.17 VFT plots of $LiPF_6$ based hybrids J-L

Table 2.5 VFT parameters of $LiPF_6$ based hybrids J-L

Sample	*T_o (K)*	*A ($Scm^{-1}K^{1/2}$)*	*B (K)*	*R^2*	*σ_i ($mScm^{-1}$) at 51°C*
J	150	2.300	730.0	0.986	2.00
K	150	1.200	590.0	0.993	2.00
L	150	1.600	700.0	0.994	1.50

To conclude, among LiTFSA based hybrids, there exists a notable difference in the carrier ion number parameter (A). However, this was not observed to be dominant factor of ionic conductivity. On the other hand, activation energy (B) significantly affected the ionic conductivity. $LiPF_6$ based hybrids showed higher ionic conductivity which should be due to the lower activation energy parameters different from those with LiTFSA based hybrids. However, the carrier ion numbers for the hybrid with $LiPF_6$ were observed to be extraordinarily low, which does not correlate well with the ionic conductivity data. This may be explained by the fact that the turbidity was due to the larger order of phase separation between the organic moiety and inorganic counterpart. This led to an improvement in the ionic conductivity through better connection between ion conductive organic components. This is in good agreement with lower activation energy for G-L.

2.4.5 Estimation of t_{Li}^+ of the hybrids

t_{Li}^+ stands for the contribution of lithium cation migration under ionic conduction of various ionic species. When the lithium cation is the only carrier ion in a system, t_{Li}^+ is 1. However, most of electrolytes suffer t_{Li}^+ at ambient temperature due to strong coordination of Lewis basic electrolyte towards lithium cation. A representative plot of the dc current measurement has been shown in Figure 2.18. The highest t_{Li}^+ was observed to be 0.16 for hybrid sample J ($LiPF_6$ as lithium ion source and TMB as boron source). t_{Li}^+ of the previously reported hybrids by Ohno group didn't exceed 0.1.

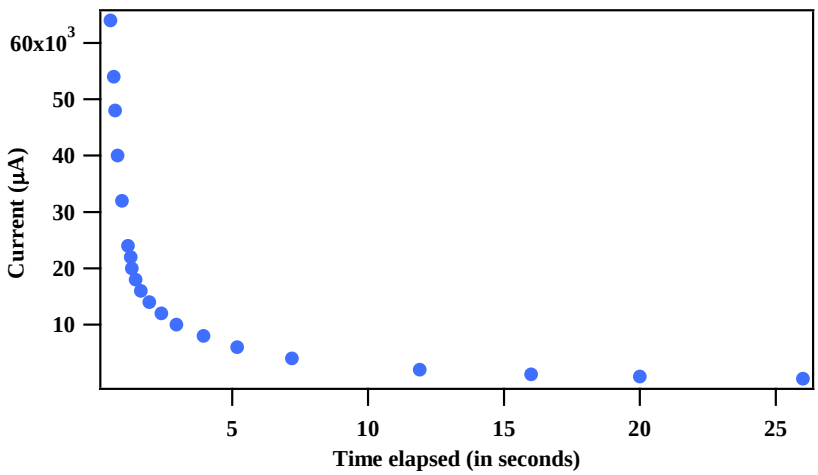

Figure 2.18 Polarisation curve of the organic-inorganic hybrid in Li/electrolyte/Li sandwich cell

2.5 Conclusion

In this study, a series of mechanically robust borosilicate type organic- inorganic hybrid ion-gel electrolytes were prepared in the presence of ionic liquid and lithium salt additives utilising a facile *in-situ* sol-gel condensation pathway. For instance, Ohno group had polymerized ionic liquid in the hybrid matrix, which results in stronger network at the cost of increased brittleness. However, this research has demonstrated the use of free ionic liquid monomer in the matrix, which are additionally low viscous type in nature. These factors contribute towards desirable properties like lesser brittleness, increased conductivity, ease of fabrication and device fabrication was possible only using the present system of hybrids. A modular approach was followed to understand the effect of alkoxyborane precursors and lithium salt additives. Lithium salt additive greatly affected the ionic conductivity and thermal properties of the materials. In TFSA based hybrids, due to its plasticizing property of TFSA anion, resulted in homogeneous profiles at optimum concentrations, which led to improved thermal stability. On the other hand, $LiPF_6$ additive by default resulted in heterogeneous profiles possibly due to its larger order of phase separation in the hybrid matrix. The larger phase separation order enables better connections between ion conductive pathways, which led to better ionic conductivity. In the ion-gels including $LiPF_6$, enhancement of ionic conductivity was observed at lower concentrations of alkoxyborane (exceeding 2.0 $mScm^{-1}$ at 51ºC), which subsequently declined at higher alkoxyborane concentrations. The order of ionic conductivity of the presently synthesised hybrids was over an order higher than the previously reported hybrids (10^{-4}-10^{-5} Scm^{-1} at 51ºC) by Ohno *et al*. On the other hand, LiTFSA based hybrids exhibited a different conductivity from that of PF_6 based hybrids. Maximum t_{Li^+} was calculated to be 0.16 among the $LiPF_6$ based hybrids, while the t_{Li^+} of the previously reported hybrids by Ohno *et al*., were not particularly high. Rheological properties for SPE are measured using a thin film of the sample. However, such a stretching is not possible for glass based hybrid ion-gels. Thus, rheological studies were not performed. Since, such studies have not been carried out by both groups, a conclusive remark on the rheological properties of this hybrid could not be drawn.

References

(1) Armand, M.; Tarascon, J.-M. *Nature*, **2008**, *451*, 652–657.
(2) Scrosati, B.; Garche, J. *J. Power Sources*, **2010**, *195*, 2419–2430.
(3) Sakaebe, H.; Matsumoto, H; Application of Ionic Liquids to Li Batteries, in *Electrochemical Aspects of Ionic Liquids*, ed. by Ohno, H. **2005**, Wiley , 171–186.
(4) Ohno, H.; Yoshizawa, M.; Mizumo, T; Ionic Conductivity, in *Electrochemical Aspects of Ionic Liquids*, ed. by Ohno, H. Wiley **2005**, Wiley, 75–81.
(5) Hwang, S. S.; Cho, C. G.; Kim, H. *Electrochem. Commun.*, **2010**, *12*, 916–919.
(6) Di Noto, V.; Lavina, S.; Giffin, G. A.; Negro, E.; Scrosati, B. *Electrochim. Acta*, **2011**, *57*, 4–13.
(7) MacFarlane, D. R.; Forsyth, M.; Howlett, P. C.; Pringle, J. M.; Sun, J.; Annat, G.; Neil, W.; Izgorodina, E. I. *Acc. Chem. Res.*, **2007**, *40*, 1165–1173.
(8) Galiński, M.; Lewandowski, A.; Stępniak, I. *Electrochim. Acta*, **2006**, *51*, 5567–5580.
(9) Garcia, B.; Lavallée, S.; Perron, G.; Michot, C.; Armand, M. *Electrochim. Acta*, **2004**, *49*, 4583–4588.
(10) Lewandowski, A.; Świderska-Mocek, A. *J. Power Sources*, **2009**, *194*, 601–609.
(11) Fernicola, A.; Croce, F.; Scrosati, B.; Watanabe, T.; Ohno, H. *J. Power Sources*, **2007**, *174*, 342–348.
(12) Sato, T.; Maruo, T.; Marukane, S.; Takagi, K. *J. Power Sources*, **2004**, *138*, 253–261.
(13) Armand, M.; Endres, F.; MacFarlane, D. R.; Ohno, H.; Scrosati, B. *Nat. Mater.*, **2009**, *8*, 621–629.
(14) Welton, T. *Chem. Rev.* **1999**, *99*, 2071–2084.
(15) Smaran, K. S.; Vedarajan, R.; Matsumi, N. *Int. J. Hydrog. Energy*, **2014**, *39*, 2936–2942.
(16) Fujinami, T.; Mehta, M. A.; Sugie, K.; Mori, K. *Electrochim. Acta*, **2000**, *45*, 1181–1186.
(17) Mehta, M. A.; Fujinami, T.; Inoue, T. *J. Power Sources*, **1999**, *81–82*, 724–728.
(18) Mehta, M. A.; Fujinami, T. *Solid State Ionics*, **1998**, *113–115*, 187–192.
(19) Shankar, S.; Matsumi, N. *Polym. Bull.*, **2012**, *68*, 721–727.
(20) a) Matsumi, N.; Chujo, Y., *Polym. Bull.*, **1997**, *38*, 531-536.
b) Evans, J.; Vincent, C.A.; Bruce, P.G. *Polymer*, **1987**, *28*, 2324-2328.
(21) Narita, A.; Shibayama, W.; Matsumi, N.; Ohno, H. *Polym. Bull.*, **2006**, *57, 109-114.*
(22) Matsumi, N.; Mizumo, T.; Ohno, H. *Polym. Bull.*, **2004**, *51*, 389-394.
(23) Matsumi, N.; Nakashiba, M.; Ohno, H., *Polym. Bull.*, **2003**, *50*, 259-264.
(24) Mizutani, T.; Kurahashi, T.; Murakami, T.; Matsumi, N.; Ogoshi, H. *J. Am. Chem. Soc.*, **1997**, *119*, 8991–9001.
(25) Miyata, M.; Matsumi, N.; Chujo, Y. *Macromolecules*, **2001**, *34*, 7331–7335.
(26) Matsumi, N.; Chujo, Y. *Macromolecules*, **1998**, *31*, 3802–3806.
(27) Matsumi, N.; Sugai, K.; Ohno, H. *Macromolecules*, **2003**, *36*, 2321–2326.
(28) Matsumi, N.; Kotera, K.; Chujo, Y. *Macromolecules*, **2000**, *33*, 2801–2806.
(29) Matsumi, N.; Sugai, K.; Ohno, H. *Macromolecules*, **2002**, *35*, 5731–5733.
(30) Matsumi, N.; Sugai, K.; Miyake, M.; Ohno, H. *Macromolecules*, **2006**, *39*, 6924–6927.
(31) Matsumi, N.; Nakashiba, M.; Mizumo, T.; Ohno, H. *Macromolecules*, **2005**, *38*, 2040–2042.
(32) Matsumi, N.; Sugai, K.; Sakamoto, K.; Mizumo, T.; Ohno, H. *Macromolecules*, **2005**, *38*, 4951–4954.
(33) Mizumo, T.; Watanabe, T.; Matsumi, N.; Ohno, H. *Polym. Adv. Technol.*, **2008**, *19*, 1445–1450.
(34) Rahman, I.A.; Padavettan, V. *J Nanomater*, **2012**, *8*, 1-15.
(35) Scrosati, B., Abraham, K.M., van Schalkwik W.; Hassoun, J.; Eds., in *Lithium Batteries-Advanced Technologies and Applications*, **2013**, Wiley.

2.1 Abstract 67
2.2 Introduction 68
2.3 Experiment 69
2.3.1 Materials and Instrments 69
2.3.2 Electrochemical Impedance Spectroscopy 70
2.3.3 Models for Ionic conductivity 73
2.3.3.1 Arrhenius model 73
2.3.3.2 Vogel-Fulcher Tammann (VFT) model 73
2.3.4 Preparation of organic-inorganic hybrid ion-gels 74
2.4 Results and discussion 75
2.4.1 Characterisation of the hybrids 77
2.4.2 Morphological studies of the hybrids 78
2.4.3 Temperature dependence of ionic conductivity of the hybrids 79
2.4.4 Study of VFT parameters of the hybrids 83
2.4.5 Estimation of $t_{Li}^{+}$of the hybrids 87
2.5 Conclusion 88
References 89

Chapter 3

Evaluation of Organic-Inorganic Hybrids as Electrolytes in Fabricated Anodic half-cells

3.1 Abstract

Organic-inorganic hybrids have been evaluated as electrolytes for Lithium-ion batteries through charge-discharge studies in anodic half-cells utilising graphite anodes. The average capacity of hybrids ranged from 120 - 160 $mAhg^{-1}$. Dynamic Electrochemical Impedance Spectroscopic (DEIS) technique was implemented as a novel tool for determination of the voltage cut-off of the anodic half-cells, instead of conventional method of determination by virtue of Open Circuit Potential/Voltage (OCP/OCV). DEIS Experiments were carried to ascertain the optimum working potential for these hybrids.

3.2 Introduction

Lithium-ion batteries have gained wide spread attention after the successful commercialisation by Sony Corporation. Apart from the everyday ubiquitous applications which are seen in our lives, the applications are further finding their way into state-of-art hybrid electric vehicles and plug-in hybrid electric vehicles. The deliberate and conscientious effort in this direction is indeed guided by various factors such as safety parameters of the electrolytes apart from product efficiency in terms of cost, conductivity and other mechanical and thermal factors.[1–6] Retention of capacity and sustained longevity of lithium ion batteries is another area of concern. The capacity limits of the batteries are not only dependent on the electrodes used but also on the electrolytes which support the diffusion of lithium ions through their matrices. The internal parameters inside a cell set-up such as the bulk resistance of the electrolyte coupled with the charge-transfer resistance and other interfacial parameters greatly affect the smooth functioning of the cell over a time period. Although, sustained longevity is a utopian concept with reference to lithium batteries, still scientists all over the world are on a discovery hunt for materials and methods towards the betterment of the existing protocols. Lithium ion batteries work on the principle of insertion and extraction of lithium-ions from the electrodes while diffusing through the electrolyte media (Figure 3.1). In Li-ion battery, graphite was one of the first type of carbon which

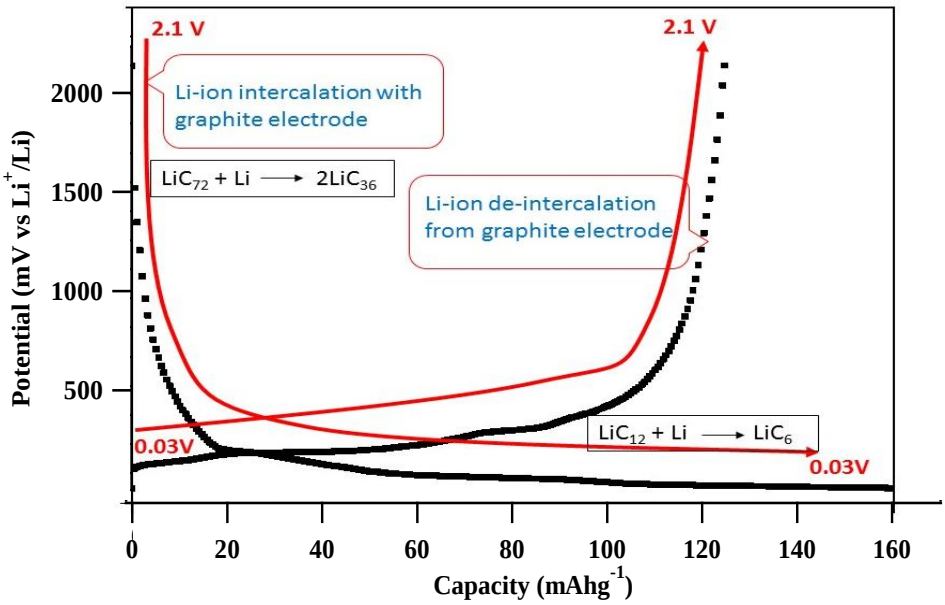

Figure 3.1 Charge-discharge as indicated by the intercalation of lithium in the graphite anode

showed reversible lithiation and is still in use as anode. It is generally used to investigate the anodic reaction in Li-ion batteries. Lithiation of graphite is an intercalation process in which Li ions are inserted between graphene planes. The process involves transition between intercalation stages. Practical graphite electrodes are usually composed of graphite bound with polymers like polyvinylidene fluoride (PVdF) to a metallic current collector. The structure thus formed is porous, allows the solution to penetrate among the graphene planes and intercalate with them. As the particles in these electrodes are more oriented, the hysteresis between the intercalation-deintercalation are smaller and the specific charge capacity may approach 372 $mAhg^{-1}$ (LiC_6), which is the theoretical value. A typical charge-discharge profile is depicted in Figure 3.1 As shown in the figure, in a conventional anodic half-cell consisting of a graphite electrode/electrolyte/Li-metal configuration, intercalation and de-intercalation of lithium ions predominantly occurs at lower voltages with respect to Li-electrode. Although intercalation and de-intercalation occur at higher voltages up to 2.1 V, the major insertion–extraction range takes place at very low potentials (approximately 0.03 V). As an over charging and discharging of the carbon electrode might lead to an irrecoverable damage to the cell, manual cut-off limits till 2.1 V.

The efficiency of the intercalation process is marked by the charge-discharge capacity profiles while the factors affecting the process can be monitored by various techniques, which includes Raman spectroscopy, (Fourier transform infrared) FT-IR spectroscopy, Atomic Force Microscopy (AFM) and Transmission electron microscopy (TEM) etc. Of the many ways of understanding the internal parameters of a battery, Electrochemical Impedance Spectroscopic (EIS) technique is a versatile, non-destructive technique successfully employed for a considerable timeframe. Thus, EIS is a powerful technique often employed for the electrochemical characterisation of the lithium-ion batteries. The intercalation of lithium ions into graphite has been extensively dealt in various articles and reviews. Basically, EIS technique, involves an infinitesimal AC perturbation at low or zero potential being applied to a sample resulting in an impedance output. The resultant data is resolved into real and imaginary vectors and are further analysed.

Lithium insertion into graphite anode is a multi-step process involving:

- Transport of lithium ions in the electrolyte solution,
- Migration through the surface films formed over anode material,
- Facilitation of charge-transfer between the lithium cation and the film,
- Solid-state diffusion of lithium ions,
- Followed by insertion and accumulation of lithium ions into graphite.

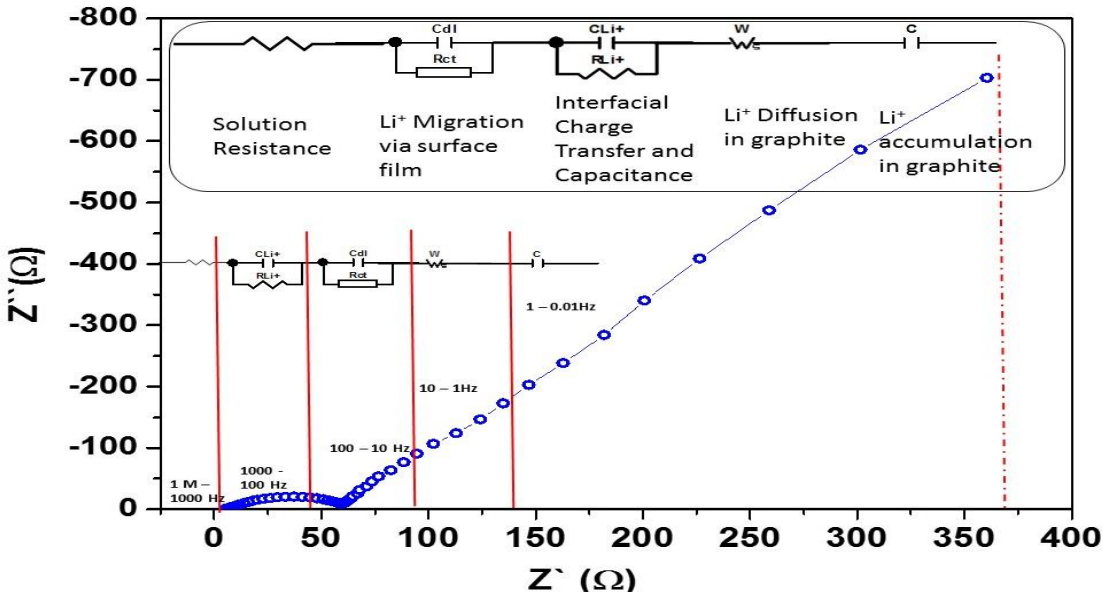

Figure 3.2 Correlation between Nyquist plot and transport of lithium ions in a battery

The impedance profiles of lithium ion batteries obtained from EIS experiments, can be explained by Figure 3.2. In the figure, the portion corresponding to lowest Z' or real impedance corresponds to the high frequency region or the resistance provided by the bulk of the electrolyte, affecting the transport of lithium ions. Further, at the intermediate frequency regions (1000 Hz till 0.1Hz) include portions corresponding to the various layers of thin films passivating the anode surface. The lowest frequency regions are associated with the diffusion of lithium ions into graphite and their subsequent accumulation. The correlation of the experimental data with the actual physical parameters is carried out with the help of electrochemical model fitting. The corresponding electrochemical model for discussed processes is depicted in Figure 3.3.

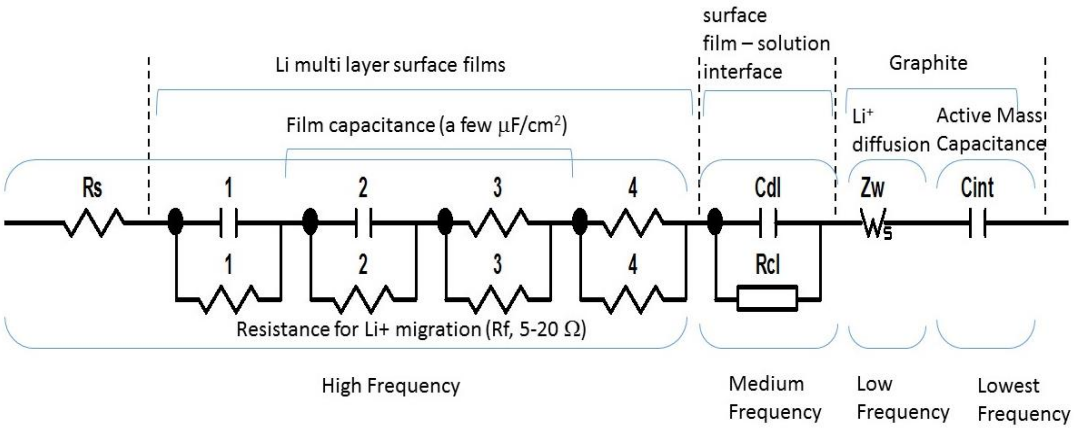

Figure 3.3 Designation of electrochemical circuit model for transport of lithium ions in batteries

The solid state potential driven lithium ion diffusion into graphite is often denoted by Warburg element in the circuit design. To be specific, Warburg impedance with finite thickness, explains this phenomenon.

Dynamic Electrochemical Impedance Spectroscopy

Dynamic Electrochemical Impedance Spectroscopy (DEIS) is a versatile characterisation technique to determine electrochemical responses for interfacial processes and structures. DEIS acquires variable frequency responses in AC superimposed with a potentiodynamic DC voltage in the same potential scan of an electrochemical cell. The spectra are usually recorded in bidirectional potential scans, which give additional information on the extent of reversibility of different constituent processes that contribute to the frequency response of a nonstationary electrochemical interface.

Generally, the potential scan and the multivariate data analysis of DEIS spectrum are plotted as a 3D plot with Z`, Z`` against the applied voltage (V). Similar to a conventional electrochemical impedance spectrum, the obtained data are fit with an equivalent electric circuit de-convoluting the AC part of the interface response into constituents related to different interfacial processes and structures. Thus, potentiodynamic electrochemical impedance spectroscopy characterizes, in a single potential scan, different interrelated processes (interfacial charge transfer, diffusion, adsorption, etc.) and interfacial structures (double electric layer, space charge layers, etc.) at non-stationary electrochemical interface. The separation of the constituent AC responses has enabled multiparametric monitoring of

atomic layer-by-layer deposition in multilayer assembly, characterisation of nonstationary semiconductor systems by acquisition of variable Mott-Schottky plots, monitoring of nonstationary stages of electropolymerization and mutually correlated adsorption of cations and anions.

A vast amount of literature is seen resorting to various variants of EIS technique, to study the State of Charge (SOC), lithiation, electrode etc. For a better understanding of the charge-discharge profiles of the lithium ion batteries, *in-situ* electrochemical impedance spectroscopy was employed by Itagaki *et al.*, who recorded impedance spectra in tandem during the charge-discharge processes of cathodic half-cells of $LiPF_6$ based electrolyte in the presence of various alkyl carbonate additives. The focus of such study was restricted to convenience in terms of experimentation, while simultaneously understanding the SEI characteristics during the charge-discharge process.[17] The same group has also reported a similar article utilising the *in-situ* technique utilising anodic half-cells as well, highlighting the nature of SEI film. Changing nature of R_{ct} values during the charge-discharge processes was a prominent find in their study.[18] However, these experiments were based on an assumption that the cell was maintained at specific SOC. Also, considering the non-stationary SOC, the effective DC potential turns up to be 0, at any point of AC perturbation signal. Thus, the experimental scheme can't be implemented for determination of a cut-off limit of a novel electrolyte. Improvising on the obtained reports, Moss *et al.*, studied commercial Li-ion battery who recorded DEIS spectra on the application of external DC. R_{ct} values of such studies showed a greater degree of dependence on the applied DC and the charging current, though variations were observed during charging and discharging steps. However, the study was more emphasised on the development of an empirical simulation to parametrise real time battery performances.[19] While, another research work by Huang *et al.*, devised a novel implementation of DEIS concerning the recording the impedance spectra at various charging DC currents, without compromising on the SOC. A cathodic half-cell of $LiMn_2O_4$/Li half-cell configuration was studied, emphasizing on the correlation of R_{ct} values with that of charging DC. The group varied its experimental technique from the previous reports while concluding similar inferences.[20] All the reported literature focusses on the study of internal kinetics of the commercial cells or cells with known capacity via DEIS. The approach of our study is fundamentally different from the abovementioned

reports. In an effort to effectively understand the fullest capacity of a novel electrolyte in fabricated cells, charge-discharge studies are carried out. However, there exists no protocol for devising a particular voltage boundary for a half/full cell for an electrolyte except an approximation based on the electrodes used. Since, "trial and error" method of optimising the voltage boundaries is a voluminous task involving time and energy, we attempt to devise a novel protocol for understanding such parameters with the help of EIS technique. Here, we propose the novel implementation of Dynamic Electrochemical Impedance Spectroscopy (DEIS) as an effective tool in understanding the R_{ct} values of the cell, thus, being instrumental in determining the cut-off limit of the cell for optimal performance of the cell. Further, DEIS studies of a half-cell or full-cell at different potentials has not been reported so far.

In this study, the impedance profiles of the anodic half-cell fabricated using Organic-inorganic hybrid electrolytes were studied over a range of potential utilising Dynamic Electrochemical Impedance Spectroscopy. The novelty of this work lies in the implementation of DEIS technique in understanding of behaviour of a novel electrolyte during cycling processes.

3.3 Experimental

3.3.1 Synthesis of organic-inorganic hybrid electrolytes

Organic-inorganic hybrids were synthesised by an *in-situ* sol-gel condensation procedure utilising tetramethylorthosilicate & alkoxyboranes viz. mesityl dimethoxyborane and trimethoxyborane in the presence of low viscous type 1,3-diallylimidazolium TFSA ionic liquids along with lithium salt additive ($LiPF_6$ and 0.1N HCl aq. as the acid catalyst). Details about the synthetic procedure and detailed composition profiles have already been described in Chapter 2. However, compositional details of the hybrids considered in this study, is given in Table3.1

Table 3.1. Compositional matrix employed for the synthesis of organic-inorganic hybrids

Sample	*Ionic liquid (in mmol)*	*Tetramethylorthosilicate (in mmol)*	*Alkoxyborane (in mmol)*[a,b]	*$LiPF_6$ (in mmol)*
A	1.0	2.5	1.0 [a]	1.0
B	1.0	2.5	1.0[b]	1.0

where *a = trimethoxyborane and b = mesityldimethoxyborane

3.3.2 Fabrication of anodic-half cells

Anodic half-cells were fabricated using CR2025 type cells, with graphite as working electrode (12 Φ, PIOTREK, capacity), lithium metal as the counter electrode (15 Φ, Honjo metals) and powdered hybrid electrolyte (~30 mg) separated by ring shaped Celgard® based separator (15 Φ) following a format as shown in Figure 3.4. Appropriate quantity of ethylene carbonate: diethyl carbonate (EC: DEC) (1:1) (~ 35 µl) was used to wet the electrolyte to ensure a steady SEI layer formation. The cells assembly was carried out in a glove box maintained under argon atmosphere. The assembled cell was allowed for pre-determined time period for stabilization purposes.

3.3.3 Charge-discharge studies

The prepared graphite based anodic half-cells (Figure 3.4) were charged and discharged in the galvanostatic mode using Hokuto Denko HA-150 and Biologic SMP-3 dual channel systems. Thereafter, the charge–discharge studies were carried out at various charging rates. During the charging process, lithium ions populate the graphite anode, while during the discharging the cell down to 1.5 V the lithium ions move out of the graphite structure.

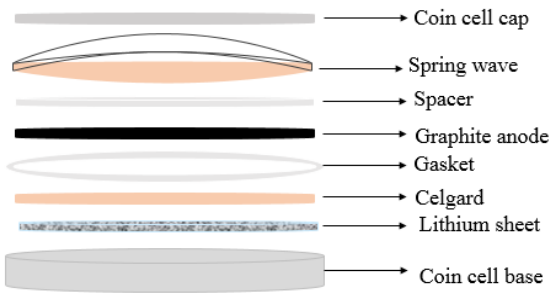

Figure 3.4 Set-up of the assembled anodic-half cells

3.4 DEIS experimental protocol

DEIS experiments were carried out using a Potentiostat/Galvanostat FRA (Biologic SMP3). The prepared cells were galvanostatically charged from designated potential value (determined from the OCP) to a potential of 0.03 V with a step potential divided equally into 16 steps. Similar protocol was employed for discharge process as well. Impedance spectra was acquired successively at every step potential during charging and discharging profiles from 0.03 V .The upper cut-off was determined on the basis of the OCP of the cell. The experimental frequency range was from 1 MHz – 0.1 mHz. While the considered data for analysis was restricted within 50 kHz till 30 mHz. In the present studies, with the constant experimental parameters being SOC, we have chosen the variable as the DC potential. Later, in Figure 3.10 the circuits used for fitting is shown.

The schematic representation the protocol is as follows in Figure 3.5:

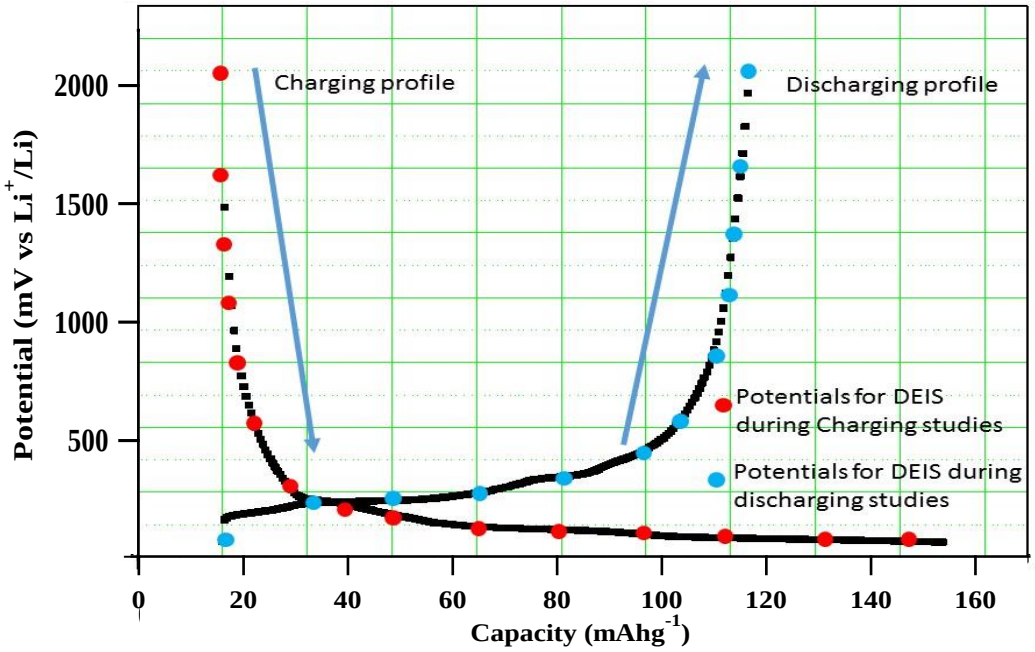

Figure 3.5 The DEIS experimental protocol highlighting the stages of experimental data extraction

3.5 Results and Discussion

From the previous studies, a basic understanding about the ion conductive behaviour of the hybrids was understood. Of all the hybrids synthesised, only two hybrids were chosen for the charge-discharge studies as electrolytes. The choice of hybrid ion-gels was solely based on the observed ionic conductivity at 51ºC. The following Figure 3.6, shows the ionic conductivity trend.

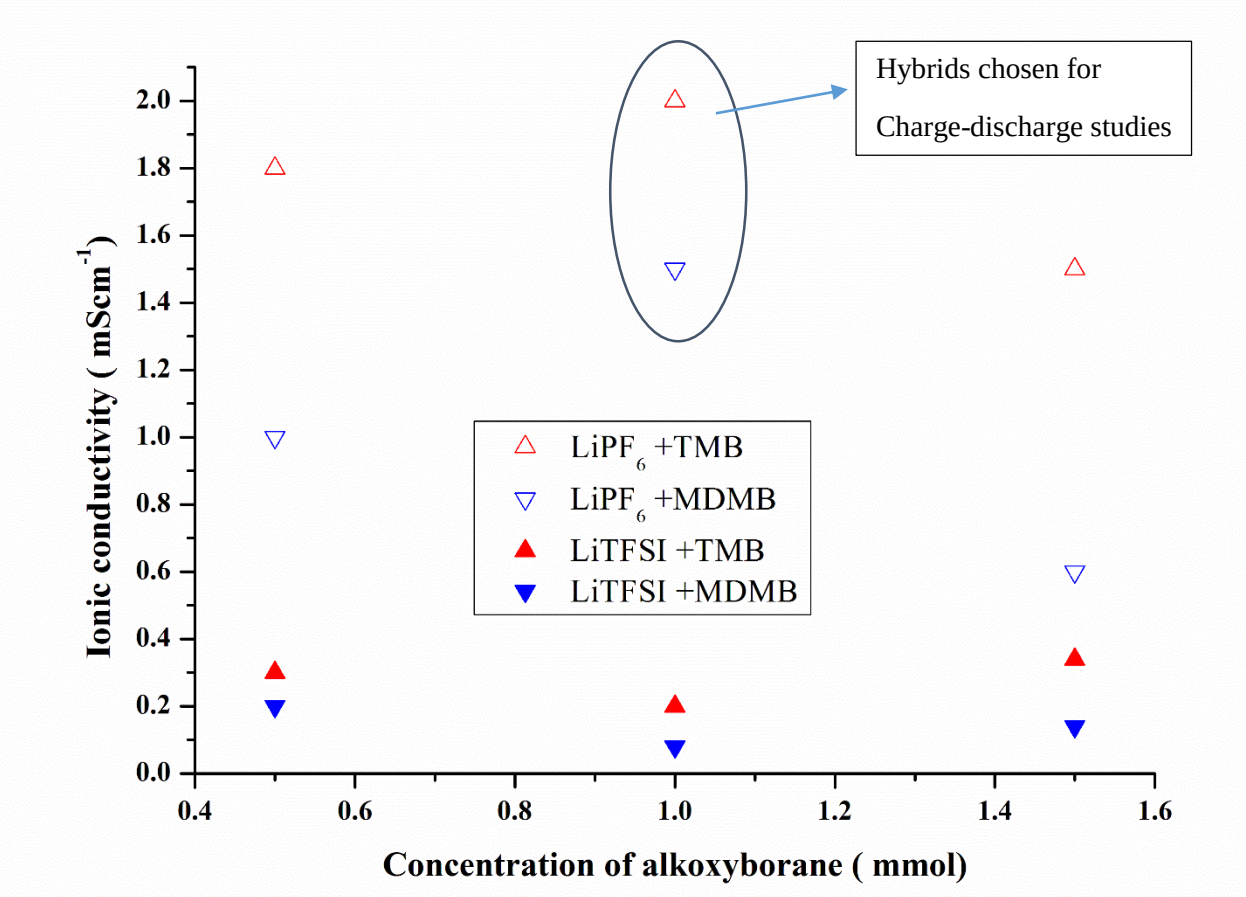

Figure 3.6 Comparative plot depicting the ionic conductivity profiles of various organic-inorganic hybrids as a function of alkoxyborane concentration and lithium salt additive

Hence, sample A and B were chosen among the $LiPF_6$ based hybrids, with different alkoxyborane precursors.

- Classified as a function of alkoxyborane precursors
- $LiPF_6$ with **trimethoxyborane (TMB)**---- Sample A
- $LiPF_6$ with **mesityldimethoxyborane (MDMB)**----Sample B

The Samples A and B were chosen not only as a function of alkoxyborane concentration but also the due to the fact that these hybrids showed high order of ionic conductivity. Sample A showed considerably high ionic conductivity in the order of 2 $mScm^{-1}$ (at 51°C), while conductivity of Sample B was also in a similar range.

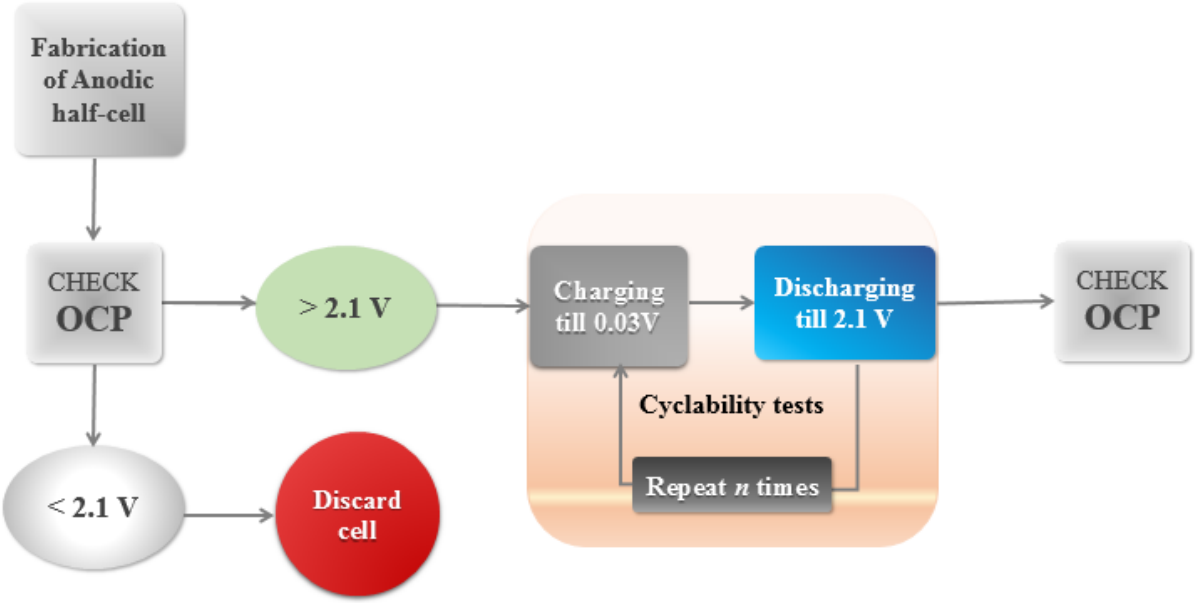

Figure 3.7 Flowchart depicting the conventional protocol employed for charge-discharge studies

Sample A

The conventional experimental protocol for the evaluation of the anodic half-cells by means of charge-discharge processes is shown in Figure 3.7. Gauging the cell potential from its initial OCP values in graphite based anodic half-cells, the maximum cut-off range is often restricted to 2.1 V. Firstly, the cell is charged by lithiating the anode till 0.03V. Further, the lithiated anode is discharged up to 2.1V and the process is repeated numerous times. The charge-discharge studies of these cells was carried out on a pilot basis, without any previous references of this kind of electrolytes. Thus, following the above mentioned protocol, the anodic half-cell prepared with Sample A was subjected to charge-discharge studies with a graphite anodes with cut-off potential of 2.1 V. The following Figure 3.8 shows the first 10 cycles of charge−discharge curves at 0.5C charging rate in the presence of organic electrolyte additives EC: DEC (1:1).

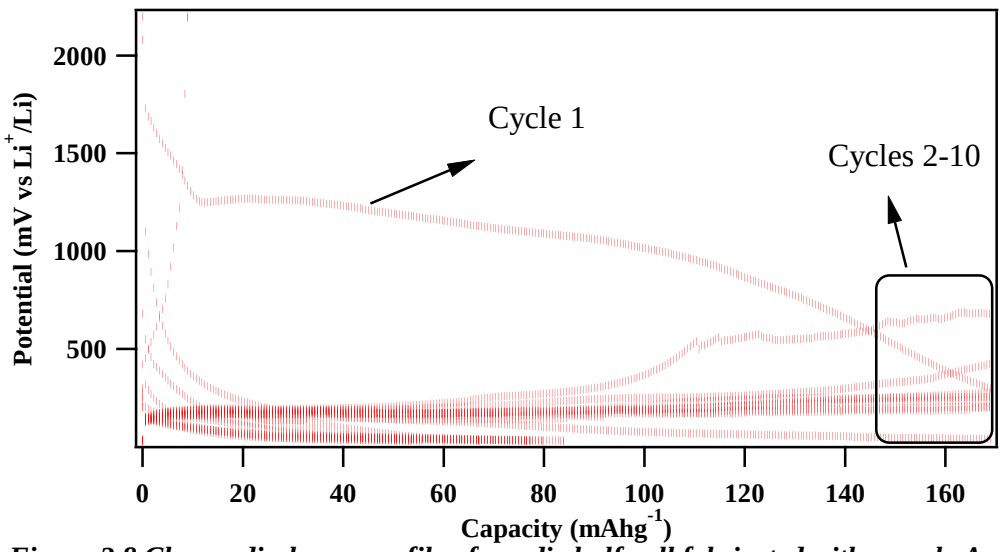

Figure 3.8 Charge discharge profile of anodic half-cell fabricated with sample A at 0.5C charging rate (voltage cut-off 0.03 V-2.1 V)

The first charge capacity was over 160 $mAhg^{-1}$. In subsequent cycles, we observed a non-ideal charge discharge pattern within a low-potential range of 500 mV, although the capacity of the cell over 160 $mAhg^{-1}$. Continuous operations at such low potentials was not deemed to be beneficial, and prompted the re-design of the experimental protocol followed. The major cause behind the unsatisfactory performances of the half-cell was possibly due to overcharging and over-discharging factors. Overcharging, would lead to permanent lithium insertion into the anode. While, over-discharging would permanently degrade the graphite anode. This kind of problem arises due to improper determination of working range of potential.

It was deemed necessary to understand the internal parameters of the cell, which would probably improve the optimum life-cycle of the cells, by smooth cycling. Estimation of working potential range is often determined by cyclic voltammetry analyses and potential window experiments. Although, voltammetric analyses and potential window measurements would lead to a practical understanding about the range of electrochemical stability of the concerned material, these methods are not sufficient to determine the optimum range within the available electrochemical window. In this regard, we chose Dynamic Electrochemical Impedance Spectroscopy (DEIS) as an effective approach towards addressing this problem. EIS has already been established as a powerful tool employed in the characterisation of batteries. The definition of DEIS technique has been dealt in different manners by

various research groups which has been discussed at length in the earlier section. Hence, the existing experimental protocol was modified to accommodate DEIS suitably. The modified protocol is shown in the flowchart (Figure 3.9). Figure 3.10 shows the electrochemical circuit used for fitting the obtained data.

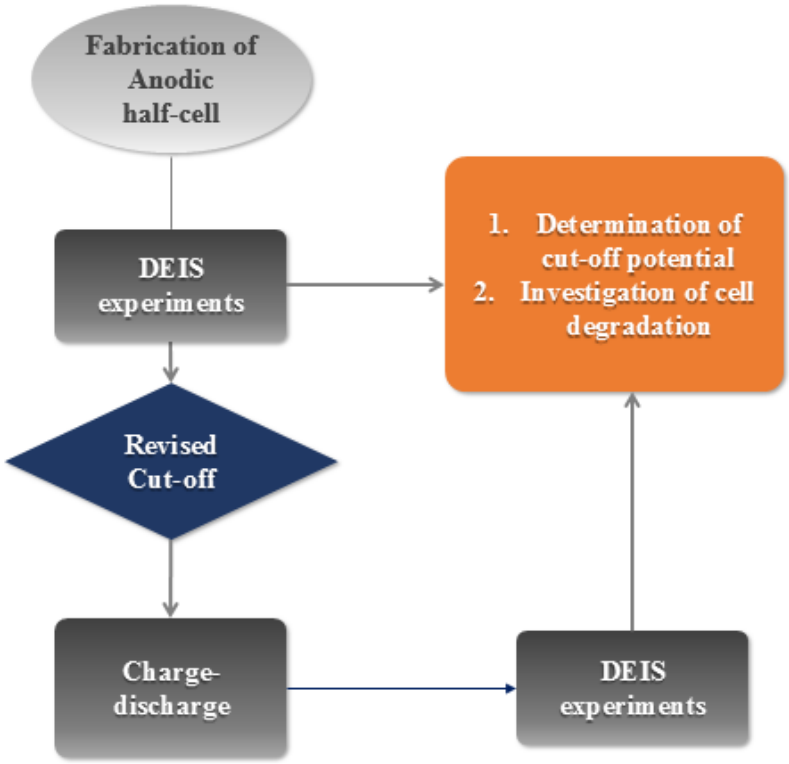

Figure 3.9 Modified protocol employed including DEIS for charge-discharge studies of organic-inorganic hybrids

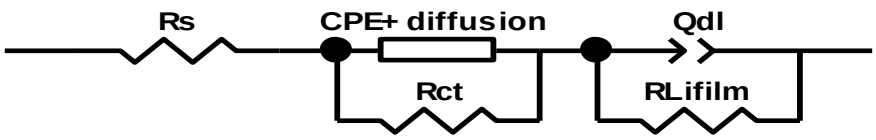

Figure 3.10 Physical circuit used for electrochemical fitting of DEIS data

DEIS profiles of freshly prepared half-cells

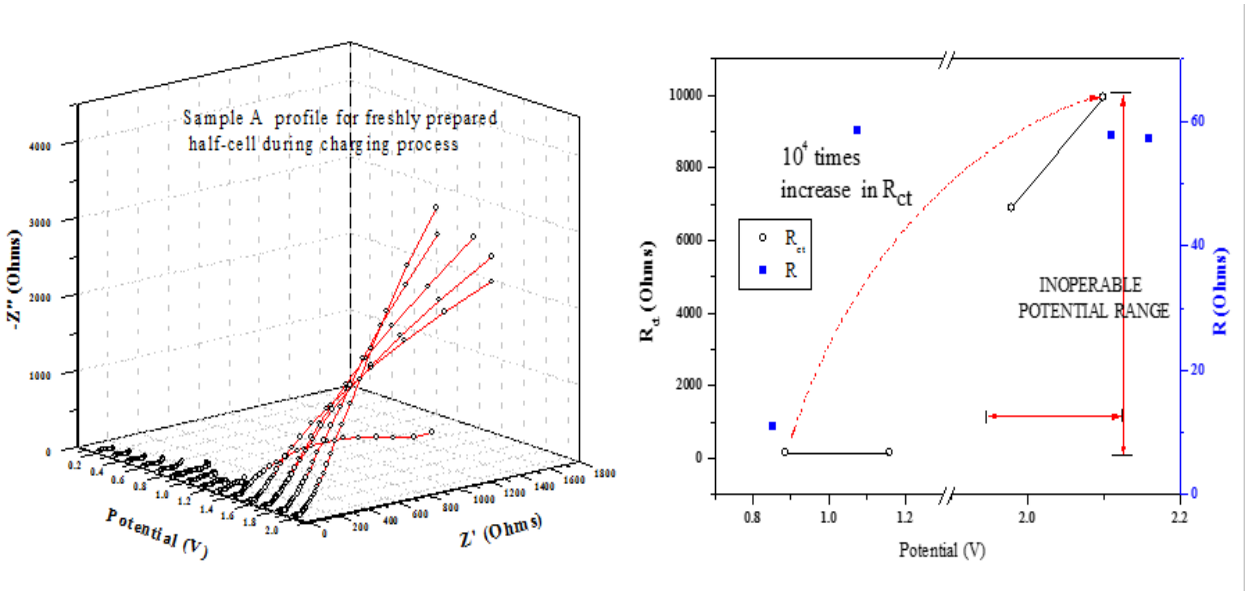

Figure 3.11 DEIS charging profile of a freshly prepared anodic-half cell fabricated using Sample A (voltage cut-off range 0.03 V-2.2 V) alongside the derived R_{ct} values

From the DEIS charging profiles, it was observed that the highly capacitive tail ends are conspicuous at higher potentials beyond 1.5 V. This kind of capacitive tails have detrimental effect on

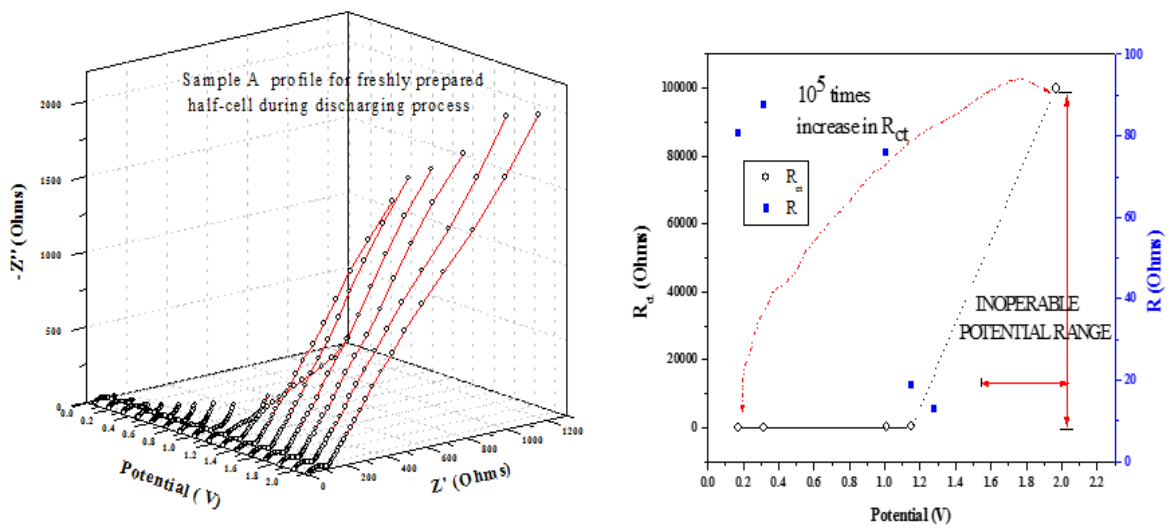

Figure 3.12 DEIS discharging profile of a freshly prepared anodic half-cell fabricated using Sample A (voltage cut-off range 0.03 V-2.2 V) alongside the derived R_{ct} values

the intercalation behaviour of lithium ions into the graphite. The fitting data reveals that the corresponding R_{ct} values at high potentials are thousands times higher than the R_{ct} values at potentials during complete lithiation (0.03 V – 1.5 V) (Figures 3.11 and 3.12). Similarly, during the discharging DEIS experiment as well, it was noticed that at high potential, tremendously high values of R_{ct} were observed. As already mentioned in the protocol, the DEIS study is instrumental in determination of the experimental cut-off potential. Hence, taking cue from this experiment the cell was put to charge-discharge studies with a revised potential range.

The cell was cycled 10 times at 0.5C charging rate within a range of 0.03 V-1.5 V as shown in Figure 3.13. Further, the cell was also run for 70 more cycles at different charging rates viz. 0.5C, 1C and 1.5C. The cell after 50 cycles of charge-discharge could reciprocate well with the DEIS experiments,

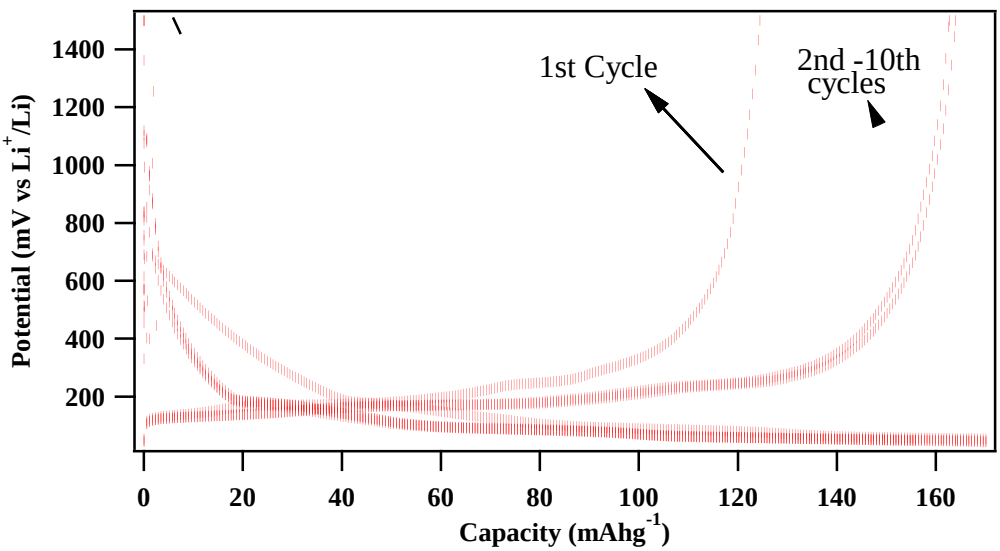

Figure 3.13 Charge-discharge profiles of anodic half-cell fabricated with sample A at 0.5C charging rate (voltage cut-off 0.03 V-1.5 V)

which was evident from the steady impedance profiles recorded over a charging curve from 1.5 V to 0.03 V. The statistics are represented in the Figure 3.14. Although the capacity at 0.5C rate was over 160mAhg^{-1}, the discharge profile reduced drastically at higher charging rates. However, the efficiency of capacity retention was in the range of 95-100%. Hence, the decrease in the capacity is not an irreversible phenomena as often attributed in ageing batteries. From the efficiency chart, it is generally understood that the charging processes at higher charging currents is often associated with lower degree of intercalation of lithium ions into the electrode.

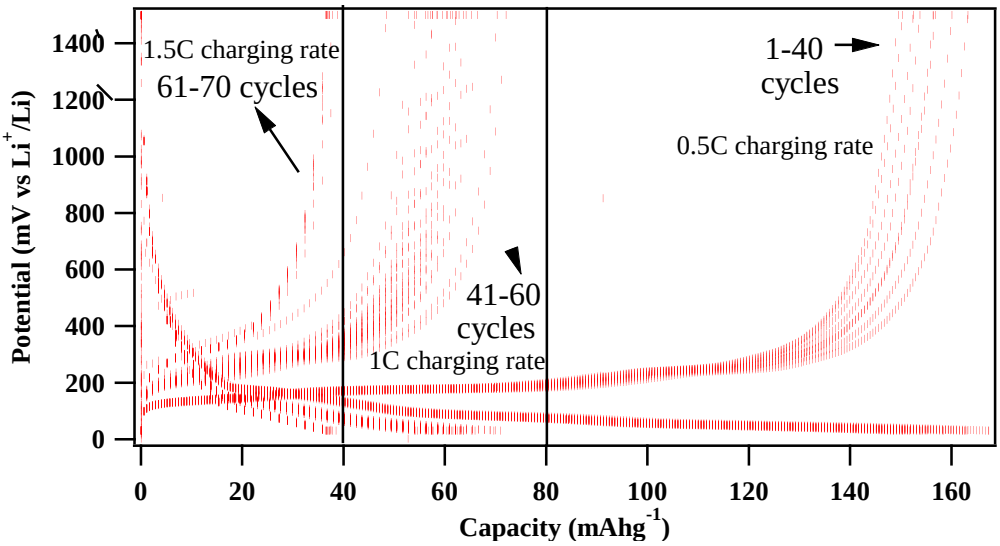

Figure 3.14 Charge-discharge profile of assembled anodic half-cell fabricated using Sample A (voltage cut-off range 0.03 V-1.5 V, at 0.5C, 1C and 1.5C charging rates)

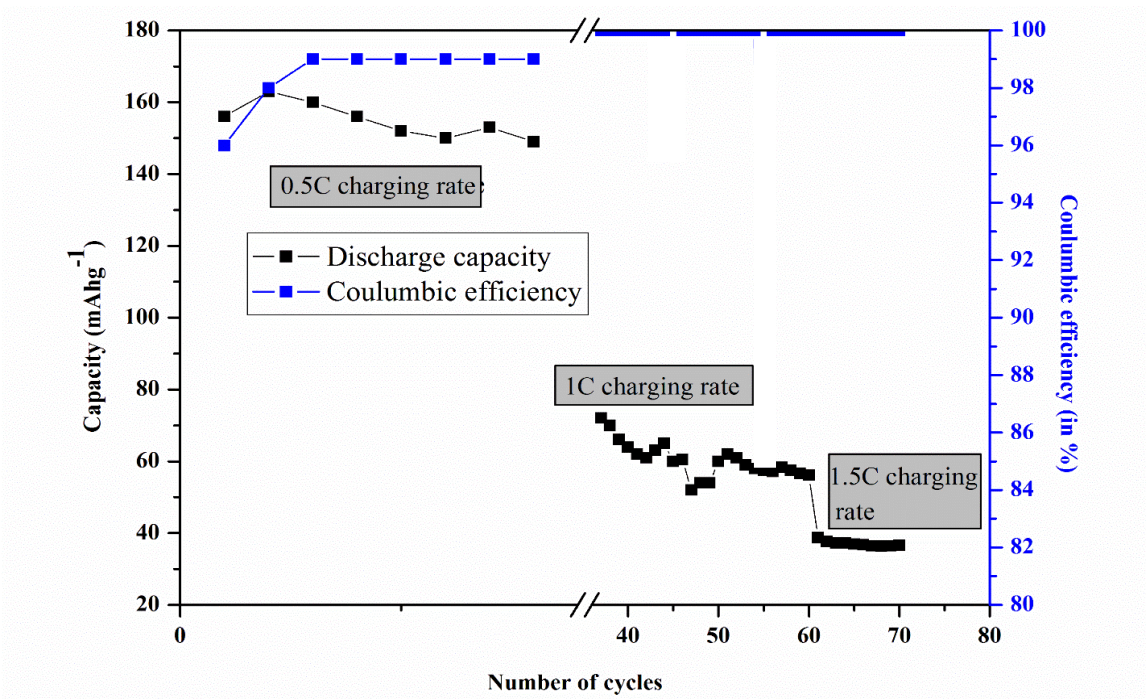

Figure 3.15 Couolombic efficiency chart for Sample A run over 70 cycles at different charging rates

The high range of coulombic efficiency indicates an of efficient extraction of the inserted lithium ions from the anode into the electrolyte matrix. The coulombic efficiency charts are shown in Figure 3.15.

Sample A Charging profile

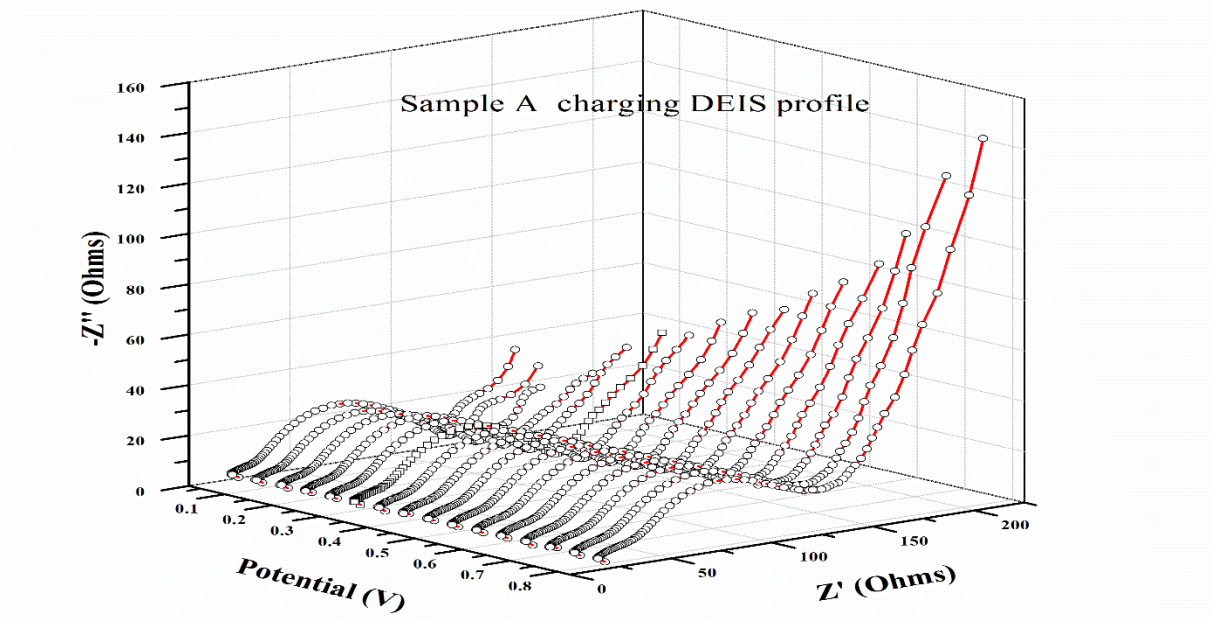

Figure 3.16 DEIS charging profile of an already pre-cycled anodic half-cell fabricated using Sample A (Voltage cut-off range 0.03 V-0.9 V)

The above Figure 3.16 shows a charging DEIS profile with a voltage cut-off from 0.9 V till 0.03 V. The choice of the cut-off voltage was taken to be the OCP of the concerned cycled cell. As we move down the potential curve, we see the capacitive tail fading out to diffusive or semi-diffusive regions. Since, the electrolyte components consist of various nano domains of heterogeneity, the corresponding effect is observed in the impedance profile of the sample. We used a circuit design of R(RM)(QR) to evaluate the DEIS results (circuit is referred to in Figure 3.3) .

The R_{ct} (charge-transfer) values along with the resistance values at the lithium cathode are highlighted in the Figure 3.17, which indicates that the charge transfer resistance values decrease during the charging potential dip, while the resistance value at the cathode, does not show changes in a large scale, and remains constant. However, the most significant observation is the revised cut-off ensured low or minimal values of R_{ct} in the cell. The devised hypotheses found good correlation with the obtained experimental data in both charging and discharging profiles.

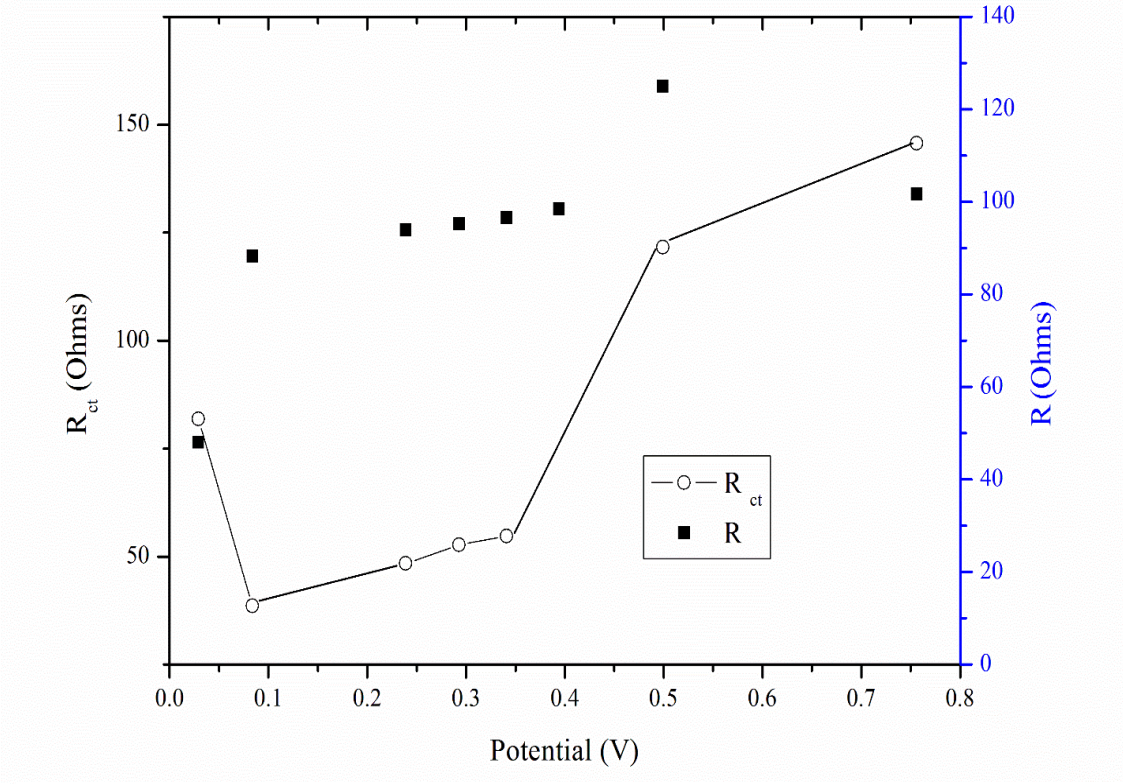

Figure 3.17 R_{ct} parameters as obtained from the DEIS charging profile of an already pre-cycled anodic half-cell fabricated using sample A

1

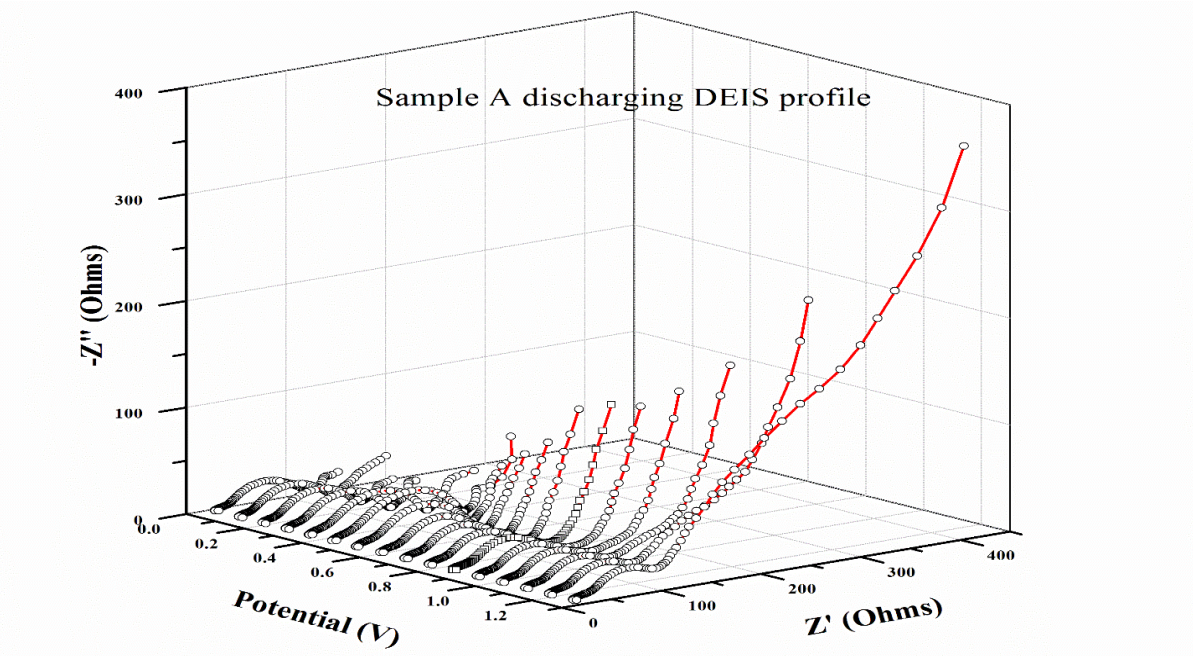

Figure 3.18 DEIS discharging profile of an already pre-cycled anodics half-cell fabricated using sample A (voltage cut-off range 0.03 V-0.9 V)

Figure 3.18 shows the impedance or Nyquist profiles recorded at different potentials at decreasing levels of SOC during the discharge process. The capacitive tail-ends are once more evident at the high potential regions (observed at high potentials as the discharge proceeds), which are conspicuously absent at the lower potentials. An electrochemical fitting of the corresponding data gave us an interesting finding concerning the R_{ct} values as shown in Figure 3.19.

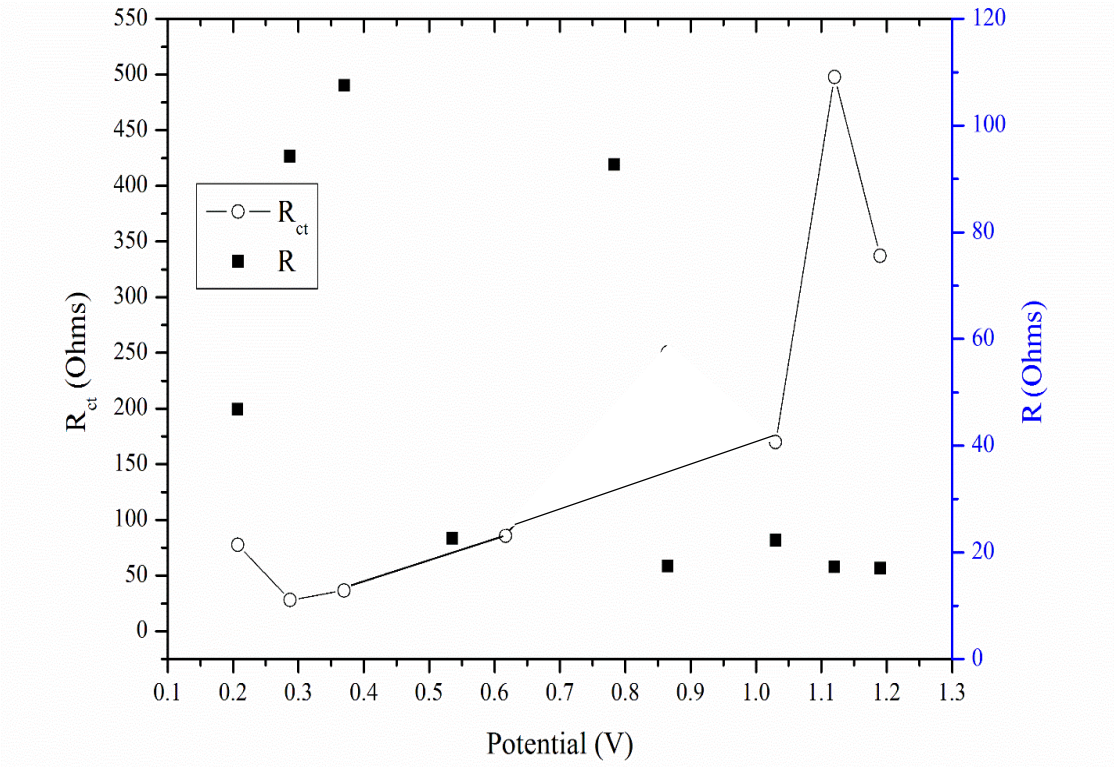

Figure 3.19 R_{ct} parameters as obtained from the DEIS discharging profile of an already pre-cycled anodic half-cell fabricated using sample A

Sample B

A similar methodology was employed for Sample B as well when it showed abnormal charge-discharge profiles on cycling governed by the OCP values. The charge-discharge profile can be seen in Figure 3.20. The cell was further subjected to DEIS experiment to determine the upper threshold limit in order to avoid high capacitive regions and further avoiding unusual charge-discharge profiles. The After circuit fitting of the impedance profiles, it was seen that beyond 1.4 V the charging profiles 3D

trajectory of the Nyquist plots over a potential range from 0.03 V till 2.2 V is shown in Figure 3.21. showed hindrance to transport of lithium ions through the surface films. At further higher potentials,

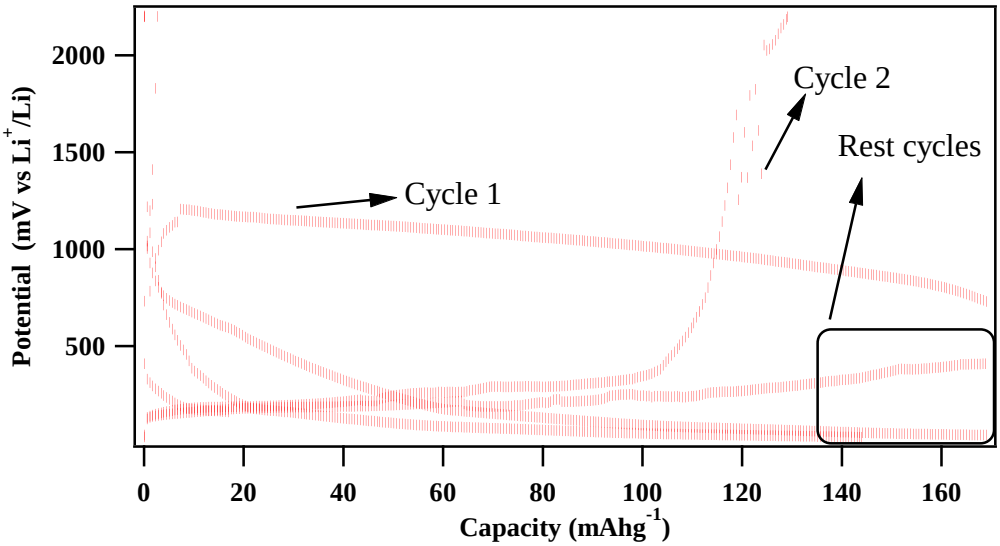

Figure 3.20 Charge-discharge profile of anodic half-cell fabricated with sample B at 0.5C charging rate (voltage cut-off 0.03 V-2.1 V)

the charge transfer resistances shot up to great extent. Generally, such high values of R_{ct} values are not ideal for smooth functioning of the cells. The associated R_{ct} values linked to the optimised range are shown in the adjacent Figure 3.21.

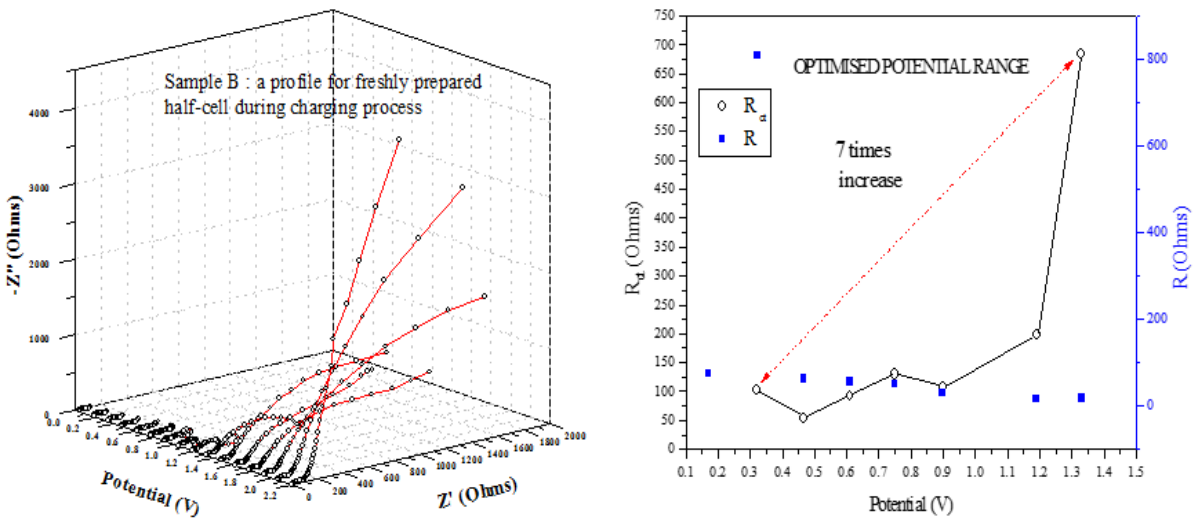

Figure 3.21 DEIS charging profile of an already pre-cycled anodic half-cell fabricated using sample B (voltage cut off range 0.03 V-2.2 V) alongside the derived R_{ct} values

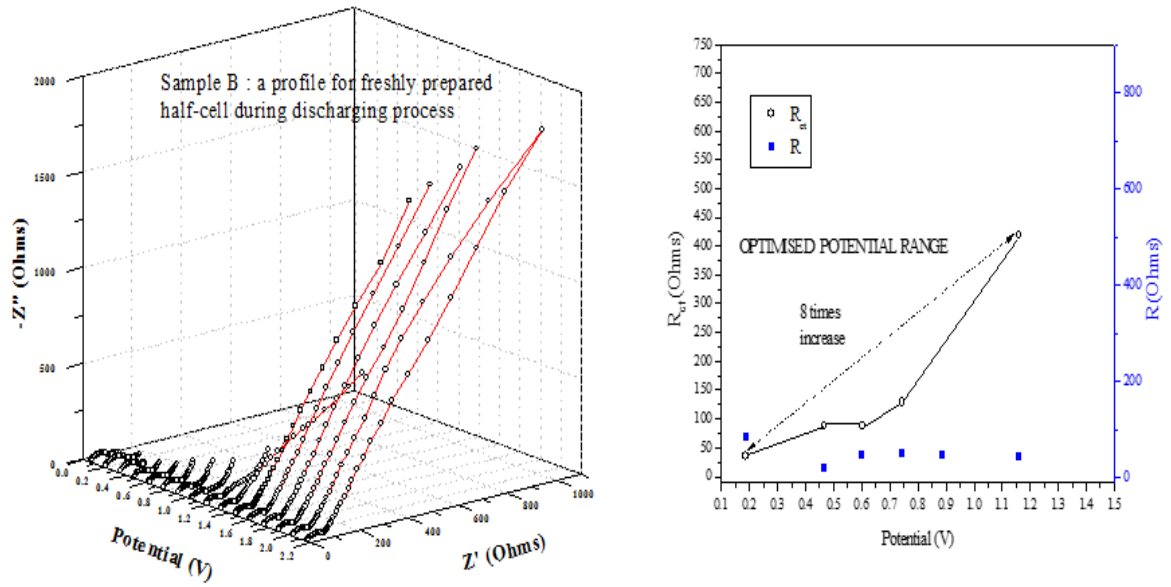

Figure 3.22 DEIS discharging profile of an already pre-cycled anodic half-cell fabricated using sample B (voltage cut-off range 0.03 V-2.2 V) alongside the derived R_{ct} values

In the discharge profile, i.e. in Figure 3.22 the high charge transfer resistance values were even more predominant after the potential crossed 1.5 V. This kind of behaviour adversely affects the lithiation and delithiation process occurring during the cycling of the cell. Hence, the results led us to the conclusion that the proper functioning of the cell can be envisaged only by reconsidering the voltage-cut off parameters of the anodic half-cell. Hence, a preventive cut-off determination in the working potential was indeed necessary to prolong the life cycle of the cell. Hence, the cell cut-off potential was revised to 1.6 V-0.03 V on the basis of DEIS results.

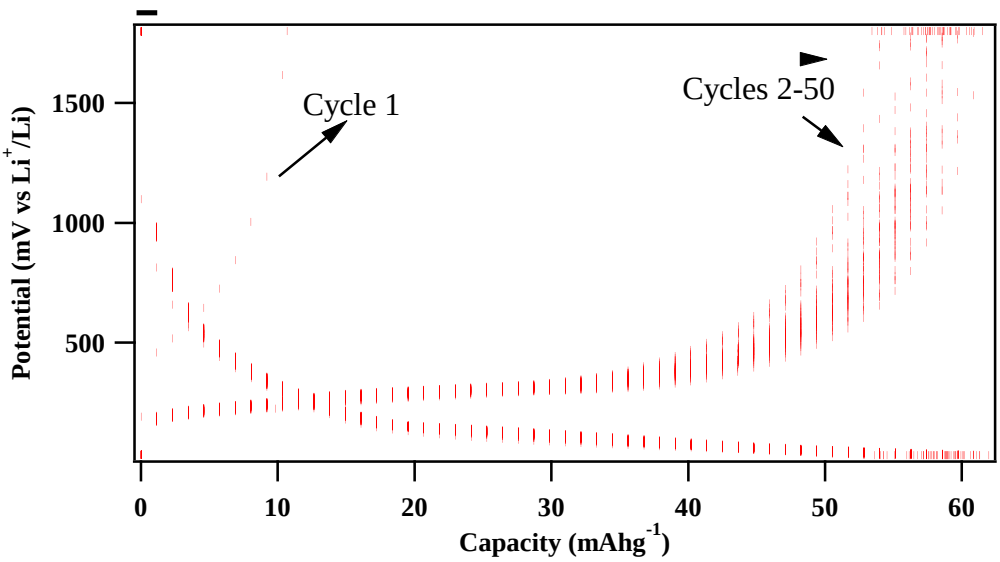

Figure 3.23 Charge-discharge profiles anodic half-cell fabricated with sample B at 0.5C charging rate (voltage cut-off 0.03 V-1.5 V)

The cell was subjected to charge-discharge experiments at 1C for 50 cycles. The results are shown in Figure 3.23 for Sample B, 1C charging rate, the profiles are much well-settled except for the first cycle. The results strengthened our hypotheses that the determination of the cut-off potential indeed proved advantageous towards improving the cycle life of the cell. The related coulombic efficiencies are also charted in the following Figure 3.24.

To further evaluate the working of the cell, the cell was further subjected to DEIS experimental protocol towards investigating the degradation of the cell over repeated cycling and if such behaviour was specific to this hybrid only.

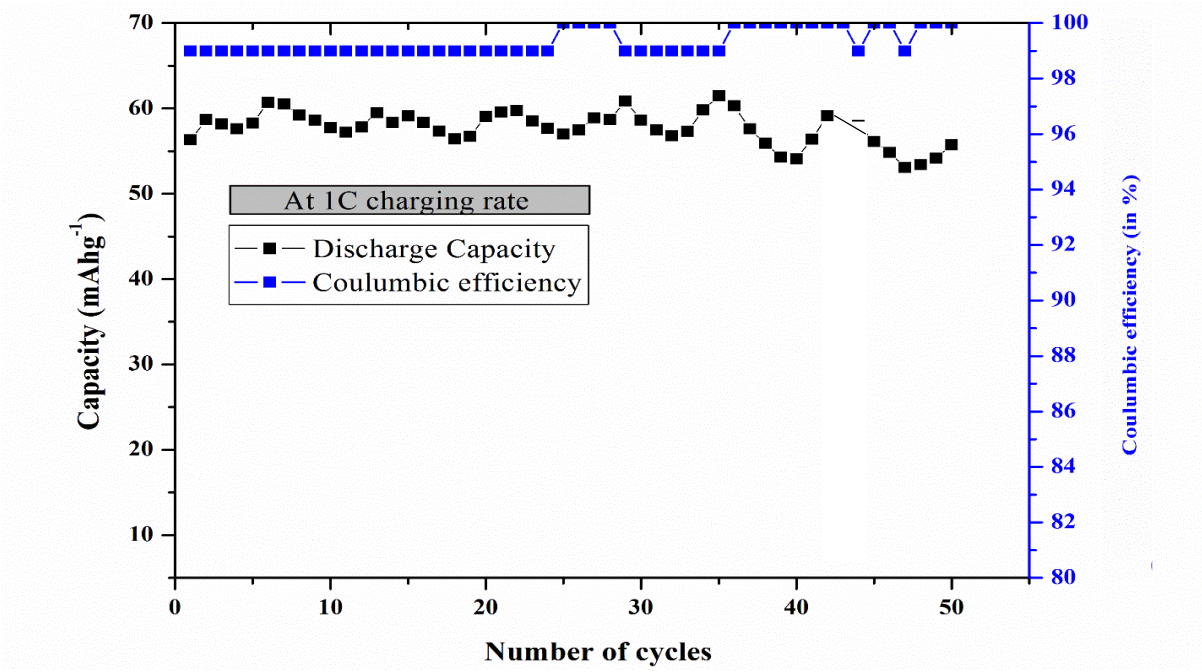

Figure 3.24 Couolombic efficiency chart for Sample B run for 50 cycles at 1C charging rate

Figure 3.25 deals with the 3D trajectory of the charging DEIS experiment of Sample B, carried out after 50 times of cycling. The experimental data obtained after fitting with the designated circuit is plotted in Figure 3.26. Within the estimated cut-off range, observed R_{ct} parameters were high only at the initial OCP, which decreased greatly once the charging process was initiated. The constant yet high value of R indicates the passivation of lithium sheet over regular cycling.

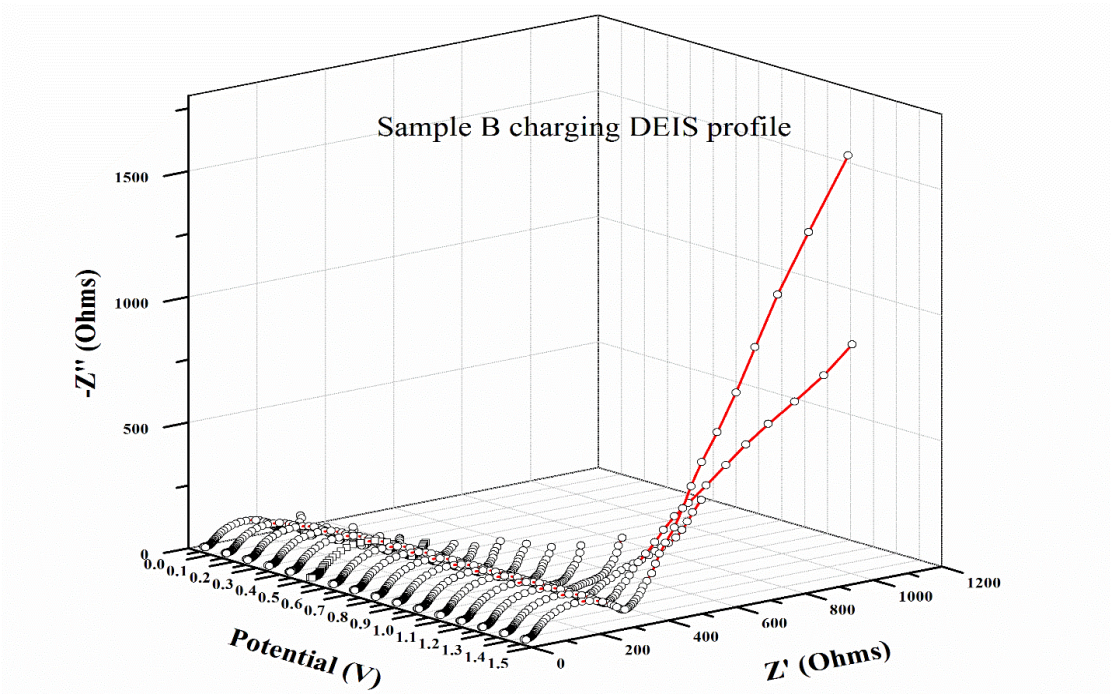

Figure 3.25 DEIS charging profile of an already pre-cycled anodic half-cell fabricated using Sample B (voltage cut-off range 0.03 V-1.6 V)

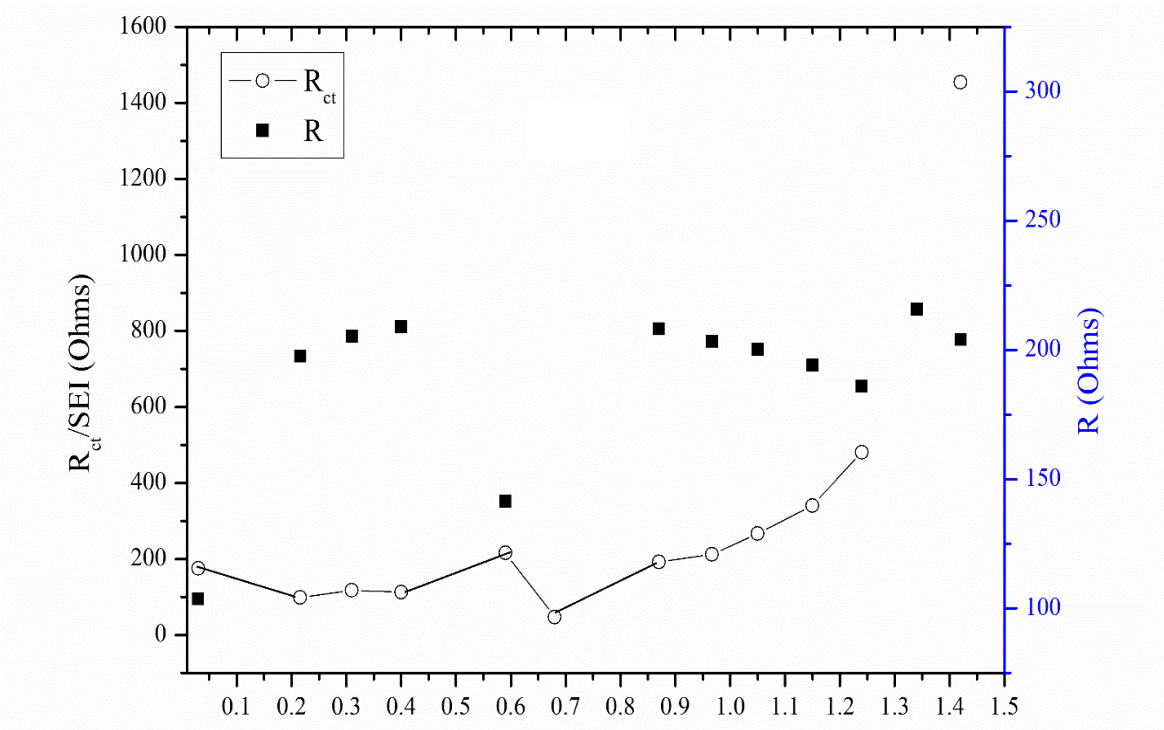

Figure 3.26 R_{ct} parameters as obtained from the DEIS charging profile of anodic half-cell fabricated using sample B

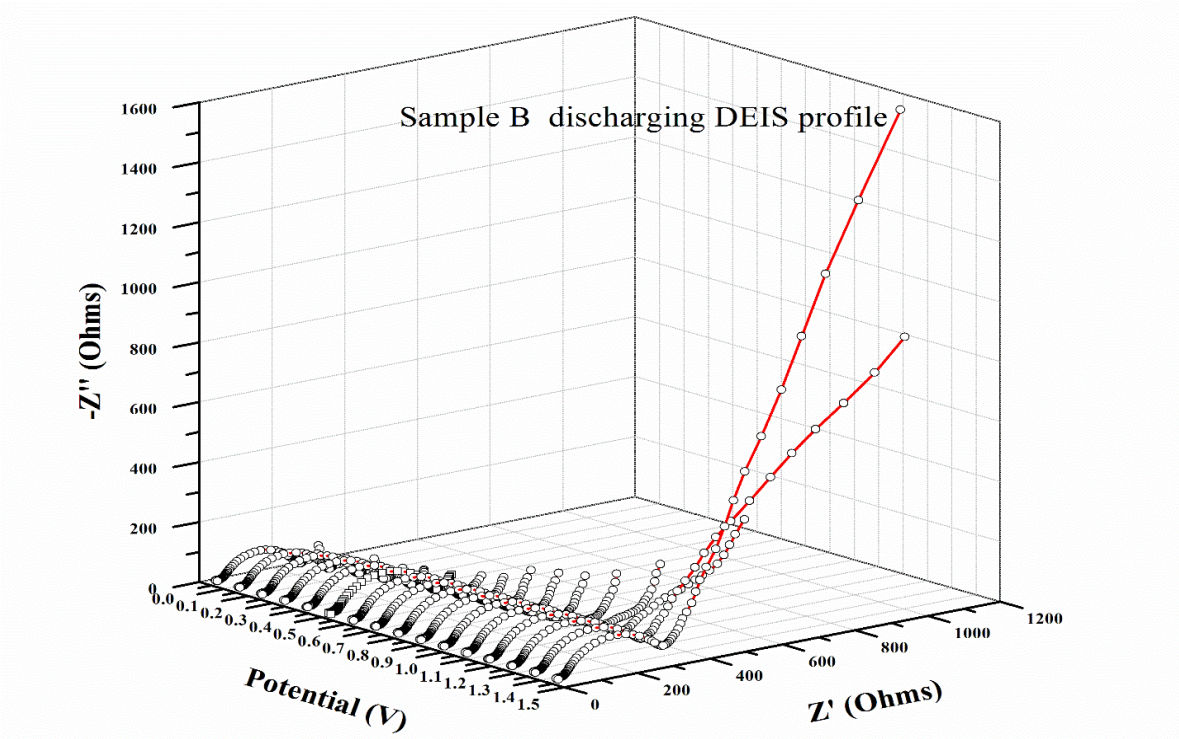

Figure 3.27 DEIS discharging profile of an already pre-cycled anodic half-cell fabricated using Sample B (voltage cut off range 0.03 V-1.6 V)

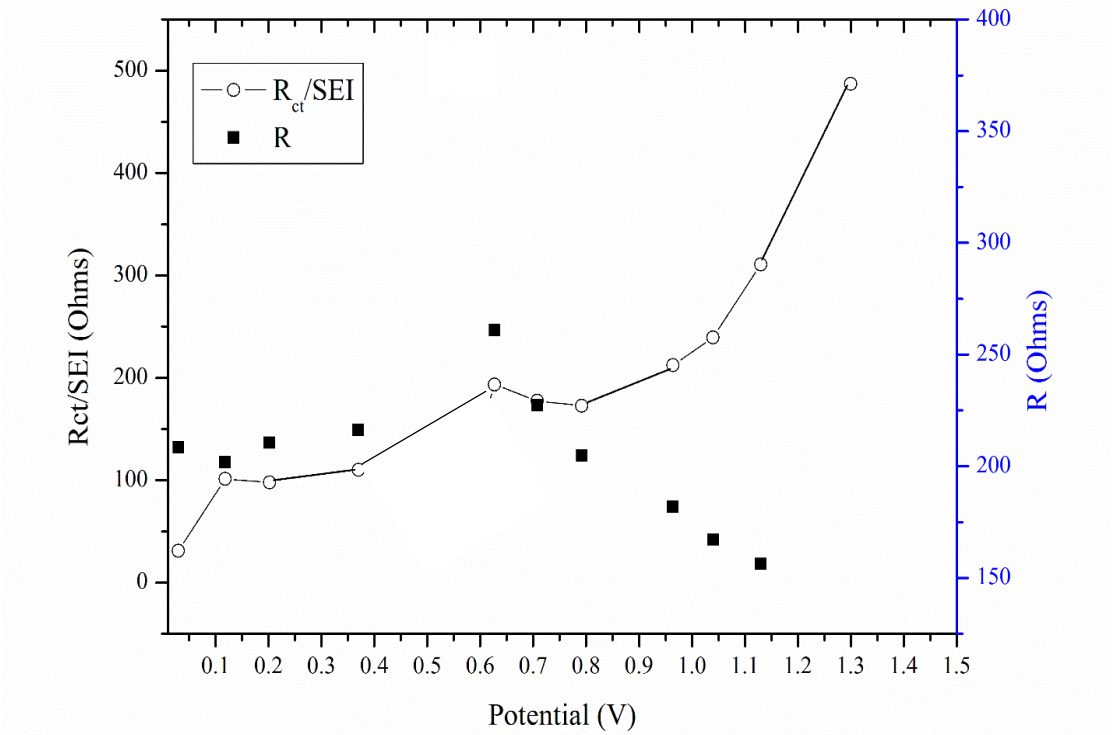

Figure 3.28 R_{ct} parameters as obtained from the DEIS discharging profile of anodic half-cell fabricated using Sample B

A study of the discharge points of Sample B showed similar R_{ct} values corresponding to charging, while the R value decreased to a great extent, indicating about a re-activated lithium cathode due to initiation of cycling, in an already cycled cell (Figures 3.27 & 3.28). From a comparative study of the processed data from the DEIS charging and discharging profiles of already cycled Sample B (Figures 3.25-3.28), it was observed the R_{ct} values were in good correlation with the data obtained from a freshly prepared cell. Hence, optimisation of cell potential is a significant parameter for improved longevity of the cell.

3.6 Conclusions

Organic-inorganic hybrid ion-gel electrolytes do not comply with the conventional protocol adapted for charge-discharge studies. DEIS technique, for the first time, was employed as a diagnostic tool for the characterization of the anodic half-cells. From the simultaneous charging and discharging patterns obtained from these tests, it was inferred that high R_{ct} values at higher potentials often took toll of the inherent capacity of the batteries. Learning from the DEIS results, a revised cut-off in the working potential range resulted in notable improvement in the discharge profiles. Although, the hybrids contain low quantity of lithium salt in the order of millimoles, still they showed impressive capacities over 120-160 $mAhg^{-1}$ at 0.5C charging rates after revised cut-off as obtained from DEIS spectra, comparable with that of commercial electrolytes. With regard to Dynamic electrochemical Impedance Spectroscopic studies, dependence of R_{ct} values provided crucial evidence towards the optimum experimental cut-off required for better functioning of battery. The overall results are tabulated in Table 3.2. Moreover, this analyses also proved beneficial in estimating the degradation features of a battery. In the present work for the simplicity as academic study, no additive was employed for SEI formation and reduction of interfacial resistance. If such additives are also employed, charge-discharge parameters will be greatly improved. But, the present purpose of this work has been to adequately evaluate the properties of organic-inorganic hybrid ion-gel itself.

Table 3.2 Overview of obtained results from charge-discharge and DEIS results

Sample name	*Capacity at 0.5C charging rate ($mAhg^{1}$)*	*Capacity at 1C charging rate ($mAhg^{-1}$)*	*R_{ct} at fully charged state (Ohms)*	*R_{ct} at fully discharged state (Ohms)*
A	160	60	75	350
B	120	60	200	500

References

(1) Cheng, F.; Liang, J.; Tao, Z.; Chen, J. *Adv. Mater.*, **2011**, *23*, 1695–1715.
(2) Armand, M.; Tarascon, J.-M. *Nature*, **2008**, *451*, 652–657.
(3) Tarascon, J.-M.; Armand, M. *Nature*, **2001**, *414*, 359–367.
(4) Goodenough, J. B.; Park, K.-S. *J. Am. Chem. Soc.*, **2013**, *135*, 1167–1176.
(5) Guerfi, A.; Dontigny, M.; Charest, P.; Petitclerc, M.; Lagacé, M.; Vijh, A.; Zaghib, K. *J. Power Sources*, **2010**, *195*, 845–852.
(6) Zaghib, K.; Charest, P.; Guerfi, A.; Shim, J.; Perrier, M.; Striebel, K. *J. Power sources*, **2004**, *134*, 124–129.
(7) Galiński, M.; Lewandowski, A.; Stępniak, I. *Electrochim. Acta*, **2006**, *51*, 5567–5580.
(8) Garcia, B.; Lavallée, S.; Perron, G.; Michot, C.; Armand, M. *Electrochim. Acta*, **2004**, *49*, 4583–4588.
(9) Fernicola, A.; Croce, F.; Scrosati, B.; Watanabe, T.; Ohno, H. *J. Power Sources*, **2007**, *174*, 342–348.
(10) Sato, T.; Maruo, T.; Marukane, S.; Takagi, K. *J. Power Sources*, **2004**, *138*, 253–261.
(11) Lewandowski, A.; Świderska-Mocek, A. *J. Power Sources*, **2009**, *194*, 601–609.
(12) Guerfi, A.; Dontigny, M.; Charest, P.; Petitclerc, M.; Lagacé, M.; Vijh, A.; Zaghib, K. *J. Power Sources*, **2010**, *195*, 845–852.
(13) Sugimoto, T.; Atsumi, Y.; Kikuta, M.; Ishiko, E.; Kono, M.; Ishikawa, M. *J. Power Sources*, **2009**, *189*, 802–805.
(14) MacFarlane, D. R.; Forsyth, M.; Howlett, P. C.; Pringle, J. M.; Sun, J.; Annat, G.; Neil, W.; Izgorodina, E. I. *Acc. Chem. Res.*, **2007**, *40*, 1165–1173.
(15) Wang, Y.; Zaghib, K.; Guerfi, A.; Bazito, F. F.; Torresi, R. M.; Dahn, J. R. *Electrochim. Acta*, **2007**, *52*, 6346–6352.
(16) Scrosati, B.; Garche, J. *J. Power Sources*, **2010**, *195*, 2419–2430.
(17) Itagaki, M.; Kobari, N.; Yotsuda, S.; Watanabe, K.; Kinoshita, S.; Ue, M. *J. Power Sources*, **2005**, *145*, 78-84.
(18) Itagaki, M.; Kobari, N.; Yotsuda, S.; Watanabe, K.; Kinoshita, S.; Ue, M. *J. Power Sources*, **2004**, *135*, 255-261.
(19) Moss, P.L.; Au, G.; Plichta, E.J.; Zheng, J.P. *J. Electrochem. Soc.*, **2008**, *155*, A986-A994.
(20) Huang, J.; Zhang, J.; Li, Z.; Song, S.; Wu, N. *Electrochim. Acta*, **2014**, *131*, 228-235.

Table of Contents

Chapter 3 90
Evaluation of Organic-Inorganic Hybrids as Electrolytes in Fabricated Anodic half-cells 90
3.1 Abstract 90
3.2 Introduction 91
3.3 Experimental 95
3.3.1 Synthesis of organic-inorganic hybrid electrolytes 96
3.3.2 Fabrication of anodic-half cells 97
3.3.3 Charge-discharge studies 97
3.4 DEIS experimental protocol 98
3.5 Results and Discussion**:** 99
3.6 Conclusions 115
References 116

Chapter 4

Flammability Studies of Organic-inorganic Hybrid Ion-gel Electrolytes

4.1 Abstract

This chapter focusses on the thermal studies of the organic-inorganic hybrid ion-gel electrolytes for lithium-ion batteries. These ion-gel electrolytes, possess ionic liquid monomers confined within the borosilicate or silicate matrices, are an ideal match for the non-flammable combination. Thermo-gravimetric analyses showed the hybrids were stable over 350 ^{o}C . Differential scanning calorimetric studies revealed that the hybrids were glassy till over 100 ^{o}C. Further, flame tests proved that the organic-inorganic hybrid electrolytes are not only lower in their susceptibility towards flame, but also do not suffer major loss of weight in flame tests. It was also observed that hybrids are not combustible in nature, unlike other commercial electrolytes used in lithium-ion batteries.

4.2 Introduction

Lithium-ion batteries are a major player in today's never ending quest for energy resources.[1,2] With energy demands sky-rocketing to greater heights, while reserves of the conventional energy sources rapidly declining, it has become inevitable to look for alternative energy resources.[3] Flexibility in terms of design and high power density has endowed them with wide spread applications in various kinds of daily use electronic gadgets, laptops and even in state-of-art electric and hybrid vehicles.[4] Lithium-ion batteries, though, immensely popular are often marred by the safety concerns especially due to the use of few specific ingredients. The inadequacies linked to lithium-ion batteries drew major attraction during the accidents linked to Boeing Dream Liner 787.[5] Prior to this mishap, there were several reports of fire accidents in laptops, electric vehicles etc. due to faulty lithium-ion batteries.[6] Most of the commercial lithium-ion batteries include an electrolyte component mainly composed of a lithium salt such as $LiPF_6$ along with linear and cyclic carbonate additives. Ethylene carbonate (EC) and Dimethyl carbonate (DMC), often used solvents in the commercial lithium-ion batteries are often marked with imminent danger of ignition at higher temperatures due to thermal runaways. Apart from these components, commonly used $LiPF_6$ also poses the risk of releasing gases such as HF on exposure to moisture apart from dangers of flammability. In order to address the issue of flammability, one approach could be external fire safety mechanism which will be able to regulate self-extinguishable properties. But, such an approach would not only be expensive but would also adversely affect the portability of the batteries. A smarter alternative can be the use of flame resistant electrolyte or flame-retardant additives.[7–11] Although, there exists no official classification of such materials, a broad classification can be assigned on the basis of few earlier reports pertaining to this category of research.[12] Roughly 4 classes can be brought on the basis of flame-resistant or flame-retardant properties (Figure 4.1). They can be discussed further in the following manner:

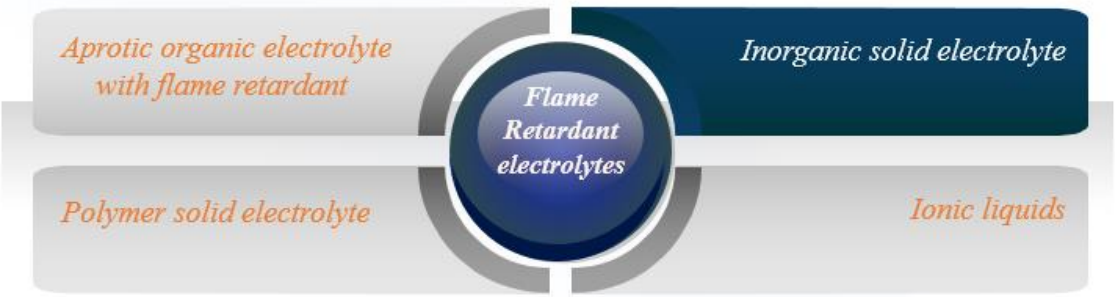

Figure 4.1 Broad classification of major flame-retardant electrolyte alternatives

As per the classification, the major categories in the flame retardant electrolytes are:

- Aprotic organic electrolyte with flame retardants: In this class of electrolytes and additives, phosphorus compounds such as phosphoric acid esters and phosphazenes are commonly considered examples. The major drawbacks in this category includes low conductivity, although long shelf-life and low-cost are the advantages linked to this category.[12–18]
- Polymer electrolytes: In this category, polymer solid electrolytes or polymer gel type electrolytes are included. Typical examples include composites of polyethylene oxide and lithium salt or composites of PEO and lithium salt along with organic solvents. Although, this category is not purely flame-resistant (in the presence of organic solvents), it's still one of the pouplar electrolyte combinations for commercial lithium-ion batteries. However, phosphorus compounds are often used as flame-retardant additives. Low conductivity due to high crystallinity and low mechanical stability are the issues seeking to be addressed in this category.[19,20]
- Inorganic solid electrolyte: Inorganic polymer electrolytes or crystalline solid electrolytes or nano particulate materials are the typical examples in this category. Well-known examples are sulfide glass i.e., Thio-LISICON or silicate glasses or nanocomposites composed of silica nanoparticles or ionic liquids loaded with silica particles, which are often flame-resistant to a great extent by virtue of their inorganic content.[19,21–27]

- Ionic liquids: Ionic liquids are one of the most popular research ingredients in recent times. Riding high on the benefits like high ionic conductivity, low vapour pressure, high thermal stability and low flammability, these molten salts are being examined as electrolytes for various types of battery technologies. Moreover, there are reports on ionic liquids being used along with alkyl carbonates for improved flame retardancy.[28–34]

The use of electrolyte additives is indispensable for the stable SEI layer formation in lithium-ion batteries. Significant research work is also being carried out towards the development of flame-retardant materials as either co-solvent or additives, which include various types of fluorinated phosphates. However, few of the commonly studied additives in this category often are associated with decomposition of graphite anodes.[35,36] Hence, use of these systems in the presence of non-graphitic anode is an alternative solution which is not economically viable.

As mentioned earlier, it's always imperative to have an internally designed safety mechanism by redesign of electrolyte or electrolyte additive system over external safety mechanism to prevent any thermal runway related disasters. Since most of the commercial batteries use organic solvents for smooth functioning of the batteries, it will be only possible to find electrolyte alternatives with flame-retardant properties or are flame-resistant in nature.

In this chapter, we present the non-flammable attributes of organic-inorganic hybrid electrolytes over the conventional commercial electrolytes evaluated by means of flame tests. The novel borosilicate type organic-inorganic hybrids by virtue of their borosilicate network and dispersed ionic liquid phase provide thermal-resistant properties, which are meritorious attributes of this solid-state electrolyte. Apart from flame tests, the thermal stability by means of thermogravimetric and differential scanning calorimetric analyses are also carried out. The novel organic-inorganic hybrid electrolyte banks on borosilicate matrix for its incombustible nature and mechanical durability, whilst utilising an ionic liquid for optimum ionic conductivity and flame resistance, which in fact is a synergistic union of two flame-resistant materials. Further, as a comparative flame test of commercial electrolyte 1M $LiPF_6$ solution (EC-DEC 1:1 solution) was also carried out to highlight the superiority of the organic-inorganic

hybrid ion-gel electrolyte. Typically, in commercial electrolyte solutions, such as 1M $LiPF_6$ in EC: DEC solutions, the carbonate additives are mainly responsible for the flammable attributes in the electrolyte.

4.3 Experimental

4.3.1 Materials

The organic-inorganic hybrids were synthesized by an *in-situ* sol-gel condensation process in the presence of alkoxyborane and alkoxysilane precursors in the presence of ionic liquid. Detailed procedure and compositional aspects are discussed in Chapter 2. However, for the purpose of quick reference the gist of the synthesized hybrids is presented in the following Figure 4.2:

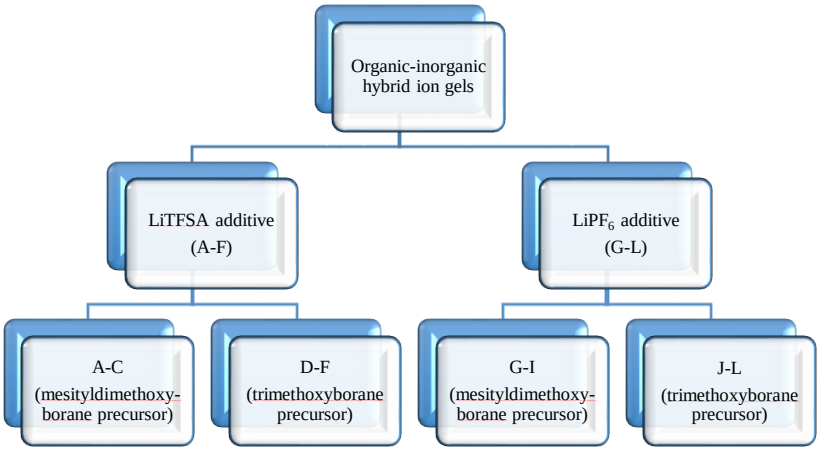

Figure 4.2 Flowchart showing the classification of all the synthesised organic-inorganic hybrids

4.3.2 Instruments

Thermogravimetric analyzer (Perkin Elmer 7) was used to determine the decomposition temperature of the sample. Thermogravimetry was conducted under nitrogen atmosphere at a heating rate of 10 ^{o}C per minute. Sample weight was in the range of 10-15 mg.

Differential Scanning Calorimetry (DSC) analyses were performed with a MDSC 2920 instrument (TA instruments) for a single scan within a temperature scan range starting from -100 till 100 ^{o}C at a heating rate of 3 ^{o}C per minute. The instrument was equipped with liquid nitrogen cooling

system for regulation of temperature. The sample weights were in the range of 10-15 mg taken in hermetically sealed aluminium pans.

Flame tests were carried out by subjecting a designated amount of hybrid to flame inside a hood. Time-sequenced study performed to verify the durability of hybrids against flame. Further, the corresponding weight loss due to flammability test was noted down.

4.4 Results and Discussion:

4.4.1 Thermogravimetric analyses

Interestingly, thermogravimetric analyses of all the LiTFSA (Figure 4.3) based hybrids showed similar profiles with stability till around 350 °C . LiTFSA based hybrids showed single step degradation profiles. The TGA profiles are reflective about the decomposition of the concerned lithium salt in every set besides the ionic liquid. The decomposition temperature of LiTFSA is often a single-step degradation with the decomposition temperature very close to that of the ionic liquid. This behaviour was observed regardless of the alkoxyborane precursor i.e. trimethoxyborane or mesityldimethoxyborane. This behaviour is in conjunction with the morphological data obtained, where LiTFSA based hybrids showed homogeneous profile, indicating a single step degradation (inset in Fig. 4.3 shows the morphological profile of LiTFSA based hybrids).

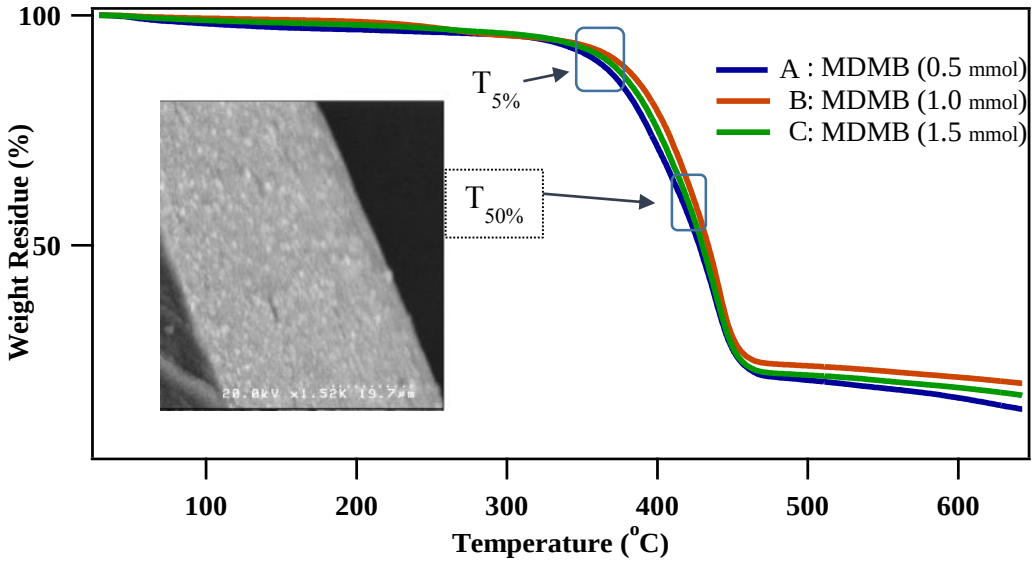

Figure 4.3 Representative TGA plots of LiTFSA based organic-inorganic hybrids A-C

Unlike LiTFSA based hybrids, $LiPF_6$ based hybrids (Figure 4.4) showed a dual step degradation profile. Although, the onset of decomposition started early, irrespective of the alkkoxyborane precursor, the final decomposition temperature was close to LiTFSA based hybrids. $LiPF_6$ based hybrids

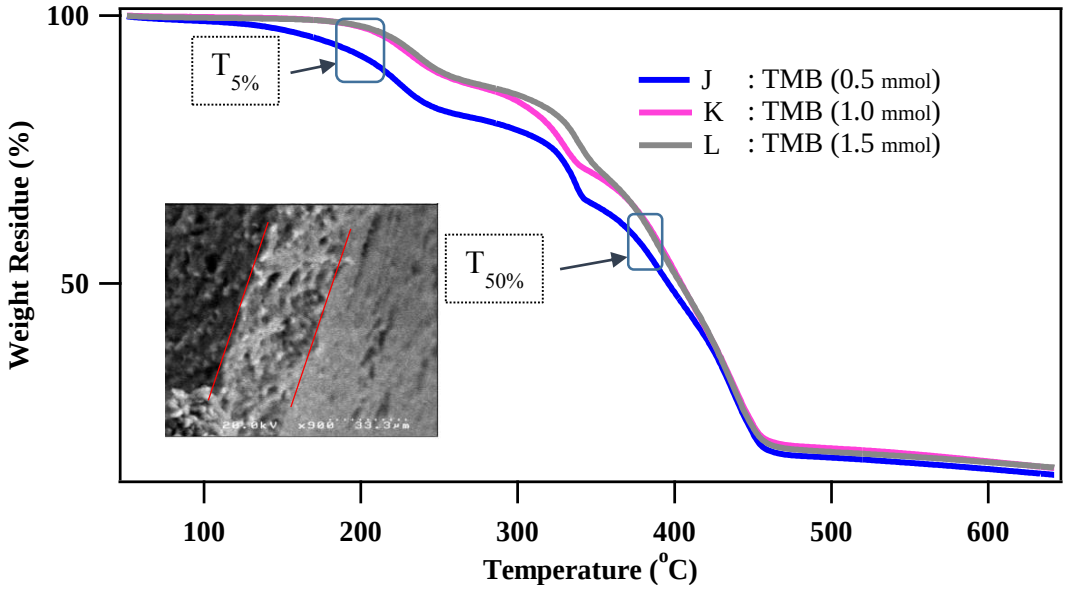

Figure 4.4 Representative TGA plots of $LiPF_6$ based organic-inorganic hybrids (J-L)

decompose in two steps. The two steps roughly can be correlated in the following manner, the first decomposition step corresponds to that decomposition of the upper porous layer as observed in morphological profile, while the next one is the homogeneous layer present beneath the porous layer. (inset in Fig. 4.4 shows the morphological profile of $LiPF_6$ based hybrids). To conclude, all the hybrids regardless of the constituents showed a similar ceramic yield. The obtained ceramic yield of the organic-inorganic hybrids from the TGA data is enlisted in the following table (Table 4.1)

Table 4.1 Thermogravimetric data of organic-inorganic hybrids

Sample	*$T_{5\%}$ (°C)*	*$T_{50\%}$ (°C)*	*Ceramic yield (%)*
A	320	427	14
B	325	435	20
C	328	431	17
D	338	439	11
E	324	437	11
F	341	436	12
G	207	409	13
H	210	401	17
I	219	414	20
J	180	396	14
K	220	404	15
L	224	404	16

4.4.2 Differential Scanning Calorimetry analyses

As an extension to the thermogravimetric studies, further Differential Scanning Calorimetric analyses was also carried to study the glass transition temperature(T_g) of the organic-inorganic hybrids. The T_g value close to -90 °C observed in the DSC thermograms of the hybrids indicative about the T_g of the ionic liquid alone.[37] Typically the T_g values of silicate or borosilicate networks are observed well above the experimental range considered at laboratory scales.

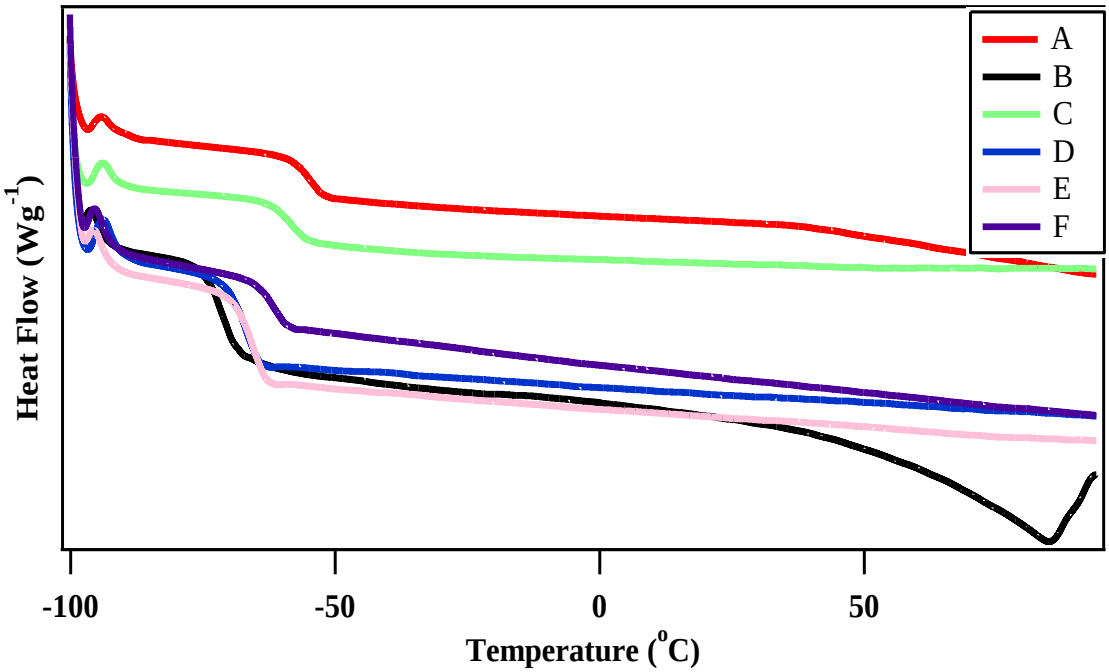

Figure 4.5 DSC plots of LiTFSA based organic-inorganic hybrids A-F

Interestingly, all the TFSA based hybrids showed a second T_g value. Although the T_g values of Samples A & C resemble each other closely in the range of -50 °C, possibly due to the bulky mesityl group interaction with the borosilicate network, while that of Sample B was around -70 °C. While, the TMB based hybrids with LiTFSA i.e., from D-F show a range of close to -60 °C. Since, the possibility of T_g of borosilicate network is ruled out at this temperature. The T_g value of the silicate network. The DSC plots of hybrids A-F is shown in Figure 4.5.

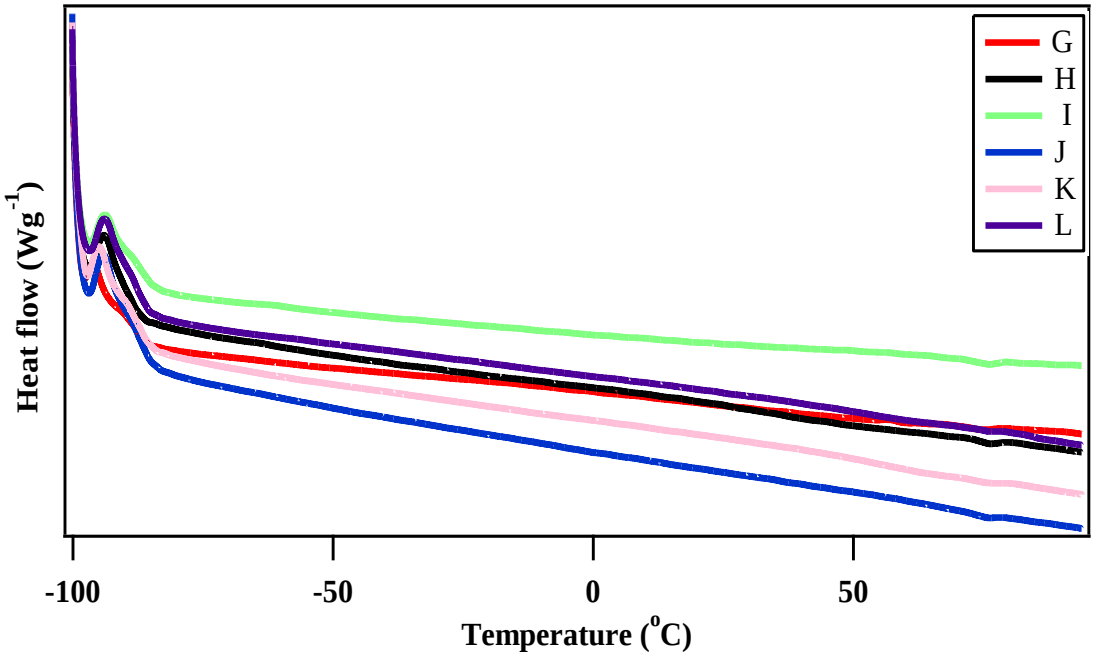

Figure 4.6 DSC plots of $LiPF_6$ based organic-inorganic hybrids J-L

On the contrary, Samples from G-L i.e., $LiPF_6$ based hybrids including trimethoxyborane and mesityldimethoxyborane as alkoxyborane precursors invariably show a Tg value close to -90 °C which corresponds to that of the pure ionic liquid as shown in Figure 4.6.

4.4.3 Flammability studies of hybrids

All the hybrids were studied for the flammability aspects, by subjecting a certain weight of the sample to constant flame, and measuring the weight changes in the samples post-flame treatment. The weight loss ratio gave an interesting insight about the effect of structural composition properties of the organic-inorganic hybrids on flammability. The samples were subjected to continuous flame for over 60 seconds time frame which was monitored by using a stopwatch.

Hybrid A

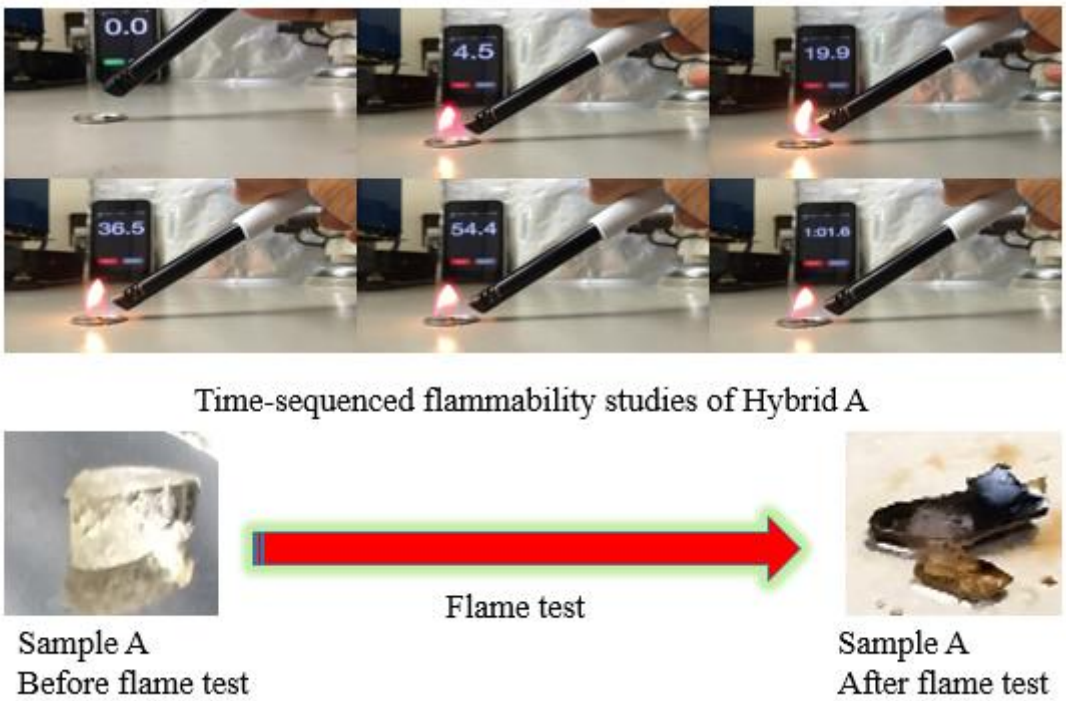

Figure 4.7 Flammability studies of Hybrid A

Hybrid A has a transparent morphology, showing flame susceptibility only at its exposed portions. The weight loss was found to be 16 % of its initial weight. The sample before and after flame test is shown in Figure 4.7. A pinkish flame was observed due to the burning of the lithium salt present within the matrix.

Hybrid B

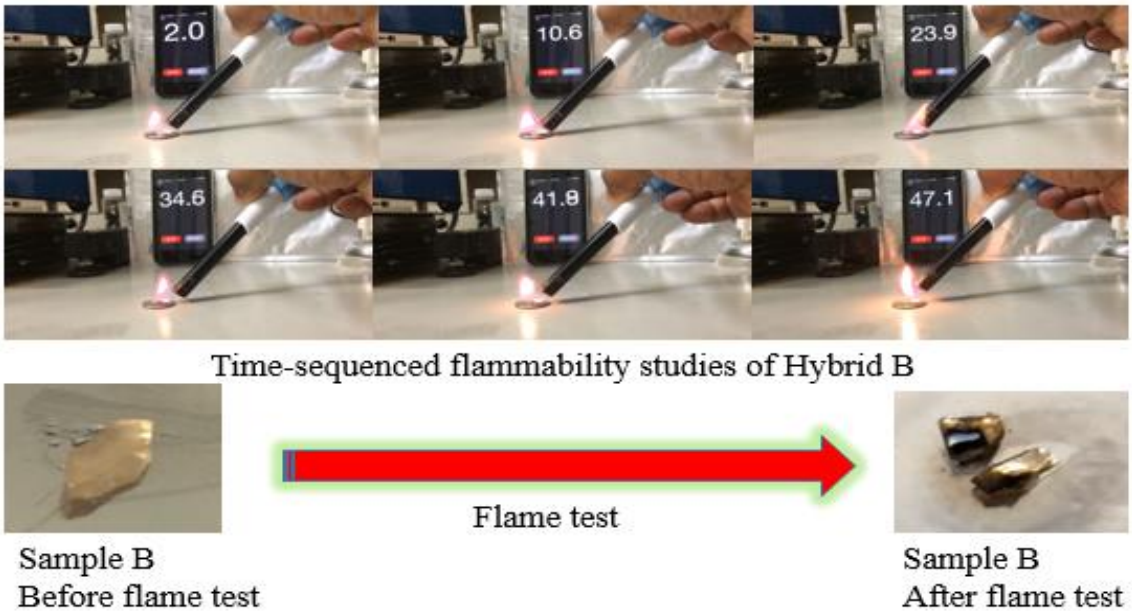

Figure 4.8 Flammability studies of Hybrid B

This sample i.e. hybrid B bore close resemblance with that of hybrid A in the flammability test. The weight loss was lower compared to Sample A (~10 %) with an evident pink flame. Even after a minute of being exposed to flame, the sample did not get carbonize. (Figure 4.8)

Hybrid C

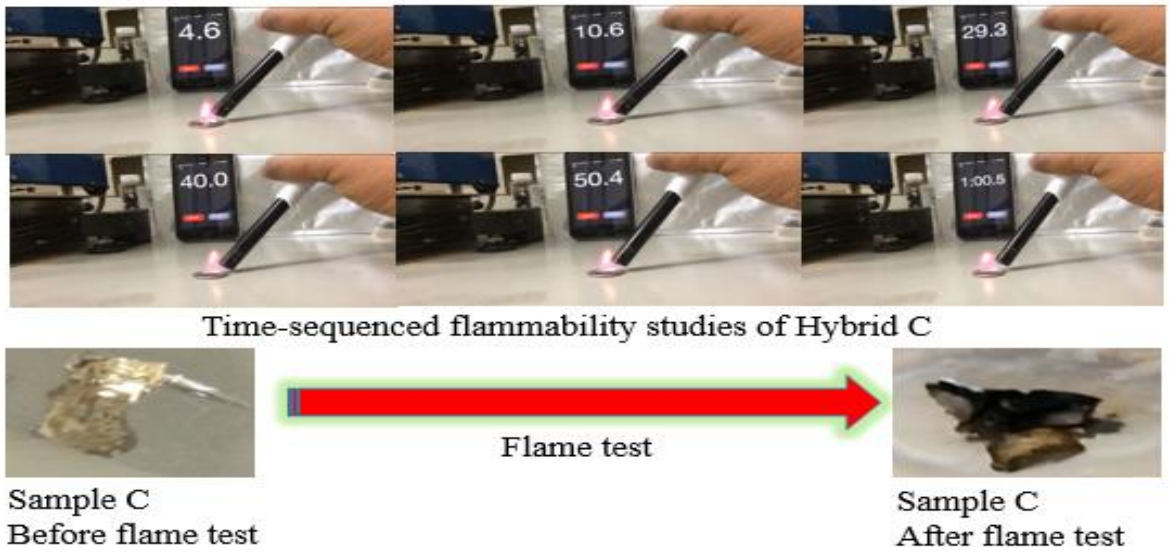

Figure 4.9 Flammability studies of Hybrid C

The transparent portions of the hybrid Cwere selected for flame test. The loss of weight in this hybrid (Figure 4.9) was greater than that of Hybrid B, in the range of 14 % quite close to that of Hybrid A.

Hybrid D

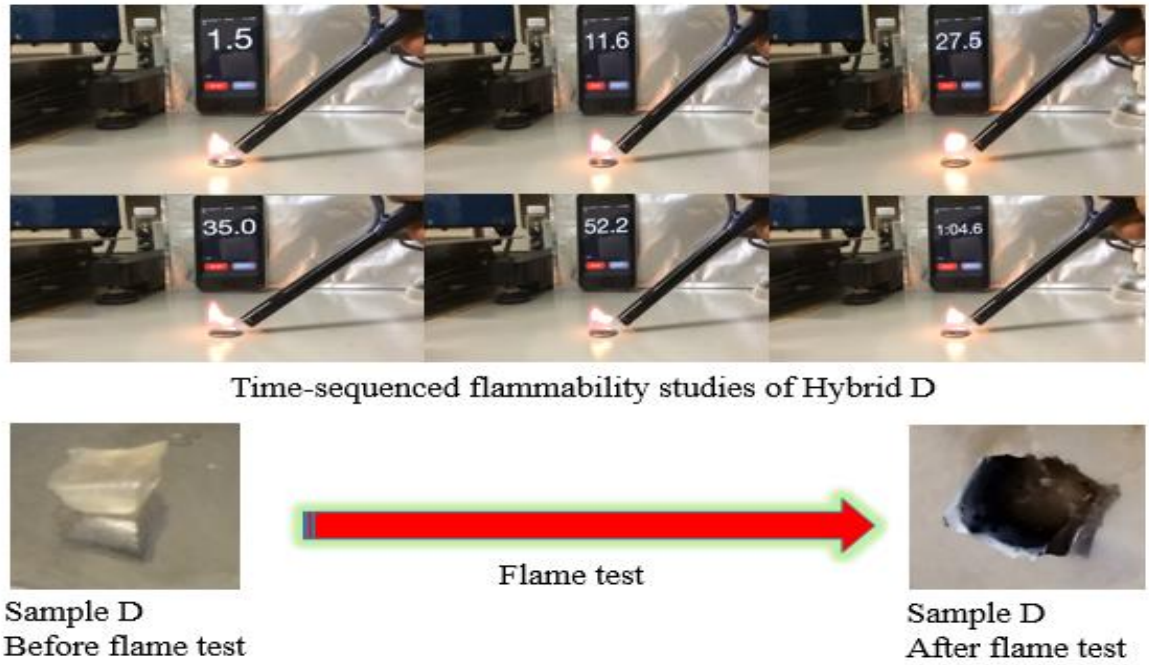

Figure 4.10 Flammability studies of Hybrid D

Hybrid D with trimethoxyborane as alkoxyborane precursor, showed charring up of the sample after a minute of exposure to naked flame, however the corresponding weight loss was restricted to around 12 %. The visuals of the flame test are shown in Figure 4.10. The pink flame was observed though to a lesser extent compared to its predecessors.

Hybrid E

Hybrid E also showed results quite close to that of hybrid D, with weight loss post flame test close to that 13 %. Although, the samples did not register a resemblance with that of hybrid D. Interestingly, the pink flame was absent in this flame test. The sequenced images of flame test are shown in Figure 4.11.

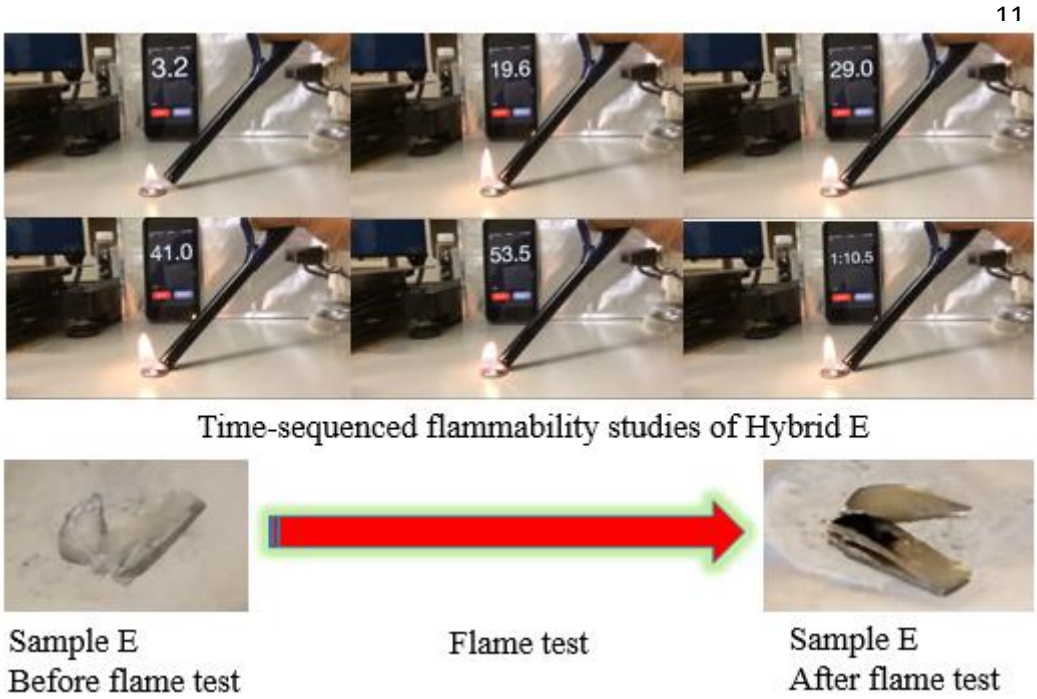

Figure 4.11 Flammability studies of Hybrid E

Hybrid F

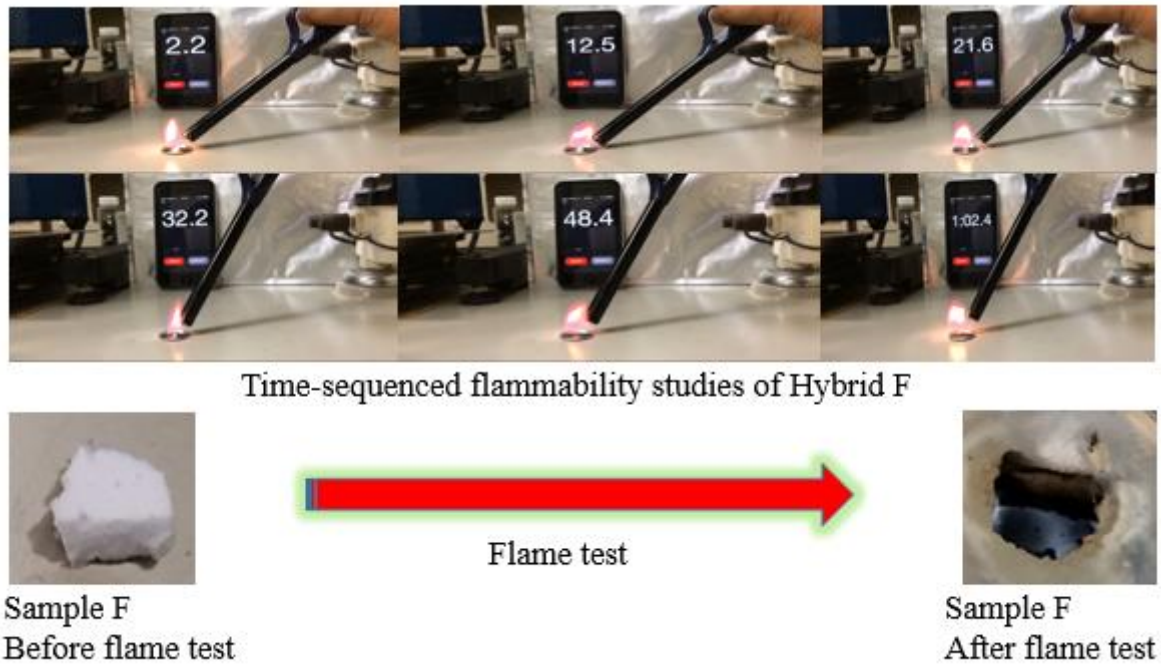

Figure 4.12 Flammability studies of Hybrid F

Hybrid F which (Figure 4.12) showed a turbid morphology quite different from that of hybrids D & E, showed a weight loss of around 16 % after being subjected to flame test. The sample was clearly charred to a greater extent compared to other hybrids.

Hence, as a general conclusion, LiTFSA based hybrids showed greater flame resistance properties. In case of all mesityldimethoxyborane additive i.e. Samples A-C and hybrids with trimethoxyborane additive such as D, F showed a pink flame which is characteristic of a lithium salt. Possibly, minute traces of lithium salt as encased in the matrices get slowly burnt up, during the progressive decomposition of the organic moiety in the hybrids, which is evident from the differently coloured flames.

Hybrid G

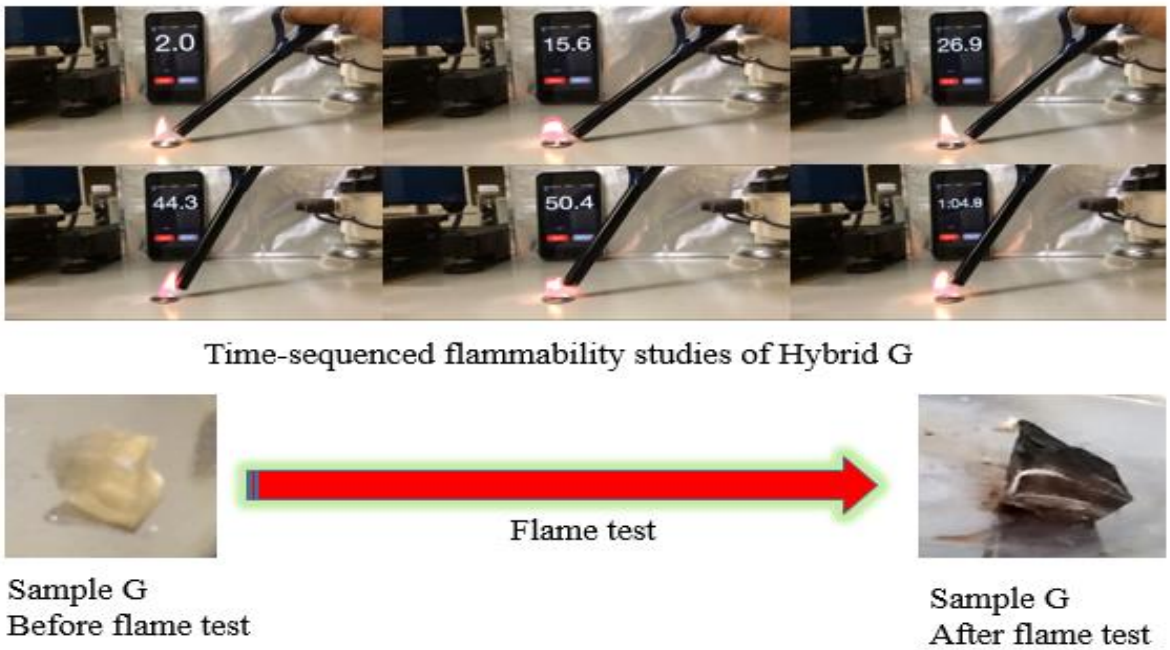

Figure 4.13 Flammability studies of Hybrid G

Hybrid G showed a weight loss of over 16 % after being subjecting to naked flame for more than 60 seconds. Although, the framework remained intact, considerable charring was evident on the areas exposed to naked flames. Visuals are shown in Figure 4.13.

Hybrid H

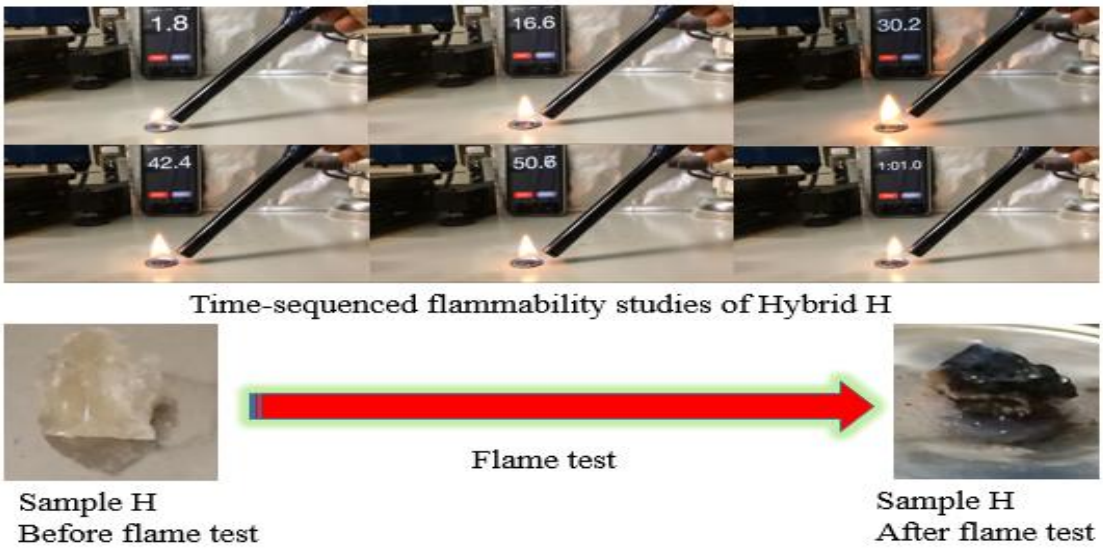

Figure 4.14 Flammability studies of Hybrid H

Sample H with a turbid matrix also burnt up to a great percent losing a weight loss as high as 16 % from its original weight. The visuals are shown in Figure 4.14 shows a highly oxidised mass.

Hybrid I

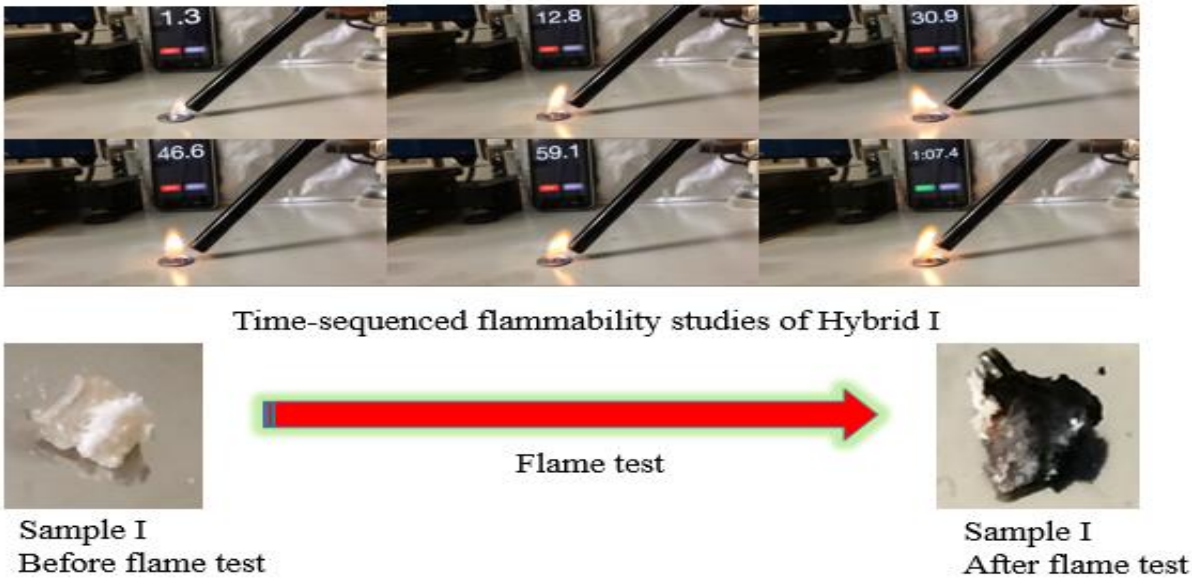

Figure 4.15 Flammability studies of Hybrid I

Hybrid I could sustain a time frame of more than a minute and the corresponding weight loss was highest (21 %) than other hybrids in this set. This turbid matrix registered a huge loss in weight due to the burning up of the excess of organic components included in the initial composition of the hybrid synthesis. The visuals are shown in Figure 4.15

Hybrid J

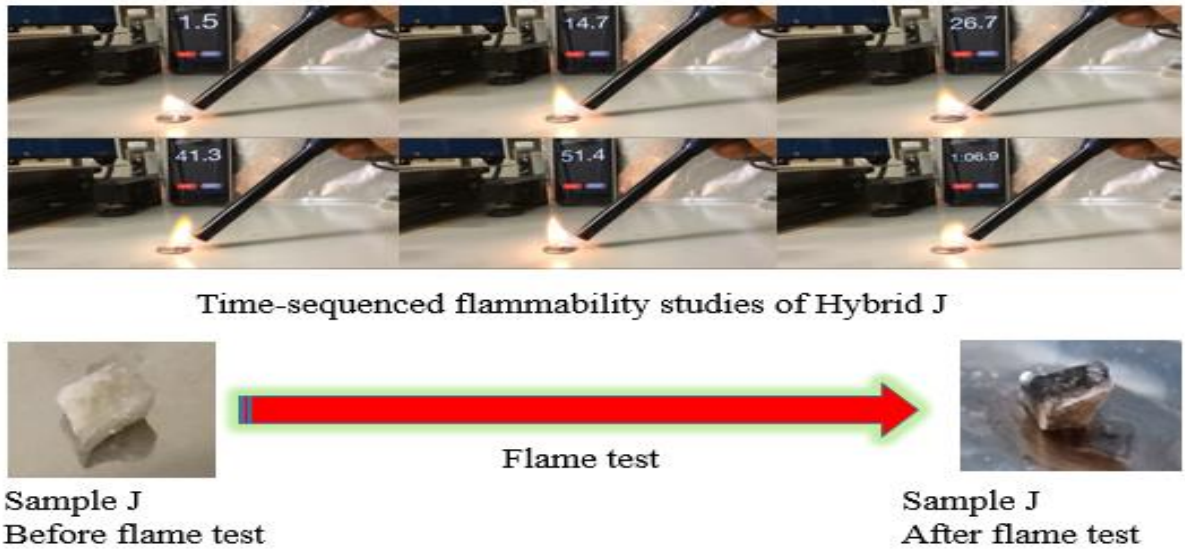

Figure 4.16 Flammability studies of Hybrid J

Hybrid J consisting of trimethoxyborane precursors suffered a weight loss of more than 33 % in the flame test, the details are shown in Figure 4.16. Although, visually, there was no significant change, the weight loss indicates the loss of organic components to great extent in this turbid matrix.

Hybrid K

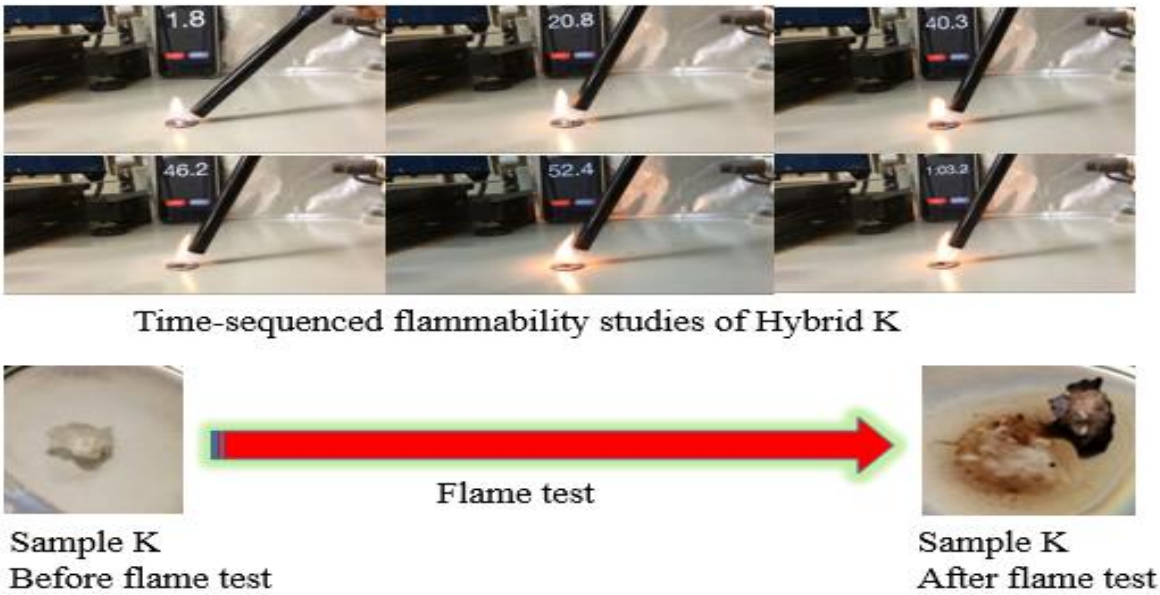

Figure 4.17 Flammability studies of Hybrid K

Hybrid K as well showed a weight loss exceeding 26 % and showed considerable charring as shown in Figure 4.17. Although, considerable loss was observed only on the side exposed to flames, the weight loss was once again high compared to other TFSA based hybrids.

Hybrid L

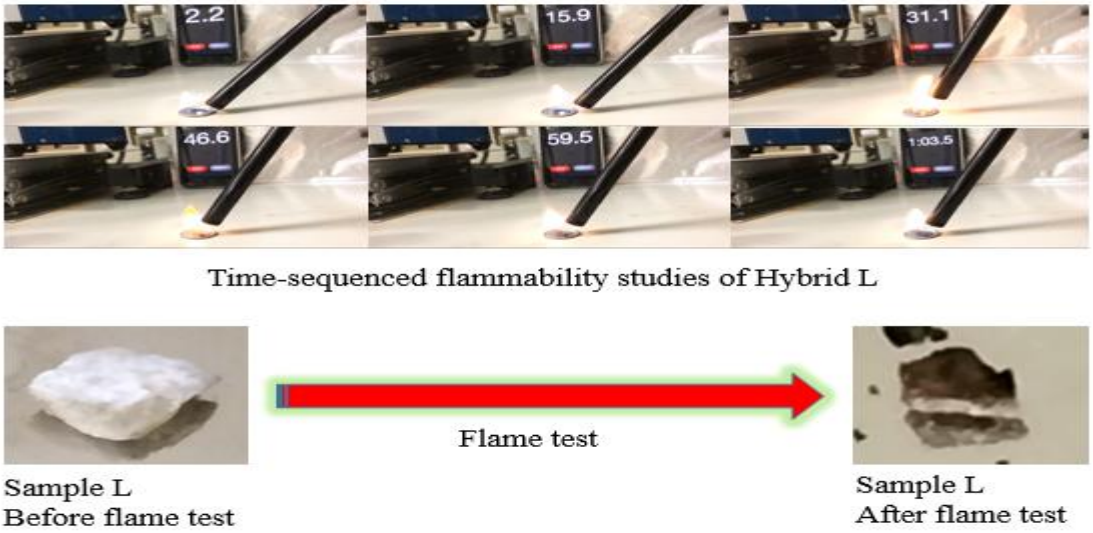

Figure 4.18 Flammability studies of Hybrid L

The turbid matrix of Sample L, showed weight loss of around 17 %. The corresponding images are shown in Figure 4.18.

Table 4.2 Table showing the observed weight loss associated during flame tests

LiTFSA based hybrids		$LiPF_6$ based hybrids	
Sample	*Weight loss (%)*	*Sample*	*Weight loss (%)*
A	15.9	*G*	16.8
B	9.77	*H*	15.5
C	13.2	*I*	21.1
D	11.5	*J*	33.5
E	10.3	*K*	25.6
F	16.9	*L*	16.9

The weight loss of all the organic-inorganic hybrids samples due to flame test, is tabulated in the above table. (Table 4.1). As a general conclusion, it was observed $LiPF_6$ underwent greater loss of weight due to flame test compared with TFSA based hybrids. Previously, we have observed that most of the LiTFSA based hybrids have transparent morphological features giving rise to robust mechanical features except for hybrids at high alkoxyborane concentrations (eg. C and F). The corresponding structural rigidity was evident even in the flame tests corresponding to lower weight losses. While, $LiPF_6$ based hybrids by default showed a turbid morphological profile, characteristic of weaker interations between the organic and inorganic moieties, leading to a weaker structural matrix. It was further corroborated with greater weight loss associated with these hybrids. The pink flame associated with LiTFSA based hybrids, is possibly due to the burning of the trapped lithium salt in the hybrid matrix. The low percentage of weight loss

Another common observation in all the hybrids irrespective of the components was the property of self-extinguishing. The hybrids did not sustain flame on their own and were oxidised only due to the subjected flame. The borosilicate or silicate matrix in addition with the ionic liquid constituent provided thermal resistance to the organic-inorganic hybrid materials. To highlight this specific merit of the organic-inorganic hybrid over other conventional electrolyte, 1M $LiPF_6$ (1:1 EC-DEC) solution was

also subjected to flame test. The sample was ignited and the flame was put off. However, the electrolyte solution was flammable and was completely consumed within 20 seconds of ignition. The visuals can be seen in the Figure 4.19.

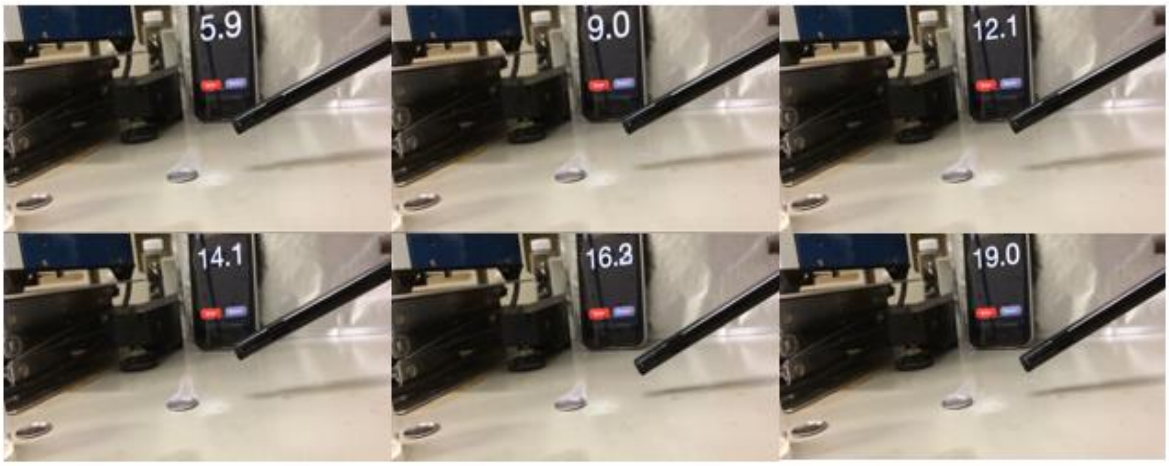

Figure 4.19 Flammability studies of 1MLiPF$_6$ (1:1 EC-DEC) solution

4.5 Conclusions:

Thermogravimetric, differential scanning calorimetric analyses and Flame tests of the organic-inorganic hybrids were carried out. LiTFSA based hybrids showed greater stability in TGA analyses over $LiPF_6$ based hybrids, although the end product in terms of ceramic yields were almost similar. While LiTFSA based hybrids registered an additional T_g value, apart from the one due to the ionic liquid; $LiPF_6$ based hybrids showed uniform T_g profiles corresponding only to the ionic liquid. While $LiPF_6$ based hybrids were showed pronounced loss of weight compared to other hybrids, LiTFSA based hybrids showed relatively stable performance over $LiPF_6$ based hybrids. The above experimental results are in good correlation with the earlier results of morphological profiles. The major finding in the previous results emphasized on the fact that robust networking is observed in the case of TFSA based hybrids which is evident from the transparent homogenous fabric of the hybrids. However, $LiPF_6$ based hybrids by default show a turbid matrix which is due to lesser interactions between the organic and inorganic phases, visualised by the turbidity of the matrix. From the weight loss measurements from the naked flame studies, it was understood that most of the hybrids registered a weight loss of around 10-30 %, mainly corresponding to the volatile organic matter and possibly partially of some ionic liquid content locked along with in the silicate/borosilicate matrices. Only TGA is the most common way to estimate the amount of inorganic component. From the thermogravimetric studies (50 ^{o}C-650 ^{o}C), it was revealed that the ceramic yield was in the range of 10-20 %, which is possibly the remnants of silicate or borosilicate matrix devoid of any organic component or lithium salt. (The thermogravimetric studies were carried beyond the decomposition temperature of the concerned lithium salts.) Apart, from the re-affirming evidence about the previously obtained results, the hybrids were also successful in flame test against the sacrificial commercial electrolyte 1M $LiPF_6$ (1:1 EC-DEC) solution.

References

(1) Tarascon, J.-M.; Armand, M. *Nature*, **2001**, *414*, 359–367.
(2) Armand, M.; Tarascon, J.-M. *Nature*, **2008**, *451*, 652–657.
(3) Goodenough, J. B.; Park, K.-S. *J. Am. Chem. Soc.*, **2013**, *135*, 1167–1176.
(4) Zaghib, K.; Charest, P.; Guerfi, A.; Shim, J.; Perrier, M.; Striebel, K. *J. Power Sources*, **2004**, *134*, 124–129.
(5) Williard, N.; He, W.; Hendricks, C.; Pecht, M. *Energies*, **2013**, *6*, 4682–4695.
(6) Wang, Q.; Ping, P.; Zhao, X.; Chu, G.; Sun, J.; Chen, C. *J. Power Sources*, **2012**, *208*, 210–224.
(7) Harris, S. J.; Timmons, A.; Pitz, W. J. *J. Power Sources*, **2009**, *193*, 855–858.
(8) Spotnitz, R. M.; Weaver, J.; Yeduvaka, G.; Doughty, D. H.; Roth, E. P. *J. Power Sources*, **2007**, *163*, 1080–1086.
(9) Kim, G.-H.; Pesaran, A.; Spotnitz, R. *J. Power Sources*, **2007**, *170*, 476–489.
(10) Lisbona, D.; Snee, T. *Process. Saf. Environ. Prot.*, **2011**, *89*, 434–442.
(11) Spotnitz, R.; Franklin, J. *J. Power Sources* **2003**, *113*, 81–100.
(12) Tsujikawa, T.; Yabuta, K.; Matsushita, T.; Matsushima, T.; Hayashi, K.; Arakawa, M. *J. Power Sources*, **2009**, *189*, 429–434.
(13) Hu, J.; Jin, Z.; Zhong, H.; Zhan, H.; Zhou, Y.; Li, Z. *J. Power Sources*, **2012**, *197*, 297–300.
(14) Wu, B.; Pei, F.; Wu, Y.; Mao, R.; Ai, X.; Yang, H.; Cao, Y. *J. Power Sources*, **2013**, *227*, 106–110.
(15) Allcock, H. R.; Taylor, J. P. *Polym. Eng. & Sci.*, **2000**, *40*, 1177–1189.
(16) Levchik, S. V.; Weil, E. D. *J. Fire Sci.*, **2006**, *24*, 345–364.
(17) Lu, S.-Y.; Hamerton, I. *Prog. Polym. Sci.*, **2002**, *27*, 1661–1712.
(18) Xu, K.; Ding, M. S.; Zhang, S.; Allen, J. L.; Jow, T. R. *J. Electrochem. Soc.*, **2002**, *149*, A622–A626.
(19) Kumar, B.; Scanlon, L.; Marsh, R.; Mason, R.; Higgins, R.; Baldwin, R. *Electrochim. Acta*, **2001**, *46*, 1515–1521.
(20) Morford, R. V.; Welna, D. T.; Kellam III, C. E.; Hofmann, M. A.; Allcock, H. R. *Solid State Ionics*, **2006**, *177*, 721–726.
(21) Romero-Guzmán, M. E.; Romo-Uribe, A.; Ovalle-García, E.; Olayo, R.; Cruz-Ramos, C. A. *Polym. Adv. Technol.*, **2008**, *19*, 1168–1176.
(22) Li, Y.-C.; Schulz, J.; Mannen, S.; Delhom, C.; Condon, B.; Chang, S.; Zammarano, M.; Grunlan, J. C. *ACS Nano*, **2010**, *4*, 3325–3337.
(23) Kanno, R.; Murayama, M. *J. Electrochem. Soc.* **2001**, *148*, A742–A746.
(24) Murayama, M.; Sonoyama, N.; Yamada, A.; Kanno, R. *Solid State Ionics*, **2004**, *170*, 173–180.
(25) Ray, S.; Easteal, A. J. *Mater. Manuf. Process.*, **2007**, *22*, 741–749.
(26) Shimano, S.; Zhou, H.; Honma, I. *Chem. Mater.*, **2007**, *19*, 5216–5221.
(27) Schaefer, J.; Lu, Y.; Moganty, S.; Agarwal, P.; Jayaprakash, N.; Archer, L., *Angew. Chem. Int. Ed.*, **2012**, *24*, 4430-4435.
(28) Byrne, C.; McNally, T. *Macromol. Rapid Commun.*, **2007**, *28*, 780–784.
(29) Ohno, H. *Bull. Chem. Soc. Jpn.*, **2006**, *79*, 1665–1680.
(30) Arbizzani, C.; Gabrielli, G.; Mastragostino, M. *J. Power Sources*, **2011**, *196*, 4801–4805.
(31) Ishikawa, M.; Sugimoto, T.; Kikuta, M.; Ishiko, E.; Kono, M. *J. Power Sources*, **2006**, *162*, 658–662.
(32) Kühnel, R.-S.; Böckenfeld, N.; Passerini, S.; Winter, M.; Balducci, A. *Electrochim. Acta*, **2011**, *56*, 4092–4099.
(33) Ohno, H.; Fukumoto, K. *Electrochemistry*, **2008**, *76*, 16–23.
(34) Fox, D. M.; Gilman, J. W.; Morgan, A. B.; Shields, J. R.; Maupin, P. H.; Lyon, R. E.; De Long, H. C.; Trulove, P. C. *Ind. & Eng. Chem. Res.*, **2008**, *47*, 6327–6332.
(35) Wang, X.; Yamada, C.; Naito, H.; Segami, G.; Kibe, K. *J. Electrochem. Soc.*, **2006**, *153*, A135–A139.
(36) Ota, H.; Kominato, A.; Chun, W.-J.; Yasukawa, E.; Kasuya, S. *J. Power Sources*, **2003**, *119–121*, 393–398.
(37) Ohno, H. *et al*. U.S. Patent No. 7517999B2, **2009.**

Table of Contents

4.1 Abstract 117
4.2 Introduction 118
4.3 Experimental 121
4.3.1 Materials 121
4.3.2 Instrumental 121
4.4 Results and Discussion 122
4.4.1 Thermogravimetric analyses 122
4.4.2 Differential Scanning Calorimetry analyses 124
4.4.3 Flammability studies of hybrids 125
4.5 Conclusions 135
References 136

Chapter 5 Conclusions

5.1 General Conclusions

With the energy demands reaching new heights compounded with technological evolution, the energy requirements are never depleting. Being at a threshold point, to bid adieu to the quick-ending non-renewable resources we are bound to look for alternative prospects to feed out energy demands. Although, renewable energy sources are supplementing the long-term demands, the areas of enormous energy density, economic viability, safety and also environmental friendly are the commonly queried aspects in present-day energy systems. Lithium–ion batteries have been leading the race grabbing many accolades such as portability, high energy density etc. Although there are various areas of concern in the present day lithium-ion batteries, the area of our main interest is in electrolytes. Electrolytes play a major role in these battery which need to be synergistic to the needs of electrodes whilst not compromising with conductivity and diffusivity of the lithium ions.

In Chapter 1, the author has carried out an exhaustive literature review about the materials concerning the Lithium-ion batteries. A negative electrode or anode, a positive electrode or cathode along with an electrolyte constitute the major components of lithium-ion batteries. The author tried to present an overview of the pros and cons of various components discussing in detail about classification, materialistic viewpoint and production value. Further, focussing on the area of interest concerning the solid-state electrolytes the author examines the loopholes of electrolytes in various categories. Further, banking on the benefits of ionic liquids, boron chemistry and sol-gel chemistry the author lays the foundation for the objectives and scope of his research.

Chapter 2, deals with the design and synthesis of novel borosilicate type organic-inorganic hybrid ion-gels composed of an inorganic borosilicate/silicate network and an organic moiety such as mobile ionic liquid and lithium salt within its matrices. The facileness of *in-situ* sol-gel condensation was exploited employing various alkoxyboranes and alkoxysilane precursors in the presence of ionic liquid which gave rise to mechanically robust organic–inorganic hybrid ion-gels. The obtained glassy hybrids were not only mechanically stable but also showed high ionic conductivity even with low

concentration of lithium salt additive in the hybrid composition. The alkoxyborane precursor played a diminutive role in ionic conductivity while the morphological features were primarily governed by the lithium salt additives. LiTFSA based hybrids proved to be homogenous over $LiPF_6$ based systems, while $LiPF_6$ based systems boasted of superior ionic conductivity profiles. In-depth study of the temperature dependence of ionic conductivity was carried out alongside estimation of lithium ion transference number which is instrumental in determining the role of the material as an electrolyte in lithium-ion batteries. Their lithium-transport parameters were comparable with other conventional electrolytes. The originality of this chapter lies in the design and synthesis of borosilicate based organic-inorganic hybrid ion-gels showing high ionic conductivity. Furthermore, morphological effect on ion-conductive behaviour of the hybrid ion-gels were clarified with the help of VFT analysis.

Chapter 3 deals with the employment of the organic-inorganic hybrid ion-gels as electrolytes for lithium-ion batteries. Organic-inorganic hybrid ion-gel electrolytes do not comply with the conventional protocol adapted for charge-discharge studies, evident in their preliminary studies. Thus, an electrochemical technique viz. Dynamic Electrochemical Impedance Spectroscopy (DEIS) was employed for the first time, as a diagnostic tool for the characterisation of the anodic-half-cells. This non-destructive technique was helpful in gaining deep insights about the internal resistances operating within the cell, thereby predicting the applicable working potential limit. Inferences drawn from these studies, led to revised experimental protocol of these batteries, showing appreciable results. Although, the hybrids are contain low quantity of lithium salt to the order of millimoles, they showed impressive capacities of over 120-160 $mAhg^{-1}$ at 0.5C charging rates at par with commercial electrolytes. The novelty in this chapter lies in the implementation of DEIS as an investigative tool in the determination of workable potential range for the organic-inorganic hybrids. This application is reported for the first time.

Chapter 4 deals with the thermogravimetric, differential scanning calorimetric analyses and flame tests of the organic-inorganic hybrids were carried out. LiTFSA based hybrids by virtue of their robust mechanical stability showed greater stability in TGA analyses over heterogeneous $LiPF_6$ based hybrids. The DSC thermograms revealed greater interactions between the organic and inorganic

moieties of LiTFSA based hybrids over $LiPF_6$ based hybrids. Irrespective of the nature of salt additive, the hybrids were found to be extremely flame resistant, registering minimum weight losses whilst showing negligible susceptibility to flame unlike commercial electrolyte 1M $LiPF_6$ (1:1 EC-DEC) solution.

5.2 Future prospects of the thesis

Building on the foundations laid by the present work, the possible or tentative offshoots of future experiments which can be tried are as follows:

1. Post-mortem studies concerning the internal kinetics in the fabricated cells is another voluminous off-shoot which needs to be understood. Given the novelty of electrolyte, the understanding of such fundamental issues can be instrumental in improvisation over the achieved results.
2. The hybrid electrolytes show high thermal stability. Successful cyclability tests of the fabricated anodic half-cells at temperatures as high as 80°C opens up avenues for applications in high-temperature lithium battery requirements.
3. Given the advantages of robust mechanical stability and tunable morphological profiles, along with flexibility in terms of choice of precursor materials the organic-inorganic hybrids pave the way for exploration into other battery technologies as well. For instance, tuning the morphological profiles alone would be an *ad hoc* solution to the permeability of gas in a solid-state media, which can be utilised in Lithium-air battery technology. Hence, organic-inorganic hybrids are likely to be promising candidates in the Lithium-air technology as well.

List of Publications and other Achievements

Name: Kumar Sai Smaran

1. Original Papers

① [Peer-Reviewed Journals, First Author]

"Design of Organic-inorganic Hybrid Ion-gel Electrolytes Composed of Borosilicate and Allylimidazolium Type Ionic Liquids", Kumar Sai Smaran, Raman Vedarajan, Noriyoshi Matsumi, International Journal of Hydrogen Energy, vol.39, pp.2936-2942, 2014.

② [Peer Reviewed Journals, Non-First Author]

"Synthesis Of Imidazolium Salt-Terminated Poly(Amidoamine)-Typed POSS-Core Dendrimers And Their Solution And Bulk Properties", Kensuke Naka, Ryusuke Shinke, Maki Yamada, Fadila Djouadi Belkada, Yoko Aijo, Yasuyuki Irie, Sonu Ram Shankar, Kumar Sai Smaran, Noriyoshi Matsumi, Shogo Tomita and Shinichi Sakurai, Polymer Journal, vol.46, pp.42-51, 2014.

1. Oral or Poster Presentations (First Author or Presenter)

International

1) "Design of Borosilicate Type Organic-Inorganic Hybrid Ion-gel Electrolytes", *{Oral Presentation}*, Kumar Sai Smaran, Noriyoshi Matsumi, PRiME-2012 (Pacific Rim Meeting on Electrochemical and Solid State Interface), Joint International Meeting of ECS—The Electrochemical Society and The Electrochemical Society of Japan, Honolulu,

Hawaii (USA), (2012, 10).

2) "Borosilicate/Ionic Liquid Hybrid Electrolytes," *{Oral presentation},* Kumar Sai Smaran, Raman Vedarajan, Noriyoshi Matsumi, JAIST International Symposium on Ionics Materials, Japan Advanced Institute of Science and Technology, (2012, 3).

3) "Morphological and Electrochemical Aspects of Borosilicate Type Organic Inorganic Hybrid Ion-gels." *{Poster presentation},* Kumar Sai Smaran, Raman Vedarajan, Noriyoshi Matsumi. "19th International Conference on Solid State Ionics 2013", Kyoto, (2013, 6).

4) "Morphological and Electrochemical Aspects of Borosilicate Type Organic Inorganic Hybrid Ion-gel electrolytes." *{Oral presentation},* Kumar Sai Smaran, Raman Vedarajan, Noriyoshi Matsumi, JAIST International Symposium on Functional Polymer Materials, Japan Advanced Institute of Science and Technology, (2013, 12).

5) "Borosilicate Type Organic-Inorganic Hybrids as Electrolytes for Lithium Ion Secondary Battery Devices." *{Oral presentation},* Kumar Sai Smaran, Raman Vedarajan, Noriyoshi Matsumi, JAIST Japan-India Symposium on Automotive Technologies (Energy, Fuels and Plastics), Japan Advanced Institute of Science and Technology, (2014, 6).

Domestic

6) "Preparation of Ion-gel Electrolytes via Borosilicate Glass Formation in the Presence of Ionic Liquids." *{Poster presentation}*, Kumar Sai Smaran, Noriyoshi Matsumi, "Annual Meeting of SPSJ (Society of Polymer Science, Japan) 2012", Yokohama, (2012, 5)

7) "Ion Conductive Properties of Borosilicate Glass/Ionic Liquid Hybrid including Allylimidazolium Type Ionic Liquids." *{Poster Presentation}*, Kumar Sai Smaran, Raman Vedarajan, Noriyoshi Matsumi. "Fall Meeting of SPSJ", Nagoya, (2012, 9).

8) "Design of Organic-Inorganic Hybrid Ion-Gel Electrolytes Including Allylimidazolium

Type Ionic Liquids," *{Poster presentation},* Kumar Sai Smaran, Raman Vedarajan, Noriyoshi Matsumi. Regional Meeting of CSJ (Chemical Society of Japan), Fukui, (2012, 11).

9) "Ion Conductive Properties of Organic-inorganic Hybrid Ion-gels Composed of Borosilicate Glass and Low Viscous Ionic Liquids." *{Poster Presentation},* Kumar Sai Smaran, Raman Vedarajan, Noriyoshi Matsumi. "Annual Meeting of CSJ (Chemical Society of Japan) 2013", Kyoto, (2013, 3).

10) "Electrochemical Properties of Borosilicate-Ionic Liquid Hybrid Ion-gels." *{Poster presentation}*, Kumar Sai Smaran, Raman Vedarajan, Noriyoshi Matsumi. "Annual Meeting of SPSJ (Society of Polymer Science, Japan) 2013", Kyoto, (2013, 5).

11) "Design of Organic-Inorganic Hybrid Ion-gel Electrolytes Composed of Borosilicate And Allylimidazolium Ionic Liquids." *{Oral presentation},* Kumar Sai Smaran, Raman Vedarajan, Noriyoshi Matsumi. "Inorganic Polymer Conference", Tokyo University of Sceince, Tokyo, (2013, 9).

12) "Charge-Discharge Characteristics of Lithium Ion Secondary Batteries Fabricated Using Borosilicate Type Organic-Inorganic Hybrid Ion-gel Electrolytes." *{Poster presentation},* Kumar Sai Smaran, Raman Vedarajan, Noriyoshi Matsumi. "Annual Meeting of SPSJ (Society of Polymer Science, Japan) 2014", Nagoya, (2014, 5).

13) "Charge-Discharge Characteristics of Lithium Ion Secondary Batteries Fabricated Using Borosilicate Type Ion-gel Electrolytes." *{Oral presentation},* Kumar Sai Smaran, Raman Vedarajan, Noriyoshi Matsumi. "Fall Meeting of SPSJ", Nagasaki, (2014, 9).